Structural and Functional Heterogeneity of Striatal Interneuron Populations

by

Farid Nashaat Garas

New College, Oxford

A thesis submitted to the University of Oxford in fulfillment of the requirements for the degree of Doctor of Philosophy

University of Oxford,

MRC Brain Network Dynamics Unit,

Department of Pharmacology,

Trinity Term 2015

Structural and Functional Heterogeneity of Striatal Interneuron Populations

Farid Nashaat Garas

New College, University of Oxford

Thesis submitted for degree of Doctor of Philosophy at the University of Oxford, Trinity Term 2015

ABSTRACT

The striatum is the largest nucleus of the basal ganglia, and acts as a point of convergence for thalamic, cortical and midbrain inputs. It is involved in both motor and associative forms of learning, and is composed of spiny projection neurons (SPNs) whose output along the so-called "direct pathway" and "indirect pathway" is modified by the activity of diverse sets of interneurons. Four "classical" or major classes of striatal interneuron can be identified according to the selective expression of the molecular markers parvalbumin (PV), calretinin (CR), nitric oxide synthase (NOS) or choline acetyltransferase (ChAT). Although the interneurons within a class are generally considered to be homogeneous in form and function, there is emerging evidence that some classes encompass multiple types of neuron, and that the heterogeneity in striatal interneurons extends beyond these four classes. Defining the extent of interneuron heterogeneity is important for understanding how the striatum processes distinct, topographically-organized inputs from the cortex and thalamus in order to govern a wide range of behaviors.

To address these issues, a combination of immunofluorescence microscopy and stereological cell counting approaches was used in striatal tissue from rat, mouse and non-human primate. This was supplemented by in vivo recording and juxtacellular labelling of single neurons in rat. A first set of experiments showed that secretagogin (Scgn), a calcium-binding protein, is expressed by a large number of interneurons in the dorsal striatum of rat and primate, but not in the mouse. In all species tested, secretagogin was expressed by a subset of PV+ interneurons and a subset of CR+ interneurons in the dorsal striatum, but also labelled a group of interneurons that did not express any of the classical markers of striatal interneurons.

A second set of experiments in the rat demonstrated that the selective co-expression of Scgn by PV+ interneurons delineates two topographically-, physiologically- and morphologically-distinct cell populations. These topographical differences in distribution were largely conserved in the primate caudate/putamen. In rats, PV+/Scgn+ and PV+/Scgn– interneurons differed significantly in their firing rates, firing patterns and phase-locking to cortical oscillations. The axons of PV+/Scgn+ interneurons were more likely to form appositions with the somata of direct pathway SPNs than indirect pathway SPNs, whereas the opposite was true for the axons of PV+/Scgn- interneurons. These two populations of GABAergic interneurons provide a potential substrate through which either of the striatal output pathways can be rapidly and selectively inhibited, and in turn mediate the expression of behavioral routines.

A third set of experiments showed that CR+ interneurons of the dorsal striatum can be separated into three populations based on their molecular, topographical and morphological properties. Small-sized ("Type 3") CR+ interneurons co-expressed Scgn and were restricted in their distribution towards the rostro-medial poles of the striatum in both rats and primates. In rats, these neurons also expressed the transcription factor SP8, suggesting that they may be newly generated throughout adulthood. Large-sized, ("Type 1") CR+ interneurons did not express Scgn, but could be further distinguished by their expression of the transcription factor Lhx7. Medium-sized ("Type 2") CR+ interneurons did not express Scgn or Lhx7, and had heterogeneous electrophysiological properties in vivo.

The expression of Scgn, but not other classical interneuron markers, identified a group of interneurons that were restricted in their distribution towards the ventro-medial aspects of the dorsal striatum. A fourth set of experiments showed that these neurons are also present in the core and the shell of the nucleus accumbens. Unlike the case of dorsal striatum, however, PV+ interneurons and CR+ interneurons of the nucleus accumbens did not co-express Scgn. Moreover, many of the interneuron populations studied had greater densities in the ventral striatum compared to the dorsal striatum, and had quantifiably strong biases in their distribution towards a variety of axes within both the core and the shell of the nucleus accumbens. These data thus highlight some major differences in the constituent elements of the microcircuits of dorsal striatum and nucleus accumbens.

In conclusion, these studies have revealed a great deal of molecular, topographical, electrophysiological and structural heterogeneity within the interneuron populations of the striatum. As several of these interneuron populations were not evenly distributed throughout the striatum, this ultimately suggests that the microcircuit of the striatum is specialized according to regions that differ in their cortical, thalamic and dopaminergic inputs.

ACKNOWLEDGEMENTS

Firstly I would like to thank my supervisors Dr. Andrew Sharott and Prof. Peter Magill, without whom this thesis would not be possible. Their scientific input helped shape a great deal of my critical thinking towards the interpretation of my own findings, as well as those of others. Their shared enthusiasm for all things basal ganglia taught me the importance of doing what you love. In particular, I would like to thank Pete for taking me on a student when he had no space and little money to spend. His faith in me was a consistent source of inspiration that pulled me through even the longest of recording sessions. A special thanks to Andy, whose presence and support throughout my studentship has meant the world to me. I only hope that I can one day repay him for all the time he spent assessing my work, irrespective of his own schedule.

I am also grateful to Prof. Paul Bolam for providing the facilities at the MRC Anatomical Neuropharmacology Unit. I am thankful for the members of the Unit for sharing this important time in my life. Special thanks go to Dan, Anna, Emilie, Eszter and Natalie for their support as well as their friendship. I also acknowledge that my work would not be possible without the funding from the Clarendon Scholarship Fund and the MRC. A special thanks to the technical staff in the lab, including Ben Micklem, Lisa Conyers, Liz Norman and Katie Whitworth, whose efforts allowed my work to be more efficient.

A huge thank you to all of my family for their seemingly endless support over the years. I am grateful for my parents, Nashaat and Manal, who gave up so much to give me this oppurtunity. A big thank you to my youngest brothers Jonathan and Andrew, who always reminded me that no matter how rough things got with work, a red pepper could always be crushed! And finally, a special thank you to my brother Shaady, whose presence in the lab during the summer months turned bench work and stereology into a nearly enjoyable adventure. Thank you for everything.

TABLE OF CONTENTS

ABSTRACT. ……i

ACKNOWLEDGEMENTS. …… ii

TABLE OF CONTENTS. …… iii

ABBREVIATIONS. …….. xiv

PREFACE……. ……..... xvii

CHAPTER 1. GENERAL INTRODUCTION. …… 1

1.1 OVERVIEW OF THE BASAL GANGLIA. …… 2

1.1.1 A brief account of the functional organization of the basal ganglia. …….. 2

1.1.2 The striatum. ……3

1.1.3 The globus pallidus (pars externa). ……..7

1.1.4 Substantia nigra pars compacta. …… 8

1.1.5 Subthalamic nucleus. ……. 11

1.1.6 The output nuclei of the basal ganglia. …….. 12

1.1.7 Summary. …… .. 13

1.2 DORSAL STRIATAL MICROCIRCUITRY. …… 15

1.2.1 Spiny projection neurons. …… 15

1.2.1.1 Anatomical properties. ……16

1.2.1.2 Pharmacological properties. ……..19

1.2.1.3 Electrophysiological properties. ……19

1.2.1.4 Summary…….. 21

1.2.2 Parvalbumin-expressing fast-spiking interneurons. …… 21

1.2.2.1 Anatomical properties. …… 21

1.2.2.2 Electrophysiological properties. …… 22

1.2.2.3 Connectivity. …… 24

1.2.2.4 Pharmacological properties. …… 26

1.2.3 NOS/NPY/SOM-expressing interneurons. ……27

1.2.3.1 Molecular characterization and morphological properties. ……27

1.2.3.2 Electrophysiological properties. ……28

1.2.3.3 Connectivity. ……28

1.2.3.4 Pharmacological properties. ……29

1.2.4 ChAT-expressing tonically active interneurons. ……30

1.2.4.1 Morphology and connectivity. ……30

1.2.4.2 Electrophysiological properties. ……30

1.2.4.3 Pharmacological properties. …… 32

1.2.5 CR-expressing interneurons. ……..33

1.2.6 Novel types of striatal interneuron. ……34

1.3 FUNCTIONAL HETEROGENEITY ACROSS THE AXES OF THE DORSAL STRIATUM IN RATS AND PRIMATES ……....37

1.4 STEREOLOGICAL CELL COUNTING IN THE DORSAL STRIATUM OF THE RAT AND PRIMATE: A BRIEF LOOK AT THE NUMBERS. ……..41

1.5 THE VENTRAL STRIATUM (NUCLEUS ACCUMBENS). ……47

1.5.1 Overview and delineation of the ventral striatum. ……47

1.5.2 The core of the nucleus accumbens. ……..…..…50

1.5.3 The shell of the nucleus accumbens. ……..51

1.6 CALCIUM BINDING-PROTEINS IN THE CENTRAL NERVOUS SYSTEM……53

1.6.1 Secretagogin. ……..54

1.7 AIMS OF THIS RESEARCH. ……59

1.7.1 Summary. ……59

1.7.2 Specific aims. ……60

1.7.2.1 Aim 1: To qualify and quantify the degree of secretagogin expression in the dorsal and ventral striatum of rodents and Rhesus Macaques (Chapters 3 and 6)……60

1.7.2.2 Aim 2: To investigate molecular, anatomical and physiological heterogeneity among the interneuron populations of the dorsal striatum of rodents (Chapters 4 and 5) ……60

1.7.2.3 Aim 3: To quantify the degree of topographical bias in the distribution of various interneuron populations in the dorsal and ventral striatum of rodents (Chapters 3, 4, 5 and 6). ……..60

1.7.2.4 Aim 4: To determine whether molecularly and topographically distinct populations of interneuron in the dorsal striatum of rodents exist in the caudate/putamen of the Rhesus Macaque (Chapters 3, 4 and 5). ……61

1.7.2.5 Aim 5: To estimate the mean density and total numbers of different populations of striatal interneuron (Chapters 3, 4, 5 and 6). …… 61

CHAPTER 2: MATERIALS AND METHODS. …… 63

2.1 STEREOLOGICAL CELL COUNTING IN THE DORSAL AND VENTRAL STRIATUM OF RATS AND MICE. …… 64

2.1.1 Preparation of brain tissue for cell counting. …… 64

2.1.2 Indirect immunofluorescence. ……64

2.1.3 Sampling and cell-counting strategies. ……...67

2.2 ANALYSES OF DATA OBTAINED FROM STEREOLOGICAL CELL COUNTS. ….… 74

2.2.1 Calculations of section area, volume and estimates of total cell number. ……..74

2.2.2 Topographical and statistical analysis of interneuron distribution…… 77

2.2.3 Measurements of mean somatic diameters. ……79

2.3 JUXTACELLULAR RECORDING AND LABELLING. …… 80

2.3.1 In vivo electrophysiological recording and juxtacellular labelling of single neurons. …….. 80

2.3.2 Tissue processing for identification of recorded and labelled neurons. …… 82

2.3.3 Data selection and analysis regarding the firing rate and regularity of identified striatal interneurons. ……83

2.3.4 Firing of identified striatal interneurons in relation to cortical oscillatory activity. …….. 84

2.4 IDENTIFICATION AND QUANTIFICATION OF AXONAL BOUTONS OF JUXTACELLULARLY-LABELED INTERNEURONS. ……86

2.4.1 Immunofluorescence labeling and confocal imaging of neurobiotin-filled axonal boutons. .86

2.4.2 Analysis and counting of appositions made by the axons of identified interneurons. …… ..87

2.5 STEREOLOGICAL CELL COUNTS IN THE CAUDATE AND PUTAMEN OF THE RHESUS MONKEY. ……89

2.5.1 Tissue preparation and indirect immunofluorescence. ……..89

2.5.2 Immunoperoxidase labeling of secretagogin-expressing neurons for light microscopy. … . 90

2.5.3 Analysis of stereological cell counts. …… 91

CHAPTER 3: SECRETAGOGIN EXPRESSION IN THE DORSAL STRIATUM OF RODENTS AND RHESUS MACAQUES. ……... 93

3.1 INTRODUCTION. …….. 94

3.2 AIMS. …… 96

3.3 METHODS…… 97

3.4 RESULTS. …… 98

3.4.1 The calcium-binding protein secretagogin is an interneuron-specific molecular marker in rat dorsal striatum. ……98

3.4.2 Secretagogin is expressed by a relatively large interneuron population in the dorsal striatum of rats with a novel spatial distribution. ……..99

3.4.3 A discrete, topographically distinct, striatal interneuron population can be identified by its expression of secretagogin in the dorsal striatum of the rat. …… 102

3.4.4 The number and distribution, but not the broad identity, of secretagogin-expressing interneurons varies dramatically according to rodent species. ……. 104

3.4.5 Secretagogin is expressed in the caudate nucleus and putamen of the rhesus macaque. … 106

3.5 DISCUSSION. …….. 111

3.5.1 Scgn is expressed by a relatively large population of interneurons in the rat dorsal striatum

……112

3.5.2The identity, but not the relative level, of Scgn expression in the dorsal striatum is consistent across multiple species. …… 113

3.5.3 Functional considerations associated with the distributional biases of Scgn-expressing neurons across multiple axes of dorsal striatum. …… . 115

3.5.4 Scgn expression identifies a group of interneurons that are topographically biased towards the ventro-medial aspect of the dorsal striatum. ……117

CHAPTER 4. DIVERSE ELECTROPHYSIOLOGICAL PROPERTIES AND SPATIAL DISTRIBUTIONS OF PARVALBUMIN- EXPRESSING STRIATAL INTERNEURONS OF RATS AND RHESUS MACAQUES ARE IDENTIFIED BY SELECTIVE EXPRESSION OF SECRETAGOGIN. …… 120

4.1 INTRODUCTION. …… 121

4.2 AIMS. …… 124

4.3 METHODS. …… ..125

4.4 RESULTS. …… 126

4.4.1 Rat striatal PV+ interneurons can be subdivided into two populations with different topographic distributions and densities based on the expression of Scgn. …….. 126

4.4.2 A population of unevenly distributed, PV+ interneurons in the caudate and putamen of the monkey can be distinguished by the co-expression of Scgn. …… .. 130

4.4.3 Spontaneous in vivo activity of identified PV+Scgn- and PV+Scgn+ interneurons during cortical SWA and activation states. …… ..133

4.4.4 PV+/Scgn- and PV+/Scgn+ interneurons show phase locking preferences to different cortical network oscillations. …….. ..138

4.4.5 A higher proportion of PV+Scgn– axonal boutons contact SPN cell bodies. ……...140

4.4.6 The axons of PV+/Scgn– and PV+/Scgn+ interneurons are preferentially apposed to different types of spiny projection neurons. …… 143

4.5 DISCUSSION. …… . 144

4.5.1 Topographical distributions of subtypes of PV+ interneurons and their relationship to the distribution of cortical inputs to the dorsal striatum. ……145

4.5.2 The topographical distribution of PV+ subsets is related to heterogenous activity in different striatal regions during behavioral tasks. ……146

4.5.3 The expression of Scgn identifies subsets of heterogeneously distributed PV-expressing interneurons in the Rhesus Macaque caudate/putamen. …….. 148

4.5.4 Molecular heterogeneity within the parvalbumin-expressing striatal population correlates with in vivo differences in firing. …… 149

4.5.5 Different types of PV+ interneurons target striatal projection neurons in a pathway-selective manner. …… 151

CHAPTER 5: MORPHOLOGICAL AND TOPOGRAPHICAL HETEROGENEITY OF CALRETININ-EXPRESSING INTERNEURONS IN THE STRIATUM OF RATS AND RHESUS MACAQUES. ……..……155

5.1 INTRODUCTION. ……156

5.2 AIMS. ……160

5.3 METHODS. …….. 161

5.4 RESULTS. ……... 162

5.4.1 Topographically-discrete populations of CR+ interneurons can be identified by the selective expression of Scgn in the rat dorsal striatum. ……..……162

5.4.2 The selective expression of Scgn is correlated with differences in the somatic diameters of CR+ interneurons. ……164

5.4.3 CR+/Scgn+ interneurons express the transcription factor SP8. …… ..165

5.4.4 A discrete population of CR+/Scgn– interneuron expresses the transcription factor Lhx7

……167

5.4.5 Differences in molecular expression, topographical distribution and somatic size within the dorsal striatal CR+ interneuron population are correlated with previously described differences in the somatodendritic structure of CR+ interneurons. …….171

5.4.6 Spontaneous in vivo activity of identified CR-expressing interneurons during cortical SWA and activation states. …… 173

5.4.7 A discrete population of CR+ interneurons expresses Scgn in the Rhesus Macaque caudate/putamen……175

5.5 DISCUSSION. …… ..179

5.5.1 Secretagogin expressing, small sized CR-expressing interneurons are preferentially distributed in the rat and Rhesus Macaque striatum near the subventricular zone, where they might be generated throughout adulthood. ……. 180

5.5.2 A relatively small population of medium-sized CR+ interneurons does not express Lhx7 or secretagogin in the rat. …….182

5.5.3 Lhx7 expression in the large-sized CR+ interneurons of the rat may link them to the large CR+/ChAT+ expressing interneurons of the primate. …….…… 184

CHAPTER 6: CHARACTERIZATION OF MOLECULARLY DEFINED CLASSES OF INTERNEURON IN THE NUCLEUS ACCUMBENS. …… ..187

6.1 INTRODUCTION. ……188

6.2 AIMS. ……191

6.3 METHODS. …….. 192

6.4 RESULTS. …… 193

6.4.1 Scgn-expressing neurons in the nucleus accumbens do not express any marker of spiny projection neurons or any classical interneuronal marker. …….. 193

6.4.2 Scgn+ interneurons have a heterogeneous distribution within the nucleus accumbens. ….194

6.4.3 ChAT+ interneuron density increases in the medial aspects of the nucleus accumbens. …197

6.4.4 NOS+ interneurons have a similar distribution to ChAT+ interneurons in both the core and shell of the nucleus accumbens. ……... 199

6.4.5 PV+ interneurons are distributed with a decreasing rostro-caudal gradient and a medial bias in the shell but not the core of nucleus accumbens. …… 201

6.4.6 CR+ interneurons are distributed with an increasing rostro-caudal gradient in the nucleus accumbens. …….. 203

6.5 DISCUSSION. …… 205

6.5.1 The ventral striatum differs from the dorsal striatum with respect to the relative proportions of the “classical” interneuronal populations. ……205

6.5.2 The densities of some types of interneuron are greater in the shell than the core. ……..206

6.5.3 Secretagogin is expressed heterogeneously within the nucleus accumbens. ……208

6.5.4 Heterogeneous distribution of ChAT-expressing interneurons matches the uneven nature of dopamine-acetylcholine signaling in the nucleus accumbens. ……. 209

6.5.5 CR+ and PV+ interneuron populations have contrasting distributional biases along the rostro-caudal axis of the ventral striatum. ……210

CHAPTER 7: GENERAL DISCUSSION. ……..213

7.1 SUMMARY. ……..214

7.1.1 A comprehensive look at the numbers and densities of interneurons in the dorsal and ventral striatum. ……215

7.1.2 The value of distribution and regional density as compared to total cell number. ……..…219

7.2 TECHNICAL CONSIDERATIONS. ……..…….221

7.2.1 Secretagogin-expressing neurons in the rat and the mouse: a weakness of chemically based methods of neural identification? ……221

7.2.2 Calibrated immunofluorescence signals: the key to replacing binary based stereological investigations? ……223

7.2.3 The variability associated with the axonal labelling of neurons using the juxtacelluluar technique. ……226

7.3 THEORETICAL CONSIDERATIONS. …….. 228

7.3.1 The definition of a “novel cell type”: a consideration of neural development and maturation

……. . 228

7.4 FUTURE STUDIES. ……..232

7.4.1 The use of genetic mouse models to investigate further heterogeneity within Scgn-expressing striatal interneuron populations. ……. 232

7.4.2 The use of genetic rat models to investigate heterogeneity amongst striatal PV-expressing interneurons. ……233

7.4.3 Correlating differences in molecular expression profiles with the morphological characteristics of PV+ interneurons. ……234

7.4.4 Electron microscopy as a powerful tool for investigating synaptic connectivity within the striatal microcircuit. ……235

7.4.5 In vivo recordings of striatal interneurons in the ventral striatum of the rat. ……..235

7.4.6 Profiling the genetic, electrophysiological and morphological features of single neurons using the Patch-seq technique……...236

7.5 GENERAL CONCLUSIONS. ……..…238

BIBLIOGRAPHY. ……240

LIST OF TABLES

Table 1.1 Absolute numbers of neurons in the dorsal striatum of the Sprague Dawley rat

…….43

Table 1.2 Percentages of protein expression associated with striatal interneurons in the Caudate and Putamen of the Primate. ……..…46

Table 2.1: Numbers of animals used in this study. ……..…… ….64

Table 2.2: Primary antibodies used in this study. …… ….66

LIST OF FIGURES

Figure 1.1 The dorsal division of the basal ganglia: Connectivity of the major nuclei and their main extrinsic inputs. …… 4

Figure 1.2 Intrinsic synaptic connectivity between the neurons of the dorsal striatum. ……...18

Figure 1.3 Approximate cortical input fields across the rostro-caudal extent of the ventral striatum (Adapted from Humphries & Prescott 2010). ……49

Figure 2.1: Coronal planes associated with the use of the stereological cell counts in the dorsal striatum of the rat. ……..69

Figure 2.2: Coronal planes associated with the use of the stereological cell counts in the dorsal striatum of the mouse. ……69

Figure 2.3: Coronal planes associated with the use of the stereological cell counts in the ventral striatum. ……..70

Figure 2.4: Immunohistochemical delineation of the borders in the ventral striatum. ……..72

Figure 2.5: Calculating medio-lateral and dorso-ventral bias in shell (blue) and core (red) of rat nucleus accumbens. ……78

Figure 3.1: The identity of cells expressing Scgn in the dorsal striatum of the rat. ……..99

Figure 3.2: The distribution of Scgn-expressing neurons in the dorsal striatum of the rat. …….101

Figure 3.3: Density and distribution of "Scgn+-only" neurons in the dorsal striatum of the rat

……103

Figure 3.4: The distribution, density and identity of Scgn expression in the dorsal striatum of the mouse. …… ….105

Figure 3.5. The expression of secretagogin in the caudate nucleus and putamen of the rhesus macaque. …… ..……107

Figure 3.6: The distribution, density and topography of Scgn expression in the caudate and putamen of the rhesus macaque. …… .110

Figure 4.1: A large subpopulation of PV-expressing striatal interneurons co-express Scgn in rats, but not mice. ……127

Figure 4.2: PV+/Scgn– and PV+/Scgn+ interneurons have different topographical bias the dorsal striatum of rat. …… 129

Figure 4.3: PV+/Scgn– and PV+/Scgn+ interneurons have different topographical bias the caudate and putamen of the rhesus monkey. …… 132

Figure 4.4: Juxtacellular recording of identified PV+/Scgn– and PV+/Scgn+ striatal interneurons. ……...…134

Figure 4.5: Electrophysiological properties of identified PV+/Scgn– and PV+/Scgn+ interneurons recorded in the dorsal striatum of anaesthetized rats. …….……137

Figure 4.6: PV+/Scgn– and PV+/Scgn+ striatal interneurons have different profiles of phase locking to cortical oscillations. …….....139

Figure 4.7: PV+/Scgn– and PV+/Scgn+ striatal interneurons have different axonal targets. …..142

Figure 5.1: CR+/Scgn+ and CR+/Scgn– interneurons have different topographical bias the dorsal striatum of rat. …… 163

Figure 5.2: CR+/Scgn+ interneurons possess the smallest somatic diameters of all CR+ interneurons, and can be distinguished from CR+/Scgn– interneurons on the basis of their mean somatic diameters. …… ...165

Figure 5.3: CR+/Scgn+ interneurons can also be identified by their expression of SP8, a marker for newly-generated neurons derived from the subventricular zone (SVZ). ……166

Figure 5.4: The selective expression of Lhx7 distinguishes some CR+/Scgn– interneurons and is correlated with differences in mean somatic diameter. …….. 168

Figure 5.5: CR+/Scgn–/Lhx7– and CR+/Scgn–/Lhx7+ interneurons have similar topographical distribution in the dorsal striatum of rat. …… .…170

Figure 5.6: The selective expression of Scgn or Lhx7 identify morphologically distinct “types” of CR-expressing interneurons. …… ..….172

Figure 5.7 Electrophysiological properties of identified CR-expressing striatal interneurons in the rat. …….174

Figure 5.8: CR+/Scgn+ and CR+/Scgn– interneurons have different topographical bias the caudate and putamen of the macaque. ……177

Figure 6.1: Immunofluorescence images of Scgn+, PV+, ChAT+ and NOS+ interneurons in the nucleus accumbens. ……..194

Figure 6.2: Density and distribution of Scgn+ neurons in the core and shell of the NAcc. ….....……196

Figure 6.3: Density and distribution of ChAT+ neurons in the core and shell of the nucleus accumbens……198

Figure 6.4: Density and distribution of NOS+ neurons in the core and shell of the ventral striatum.

…… ……..…200

Figure 6.5: Density and distribution of PV+ neurons in the core and shell of the ventral striatum.

…… ….202

Figure 6.6: Density and distribution of CR+ neurons in the core and shell of the ventral striatum.

…… ..…204

Figure 7.1 Estimated total numbers and mean densities of molecularly-distinct interneuron populations in the dorsal striatum of the rat. 216

Figure 7.2 Estimated total number and mean density of molecularly distinct interneuron populations in the core and the shell of the rat ventral striatum. 217

ABBREVIATIONS

2D	Two dimensional
3D	Three dimensional
AC	Anterior Commissure
ACT	Activation
Ach	Acetylcholine
AMCA	Aminomethylcoumarin acetate
AMPA	α-amino-3-hydroxy-5-methyl-4-isoxazolepropionic acid
BSA	Bovine serum albumin
Ca_v	Voltage-gated Ca^{2+} channel
CB	Calbindin
CBP	Calcium binding protein
ChAT	Choline acetyle transferase
CNS	Central Nervous System
CPu	Caudate/Putamen
CR	Calretinin
CV	Coefficient of variation
CY3	Cyanine 3
CY5	Cyanine 5
DAB	Diaminobenzidine
DAPI	4',6-diamidino-2-phenylindole
DARPP-32	Dopamine- and cAMP-regulated phosphoprotein
Dk	Donkey
DLS	Dorsolateral striatum
DMS	Dorsomedial striatum
Dor	Dorsal
ECoG	Electrocorticogram
EPSP	Excitatory post synaptic potential
FSI	Fast spiking interneuron
GABA	Gamma-aminobutyric acid
GFP	Green fluorescent protein
Gp	Guinea pig
GP	Globus pallidus
GPe	External globus pallidus
GPi	Internal globus pallidus
Gt	Goat

ABBREVIATIONS (CON'T)

HD	Huntington's disease
IPSP	Inhibitory postsynaptic potential
I.P.	Intra-peritoneal
ISI	Inter-spike interval
Lat	Lateral
LBH	Lateral habenula
Lhx7	Lim homeobox 7
Med	Medial
Ms	Mouse
MSN	Medium spiny neuron
NA	Numerical aperture
NAcc	Nucleus Accumbens
NB	Neurobiotin
NMDA	N-Methyl-D-aspartate
NOS	Nitric oxide synthase
OCD	Obsessive compulsive disorder
PB	Phosphate buffer
PBS	Phosphate buffered saline
PD	Parkinson's disease
PLTS	Plateau low-threshold spiking
PPE	Preproenkaphalin
PPN	Pedunculopontine nucleus
PV	Parvalbumin
Rb	Rabbit
RF	Reticular formation
Rt	Rat
R.T.	Room temperature
Scgn	Secretagogin
SC	Superior colliculus
SD	Standard deviation
SEM	Standard error of mean
SNpc	Substantia nigra pars compacta
SNpr	Substantia nigra pars reticulate
SOM	Somatostatin
SP-8	Specificity protein 8

ABBREVIATIONS (CON'T)

SPN	Spiny projection neuron
STN	Subthalamic nucleus
SWA	Slow wave activity
TAN	Tonically active neuron
Ven	Ventral
VTA	Ventral tegmental Area
VP	Ventral pallidum

PREFACE

The following minor components of this D.Phil. Thesis were not performed by the candidate:

- **In Chapter 3**:
  - Rhesus Macaque tissue was obtained from Dr. Yoland Smith's group in Emory University, Atlanta, GA, USA
- **In Chapter 4**:
  - Recordings of 7 of the 24 juxtacellularly-labelled interneurons presented in this Chapter were performed by other members of my host lab. I analyzed, interpreted and wrote-up all data presented in this Chapter.
  - Rhesus Macaque tissue was obtained from Dr. Yoland Smith's group in Emory University, Atlanta, GA, USA
- **In Chapter 5**
  - Recordings of the juxtacellularly-labelled interneurons presented in this Chapter were performed by other members of my host lab. I analyzed, interpreted and wrote-up all data presented in this Chapter.
  - Rhesus Macaque tissue was obtained from Dr. Yoland Smith's group in Emory University, Atlanta, GA, USA
- **In Chapter 6**
  - A fraction (approximately 25%) of the stereological data was collected by an undergraduate student, Mr Thomas Gill. I analyzed, interpreted and wrote-up all data presented in this Chapter.

Research carried out by the DPhil candidate contributed to the following publication, but was not included in this thesis:

Prototypic and arkypallidal neurons in the dopamine-intact external globus pallidus.

Abdi,A.; Mallet,N.; Mohamed,F.Y.; Sharott,A.; Dodson,P.D.; Nakamura,K.C.; Suri,S.; Avery,S. V.; Larvin,J.T.;**Garas,F.N.**; Garas,S.N.; Vinciati,F.; Morin,S.; Bezard,E.; Baufreton,J.; Magill,P.J

J. Neurosci. **35**, 6667-6688 (2015).

Distinct developmental origins manifest in the specialized encoding of movement by adult neurons of the external globus pallidus.

Dodson,P.D.; Larvin,J.T.; Duffell,J.M.;**Garas ,F.N.**; Doig,N.M.; Kessaris,N.; Duguid,I.C.; Bogac z,R.;Butt,S.J.B.; Magill,P.J.

Neuron **86**, 501-513 (2015).

CHAPTER 1.

GENERAL INTRODUCTION

1.1 OVERVIEW OF THE BASAL GANGLIA

1.1.1 A brief account of the functional organization of the basal ganglia

The basal ganglia are a group of subcortical nuclei that participate in a wide range of motor and cognitive processes. They receive substantial inputs from many regions of the cerebral cortex as well as the thalamus, and target the thalamus, midbrain and brainstem (Alexander et la., 1986; Bolam et al., 2000). As such, they are well suited to the integration of a diverse range of sensorimotor information as well as to governing specific, context-dependent responses. Such functionality is not, as previously hypothesized, exclusive to motor processing, as it is now understood that the basal ganglia are involved in complex functions ranging from reward-based learning to the processing of emotionally-guided behaviors. The importance of the basal ganglia in performing these functions is demonstrated by the symptomatic sensorimotor and cognitive deficits associated with neurological diseases affecting these nuclei.

At the functional and anatomical level, the basal ganglia can be broadly segregated into a ventral and a dorsal division. The ventral division is associated with limbic functions and is discussed in more detail in section 1.5. Structurally, it is made up of the nucleus accumbens (NAcc – also simply called the ventral striatum), the ventral pallidum, and the ventral tegmental area (VTA) (Bolam et al. 2000). The dorsal division is mainly associated with sensorimotor functions, and consists of the dorsal striatum (made up of the caudate and the putamen in primates and other animals), globus pallidus pars externa (GPe - in rodents this is known as the globus pallidus), the globus pallidus pars interna (GPi) the subthalamic nucleus (STN) and the substantia nigra (SN). The substantia nigra can be further divided into the substantia nigra pars compacta (SNpc) and the substantia nigra pars reticulata (SNpr). Each of these nuclei carries out specific roles in the basal ganglia. Although the connectivity of these nuclei is the topic of much research and debate, a simplified model is often referenced in which the striatum receives the majority of inputs into the basal ganglia. Many of these inputs are topographically organized, and they predominantly originate from the cerebral cortex and the intralaminar thalamic nuclei. The striatum receives these inputs and sends a representation of this information to the output nuclei

of the basal ganglia, the Gpi and the SNpr via the direct and indirect pathways respectively (Gerfen, 1992; Flaherty & Graybiel, 1993). The STN also receives a direct input from the cortex as part of the so-called hyperdirect pathway, while also receiving input from the GPe as part of the indirect pathway (Aron & Poldrack, 2006). The STN processes these inputs, where its constituent projection neurons will target the basal ganglia's output nuclei. From there, information is sent to the superior colliculus (SC), the reticular formation (RF), the lateral habenula (LBH) and the thalamus, which constitute the major targets of the basal ganglia (Figure 1.1).

1.1.2 The striatum

The striatum is the largest nucleus in the basal ganglia, and acts as a point of convergence for thalamic, cortical (glutamatergic) and midbrain (dopaminergic) inputs (Smith et al., 1994; Kincaid et al., 1998; Bolam et al., 2000). Historically, striatal neurons have been divided into distinct populations on the basis of anatomical, physiological and/or neurochemical properties (Kubota & Kawaguchi, 1993; Kawaguchi et al., 1995). Anatomically, a division exists between spiny projection neurons and aspiny interneurons. GABAergic medium-sized densely-spiny projection neurons (SPNs) make up 90-95% of striatal neurons (Oorschot, 1996), which can be further subdivided into direct pathway neurons, which express the D1 dopamine receptor and project to the basal ganglia output nuclei (i.e. GPi and SNpr), and indirect pathway neurons which express the D2 dopamine receptor and project to the GPe only (Gerfen, 1992; Hersch et al., 1995; Yung et al., 1995; Surmeier et al., 1996).

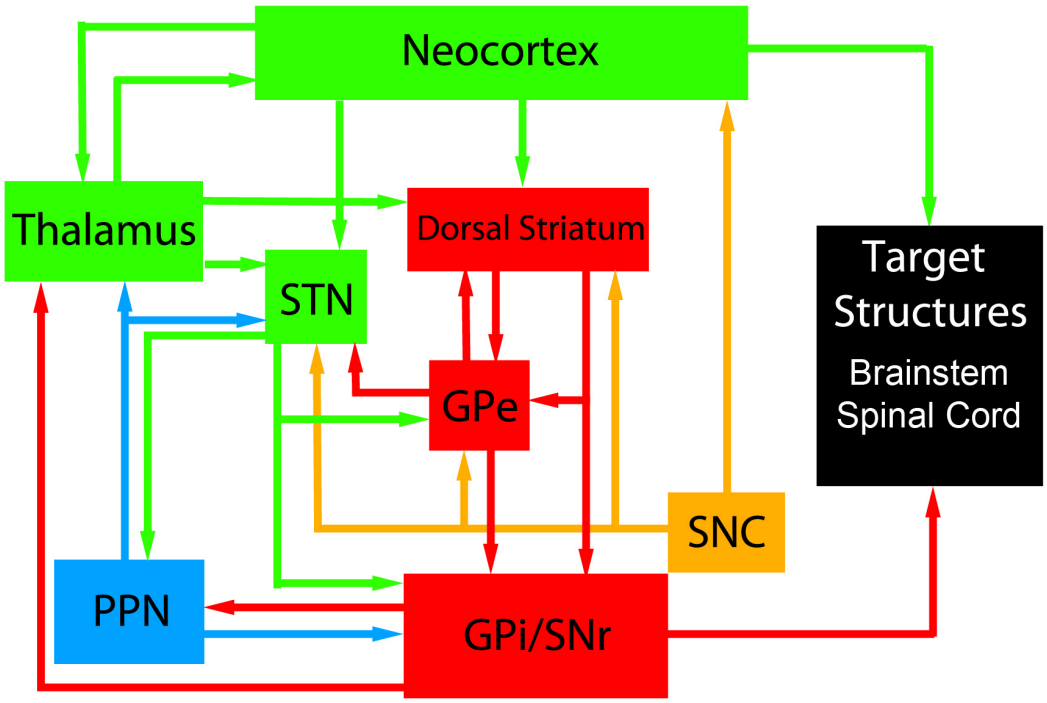


Figure 1.1 The dorsal division of the basal ganglia: Connectivity of the major nuclei and their main extrinsic inputs.
Schematic diagram demonstrating the connections between the nuclei of the basal ganglia and their target structures (Bolam 2009). Inhibitory (GABAergic) nuclei and their projections are shown in red, while excitatory (glutamatergic) nuclei are shown in green. The pedunculopontine nucleus (PPN) is shown in blue as the major source of extrinsic cholinergic input to the basal ganglia (Dautan et al., 2014), while the subtantia nigra pars compacta (SNc) is shown in orange as the major source of dopamine in the basal ganglia. The target structures of the basal ganglia, including the thalamus, midbrain and brainstem are shown in black. Processed information in the dorsal striatum leaves via a projection known as the "direct pathway" that monosynaptically targets output nuclei of the basal ganglia (SNr/GPi) or via the "indirect pathway" projection that reaches the SNr/GPi via the GPe and the STN.
GPi/e – internal/external segment of the globus pallidus. **SNpc/pr** - Substantia Nigra pars compacta/reticulata. **STN –** Subthalamic nucleus. **PPN** – pedunculopontine nucleus.

Aspiny interneurons make up 2-3% of striatal neurons (in adult rats) and can be divided into medium-sized GABAergic cells and large cholinergic neurons (Kawaguchi et al., 1995; Kreitzer 2009). The GABAergic interneurons can be subdivided into three major classes according to their expression of the calcium-binding proteins parvalbumin (PV) or calretinin (CR), or by the co-expression of nitric oxide synthase (NOS), somatostatin and neuropeptide Y (Smith & Parent 1986; Cowan et al., 1990; Chang & Kita 1992; Bennet & Bolam 1993; Bennett

& Bolam 1993). Respectively, these interneuron populations account for about 0.6% (Luk & Sadikot, 2001), 0.5% (Rymar et al., 2004), and 0.8% (West 1996) of striatal neurons in the adult rat. Cholinergic interneurons identified by their expression of choline acetyltransferase (ChAT), account for about 0.4% of rat striatal neurons (Oorschot et al., 1999). Because these 4 cell classes account for 2.6% of all striatal neurons, they are considered the major types of striatal interneurons. Functionally, these interneurons innervate SPN as well as some interneurons, and are therefore believed to be key players in shaping striatal outputs and thence, basal-ganglia-mediated behaviors (Kreitzer, 2009; Tepper & Bolam, 2004; Silberberg & Bolam 2015). It is important to note however that the expression of PV, CR, NOS or ChAT does not fully capture the diversity of striatal interneurons. Indeed, minor cell classes (each accounting for <0.1% of striatal neurons in adult rat) may also be identified according to their expression of tyrosine hydroxylase (Ibáñez-Sandoval, O. et al. 2010; Ünal et al., 2011), the 5HT3a receptor, cholecystokinin (De Deyn et al., 1992), certain subunits of type-A GABA receptors (Caruncho et al., 1996) or vaso-active intestinal peptide (Chang & Tian, 1991). As some of these cell types were discovered in transgenic mouse models, they are discussed in detail later.

At the macroscopic level, the striatum is composed of patches (sometimes called 'striosomes'), which have been shown to express relatively high levels of mu opioid receptors and low levels of acetylcholinesterase (Graybiel & Ragsdale, 1978; Graybiel et al., 1979; Gerfen, 1992). These patch regions are embedded within the striatal matrix, a compartment defined by its enriched expression of calbindin (Gerfen, 1992). Such a division at the macroscopic level is important, as it is maintained at the level of the striatum's output. With respect to its cortical input, the cortical neurons that make up the cortico-striatal pathway which project to the patch compartment are found in deep layer V, while cortico-striatal neurons innervating the matrix compartment are found in superficial layer V and layer III (McGeorge & Faull, 1989). These cortico-striatal neurons, as well as the thalamo-striatal neurons, have been shown to form synapses with both direct and indirect pathway SPNs in the same relative proportions (Doig et al., 2010). Moreover, a single direct or indirect pathway neuron can receive inputs from both cortical

and thalamic projection neurons. Once these inputs are processed within the microcircuitry of the striatum, the compartmental divisions described above are maintained in the striatum's output. SPNs in the patch compartment project to the SNpc, while those of the matrix send their axons to the SNpr and the globus pallidus. As indicated in Figure 1.1, the SNpc provides the major dopaminergic input into the striatum (Moss & Bolam, 2008; Matsuda et al., 2009). Thus, the specificity by which SPNs of patches target the SNpc is of great importance in regulating the activity of SNpc neurons, and hence regulating the processing of reward related activity in the basal ganglia (Fujiyama et al., 2011). Despite the further functional significance of this compartmental divide within the striatum has been unclear until recently (Friedman et al., 2015), it is believed that the specificity of the striatum's afferent and efferent connectivity is a vital aspect of its function as the basal ganglia's central processor.

As a result of its inherent diversity and complexity, the striatum's microcircuity is subject to the action of a variety of extrinsic and intrinsic neuromodulators (intrinsic modulators are covered later). Dopamine is the best studied of these modulators, and it is released by SNpc neurons projecting unto the dorsal striatum, where it modulates the activity of SPNs and certain interneurons. The role of dopamine will be discussed in further detail below. The striatum also receives neuromodulatory inputs from other nuclei, including a serotonergic input from the dorsal raphe nucleus. The high levels of serotonin (5-hydroxytryptamine; 5-HT) receptor expression found in the striatum highlight the importance of this input (Burke et al., 2014; Eskenazi et al., 2015). In this manner, serotonin is likely to modulate the output of the striatum in an indirect manner. Interestingly, the role of serotonin in the basal ganglia is the subject of much research, as it is believed to interact with dopamine at the level of the striatum to produce some of its neuromodulatory effects (Di Giovanni et al., 2008; Navailles & Deurwaerdere, 2011; Navailles et al., 2011). Such complexity is evidenced by the multitude of disorders associated with abnormalities in serotonergic transmission, ranging from obsessive-compulsive disorder (OCD) to depression (Soomro et al., 2008).

The striatum also receives a histaminergic input, originating from projection neurons of the tuberomamillary nucleus in the posterior hypothalamus. In the CNS, histamine has been show to play a role in the regulation of circadian rhythms via its action on H3 receptors (Pollard et al.,, 1993). Interestingly, the striatum possesses the highest level of histamine receptors in the basal ganglia (Kubota et al., 1999). In this manner, histamine is said to act presynaptically, where it can modulate the release of neurotransmitters such as dopamine (Ito et al., 1996), acetylcholine (Prast et al., 1994; 1997), serotonin and glutamate (Pollard et al., 1993). Recently, it has been shown that histamine transmission can decrease the degree of lateral inhibition between SPNs, in addition to its suppression of striatal excitatory inputs (Ellender et al., 2011). Clearly, neuromodulation is an important and complex aspect of striatal function, as these transmitters are capable of influencing the spatio-temporal activity within the microcircuitry of this structure (Silberberg & Bolam 2015). The anatomical and the physiological properties of some of the cells that form this microcircuit represents the major focus of this thesis, and it will be discussed in greater detail below.

1.1.3 The globus pallidus (pars externa)

In rodents, the external part of the globus pallidus is known simply as the globus pallidus, and is located medial to the striatum. In terms of its electrophysiological properties, in vivo recordings in combination with genetic fate mapping have provided evidence to support the idea that two developmentally and physiologically distinct neuronal populations exist within this GABAergic structure (Gardiner & Kita, 1992; Magill et al., 2000; Abdi et al., 2015; Dodson et al., 2015). The first population is composed of prototypic (spiny) neurons that fire antiphase to STN neurons, and express PV (Mallet et al., 2012). These neurons target downstream basal ganglia nuclei such as the STN and the SNpr/GPias part of the indirect pathway of basal ganglia processing. These projection neurons also give off axon collaterals, which produce local inhibition within the GPe (Kita, 1994; Kita & Kitai, 1994; Bevan et al., 1998; Sadek et al., 2007; Mallet et al., 2012). The second, smaller population is composed of “arkypallidal” neurons, which have been shown to fire in-phase with STN neurons, and express preproenkephalin (PPE). These

neurons do not innervate the STN and instead provide the striatum with its largest extrinsic GABAergic input, where they target both interneurons and projection neurons (Mallet et al., 2012; Abdi et al., 2015), allowing them to influence the processing of information within the striatal circuit (Kita, 2007). Similarly to the scenario with projection neurons of striatum, this dichotomy is now believed to be essential to the organization and processing of the GPe.

The GPe receives input from indirect pathway SPNs, while also receiving inputs from collateral axons of direct pathway SPNs as they project to the SNpr/GPi (Bolam et al, 2000; Fujiyama et al., 2011). It also receives a glutamatergic input from the STN, as well as a small dopaminergic input from the SNpc (Kita, 2007). Thanks to its connectivity with many structures of its nuclei, the GPe is well positioned to alter the processing and output of the basal ganglia.

1.1.4 Substantia nigra pars compacta

The substantia nigra pars compacta is a midbrain nucleus whose dopaminergic neurons primarily innervate the dorsal striatum and thus form the nigrostriatal pathway (Bolam et al., 2000). These dopaminergic cells are known as cell group A9, which differ from the neurons of cell group A10 found in the ventral tegmental area (VTA) that predominately project to the ventral striatum and form the mesostriatal pathway (Grenhoff et al., 1988; Morrow et al., 2005). In vivo, dopaminergic neurons of the SNpc are tonically active, and fire at a frequency of 2-8 Hz in the anaesthetized rat (Brown et al., 2009). These neurons can also exhibit a variety of firing patterns, including irregular, pacemaker and bursting activity (Brown et al., 2009). The SNpc is a heterogenous structure, and can be divided into ventral and dorsal "tiers" based on the expression molecular markers. Neurons in the ventral tier can be partly distinguished from those of the dorsal division by the expression of the calcium-binding protein calbindin (Smith & Kieval, 2000). Dopaminergic SNpc neurons expressing calbindin tent to fire slower than SNpc dopamienrgic neurons that do not. (Brown et al., 2009). Importantly, the neurons of the ventral and dorsal tiers of the SNpc have different susceptibilities to degeneration in Parkinson's disease (Yamada et al., 1990). The calbindin-expressing neurons of the ventral SNpc are known to be protected to some

degree from the pathological processes underlying the degeneration of dopaminergic neurons in Parkinson's disease (Yamada et al., 1990). As a result, the differences among these populations are the subject of much attention and research.

The SNpc receives its input from a variety of brain areas found both within and outside of the basal ganglia. From the striatum, it receives a GABAergic input from the projection neurons of the direct pathway, as evidenced by the reported co-localization of substance P and GABA in the presynaptic terminals that form synapses with the tyrosine hydroxylase expressing dopaminergic neurons of the SNpc (Bolam & Smith, 1990). This striatal input originates from direct pathway SPNs that are located within the patch compartment, and they differ from the striatal projection neurons innervating the SNpr (Fujiyama et al. 2011). The GPe and the SNpr also provide the SNpc with GABAergic innervation (Bevan, 1998; Misgeld, 2004).

The principal target of the dopaminergic neurons of the SNpc is the dorsal striatum (Tassin et al., 1976; Bockaert et al., 1976). Individual SNpc neurons have large axonal arborisations that can extend up to 50cm in length, and can simultaneously innervate both the patch and matrix compartments of the striatum (Matsuda et al., 2009), although past reports suggest that they have are more densely organized in patches (Graybiel et al., 1981). Moreover, this innervation is not specific to particular cell types, as all striatal cells within 1um of a TH-positive synapse are subject to dopaminergic transmission, as dopamine acts as a volume transmitter (Moss & Bolam, 2008; Rice & Cragg, 2008). The effect of dopaminergic transmission in the striatum is therefore a product of the level of available dopamine and the type of receptors expressed by striatal cells (Gerfen & Surmeier, 2011). As a result, dopamine is able to influence the activity of small regions of striatum, rather than any one specific group of cells. To a lesser extent, SNpc neurons have also been shown to target the GPe and STN (Hassani et al., 1997; Matsuda et al., 2009).

The dopamine released from SNpc neurons is required for a variety of functions in the brain, including reward-related behavior, movement, cognition, mood, sleep, attention, memory and learning. The importance of dopamine for movement, cognition and mood to some extent, is evidenced by the behavioural deficits concomitant with dopamine loss, such as that occurring in Parkinson's disease (Lotharius & Brundin, 2002). The role of the SNpc with respect to the prediction of reward and the reinforcement of reward-related activity has been the subject of much interest, as it may provide important clues in the understanding of addiction (Berke et al., 2000; Volkow et al., 2004). When primates are asked to perform behavioral tasks, dopaminergic neurons of the SNpc have been shown to exhibit distinctive firing patterns in relation to reward, as well as the cues that predict those rewards (Schultz et al., 1997; Schultz 1997). When a reward is presented without the presence of a cue, or when a cue associated with a reward is presented, dopaminergic SNpc neurons increase their firing rate (Shultz et al., 1997). In contrast, dopamine neurons decrease their firing rate when a predicted reward is omitted, and they show no response when a predicted reward is presented (Shultz et al., 1998). For these reasons, dopamine neurons are said to be the neural substrates of reward processing or the "reward error prediction signal" (Schultz 2010; Parush et al., 2011)

In the striatum, dopamine mediates its effects via the D1-like or D2-like receptors expressed on SPNs and certain interneurons, where it is required for the induction, maintenance and reversal of plasticity (Kreitzer & Malenka, 2005; Calabresi et al., 2007). The D1 family of receptors encompasses the D1 and D5 dopamine receptors, which are G-protein coupled receptors, that activate adenylyl cyclase and thus increase cAMP production, whereas the D2 family of receptors encompasses the D2, D3, and D4 dopamine receptors, which inhibit adenylyl cyclase and cAMP production. These secondary messenger cascades are then used to influence the activity of specific cell types within the striatum, including direct and indirect pathway SPNs (Sesack et al., 1994), as well as cholinergic interneurons (Chuhma et al., 2014). The role of these cascades, and hence dopamine, in modulating cortico-striatal plasticity is a subject of much

research, as it may account for the effect of dopamine in influencing reward-related behaviors (Wickens et al., 1996; Reynolds et al., 2001).

1.1.5 Subthalamic nucleus

The STN represents the only glutamatergic structure in the basal ganglia. Its neurons fire tonically at a rate of approximately 5-15Hz (Bevan et al., 2007). Functionally, it is believed to play an excitatory role in the basal ganglia in which it drives the activity of its targets (Bevan et al., 2007). These include the GPe and the GPi/SNr. The STN receives a glutamatergic input from the motor cortex and the intralaminar thalamic nucleus, as well as a dopaminergic input from the SNpc (Cragg et al., 2004; Janssen et al., 2012) . These inputs act to modify the tonic activity of STN neurons, with the dopaminergic input (or lack thereof) being of particular interest in the context of Parkinson's disease (Batens et al., 2015; Galvan et al., 2015). Importantly, the activity of STN neurons is tightly regulated via its reciprocal network with the GPe (Shink et al., 1996; Bevan et al., 2007). This network is of great importance, as it is thought to play the role of the pacemaker within the basal ganglia, abnormalities in which underlie various aspects of neurological dysfunction (Plenz & Kitai, 1999). For example, the functional ablation of this nucleus in 'deep brain stimulation' to treat patients with Parkinson's disease results in a paradoxical improvement of motor deficits. With respect to its function, recent reports have provided evidence to suggest that the subthamlamic nucleus and its hyperdirect pathway acts as a "brake" of ongoing behavior (Schmidt et al., 2013).

1.1.6 The output nuclei of the basal ganglia

The SNpr and the GPi (known as the entopeduncular nucleus in rodents) produce the output of the basal ganglia, and these nuclei therefore represent the last stage of basal ganglia processing (Parent & Hazrati, 1995i; 1995ii). The SNpr/Gpi receive the following major inputs from within the basal ganglia: The first input originates from the striatum as part of the direct pathway (Smith et al., 1998; Bolam, 2000). Due to the larger size of the striatum in comparison to that of the SNpr/Gpi, it is believed that these inputs converge extensively within the SNpr/GPi (Smith et al., 1998). The second of these inputs is glutamatergic, and originates from the STN,

while a third, GABAergic input, originates from the GPe (Smith et al., 1998; Deniau et al., 2007). In this manner, the output nuclei are able to receive processed information from both the direct and the indirect pathway.

With respect to their output, the GABAergic neurons of the SNr and GPi project to specific thalamic nuclei, and other subcortical structures such as the superior colliculus and the pedunculopontine nucleus (PPN) (Hauber, 1998). Within the thalamus, the SNr/GPi target the ventromedial-ventrolateral complex, which has a diffuse cortical projection. The intralaminar thalamic nucleus, which projects to the striatum, is also innervated by the SNr/Gpi (Hauber et al., 1998). The targets of the SNr/GPi are normally under a constant state of inhibition due to the tonic activity of these GABAergic output neurons (Hikosaka et al., 2007). This tonic activity has been demonstrated in both in-vivo and in-vitro preparations (Hikosaka et al., 2007). Clearly, the output of the basal ganglia during activity is not one of excitation, but rather one of disinhibition, as discussed below.

The projection from the SNr/Gpi to the superior colliculus (SC) has been the subject of much research due to the relatively simple relationship between the activity of this nucleus and that of the occulomoter system. Indeed, it has been demonstrated in primates that during the preparation of a saccade movement, SNr neurons show a transient decrease in firing rate that results in a disinhibition of topographically-specific sets of SC neurons (Hikosaka et al., 2007). The increased activity of SC neurons ultimately results in a saccadic movement that matches the topographic position of the disinhibited neurons. Ultimately, such an example helps to illustrate the direct effect of basal ganglia processing on influencing context-dependent sensorimotor behavior. Although this represents a rather oversimplified account of the basal ganglia's role in the selection of motor actions, it is currently believed that a similar model may also apply to the processing of complex motor patterns and even high level cognition (Alexander et al., 1990; Middleton & Strick, 2000).

1.1.7 Summary

From lampreys to rodents and primates, the organization of the basal ganglia is conserved, with many of the prototypic cellular and neurochemical features being found in all species. For example, the downstream processing of information through the basal ganglia of the lamprey is also divided into a direct and indirect pathway (Stephenson-Jones et al., 2011). In song birds, the basal ganglia is known to be required for vocal experimentation, a trial and error process requiring sensorimotor processing in which learning is essential (Olveczky et al., 2005; Goldberg & Fee, 2012). The conservation of this basic organization in vertebrates indicates that the basal ganglia are involved in the processing of information essential to survival. These include the selection of motor patterns in the presence of a multitude of competing sensory inputs and competing motor systems (Grillner et al., 2005; Stephenson-Jones et al., 2011).

An often-debated feature of basal ganglia processing is the existence of parallel circuits, each of which is anatomically and functionally distinct (Alexander et al., 1990). In one view, the inputs to the basal ganglia, the microcircuitry of each individual nucleus as well as the organization of the output structures are incorporated in order to account for the division of the basal ganglia into at least five separate functional circuits; motor, oculomotor, dorsolateral, lateral orbitofrontal and anterior cingulate in the non-human primate (Alexander et al., 1986; Alexander et al., 1990). By dividing the downstream processing of information within the basal ganglia into parallel circuits, this hypothesis is able to explain the wide range of behaviors associated with healthy basal ganglia activity. From its inception, this theory has been opposed by a variety of anatomical studies, especially those performed on primates (Percheron & Filion, 1991), and more recently Bergman's group, which argue for the existence of converging pathways as information progresses through the basal ganglia's downstream nuclei (Adler et al., 2013).

In terms of function, the basal ganglia's role in the generation of context-dependent behaviors was originally thought to be best illustrated by the clinical manifestations of

neurological disorders affecting the basal ganglia (Delong, 1990; Delong, 2000). These symptoms can vary from the motor impairments found in patients with Parkinson's and Huntington's disease to the cognitive impairments seen in obsessive-compulsive disorders (OCD). The study of these disorders has proven important for the proposal of functional models of basal ganglia organization (Albin et al., 1989). However, given that these disorders produce large changes to the overall activity of the basal ganglia, they often provide a skewed view of normal basal ganglia function. For example, the motor impairments in PD give the impression that the BG are heavily involved in the control of motor activity, but recent studies have provided an ever growing amount of evidence to suggest that the BG (and the striatum) is particularly involved in the phases of procedural learning and decision making (Smith & Graybiel 2014; Friedman et al., 2015). Thus, in order to understand the underlying abnormalities associated with these basal ganglia disorders, examinations of these nuclei in health are of great importance. Indeed, most therapeutic advances for Parkinson's disease in the past decade have been the product of results obtained from the research of basic scientific principles.

1.2 DORSAL STRIATAL MICROCIRCUITRY

1.2.1 Spiny projection neurons

Spiny projections neurons (SPNs; also referred to as "medium spiny neurons") are the main unit of computation within the striatum, and they account for approximately 95% of its total cell population in the adult rat (Oorschot, 1996). Their name describes their size, as well as the fact that their higher-order dendrites are densely laden with spines (Chronister et al., 1976; Wilson et al., 1983). As projection neurons, these GABAergic cells are responsible for assimilating and subsequently transmitting the information carried by neurons innervating the striatum. SPNs are dichotomous in their organization within the striatum, giving rise to the concept of the direct and indirect pathways of information flow through the basal ganglia. Direct pathway SPNs innervate the SNpr and the Gpi (Somogyi & Smith, 1979; Somogyi et al., 1981). They can be histochemically identified by their expression of the D1 dopamine receptor and the neuropeptides substance P and dynorphin (Gerfen et al., 1990; Yung et al., 1995). Indirect pathway SPNs on the other hand project to the GPe to form the striatopallidal pathway (Kawaguchi 1990), and expression of D2 dopamine receptors and the neuropeptide enkephalin (Gerfen et al., 1990; Yung et al., 1995).

This dichotomy of striatal output is a fundamental tenant of the "Albin-Delong model" of basal ganglia organization and it remains to this day an important foundation by which the function of the basal ganglia in both health and disease is understood. In the simplest terms, the direct and indirect pathways are balanced to produce a healthy output, while hypo- and hyperkinetic disorders are the result of imbalances within the activity of these outputs (Delong 1990). Patients with hypokinetic disorders such as Parkinson's disease present with bradykinesia (or akinesia) and rigidity. These changes can in theory be explained by an increased inhibition of the basal ganglia's targets (especially those in the motor thalamus). This increased inhibition is the result of increases in the activity of the indirect pathway and decreases in the activity of the direct pathway. This ultimately results in the inhibition of the GPe (Albin et al., 1989) and an

increase in the excitatory activity of the STN, resulting in a disinhibition of the basal ganglia output nuclei. This will lead to an increase in the degree to which the motor output of the CNS is inhibited (Albin et al., 1989). Hyperkinesia, as demonstrated by patients suffering from ballisms, presents with an inability to suppress the movement of distal, and in some cases proximal, joints. These disorders can also be explained by the dichotomous nature of striatal output. In these cases, an increase in the activity of the direct pathway (or conversely decrease in the activity of the indirect pathway) results in a decrease in the activity of the basal ganglia output nuclei (Delong 1990). This ultimately results in a disinhibition of the motor thalamus as well as other basal ganglia targets, leading to hyperactive behaviour.

1.2.1.1 Anatomical properties

As discussed above, striatal dichotomy is a fundamental feature of basal ganglia organization that can be used to understand a variety of disorders. However, anatomical studies have uncovered that the division of striatal output into two pathways with specific targets is not a perfect one (Kawaguchi et al., 1990; Parent et al., 1995; Wu et al., 2000). For example, the axon terminals of both direct and indirect pathway SPNs are found in the GPe (Kawaguchi et al., 1990; Wu et al., 2000). The terminals of direct pathway SPNs found in the GPe are believed to be axon collaterals, but their arborization within the GPe is much smaller than the arborization in the output nuclei (Kawaguchi et al., 1990; Wu et al., 2000). Thus, direct pathway neurons are divided into two groups. The first consists of SPNs that have a focused arborization in the SNr, while sending a smaller set axon collaterals to the GPe. The second group is composed of SPNs that arborize in both the GPe and the GPi/EP, while sending a projection with a much greater arborization within the SNr (Wu et al., 2000). Indirect pathway SPNs on the other hand project to the GPe and their axons arborize to a greater extent in GPe than those the direct pathway SPNs that terminate in this nucleus (Bolam et al., 2000). Ultimately, the results of these investigations illustrate that both the indirect and direct pathway SPNs are able to influence the activity of the GPe and the output nuclei to different degree. In this manner, the striatum is able to control the

activity of its targets to a greater extent than that proposed by a pure dichotomous division of striatal outputs (Bolam et al., 2000).

Before the axons of SPNs exit the striatum, they often give off collaterals that provide a local inhibitory innervation of other SPNs (Wilson & Groves 1980). This connectivity, as well as other intrastriatal connections are summarized in Figure 1.2. As shown in Figure 1.2, neurons of the direct pathway contact neurons of the indirect (Wilson & Groves, 1980; Somogyi et al., 1981) and direct pathway (Difiglia et al., 1982; Pickel et al., 1992). Moreover, neurons of the indirect pathway form synapses with direct and indirect pathway neurons (Aronin et al., 1986; Yung, 1996). In all cases, these synapses are formed onto the dendritic shafts and spine necks of efferent SPNs (Wilson, 2007). In vitro, the connections of direct pathway SPNs and those of indirect pathway SPNs did not have significantly different amplitudes (Planert et al., 2010). This high degree of interconnectivity within the striatum therefore ensures that these two populations are capable of functionally influencing each other's outputs. Importantly, in vitro recordings have demonstrated that the strength of the IPSCs at these synapses is relatively weak; meaning that activity at a single synapse is of little consequence to the striatum's overall output (Jaeger et al., 1994). However, given that each individual spiny neuron receives many inputs from surrounding projection neurons, it is likely that the activity of spiny neurons is influenced by the activation of its neighboring projection neurons (Yung & Bolam 2000). Moreover, it has been previously shown that although the effect of SPN collateral input unto neighboring SPNs is weak when measured at the soma compared to those of fast spiking interneurons (Planert et al., 2010; Koos & Tepper, 1999), the release probability and the quantal size of release was similar for both types of synapses (Koos et al., 2004). Thus, it is likely that the focal activation of SPNs can result in a powerful inhibition of surrounding SPNs.

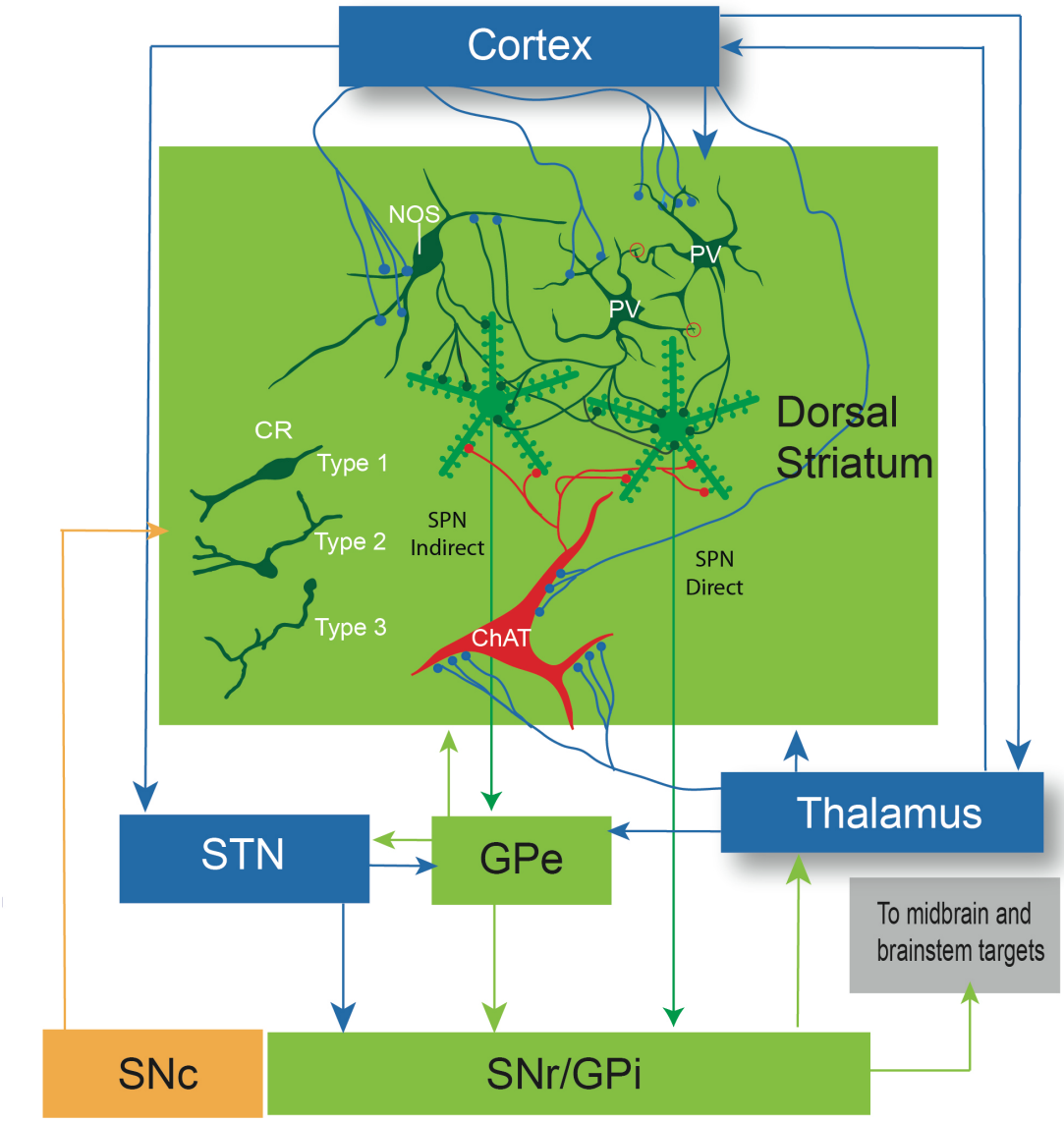


Figure 1.2 Intrinsic synaptic connectivity between the neurons of the dorsal striatum.
Schematic diagram illustrating the known connections (either physiologically or anatomically) between the neurons within the striatum. Excitatory (glutamatergic) input into the striatum from the thalamus and the cortex targets parvalbumin (PV)-, nitric oxide synthase (NOS)- and choline acetyl transferase (ChAT)-expressing interneurons. These inputs also target spiny projection neurons - SPNs (not shown for the sake of simplicity). Inhibitory (GABAergic) spiny projection neurons (light green) project to the SNr/GPi as part of the direct pathway or to the GPe as part of the indirect pathway. Within the dorsal striatum, inhibitory (GABAergic) interneurons expressing PV or NOS inhibit the activity of SPNs. The connections of the three morphologically distinct types of calretinin (CR)-expressing interneurons are not known. Cholinergic, ChAT-expressing interneurons (shown in red) also contact SPNs directly. **GPi/e** – internal/external segment of the globus pallidus. **SNc/r** - Subtantia Nigra pars compacta/reticulate. **STN** – Subthalamic nucleus

1.2.1.2 **Pharmacological properties**

Direct pathway SPNs release substance P, a neuropeptide that mediates its effect through the binding of the G-protein coupled neurokinin receptor (NK1). Functionally, the release of substance P in the striatum has been shown to have an excitatory effect on SPNs which also facilitates the effect of glutamatergic inputs to target SPNs (Blomeley & Bracci, 2008; Blomeley et al., 2009). Besides the transmission via GABA, SPNs of both the direct and indirect pathways release opioids, which have been shown to have an overall inhibitory effect in the striatum. Direct pathway SPNs release dynorphin and indirect pathway SPNs release enkephalin. The release of either of these opioids also functions to inhibit glutamatergic inputs unto neighboring SPNs (Jiang & North, 1992; Blomeley & Bracci, 2011). Clearly, SPNs can no longer be thought of as purely GABAergic cells. Indeed, their release of (excitatory) neuropeptides and (inhibitory) opioids further illustrates that striatal SPNs are not simply responsible for the reception and transmission of cortical/thalamic information, but are also heavily involved in its processing.

1.2.1.3 Electrophysiological properties

Although striatal SPNs are often described as existing in two separate groups with respect to their anatomical projections and molecular expression profiles, it is believed that these cells share many electrophysiological properties. Typically, SPNs have a low basal firing rate (0.1-5 Hz) in vivo, and display tonic or phasic activity depending on the cortical brain state and the animal's behaviour. Importantly, SPNs can also remain completely silent, making them difficult to record in vivo without the use of cortical stimulation (Wilson & Groves, 1981). The intrinsic electrophysiological properties of these neurons include a resting membrane potential of approximately -70 to -80 mV, a low input resistance and a strong, inward rectification when hyperpolarized (Kita et al., 1984; Kawaguchi et al., 1989). Both the resting membrane potential and the strong inward rectification are caused by the activation of an inwardly-rectifying potassium channel (Kir) (Nisenbaum & Wilson, 1995). One of the fundamentally unique features of SPN electrophysiology is their ability to periodically shift between two differing membrane states. These consists of a hyperpolarized 'Down state' (-90 to -70mV) and a more depolarized

'Up state' (-60 to -40mV) where the SPN can fire action potentials (Wilson & Kawaguchi, 1996). Typically, SPNs are in the 'down state' until they receives enough glutamatergic excitation (Blackwell et al., 2003). Once in the 'up state', an SPN can maintain its depolarized membrane potential as long as its excitatory drive is present. Importantly, this state transition is regulated by voltage-sensitive potassium conductances that are activated in response to depolarization of the membrane, where they act to limit the amount of synaptically driven depolarization (Wilson & Kawaguchi 1996). Up state transitions also influence an SPN's synaptic conductances by activating NMDA receptors as well as low-voltage gated L-type calcium channels (Carter & Sabatini 2004). This activation is an essential step for the induction of striatal long-term depression (Choi & Lovinger 1997, Kreitzer & Malenka 2005). Currently, it is believed that the shift to the 'Up state' represents an enabling event that allows for the processing of information through the downstream nuclei of the basal ganglia (Kasanetz et al., 2002). However, the cause, origin as well as the function of these transitions in SPNs has yet to be entirely established.

In urethane-anaesthetized rats, SPN state transitions are directly related to the activity of the cortical electro-encephalogram (EEG). This therefore implies that the cortex plays a central role in altering the state of SPNs, and hence their ability to transmit information throughout the basal ganglia (Mahon et al., 2001; Kasanetz et al., 2002). This relationship is further demonstrated by the fact that decortication abolishes transitions between up and down states in striatal SPNs (Wilson, 1993). Within the striatum, SPNs do not undergo these transitions alone, as striatal state transitions can often be correlated amongst groups of SPNs. Although the functions of these transitions are poorly understood, these results ultimately suggest that cortical input acts to produce synchronized activity within the striatum by influencing specific groups of neurons (Stern et al., 1998). Moreover, the transmission of local (eg. opioids) as well as extrinsic (eg. Dopamine) neuromodulators within the striatum is believed to influence the temporal and spatial properties of these state transitions. Importantly, these state transitions are far more prominent and clear in anaesthetized preparations (as well as slow-wave sleep). During wakefulness, SPNs display a greater range of spontaneous patterns of dynamic activities (Mahon et al., 2006)

meaning that the data provided by anaesthetized models may represent an oversimplification of striatal activity.

1.2.1.4 Summary

In the striatum, the spiny projection neurons act as receivers, integrators and transmitters of much of the extrinsic information that enters the basal ganglia. Two distinct sub-populations of SPNs, identified by their anatomical and molecular differences, carry out this complex information processing. Importantly, the processing of information within the striatum is heavily influenced by the activity of its diverse interneuron populations, the functions (and indeed identities) of which have yet to be fully understood. Ultimately, it is the combined activity of these heterogeneous populations that shape the content of the striatum's, and hence the basal ganglia's, output.

1.2.2 Parvalbumin-expressing fast-spiking interneurons

1.2.2.1 Anatomical properties

Striatal neurons expressing parvalbumin (PV+) are medium-sized, aspiny cells first described by Gerfen et al., (1985). These interneurons also express high levels of GAD67 while displaying high levels of ^{3}H-GABA uptake, and are therefore GABAergic (Gerfen et al., 1985; Lenz et al., 1994). As with other aspiny GABAergic interneurons, the nuclear envelope of these neurons is invaginated (Kita et al., 1990). Importantly, PV-expressing interneurons are also identified molecularly by their expression of the shaw-like potassium channel Kv3.1 (Lenz et al., 1994). Within the striatum, they can be found in both the matrix and patch compartments of the striatum. These interneurons are often described as one homogenous population (Kita et al., 1990; Kawaguchi, 1993), although intracellular labeling studies have described a second, larger interneuron whose axonal and dendritic fields arborize to a greater extent (Kawaguchi 1993). Parvalbumin-expressing interneurons heterogeneously distributed within striatum, with greater cell densities being reported in the dorsal, lateral and rostral aspects (Mura et al., 2000; Wu and Parent, 2000; Ma et al., 2014).

The dendritic fields of these medium-sized neurons are spherical, extending 200-300 μm around the parent somata (Kawaguchi, 1993). Parvalbumin-expressing neurons typically emit five to eight aspiny dendrites that can be both smooth and varicose, with branch points first occurring within 10μm of the soma (Cowan et al., 1990; Kita, 1993). Beyond this however, branch points occur infrequently with 5th order dendrites (or greater) being rare. The size and complexity of these dendrites is of great importance when considering how PV+ interneurons fit into the striatal microcircuit, in part because they form dendro-dendritic gap junctions with other PV+ dendrites (Kita et al., 1990; Kita, 1993). The axonal arborizations of PV+ interneurons are very dense (branching profusely) and are approximately double the size of the dendritic field diameter (Koós and Tepper, 1999; Tepper and Bolam, 2004).

1.2.2.2 Electrophysiological properties

With respect to their electrophysiology, parvalbumin-expressing striatal interneurons have been recorded in vitro using juvenile and mature rats/mice (Kawaguchi, 1993; Kawaguchi et al., 1995; Centonze et al., 2003). The results from these investigations have consistently classified these neurons as "fast-spiking" interneurons (FSI), so named because they can fire at frequencies over 400 Hz with little spike frequency adaptation when injected with strong depolarizing currents. These interneurons are hyperpolarized in vitro (-90mV), with a low input resistance and little inward rectification. As with PV+ FSIs in cortex and hippocampus, striatal PV+ interneurons are not spontaneously active in vitro, and depolarizing current injections produce action potentials that are short in duration (<0.5 ms) and exhibit deep, after-hyperpolarizations with a rapid onset (Freund and Buzsáki, 1996; Galarreta and Hestrin, 1999, 2001, 2002; Tepper et al., 2010). These properties are the result of PV+ interneurons expressing Kv 3.1 voltage-gated K+ channels, which are high-threshold, rapidly activating and slowly inactivating (Lenz et al., 1994; Rudy and McBain, 2001).

Unlike other FSIs, striatal PV+ interneurons are unusual in that they cannot fire repetitively at low frequencies (Tepper et al., 2010). Indeed, as the amplitude of the injection current increases towards the neuron's depolarization threshold (approximately -50mV), a single

delayed spike is recorded. However, as the increments of injected current continue to increase, the neuron's firing rate does not continue to increase (Bracci et al., 2003; Koos & Tepper 1999). Once the strength of the injected stimulus current reaches a level slightly beyond the neuron's firing threshold, it begins to fire at its minimal sustainable frequency (approximately 20 Hz). The in vitro response of a neuron to injected current is an important electrophysiological criterion that defines 2 categories of FSIs. One type of FSI fires continuously in response to current injection, with spikes being maintained for the duration of the current injection (except when the current's amplitude is too great, whereby the action potential is terminated earlier). The second type of FSI is characterized by "stuttering" responses where bursts of action potentials are separated by silence, during which sub-threshold oscillations of the membrane potential are observed (Kawaguchi, 1993; Bracci et al., 2003). Whether or not these differences reflect separate states of the same cell type or reflect two distinct FSI populations still remains unclear. Importantly, both of these responses have been described in the dorsal striatum of both rats (Bracci et al., 2002; Plotkin et al., 2005) and mice (Centonze et al., 2003; Gittis et al., 2010). In one study, BAC-PV-EGFP transgenic mice were used to target PV interneurons for current injections, and only the continuous firing pattern was observed in EGFP-expressing neostriatal FSIs (Freiman et al., 2006). In contrast, stuttering responses have been observed in neurons expressing PV as determined using immunohistochemistry (Kawaguchi, 1993). An explanation for these findings is currently unclear, as it may be the effect of species and cell type-specific differences or may be the result of different in vitro preparations producing variable recording environments.

Another electrophysiological property of FSIs is the presence of 2-3 mV membrane oscillations at depolarized membrane potentials below threshold, a feature that is prominent in stuttering neurons during the silences between bursts of activity (Koós and Tepper, 1999; Bracci et al., 2003). These oscillations are believed to be due to the interaction between voltage-dependent potassium currents and the inactivating sodium conductance responsible for spike generation (Bracci et al., 2003). Of the cell types in the striatum, PV+ interneurons are unique in that they are functionally interconnected with one another by "electrical synapses" i.e. gap

junctions (Koós and Tepper, 1999). The coupling ratio allowed by these gap junctions is not large enough to evoke spiking in neighboring cells, but it allows electrotonically coupled FSIs to fire synchronously with one another (Tepper et al., 2010). Interestingly, the role of this synchronous firing is not clear, as in vivo recordings from striatal FSIs (identified on the basis of firing properties) have shown that their activity is uncoordinated during the presentation of cues and rewards (Berke, 2008).

In vivo recordings in the urethane-anaesthetized rat have provided evidence for the firing of identified PV+ interneurons during different cortical states (Sharott et al., 2012). During cortical slow wave activity (SWA), striatal FSI activity is variable, with some neurons firing a single spike every 30-60 seconds while others demonstrated bursts of high frequency activity during the active component of the cortical slow oscillation (Mallet et al., 2005; Sharott et al., 2012). These variances in firing were not related with the power of cortical slow oscillations (0.4 – 1.6 Hz). During the spontaneously activated brain state, all PV+ interneurons fire at greater frequencies, with the firing being much more regular. In response to somatosensory stimuli (eg. paw pinch), PV+ interneurons are observed to increase their firing rate in a sustained manner (Sharott et al., 2012).

1.2.2.3 Connectivity

Although the somata of PV+ interneurons revived few inputs, the dendrites of PV+ neurons are in synaptic contact with a host of axon terminals. Two thirds of PV+ interneuron afferents form asymmetric (Gray's type I) synapses, most of which are of cortical origin, with some synapses originating from the thalamus (Kita et al., 1990; Kita, 1993). A single cortical axon can makes multiple contacts with a single PV+ interneuron, and this is believed to partly account for the heightened responsivity of these interneurons to cortical stimulation (Parthasarathy & Graybiel, 1997; Ramanathan et al., 2002). The remaining synaptic inputs are symmetric (Gray's type II), arising from both extrinsic and intrinsic GABAergic inputs and extrinsic dopaminergic inputs (Kubota et al., 1987; Bevan et al., 1998). Importantly, one type of

GABAergic GPe neuron selectively targets striatal PV+ interneurons (Bevan et al. 1998), as suggested by the increased firing of FSIs coinciding with a decrease in the firing of GPe neurons during choice selection (Gage et al., 2010). Boutons immunoreactive for choline acetyltransferase also make synaptic contact with PV+ interneurons, and in vitro stimulation of non-desensitizing nicotinic receptors excites PV+ interneurons (Chang & Kita, 1992; Koos & Tepper, 2002).

Striatal PV+ interneurons make efferent connections with different cell types within the striatum. Action potentials fired by these interneurons produce large amplitude IPSPs in both direct and indirect SPNs in cell culture (Plenz and Kitai, 1998). Fast-spiking interneurons in the striatum have been shown to form synapses unto the somata and proximal dendrites of SPNs, and have a failure rate of less than 1%, as evidenced by paired recordings (Kita et al., 1990). Within the radius of an FSI's axonal field, the probability of a synaptic connection between an FSI and an SPN is relatively high, ranging between 25% and 75% (Koos & Tepper, 1999; Gittis et al., 2010; Planert et al., 2010). Such numbers contrast heavily with the connection probability between SPNs, which is reported as 10-20% (Czubayko & Plenz 2002; Taverna et al., 2004). Unlike the rather weak and distal synapses between striatal SPNs, activity at FSI-SPN synapses is powerful enough to delay or even block spiking in postsynaptic SPNs (Wilson & Groves, 1980; Koos & Tepper, 1999). As such, striatal PV+ neurons are believed to produce a powerful feed-forward inhibition that regulates striatal output by modifying spike timing in SPNs. FSIs also make reciprocal synaptic connections with other FSIs, and have recently been shown to have sparse connectivity with low-threshold spike (LTS) interneurons while cholinergic interneurons do not receive any synaptic inputs from fast-spiking striatal neurons (Szydlowski et al., 2013).

1.2.2.4 Pharmacological properties

Due to the powerful influence of PV+ interneurons in the striatum, their pharmacological properties are the subject of much research. The application of dopamine, as well as D1/D5 receptor agonists has been shown to depolarize and increase the input resistance of striatal FSI; an effect that is prevented by the application of selective D1/D5 receptor antagonists (Bracci et al.,

2002). The intracellular mechanisms responsible for these effects are not fully understood, although the use of D1 knockout mice has established that they are D5 receptor-dependent (Centonze et al., 2003). In contrast, D2 receptor agonists inhibit the firing of FSIs, while antagonists of the D2 receptor cause an increase in firing rate (Wiltschko et al., 2010). Interestingly, striatal FSIs do not express D2 receptors, and this effect is believed to be mediated by the modulation of presynaptic GABAergic inputs which may be intrinsic or extrinsic (GPe). Amphetamines have also been shown to increase the firing of FSIs in vivo. Acetylcholine (Ach) has been shown to depolarize and induce the firing of striatal FSIs (Tepper et al., 2010). This response is reproduced by bath application of the nicotinic-receptor agonist carbachol. In addition to this proposed nicotinic receptor activation, ACh may also be involved in inhibiting activity at FSI-SPN synapses, an effect that is removed by the application of pirenzapine (Koos & Tepper, 2002). Functionally, this effect may become more pronounced during periods of cortical activation, where ACh levels and the firing rates of FSIs are increased (Mallet et al., 2005; Sharott et al., 2012).

1.2.3 NOS/NPY/SOM-expressing interneurons

1.2.3.1 Molecular characterization and morphological properties

In the rat, striatal interneurons that are immunoreactive for NOS also express the enzyme NADPH diaphorase (the equivalent of nitric oxide synthase (NOS)), neuropeptide Y (NPY) and somatostatin (SOM), but not ChAT or PV (Vincent & Johansson, 1983; Hope et al., 1991). When treated with colchicine to inhibit axonal transport, NOS-expressing interneurons are immunoreactive for GAD-67, a finding that indicates that they are GABAergic (Kubota & Kawaguchi, 2000). Originally, SOM/NOS/NPY expressing interneurons were believed to represent a single population of neurons, but cell counting studies in rats have shown that the number of NPY+ and SOM+ neurons in the striatum do not match (Oorschot, 2013). Moreover, nearly 25% of interneurons that express either NOS, SOM or NADPH diaphorase did not express NPY, thereby indicating that at least three distinct subpopulations of striatal interneurons expressing a combination of SOM, NOS, or NPY (see later) may exist (Figueredo-Cardenas et al., 1996). Such findings are relevant, as they call into question whether the electrophysiological properties of these neurons discussed later apply to all of these cells, or only to certain subpopulations.

In terms of their morphological properties, SOM/NOS/NPY-expressing interneurons are medium-sized, and emit 3-5 aspiny, thick and non-varicose proximal dendrites that branch sparsely. The dendritic fields of these neurons extend to a diameter of 600μm, with dendrites becoming more varicose the further they are from the soma (Difiglia & Aronin, 1982; Aoki & Pickel, 1988; Kawaguchi, 1993). The axonal arborization of SOM/NPY/NOS+ interneurons are sparce, but as compared to other striatal interneurons, it is the largest in overall span and can extend up to 1 mm from the parent somata (Kawaguchi, 1993; Kubota & Kawaguchi, 2000).

1.2.3.2 Electrophysiological properties

The key electrophysiological characteristics of NOS/NPY/SOM+ interneurons that distinguish from other striatal cells is the presence of low threshold Ca^{2+} spikes (LTS), a high input resistance (>600 MΩ), a relatively depolarized resting membrane potential (-55mV), a relatively long-duration action potential as well as the presence of long-lasting plateau potentials upon depolarization of the cell from rest (Kawaguchi, 1993). This plateau is believed to occur in rebound from strong hyperpolarization currents that are present after depolarization, or in response to strong excitatory synaptic inputs (Kawaguchi, 1993). These properties of NOS/NPY/SOM+ interneurons have been replicated in both rats and mice (Kubota & Kawaguchi, 2000; Centonze et al., 2002, 2003; Ibanez-Sandoval et al., 2010). Recently, in vivo recordings of these interneurons in rats have provided evidence for their activity in both activated and cortical slow wave activity. Importantly, NOS+ cells were shown to be autonomously active in the anaesthetized rat (Sharott et al., 2012). During SWA, NOS+ interneurons fire bursts of action potentials in time with the active component of the cortical slow oscillation (Sharott et al., 2012). These bursts normally contained 3-5 spikes of decreasing amplitudes with short ISIs. During spontaneous cortical activation, NOS+ interneurons were shown to fire single action potentials at frequencies much lower than those that occur during the active component of the cortical slow oscillation (Sharott et al., 2012).

1.2.3.3 Connectivity

Striatal NOS/SOM/NPY+ interneurons receive synaptic contacts from cholinergic and dopaminergic axons on their proximal dendrites, and glutamatergic asymmetric synaptic inputs from the cortex on their distal dendrites (Kubota et al., 1988). The cortical inputs have been examined electrophysiologically using BAC-NPY-GFP transgenic mice. These studies have shown that AMPA and NMDA receptor activity is relatively weak in response to cortical input (Partridge et al., 2009; Gittis et al., 2010). Data from juxtacellular labeling studies has shown that NOS immunoreactive neurons receive GABAergic synaptic inputs from the globus pallidus (Bevan et al., 1998). They are also depolarized by D1-family agonists in the presence of D1-

receptor antagonists, indicating the involvement of D5 receptors. Acetylcholine also influences the activity of NPY+ neurons via the activation of M2 muscarinic receptors (Bernard et al., 1998). Parvalbumin-expressing interneurons are also known to innervate NOS+ interneurons (Morello et al., 1997). This connection has been demonstrated electrophysiologically as being relatively sparse, as the photostimulation of PV+ interneurons did not produce many responses in LTS interneurons (Szydlowski et al., 2013).

As depicted in figure 1.2, the major efferent targets of NOS+ interneurons are the SPNs, with synapses being made with distal regions of dendrites and with the spines (Difiglia & Aronin, 1982; Vuillet et al., 1989a, b; Kubota & Kawaguchi, 2000). The functional relevance of this connection has been studied in vitro, with activity in PLTS interneurons evoking only weak GABAergic IPSCs in SPNs with a high failure rate (Gittis et al., 2010). Anatomical studies have also shown that NPY+ boutons form symmetrical synapses with cholinergic interneurons (Vuillet et al., 1989a; 1992). Despite this evidence, in vitro recordings using BAC transgenic mice in which ChAT+, PV+ and NPY+ neurons expressing Lhx6 were made to express EGFP have demonstrated that activity in NPY+ neurons do not evoke IPSCs in postsynaptic LTS neurons, PV+, or cholinergic interneurons (Marin et al., 2000; Tepper et al., 2010). Thus, although the anatomical evidence suggests that NPY+ neurons make synaptic contacts with different cell types, electrophysiological evidence (see above) indicates otherwise, and this is likely explained by the pharmacological properties of SOM/NOS/NPY+ interneurons.

1.2.3.4 Pharmacological properties

This may be explained by the fact that PLTS interneurons do not principally release GABA, an idea that is supported by the low levels of GABA and GAD expression previously reported in NOS-expressing interneurons (Chesselet & Robbins, 1989; Kubota et al., 1993). Thus, it is currently believed that these neurons release SOM, nitric oxide and/or NPY, which could exert long-term neuromodulatory effects on their postsynaptic targets rather than fast synaptic effects (Tepper et al., 2010). Indeed, the application of SOM has been shown to inhibit the release

of GABA at SPN-SPN synapses (Lopez-Huerta et al., 2008), thereby allowing PLTS neurons to subtly modify the striatal processing and output of information. Importantly, the release of nitric oxide and the subsequent activation of the cyclic guanosine monophosphate (cGMP) pathway in spiny projection neurons has been shown to play an important role in spike time dependent plasticity, as long-term depression induced by high frequency stimulation of corticostriatal fibers can be blocked by the inhibition of nitric oxide synthase (Calabresi et al., 1999).

1.2.4 ChAT-expressing tonically active interneurons

1.2.4.1 Morphological properties and connectivity

Cholinergic interneurons in the striatum are large, aspiny neurons that make up 1-2% of striatal cells in the primate (Kemp & Powell 1971a) and 0.4% of all striatal cells in the rat (Oorschot, 1999). Their ovoid shaped somata have a diameter of 20-50μm, and they possess a large axonal field that forms synapses with both direct and indirect pathway SPNs as well as PV+ interneurons (Bolam et al., 1984; Phelps et al., 1985; Koos & Tepper 2002). These neurons are thought to receive a relatively small excitatory innervation that originates mostly from the thalamus, with little originating from the cortex (Lapper & Bolam 1992; Thomas et al., 2000; Doig et al., 2014). SPN boutons immunoreactive for GABA have been shown to make contact with ChAT+ interneurons, providing them with an inhibitory input (Bolam et al., 1986).

1.2.4.2 Electrophysiological properties

Cholinergic interneurons are electrophysiologically described as tonically active neurons (Sharott et al., 2012) due to their continuous firing in vivo, a feature that allows them to be identified during blind recordings in primates (Aosaki et al., 1994). In vitro recordings of cholinergic interneurons have demonstrated that these neurons possess a depolarized resting potential as well as a high input resistance (Kawaguchi, 1993). Identified cholinergic interneurons recorded in vivo fire spontaneously at relatively slow rates (4 spikes/second) due to the presence of resting sodium currents and hyperpolarization-activated cation currents (Bennett et al., 2000).

Importantly, a prominent after-hyperpolarization produced by the activity of calcium-activated potassium currents follows each spike, thereby limiting the frequency of these neurons to 2-10 Hz (Wilson et al., 1990; Wilson & Goldberg 2006). Both the in vivo and the in vitro firing of ChAT expressing interneurons is often described as having 3 "modes" of firing that do not affect its mean firing rate: bursting, regular or irregular (Bennett and Wilson, 1999; Sharott et al., 2012). These 3 modes are distinguished by the percentage of spikes within bursts as well as the CV of the inter spike intervals. A given mode is maintained during both cortical activation and cortical slow wave activity, and transitions between the two states in vivo do not affect the firing pattern of a given $ChAT^+$ interneuron (Sharott et al., 2012).

The study of cholinergic interneurons is of particular interest due to their potential role in the processing of salient cues in primates, including reward and reward prediction (Ravel et al., 1999; Morris et al., 2004). In vivo recordings made in awake animals have demonstrated the presence of a pause in the tonic firing of tonically active neurons (presumed to be cholinergic interneurons) that coincides with the presentation of salient cues (Aosaki et al., 1994b; Graybiel et al., 1994). This response is dependent on the thalamic and dopaminergic innervation of the striatum (Joshua et al., 2008), but the intrinsic membrane properties of cholinergic interneurons are also important (Matsumoto et al., 2001). The capacity to pause for prolonged periods is largely due to the expression of K_{irs} that become unblocked at hyperpolarized potentials, thus prolonging the cell's silence (Wilson 2005). The role of other striatal interneurons in the processing of salient queues has yet to be determined, and it is within the realm of possibility that no other interneuron population plays a role in saliency.

1.2.4.3 Pharmacological properties

One of the major distinguishing features of ChAT-expressing interneurons is their synthesis and release of acetylcholine (Ach) (Calabresi et al., 2000; Zhou et al., 2002). Despite the relatively small population of these interneurons, their dense and large axonal arborizations allow ACh to have widespread effects on local synapses with medium spiny neurons (Izzo & Bolam 1988). Acetylcholine can also act via volume transmission to further influence striatal activity, but this effect is limited due to its rapid degradation in the extracellular space (Contant et al., 1996). These effects are mediated by both nicotinic (nAChR) and muscarinic (mAChR) receptors. The nicotinic receptors are ligand-gated ion channels that are expressed presynaptically, mainly on axon terminals of dopaminergic neurons and the dendrites of parvalbumin expressing interneurons within the striatum (Koos & Tepper 2002; Schwartz et al. 1984; Zhou et al. 2002; Threlfell et al., 2012). Activity at these nicotinic receptors is believed to modulate the release of dopamine from SNc neurons in the dorsal striatum as well as modulate the electrical activity of striatal neurons (Threlfell et al., 2012). Muscarinic receptors are G-protein coupled receptors that exist as 5 separate subtypes (M1-M5), with M1, M3 and M5 being Gq-coupled, and M2 and M4 receptors being Gi-coupled. All of these subtypes are expressed in the striatum; they are expressed on indirect pathway SPNs (M1, M4) and direct pathway SPNs (M1), cholinergic interneurons (M2, M4) as well as GABAergic interneurons (M1, M5) (Bernard et al., 1992; Weiner et al., 1990; Yan & Surmeier 1996; Yan et al., 2001). By acting at muscarinic receptors, acetylcholine can trigger secondary messenger cascades to influence the short-term and the long-term activity of striatal neurons. At a macroscopic level, the spatio-temporal release of acetylcholine in the striatum is heavily implicated in prediction-reward error as well as cue-dependent responses (Ravel et al., 1999).

Cholinergic interneurons express D1-like (D5) and D2-like (D2) dopamine receptors (Hersch et al., 1994; Bergson et al., 1995). The expression of both D5 and D2 receptors allows dopaminergic terminals to excite cholinergic neurons via a cAMP-dependant mechanism that is initiated by D5 receptor activation, while activation of D2 receptors inhibits depolarization via the

inhibition of voltage-gated sodium channels (Aosaki et al., 1998; Maurice et al. 2004). In contrast, both M2 and M4 receptor activation by acetylcholine reduces the excitability of target cholinergic interneurons via a mechanism involving the activation of potassium currents (Calabresi et al., 1998). Immunohistochemical studies have shown that M2 receptors are expressed on efferent cholinergic boutons, indicating that they may function as presynaptic autoreceptors responsible for inhibiting the release of ACh (Yan & Surmeier 1996).

1.2.5 CR-expressing interneurons

Although CR+ interneurons are relatively numerous, accounting for 0.5% of all striatal neurons, the properties and functions of these interneurons are poorly understood (Rymar et al., 2004). The current understanding of these interneurons is effectively limited to the results of immunohistochemical studies. The absence of these results has limited any potential descriptions of the axonal arborization of these cells. There are also no current EGFP-CR+ transgenic mice (Tepper et al., 2010), making in vitro electrophysiological recordings of these neurons difficult. Importantly, the proportion of striatal CR+ interneurons increases from rodents to primates, where they outnumber PV+ and NOS/SOM/NPY+ neurons by a factor of 4 to 1 (Wu & Parent, 2000). This potentially indicates their importance in the processing of more complex cognitive processes.

Immunohistochemical studies performed in rats described CR+ interneurons as medium-sized aspiny neurons that emit a small number of smooth, aspiny dendrites with a sparse branching pattern (Bennett & Bolam, 1993). However, more recent studies have described three potentially distinct types of striatal CR+ neurons on the basis of their somatodendritic structures (Prensa et al., 1998; Schlosser et al., 1999; Wu & Parent, 2000; Tepper et al., 2010. Briefly, these neurons are divided into those with large somata and infrequently branching dendrites (“Type 1”), those with medium sized, bifurcating somata (“Type 2”) and those with small somata and tortuous dendrites (“Type 3”) (Tepper et al., 2010). The expression of calretinin within the

striatum is of interest due to its apparent role in disease. For example, neonatal hypoxia in rats causes the exclusive neurogenesis of CR+ interneurons in striatum (Yan et al., 2008). In post-mortem studies of Huntington's disease patients, large CR-expressing striatal interneurons were shown to be spared from degeneration despite a decrease in the degree of calretinin expressed by these cells (Massouh et al., 2008). Thus, the neurodegenerative processes present in Huntington's disease may influence the degree of CR expression without causing the degeneration of the cells themselves.

1.2.6 Novel types of striatal interneuron

Recent work in BAC transgenic mice has revealed the existence of substantial heterogeneity within striatal interneuron populations by identifying novel types of interneurons that express either NPY (without the co-expression of SOM or NOS) (Ibáñez-Sandoval et al., 2011), TH (Ibáñez-Sandoval et al., 2010) or the 5HT3a serotonin receptor (Lee et al., 2010; Munoz-Manchado et al., 2014; Silberberg & Bolam 2015). Due to technical limitations associated with the histochemical detection of these proteins in the rat, their presence has only been shown in the striatum of the mouse (Unal et al., 2011). As such, they are presented briefly here as a demonstration of the heterogeneity that exists within the interneuron populations of the striatum.

In the dorsal striatum of mice, TH-expressing interneurons did not express NOS, PV or CR (Ibáñez-Sandoval et al., 2011), suggesting that they represent a novel group of interneurons. Interestingly, the number of TH-expressing interneurons in the striatum is increased by lesioning of the dopaminergic system. Although this may suggest a potential compensatory mechanism, these interneurons do not produce or release dopamine, and have been shown to be GABAergic interneurons (Xenias et al., 2015). In vitro electrophysiological recordings of these interneurons suggest that there are 4 different types of TH-expressing interneurons (Ibáñez-Sandoval et al., 2011). Although they are few in number, dopaminergic activity in the striatum has been shown to generate long-lasting depolarizing plateau potentials in these interneurons, suggesting that these

TH-expressing neurons may be critical in the computing and transmission of dopaminergic signals within the striatal microcircuit (Ibáñez-Sandoval et al., 2015).

The recent finding that 5HT3a receptor expression identifies multiple groups of interneurons in the dorsal striatum of eGFP-5HT3a mice suggests additional heterogeneity within existing populations of striatal interneurons (Munoz-Manchado et al., 2013). Indeed, it has been shown that some, but not all PV-expressing interneurons also co-express the 5HT3a receptor (Munoz-Manchado et al., 2013). This co-expression is reflected in the fast spiking nature of nearly one-third of all 5HT3a-GFP interneurons (Munoz-Manchado et al., 2013; Silberberg & Bolam, 2015). Importantly, the connectivity of these interneurons within the striatal microcircuit has been briefly investigated, and they have been shown to receive cholinergic input, while making contacts with striatal projection neurons (Faust et al., 2015).

Using GFP-NPY reporter mice, the expression of NPY within the dorsal striatum has been shown to identify two distinct groups of interneurons (Ibáñez-Sandoval et al., 2011). The first group belongs to the "classical" NPY-SOM-NOS neurons electrophysiologically characterized by the low threshold spikes (LTS) they produce when recorded in slice preparations (Kawaguchi et al., 1997). The second group did not express SOM or NOS, and was characterized as the NPY-neurogliaform cell, so called due to its morphological similarities to neurogliaform cells in the cortex (Overstreet-Wadiche & McBain 2015). Similarly to cholinergic interneurons, these NPY-NGF cells were tonically active in the mouse. This matches results from in-vivo recordings of NPY-expressing interneurons in the rat, as these also displayed tonic activity (Sharott et al., 2012).

Ultimately, the existence of these novel striatal populations within the dorsal striatum of eGFP mice suggests that the identity of striatal interneurons extends far beyond the 4 "classic" types of interneurons. As the field continues to expand, it appears that the diversity of structural and electrophysiological properties among striatal interneurons has begun to mirror the

heterogeneity that is well established in cortical and hippocampal circuits (Klausberger & Somogyi, 2008). Indeed, both the NPY-NGF neuron and the 5HT3a interneuron were identified thanks to their previous descriptions in the cortex (Lee et al., 2010; Overstreet-Wadiche & McBain 2015). The presence of these novel types of interneurons, in combination with evidence to suggest that further heterogeneity exists within the classical interneurons of the striatum (Kawaguchi, 1993; Tepper et al., 2010) ultimately implies that a great deal of structural and electrophysiological heterogeneity within the striatal microcircuit remains to be defined .

1.3 FUNCTIONAL HETEROGENEITY ACROSS THE AXES OF THE DORSAL STRIATUM IN RATS AND PRIMATES

The first description of the basal ganglia in the Albin-DeLong model hypothesized that the striatum could be functionally divided into discrete sub-circuits that would each perform different motor and associative tasks (Albin, Young and Penney 1989; DeLong 1990). Although they were simplified, such conclusions were drawn from the heterogeneous nature of cortical inputs into the striatum such that different regions of the striatum received inputs from functionally distinct cortical domains (McGeorge & Faull, 1989). These findings, combined with recent studies demonstrating the existence of heterogeneous spatial distribution of both striatal projection neurons (Gangarossa et al., 2013) and striatal interneurons (Kawaguchi 1993; Rymar et al., 2004) suggests that topographical heterogeneity at the may also exist within the striatum. Recently, this potential spatial heterogeneity has been linked to a variety of striatal functions. For example, the striatum has been shown to be critical for decision-making involving both goal-directed behaviour as well as stimulus-response driven mechanisms. The transition from the former to the latter behaviour is a requirement for all learning, and yet the neural correlates for these behaviors are thought to take place in the lateral and medial regions of the striatum respectively (Haber et al., 2000; Niv & Schoenbaum, 2008). Thus, given that the interneuron populations described in this study are biased in their distribution throughout the medio-lateral and dorso-ventral axes of the dorsal striatum, it is important to briefly present the evidence that links the spatial and functional heterogeneity of the caudate-putamen in rats and monkeys.

One of the most recently studied functional segregations along the dorsal striatum of rats lies along its medio-lateral axis. One of the major functions associated with healthy striatal activity is the selection of reward-related actions through the integration of goal-directed behaviors and the acquisition of habits. These learned behaviors are often investigated through a variety of tasks that can be simplified in the following manner: an external stimulus triggers a response from the animal, often followed by the delivery of an associated reward. As its name suggests, goal-directed action involves an association of a specific behavior with a reward. Neural

circuits responsible for the processing of these behaviors can be studied by changing the value of the reward, and studying the effect that this has on an animal's behavior. As the apparent value of the reward is devalued for example, the behavior associated with that reward would disappear over time. In contrast, habit acquisition describes the relationship between a stimulus and an associated behavior (Gremel & Costa, 2013). It is not influenced by changes to the value of the reward. Importantly, recent studies have shown that lesions to the dorso-medial striatum disable goal-directed behaviors, while lesions to the dorso-lateral striatum prevent associations between stimulus and response (i.e. habit formation) (Gremel & Costa, 2013). Importantly, lesions to these striatal regions does not prevent animals from completing the task, but caused both groups to use different functional mechanisms (Gremel & Costa, 2013). Specifically, animals with dorsomedial striatal (DMS) lesions were impaired in the use of goal-directed behavior, but could complete the task using habitual behavior (Gremel & Costa 2013). Thus, goal driven and habit driven behaviors are seemingly processed in parallel during task completion, but one could argue that modulation of these behaviors is dependent on the activity of the dorso-medial or the dorso-lateral striatum, respectively (Balleine & O'Doherty, 2010).

The involvement of both the dorsomedial striatum (DMS) and the dorsolateral striatum (DLS) in task completion is best exemplified by the finding that single cells recorded in both regions respond throughout the performing of an odor guided task (Gremel & Costa, 2013). This implies that both striatal domains are involved in goal driven and habit driven behaviors. However, by using a task that dissociated goal driven and stimulus driven behavior, Costa and colleagues were able to show that the modulation of firing in the dorso-medial striatum was greater during goal directed behaviors (Gremel & Costa, 2013). In contrast, the dorso-lateral striatum's activity was more strongly modulated during stimulus driven behaviors (Gremel & Costa, 2013). Further discrepancies have also been described regarding the activity of interneurons in these domains. For example, a select group of fast spiking interneurons in the dorso-medial but not the dorso-lateral striatum responded to reward prediction such that their firing rate was affected by the difference between the anticipated and actual reward delivered to

the animal (Stalnaker et al., 2012). In addition to these differences, other studies have found that activity in the DLS and DMS differs during the early and later stages of training. For example, neurons in the DLS are more selective during the action portion of task acquisition while DMS neurons were more active when animals were making cue-based associations early on in their training (Yin et al., 2009; Thorn et al., 2010). These results are in agreement with the finding that lesions of the DMS impair the early stages of training for association tasks, but do not influence animal behavior during later stages of training (Koralek et al., 2012; Gremel & Costa 2013). Moreover, the increased involvement of the DLS during the active or "motor" components of behavior acquisition is not surprising, given the increased connectivity of this region with the sensory-motor cortices (McGeorge & Faull, 1989). Thus, although both the DMS and the DLS are both equally involved in the acquisition of novel activities, the results from behavioral studies investigating the DMS and DLS have provided concrete evidence to suggest that these regions are responsible for processing different and specific components of learned behavior. These differences are important, as they imply that the striatal circuitry making up the DMS and the DLS may itself reflect the different functional requirements of these two striatal domains.

In rodents, both the functional and structural heterogeneity along the dorso-ventral striatal axis (of the dorsal striatum) has not been investigated to a large degree. Although CR+ (Rymar et al., 2004; Ma et al., 2014) and PV+ interneurons (Ma et al., 2014) have been described as having potential dorsal biases along specific coronal planes, dorso-ventral biases in the striatum have not been quantifiably defined for any striatal interneuron or for spiny projection neurons (Oorschot, 2013). In the primate striatum however, studies have attributed distinct behavioral functions to the dorsal, central, and the ventral regions of the caudate-putamen. The results from these behavioral studies are briefly discussed below. Unsurprisingly, these 3 regions are distinguished by their anatomical connections with cortical and subcortical circuits (Haber & Knutson, 2010), and are well aligned with previously described tripartite divisions that have been ascribed to the human caudate/putamen (CPu) (Karachi et al., 2002). These findings help to further strengthen the hypothesis that the heterogeneity of inputs to distinct striatal sub-domains is reflected in the

functional heterogeneity of those sub-domains. Whether or not this heterogeneity is reflected in the cellular circuitry of these sub-domains however, remains to be seen.

When monkeys were trained to make saccades in response to visual cues that provided rewards of unequal value, recordings in the dorsal regions of the caudate found that single neurons were highly responsive prior to saccades along a specific direction. These responses were seen for saccades that produced both small and large rewards. These neurons are therefore believed to encode the value of specific actions (Doya & Kimura, 2005; Haber & Knutson, 2010; Stalnaker et al., 2010). In contrast (and perhaps unsurprisingly), neurons in the ventral caudate were highly responsive to the inherent value of the delivered reward, while very few responded to the direction of the saccade that was performed (Haber & Knutson, 2010). These results are in agreement with previous studies in primates involving a Go/No-go task, in which ventral neurons responded almost exclusively to the size of the delivered reward, while neurons in the dorsal caudate as well as the head of the caudate were responsive to the type of movement being made even when no reward was delivered during an error trial (Apicella et al., 1991; Hollerman et al., 1998). Clearly, the existence of functional heterogeneity in the medio-lateral and dorso-ventral striatum is of vital importance for the development of learned behaviors as well as reward association. Although it should be stressed that this compartmentalization is partial, its existence strongly suggests that striatal circuits associated with these functions must either be composed of different processing units (i.e. cell types) or must process that information in a different manner (i.e. via distinct connectivity). For this reason, it is imperative that the cellular or circuit-based heterogeneity implied by the functional and anatomical heterogeneity of the striatum be explored in more detail.

1.4 STEREOLOGICAL CELL COUNTING IN THE DORSAL STRIATUM OF THE RAT AND PRIMATE: A BRIEF LOOK AT THE NUMBERS

The common understanding of striatal cytoarchitecture in the dorsal striatum is that it is mostly composed of spiny projection neurons with aspiny interneurons making up a relatively small proportion of this structure (Kawaguchi et al., 1993). Various studies have now attempted to quantify the exact proportions occupied by striatal cell types, including their subdivisions. These studies have reported many different values regarding the relative proportions occupied by the aspiny interneuron population of the striatum. In the case of the rat, these differences are small, with some studies reporting less than 3% (Oorschot, 1996) while others reported values as high as 6% (Graveland and DiFiglia, 1985). Although such differences appear small in nature, they should nevertheless be taken seriously given the strong influence that a few interneurons can exert on SPN activity (see sections 1.2.2-1.2.6), and hence striatal output (Koos & Tepper, 1999). In the monkey, studies have reported an even larger disparity with respect to interneuron numbers, with reports suggesting that the overall proportion of interneurons does not change in the monkey (4-6%) compared to the rat, while others suggest that interneurons make up nearly a quarter (~23%) of the caudate-putamen's neurons (Graveland and DiFiglia 1985; Deng et al., 2010). Such disparate results in the monkey merit further investigation, as they either suggest that the relative numbers of interneurons do not change from rodents to primates, or that they change dramatically.

One of the first studies investigating the percentage of interneurons and medium spiny neurons in the dorsal striatum in both rats and monkey was performed by Graveland and DiFiglia (1985). Importantly, interneurons were identified using electron microscopy by the presence of indented nuclei, while SPNs were identified by their unindented nuclei. In the rat (and the mouse), this technique is reliable, as indentation of nuclei has been shown to correctly identify aspiny interneurons in the striatum (Bolam et al., 1981; Kawaguchi et al., 1993). Thus, the value of 4-5% that was obtained by averaging the results of 14 sample regions of neostriatum (they did

not perform counts in an entire section) are most likely accurate. In the monkey however, the method of classifying striatal neurons based on their nuclear indentation is not full proof because studies using similar techniques in humans found that nearly 8% of SPNs (identified by the presence of spines and their expression of substance P) had a shallow indentation in their nuclei (Hutcherson & Roberts, 2005). Importantly, Graveland and DiFiglia reported that approximately 12% of their counted neurons also had shallow indented nuclei, and these were classified as interneurons at the time. For this reason, their value of 23% for striatal interneurons in the monkey may represent an overestimation, and a value of 11% may prove to be more accurate. Thus, caution should be taken when citing values obtained from older stereological studies, as newer, more accurate techniques have arisen in the past 2 decades. These are described below.

Modern stereological techniques (such as the optical disector technique described in chapter 2 – West, 1999) are defined by their lack of reliance on features of neurons that are variable such as nuclear shape and cell size. Moreover, modern studies look to measure absolute numbers of neurons rather than using density measures, which can prove inaccurate unless the volume of the entire structure is calculated using the Cavalieri estimator method for complex volumes (West et al., 1993, Oorschot 1994, West et al., 1999). In the striatum of adult rats (the Sprague-Dawley strain), these techniques have been used in several studies to provide estimates for the absolute numbers of the 4 major types of striatal interneurons, as identified using immunohistochemistry or in situ hybridization. The results from these studies are summarised in Table 1.1. In most of these studies, it should be noted that the striatum's rostro-caudal axis was defined as extending from 2.2mm rostral of Bregma and 2.6mm caudal of Bregma, according to a standard stereotaxic atlas (Paxinos & Watson, 2007). Importantly, most stereological studies have neglected the region of striatum caudal to the plane at 2.6mm. This caudal-most region extends a further 1.2mm towards the caudal pole of the dorsal striatum and therefore represents a major part of the structure (Paxinos and Watson, 2007). Recently, the very caudal aspects of the striatum in mice have been shown to possess a particularly specialized composition of neurons, where almost all of the SPNs express D1 (i.e. direct pathway) and there also is a relatively high proportion of

ChAT-expressing interneurons (Gangarossa et al., 2013). This oversight is of particular importance with respect to the absolute number of PV+ interneurons, where the striatum was limited in the rostro-caudal axis from 1.7mm rostral of Bregma to 1.4mm caudal of Bregma. Thus, although the results in Table 1.1 are informative with respect to the absolute numbers of striatal interneurons, the contributing studies have nevertheless neglected a large portion of the striatum and their numbers may therefore represent underestimates. More importantly, the recent findings that some striatal neurons (Gangarossa et al., 2013) are preferentially distributed in the caudal striatum could also imply that this region is functionally specialized, and may therefore hold further heterogeneity that has yet to be fully explored.

Table 1.1 Absolute numbers of neurons in the dorsal striatum of the Sprague Dawley rat

Neuron Type	Absolute Number	%	Reference	Additional Notes
All striatal neurons	2854600	100%		Obtained by summing all other absolute numbers
SPNs	2791000 2540000	97.8%	Oorschot, 1996 Luk & Sadikot, 2001	
Parvalbumin-expressing	~16900	0.6%	Luk & Sadikot, 2001 Larsson et al., 2001	The striatum was limited in the rostro-caudal axis. Larsson worked in Wistar rats.
Calretinin-expressing	13200	0.5%	Rymar et al., 2004	
NOS-expressing	21300	0.8%	West, 1996	
ChAT-expressing	12200	0.4%	Oorschot, 1999	

When the absolute numbers of all striatal neurons are summed, the results from these studies suggest that striatal interneurons make up a mere 2.3% of the striatum's cytoarchitecture, a value that is nearly half of what was reported by Graveland and DiFiglia. However, it should be considered that these values represent underestimates due to the selective sampling of the striatum in these studies. Moreover, none of these studies were as thorough with respect to their sampling areas as the study by Graveland and DiFiglia (1985), which further supports the idea that a value of 2.3% may be a minimal value. The importance of regional sampling in the striatum is particularly evident in the case of PV+ interneurons. For example, Celio used a highly robust sampling method in which all PV-expressing interneurons were counted in every other 50um-sagittal section across a large portion of the dorsal striatum (Celio, 1990). He reported that PV-expressing interneurons alone accounted for nearly 2% of all striatal neurons. Although this study did not specify the particular strain of rat that was used for the counts (for this reason it is not in Table 1), it suggests that the 0.6% value (Larsson et al., 2001; Luk and Sadikot 2001) that is often cited for the rat is indeed an underestimate. Additionally, the non-stereological work of Kita and Kitai reported that nearly 3-5% of striatal neurons expressed parvalbumin on the basis that PV+ interneurons also stained strongly for glutamate decarboxylase (Kita et al., 1990). Unlike the study by Luk and Sadikot, which sampled 5 sections along a limited portion of the striatum's rostro-caudal axis, the study by Kita and Kitai sampled $1mm^2$ areas near the lateral ventricle, which has been noted anecdotally in the past to contain a relatively large proportion of PV+ interneurons (Kawaguchi et al., 1993). Thus, the results obtained from these studies clearly indicate the importance of sampling when making stereological estimates, particularly in the case of striatal interneurons whose distribution might not be uniform along the rostro-caudal and medio-lateral axes. Indeed, given the lack of consistent sampling across stereological studies investigating striatal interneurons, it is perhaps inappropriate to sum the results from these studies in order to conclude that striatal interneurons make up less than 3% of all striatal neurons in rodents (Tepper et al., 2010).

Stereological estimates of cell types in the caudate nucleus and putamen in the monkey are less complete than the data in the rat. Past studies have attempted to compare the densities of cells expressing calretinin, parvalbumin and somatostatin expression in the rat and the monkey (Wu and Parent, 2000). In agreement with past studies, Wu and Parent (2000) found that the density of all 3 of these interneuron populations was higher in the monkey than in the rat. However, as these authors did not normalize tissue shrinkage (which will be different for the rat and the monkey due to the different composition of white matter and grey matter in the respective tissues), their comparisons of relative densities should be taken as inconclusive (Oorschot 1994). With respect to the relative abundance of interneurons in the monkey caudate/putamen, the absolute numbers most commonly cited are those reported by Deng and colleagues (Deng et al., 2010). Their results are summarized in Table 1.2. In the squirrel monkey, it should be noted that calretinin is expressed in a subset of spiny projection neurons and ChAT+ interneurons (Deng et al., 2010), and so the values for calretinin-expressing interneurons are obtained by subtracting all other percentage values from 100. This is potentially incorrect as it assumes that other interneurons positive for calbindin (the marker used for projection neurons) do not exist in the caudate-putamen of the monkey. Moreover, the extent of the stereological sampling, as well as the regions used is not well defined in this study, which indicates that the reported values may be prone to error.

Ultimately, one should be careful when interpreting the cell counts reported in monkey tissue given the potential for sampling bias. These problems are further complicated by the degree of complexity associated with protein expression in striatal interneurons of the monkey, where some interneuron classes often express multiple proteins (Wu & Parent 2000; Deng et al., 2010). Thus, stereological data in the monkey should often describe protein expression, rather than a distribution of a particular type of interneuron, as these are poorly defined in the primate. Clearly, a more complete stereological count is required in order to further elucidate the distribution and absolute numbers of these interneurons in the primate striatum.

Table 1.2 Percentages of protein expression associated with striatal interneurons in the Caudate and Putamen of the Primate

Expression	Caudate	Putamen
Parvalbumin-expression	1.0%	2.4%
Calretinin-expression	2.0%	1.5%
NOS-expression	1.9%	1.2%
ChAT-expression	1.1%	0.9%

1.5 THE VENTRAL STRIATUM (NUCLEUS ACCUMBENS)

1.5.1 Overview and delineation of the ventral striatum

The ventral striatum (most commonly referred to as the nucleus accumbens - NAcc) of rodents (Paxinos & Watson 2007) is anatomically delineated by the external capsule rostrally and lateraly, while its medial borders are limited by the septum and the lateral ventricle. In the rostro-caudal axis, the ventral striatum merges with the stria terminalis caudally, and is rostrally limited by the olfactory tubercle. Its dorsal border lies ventrally to the dorsal striatum, and can be delineated by staining the structure for immunohistochemical markers such as acetylcholinesterase and calbindin (Jongen-Relo et al., 1994; Groenewegen et al., 1999). In all planes, the nucleus accumbens can be further divided into 2 major regions: the core and the shell. The core region wraps around the anterior commissure (white matter) and is medially and ventrally delineated by the shell. The borders of the core are best defined by immunohistochemical staining for acetylcholinesterase, which is expressed as low levels in the entirety of the core but is enriched in the surrounding shell as well as the dorsal striatum. The borders of the shell are best outlined by staining for calbindin, which strongly labels the core of the NAcc and weakly labels the shell. However, the use of these markers does not fully delineate the medial or the ventral borders of the shell because the surrounding structures also express calbindin to some degree. The lack of a concrete method to fully delineate the borders of the shell has therefore represented a hurdle for various anatomical studies of the nucleus accumbens. This is especially relevant for the accuracy for stereological studies looking at absolute cell numbers and densities for the various cell types in the core and shell of the NAcc. A potential immunohistochemical solution to this "delineation problem" is presented in chapter 2.

Anatomically, the nucleus accumbens is often divided into domains that are distinguished by the unique inputs and outputs of the core and the shell. Moreover, the core and the shell are sometimes further divided based on the extensive heterogeneity of inputs into the different regions within the core and the shell. These inputs have often been described as occupying

overlapping domains, such that regions of the medial shell receive different cortical and tegmental inputs that overlap with those distinct inputs of the lateral shell. A similar pattern is noted for the discrete and distinct inputs to the different regions of the core. These distinct inputs and outputs are important, as they have provided the basis for a variety of the hypothesized functions of the core and the shell which are covered in detail throughout chapter 6. As such, they are briefly described in sections 1.5.2 and 1.5.3, and are summarized in Figure 1.3 (adapted from Humphries & Prescott, 2010)

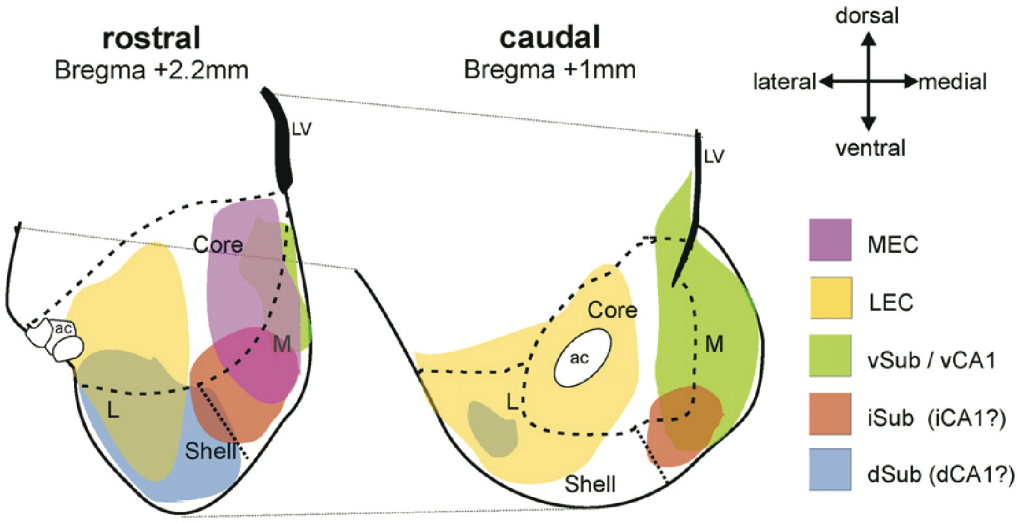


Figure 1.3 Approximate cortical input fields across the rostro-caudal extent of the ventral striatum (Adapted from Humphries & Prescott 2010). Schematic diagram demonstrating the input fields of various cortical areas into the rostral (left) and caudal (right) planes of the nucleus accumbens. The core and the shell are outlined in both coronal planes, along with the anterior commissure (ac) and the lateral ventricle (LV). The shell has been divided in both planes down the midline in accordance with anatomical descriptions of the medial and lateral inputs and outputs of the ventral striatum. These are indicated as M and L respectively.
MEC – Medial entorhinal cortex. **LEC** – Lateral entorhinal cortex. **v/i/dSub** – ventral, intermediate and dorsal subiculum. **v/i/dCA1** – ventral, intermediate and dorsal cornu ammonis.

1.5.2 The core of the nucleus accumbens

Much like the dorsal striatum, the spiny projection neurons of the NAcc core can be divided into two groups based on their expression of either D1 or D2 dopaminergic receptors (Gerfen & Surmeier, 2011). The morphology of neurons in both the dorsal striatum and the NAcc core is also similar with respect to both axonal arborisations and dendritic fields (Meredith et al., 1992). Given these similarities, it is not surprising that D1/Substance-P expressing SPNs of the core project to the output nuclei of the basal ganglia (the SNr in particular), a system analogous to the "direct pathway" of the dorsal striatum (Deniau et al., 1994; Maurice et al., 1997, 1999; Zhou et al., 2003). Continuing with this trend of similarity, all D2-expressing spiny projection neurons of the NAcc core project to the dorsolateral portions of the ventral pallidum, whose projections can be traced to the subthalamic nucleus and the dorsomedial SNr (Heimer et al., 1991; Maurice et al., 1997). This organization therefore seems to mirror that of the "indirect pathway" described in the dorsal striatum (Ikemoto, 2007). Importantly however, studies have shown that this "mirroring" of the dichotomy present in the dorsal striatum does not represent a perfect match (Kupchik et al., 2015). Indeed, a large subset of D1 receptor-expressing SPNs in in the core of the nucleus accumbens has been shown to project to the VP (Kupchik et al., 2015). This population of D1-receptor expressing SPNs which does not conform to the "direct pathway" has been estimated by some to be larger than the D2 receptor-expressing SPN population in the NAcc core that primarily targets the VP (Zhou et al., 2003). With respects to its inputs, the core of the NAcc receives three major (glutamatergic) inputs from the hippocampus, the prefrontal cortices and the amygdala (Mcgeorge & Faull, 1989; Humphries & Prescott, 2010). The core also receives a GABAergic input from the dorsolateral VP (Hakan et al., 1992; Groenewegen et al., 1993), an input that is reminiscent of the GPe projection to the dorsal striatum (Hanley and Bolam, 1997; Bevan., 1998; Mallet et al., 2012).

1.5.3 The shell of the nucleus accumbens

The NAcc shell differs greatly from the dorsal striatum with respect to the structure of the cells therein as well as its inputs and outputs. In the shell, projection neurons have a lower spine density, and are also smaller than those in the core (Meredith et al., 1992). Those SPNs that express the D1 receptor project mainly to the VTA in a reciprocal fashion such that lateral shell D1-expressing SPNs project to the lateral VTA (and vice-versa) while D1 receptor-expressing SPNs in the medial shell project to the medial VTA (Zhou et al., 2003; Ikemoto, 2007). Whether or not the projection from the shell to the VTA is inhibitory is currently unknown, as these cells have not been characterized electrophysiologically. Indeed, even the SPN targets in the VTA have yet to be identified, but it has been hypothesized that they may be the same GABAergic neurons that project back the NAcc shell (Carr and Sesack, 2000).

In the shell, medially located D2-expressing SPNs project to the medial VP while those located laterally project to the lateral VP (Ikimoto, 2007). This connection is reciprocated in a topographic manner (Groenwegen et al., 1993). A small subset of D1-expressing SPNs also projects to the VP in a similar fashion. This once again serves to highlight the importance of the medial and lateral divide that has been anatomically defined in the shell (but not for the core). Thus, although the shell differs from the core with respect to its overall structure, the distinction between D1-expressing SPNs (mostly) projecting to the SNr and D2-expressing SPNs projecting entirely to the VP remains consistent. Once again however, it should be noted that the expression of D1 and D2 receptors does not perfectly distinguish 2 separate neural populations, as recent studies have shown that 17% of SPNs co-expressed both D1 and D2-dopaminergic receptors in the shell (Bertran-Gonzalez et al., 2008). This contrasts with the levels of D1 and D2 co-expression found in the dorsal striatum (5%) and in the NAcc core (6%) (Bertran-Gonzalez et al., 2008). With respect to its output, spiny projection neurons of the shell once again distinguish themselves by targeting structures that do not lie within the basal ganglia. For example, the lateral shell projects to the lateral hypothalamus but most of its projections remain within the basal

ganglia (Usuda et al., 1998). The medial shell projects to a variety of non-basal ganglia structures such as the parabrachial nucleus (Mogenson et al., 1983). These features of the shell therefore help to illustrate the principle that the shell represents a potentially different striatal processing unit, which can further be divided into medial and lateral regions.

1.6 CALCIUM-BINDING PROTEINS IN THE CENTRAL NERVOUS SYSTEM

Calcium (Ca^{2+}) is an essential divalent ion present in the nervous system, where both its intracellular and extracellular concentration governs a variety of biological and physiological processes from neurotransmitter release to the development of neurons (Pang & Sudhof, 2010). Pathological changes in Ca^{2+} concentration therefore underlie a variety of neurological disorders such as ataxia, Alzheimer's disease and epilepsy (Ben-Ari, 2001). In order to maintain Ca^{2+}homeostasis, neurons store Ca^{2+} ions in intracellular stores or chelate free, cytosolic Ca^{2+} with Ca^{2+}-binding proteins (CBPs) (Andressen et al., 1993).

Structurally, CBPs in the nervous system are defined by the presence of the "EF-hand" Ca^{2+} binding site, which is made up of a Ca^{2+} binding site flanked by two alpha-helices (Kretsinger, 1980). Functionally, CBPs are defined as either "calcium sensors" such as synaptotagmin and calmodulin, or "calcium buffer"s such as parvalbumin and the calbindin subfamily of proteins (Matthews & Dietrich, 2015). Although the distinction between calcium sensors and buffers is not always clear, calcium sensors typically display conformational changes upon binding to Ca^{2+} ions that allow them to take part in secondary messenger cascades. In contrast, calcium buffers function to dissipate local Ca^{2+} ions. Importantly, the calcium buffers PV, CR and calbindin (CB) are often expressed by distinct subtypes of neurons (Celio, 1990). The expression of these proteins by select neural populations is potentially responsible for determining their electrophysiological characteristics to some extent. This relationship exists in neural populations found in a multitude of functionally distinct regions within the nervous system, and is best exemplified by the so-called "fast-spiking" firing patterns of neurons expressing PV (Cauli et al., 1997).

By acting as both calcium buffers and sensors, CBPs are therefore primed to play an important role in the function of the nervous system. What is perhaps the most intriguing aspect of CBP expression in neural populations is that although certain populations can co-express

different CBPs, each one seems to perform a highly specialized function within the cell, as exemplified by the fact that the deletion of one CBP is not compensated for by the upregulation of another CBP (Fossner et al., 2013). Because this specialized and selective expression of CBPs by distinct groups of neural populations is reflected in their physiological properties, CBP expression in the central nervous system is therefore a tool which may be used to identify different and potentially novel classes of neurons on a molecular basis (Klausberger & Somogyi, 2008; Fishell & Heintz 2013). Recently, an EF-hand calcium-binding protein known as secretagogin (Scgn), has been shown to label specific populations of forebrain neurons in both the developing and adult brain (Mulder et al., 2009; 2010). Due to their value as molecular tags for specific subsets of neurons, as well as their relevance to this study, the structure and hypothesized functions of Scgn are summarized briefly below.

1.6.1 Secretagogin

Secretagogin (Scgn) is a cytosolic, hexa EF-hand CBP recently cloned from insulin producing cells in the islets of Langerhans (Wagner et al., 2000). The predominant form of Scgn in the nervous system is a 32kDa protein capable of simultaneously binding 4 Ca^{2+} ions. Importantly, a splice variant known as secretagogin-R22 (32kDa) is also found in both rodent and human tissue, which contains a single Q/R switch at codon 22 (Zierhut et al., 2005). As this codon is not located in proximity to any of the calcium binding motifs, this variant does not display any changes to its Ca^{2+}-binding activity. A third variant, setagin, is a 49 amino acid peptide that does not bind calcium, and has only been detected in pancreatic tissue (Zierhut et al., 2005).

When tested in quasi-physiological salt buffers, the half-maximal $Ca2^{+}$ binding affinity of Scgn is approximately 25 μM, a value that is significantly lower than that of PV (Rogstam et al., 2007). Given this value, it is believed that only ~10% of all cytosolic Scgn is saturated at resting levels of intracellular Ca^{2+}, implying that Scgn may be sensitive to increased intracellular Ca2+

during periods of elevated cellular activity. In further contrast to PV, Scgn undergoes conformational changes in its tertiary structure upon binding to Ca^{2+} (Alpar et al., 2011). This, along with the finding that the Ca^{2+} affinity of Scgn is similar to that of synaptotagmin, suggests that secretagogin does not function as a buffer for intracellular calcium, but instead behaves as a "calcium sensor" (Alpar et al., 2011). Thus, variations in intracellular calcium levels promote the interaction of Scgn with a host of other protein networks in order to coordinate a multitude of cellular responses.

The first example of Scgn interaction with other cellular proteins was demonstrated when tissue homogenates from the central nervous system are superfused over recombinant Scgn (Rogstam et al., 2007). This results in a high affinity interaction between Scgn and soluble N-etylmaleimide-sensitive factor attachment protein of 25 kDa (SNAP-25), which occurs only in the presence of Ca^{2+} (Rogstam et al., 2007). Since then, the use of affinity chromatography and surface plasmon resonance have identified a variety of proteins that have a Ca^{2+} dependent interaction with Scgn and are involved in processes ranging from intracellular trafficking to vesicular exocytosis (Yang et al., 2005; Bauer et al., 2011). These include DOC2alph and ARFGAP2, which are involved in the regulation of vesicle fusion, as well as B-tubulin and kinesin 5B that have been shown to be involved in the transport of vesicles. Such findings are promising, particularly an interaction with SNAP-25 and SNAP-23, as they both belong to the SNARE family of proteins whose activity represents an important regulatory step in the docking and fusion of vesicles with the membrane (Milovanovic & Jahn, 2015). Thus, in some cell types, Scgn may act as a major Ca^{2+} sensor essential in regulating certain aspects of this process. This is best exemplified by recent reports demonstrating that Scgn expression is required for the secretion of corticotropin releasing hormone in the mammalian hypothalamus (Romanov et al., 2014). Cleary, Scgn possesses many of the key properties required for functional calcium sensing, implying that its selective expression by a discrete population of cells may impart novel functionality to that population.

In the nervous system, the expression of Scgn was first demonstrated thanks to histological analysis of post-mortem tissues. These studies revealed that Scgn mRNA and protein can be found in the olfactory bulb, the non-cholinergic neurons of the medial septum and dorsal striatum, the anterior hippocampal continuation as well as the cerebellum (Mulder et al., 2009; 2010). Co-localization studies later revealed that Scgn expression was limited to neuronal populations, and that dentate gyrus cells, olfactory periglomerular cells and cells in the ventral pallidal territory expressing either PV, CR or CB (respectively) also expressed Scgn. The existence of this co-expression in multiple regions of the nervous system suggests that Scgn may be co-localized with these calcium-binding proteins in other areas of the brain. Additionally, the retention of Scgn expression in the adult nervous system is perhaps not surprising, since Scgn expression in the fetal mouse brain first appears in postmitotic neurons migrating to the olfactory bulb and the subpallium (Mulder et al., 2009). Indeed, the finding that Scgn is found during the development of several postmitotic neural populations (Mulder et al., 2009) is in and of itself important, as it implies that the expression (or lack thereof) of Scgn might help to elucidate the developmental origins of entire neuronal circuits. This idea has recently been put into practice in order to solve a long-standing question regarding the development of the anterior hippocampal continuation, whose origin is debated as either being olfactory or hippocampal in nature (Wyss et al., 1983). Given that neurons of the indisium griseum express Scgn, Harkany and colleagues have recently used this to argue that these neurons might develop from the same group of post-mitotic neurons that gives rise to the Scgn-expressing granule cells of the dentate gyrus (Mulder et al., 2010). Taken together, these findings support the notion that Scgn expression complements that of other well-known and functionally important CBPs, and that Scgn expression may distinguish neuronal populations on the basis of their developmental origins and other functional properties.

Given the apparent importance of Scgn expression in the nervous system of rodents, the expression of this calcium binding protein in the primate was of particular interest. In both humans as well as non-human primates, the amino-acid sequence of secretagogin is not significantly different than that found in mice and rats (Pruitt et al., 2013; Gartner et al., 2007). Indeed, mouse Scgn has a 93% sequence homology with the Scgn protein expressed in the rat, and has an 85% sequence homology with the human Scgn. Moreover, rat Scgn has an 83% sequence homology with human Scgn. This would imply that the structure and Ca^{2+} binding capacity of Scgn described in rodents is highly conserved at the level of the primate, including humans. Although Scgn expression in endocrine tissue is relatively retained across all species, the expression of Scgn in the nervous system of the primate is greater than in the rodent (Attems et al., 2008). For example, regions of the rodent brain such as the dentate gyrus where Scgn is only expressed in granule cells, have a far greater diversity of Scgn expression in the primate, where many of the morphologically diverse sub-populations of hippocampal neurons display Scgn immunoreactivity (Attems et al., 2008; Mulder et al., 2009). Thus, Scgn expression is retained throughout multiple phylogenies, and its increased expression in primates (as with PV, CR and CB) suggests that Scgn plays an important role in the development and function of an ever increasing number of neuronal populations throughout evolution.

The extensive distribution of Scgn within a variety of neuronal networks in multiple species implies that its importance as a CBP may mirror that of PV, CR and CB. For this reason, many potential functions for Scgn in the CNS have been hypothesized in recent studies. For example, if Scgn is able to moderate the intracellular Ca^{2+} concentration of the neurons in which it is expressed, it may play a major role in shaping the electrophysiological activity of those neurons in novel ways. Such a thought is enticing; particularly when one considers the possibility that certain neurons may express Scgn and not any other known type of CBP. Moreover, the expression of Scgn during the development of post-mitotic neurons suggests that it plays a role in cellular motility and migration. During ischemic attacks resulting in cell death Scgn can be found in the circulation, suggesting that it may represent a mechanism by which cell death is

communicated, and its release may indeed trigger “neuroprotective” responses (Montaner et al., 2008; 2010). Thus, the calcium binding protein Scgn is selectively expressed in the brain of both rodents and primates, where it behaves as a putative calcium sensor whose presence is associated with cellular motility in development, vesicular exocytosis and neuroprotection from excitotoxicity.

1.7 AIMS OF THIS RESEARCH

1.7.1 Summary

By thoroughly examining the structural and electrophysiological properties of the "classical" types of striatal interneurons, this chapter has provided considerable evidence to suggest that there may be further molecular heterogeneity within the neostriatum of rodents and potentially primates. This hypothesis is strengthened by the recent identification of several novel types of striatal interneuron identified by their unique molecular and electrophysiological signatures. This, in combination with the broad expression of the calcium binding protein secretagogin in the striatum ultimately implies that the diversity of striatal interneurons may mirror that which has been previously described in the neocortex. If this molecular and physiological diversity does indeed exist within the neurons that make up the striatal microcircuit, it follows that not all striatal microcircuits are equivalent in their cellular organization. The potential for this regional heterogeneity amongst the different striatal populations is promising given the recent findings in both rats and primates (described above) that different striatal regions contribute to very specific components of learnt behaviors. As these functionally distinct striatal areas receive highly specialized input from different regions of the neocortex, it is likely that the processing units of these regions are subtly different from one another. Finally, the finding that the recently described calcium-binding protein secretagogin identifies developmentally and functionally distinct populations of neurons in the forebrain and the hypothalamus, suggests that it may represent a molecular marker whose selective expression may highlight the existence of further heterogeneity within the striatum.

1.7.2 Specific aims

1.7.2.1 Aim 1: To qualify and quantify the degree of secretagogin expression in the dorsal and ventral striatum of rodents and primates (Chapters 3 and 6)

The finding that Scgn is expressed in the non-cholinergic neurons of the dorsal striatum of mice implies that it may be selectively expressed by certain subpopulations of interneurons in the striatum of rodents and perhaps primates. The expression of Scgn may also label previously identified populations of striatal neuron in both the dorsal and the ventral striatum. As Scgn has been shown to be a functional calcium binding protein involved in calcium sensing and the regulation of vesicular exocytosis, it is likely that its selective expression by certain striatal neurons may underlie a variety of anatomical and physiological differences within those populations.

1.7.2.2 Aim 2: To investigate molecular, anatomical and physiological heterogeneity among the interneuron populations of the dorsal striatum of rodents (Chapters 4 and 5)

Given that the activity of striatal interneurons can heavily influence the output neurons of the striatum, investigations into the potential molecular, anatomical and physiological heterogeneity within these populations is likely to be important when considering that the influence of each class of interneuron over the output of the striatum is specialized. With this in mind, this study will aim to identify molecular, structural and electrophysiological heterogeneity that may exist within the "classic" and potentially novel populations of interneurons within the dorsal striatum.

1.7.2.3 Aim 3: To quantify the degree of topographical bias in the distribution of various interneuron populations in the dorsal and ventral striatum of rodents (Chapters 3, 4, 5 and 6)

In the past, certain populations of interneuron have been described as having preferences towards certain regions of the dorsal striatum in the rat, but this has yet to be quantified in a consistent manner in either the dorsal or the ventral striatum. The finding that both the dorsal and the ventral striatum receive topographically distinct, non-overlapping input from various cortical

areas, in combination with the recent finding that the output of the striatum is significantly different in the caudal pole of the dorsal striatum of mice suggests that both the functional input and output of the striatum is regionally heterogeneous. As striatal interneurons have been shown to receive (and therefore process) these inputs while simultaneously influencing the activity of SPNs (the striatum's output), it is likely that subpopulations of these interneurons are biased in their distribution throughout both the dorsal and ventral striatum.

1.7.2.4 Aim 4: To determine whether molecularly and topographically distinct populations of interneuron in the dorsal striatum of rodents exist in the caudate/putamen of the primate (Chapters 3, 4 and 5)

Although the dorsal striatum of primates is structurally different than that of the rodent (i.e. it exists as 2 separate structures: the caudate nucleus and the putamen), it nevertheless receives topographically distinct cortical inputs. Moreover, the results from behavioral studies discussed in section 1.3 have shown that the primate caudate/putamen can be functionally divided into 3 distinct regions along its dorso-ventral axis. These findings therefore suggest that the microcircuit of the primate striatum may also be organized in a topographically specific manner.

1.7.2.5 Aim 5: To estimate the mean density and total numbers of different populations of striatal interneuron (Chapters 3, 4, 5 and 6)

An in-depth look at stereological studies of the dorsal striatum (see section 1.4) reveals a great deal of inconsistency associated with the methods and the sampling strategies used to quantify the interneuron populations of the dorsal striatum. Thus, there is a pressing need for a more rigorous (stereological) analysis of the different interneuronal populations in the ventral striatum. Using a robust, highly repeatable sampling method and technique (see chapter 2 for details), this study will provide estimates for both the mean density and the total numbers of various types of striatal interneuron

Briefly, these broad aims will be achieved using a combination of stereological cell counting, in vivo juxtacellular recordings and immunofluorescence/confocal microcopy. These methods are covered in detail in Chapter 2.

CHAPTER 2.

MATERIALS AND METHODS

2.1 STEREOLOGICAL CELL COUNTING IN THE DORSAL AND VENTRAL STRIATUM OF RATS AND MICE

2.1.1 Preparation of brain tissue for cell counting

The experimental procedures described below were carried out using 24 adult (3 months old, 280-350g; Table 2.1) male Sprague Dawley rats (Charles River) and 12 adult, (Table 2.1) 6-week old C57B1/6J male mice (Charles River) in accordance with the Animals (Scientific Procedures) Act, 1986 (UK). After being deeply anaesthetized using isoflurane (4% v/v in oxygen), each rat was given a lethal dose of pentobarbitone (1.3g/kg; i.p.) followed by transcardial perfusion with approximately 50ml of 0.05M phosphate-buffered saline, pH7.4 (PBS) followed by 300 ml of fixative (4% w/v paraformaldehyde with 0.1% w/v glutaraldehyde in 0.1 M phosphate buffer, pH7.4 (PB)). This was followed by a third perfusion of approximately 200 ml of fixative (4% w/v paraformaldehyde in PB). Mice were deeply anesthetized with pentobarbitone and perfused transcardially using 20 ml of PBS, followed by 20 ml of fixative (4% w/v paraformaldehyde in 0.1 M PB). For both species, once the brain was removed, the tissue was post-fixed in this solution for 24 hours at 4^{o}C. Using a vibrating microtome (Leica VT1000S), 50 µm-thick parasagittal sections containing the striatum as identified using (when appropriate) either a rat brain atlas (Paxinos & Watson, 2007) or a mouse brain atlas (Franklin & Paxinos, 2008) were cut and collected in four vials for immunofluorescence processing.

Table 2.1: Numbers of animals used in this study

Animal Species	**Experimental procedure**	**Number**
Rat	Stereological cell counting	24
Rat	Juxtacellular recording and labeling	26
Mouse	Stereological cell counting	12
Rhesus Macaque	Stereological cell counting	2

2.1.2 Indirect immunofluorescence

Sections were washed with PBS (four 10-minute washes) and pre-incubated for 2 hours in a solution consisting of 10% v/v NDS (normal donkey serum) and 0.3% v/v Triton X-100 in PBS. After further washing using PBS, sections were incubated overnight at room temperature in a solution of 0.3%v/v Triton X-100 in PBS containing primary antibodies. Refer to Table 2.2 for details, source, and dilutions of antibodies used. After exposure to primary antibodies, sections were washed in PBS and incubated overnight at room temperature in Triton-PBS which contained a mixture of secondary antibodies (all raised in donkey) which were conjugated to the following fluorophores: DyLight 649 (1:500; Jackson ImmunoResearch Laboratories); Cy3 (1:1000; Jackson ImmunoResearch Laboratories); AlexaFluor-488 (1:500; Invitrogen); or AMCA (1:250 dilution; Jackson ImmunoResearch Laboratories). To ensure minimal cross-reactivity, these antibodies were cross adsorbed by the manufacturers. After further washing in PBS, sections were mounted on glass slides (VWR Super Premium Microscope slides) using fluorescence mounting medium (Vectashield; Vector Laboratories), followed by the addition of a coverslip.

Table 2.2: Primary antibodies used in this study

Molecular Marker	Host Animal	Dilution	Source and catalog number	B-cell lineage	Specificity Reference
Calbindin D28K	Guinea Pig	1:200	Synaptic Systems 214 004	Polyclonal	See below[1]
Calretinin	Goat	1: 500	Swant CG1	Polyclonal	Simmons et al., 2010
Calretinin	Rabbit	1:1000	Synaptic Systems 214102	Polyclonal	See below[1]
Choline acetyl transferase	Goat	1:500	Millipore AB144P	Polyclonal	Stacy et al., 2005
Choline acetyl transferase	Mouse	1:250	Gift, C. Cozzari mAb5	Monoclonal	Von Engelhardt et al., 2007
CTIP-2	Rat	1:500	Abcam AB18465	Monoclonal	Huang et al., 2012
Dopamine- and cAMP-regulated phosphoprotein -32	Goat	1:100	Santa Cruz SC-8483	Polyclonal	Yang et al., 2008
Forkhead box protein P1	Rabbit	1:50	Abcam AB16645	Monoclonal	Wang et al., 2011
Gephyrin	Mouse	1:500	Synaptic Systems 147 011	Monoclonal	Sakagami et al., 2013
Lim-homeobox 7/8	Guinea Pig	1:500	Gift, A. Rajkovic	Polyclonal	Pangas et al., 2006[1]
Neuronal nuclear antigen	Mouse	1:200	Millipore MAB377	Monoclonal	Foxworthy et al., 2013
Neuronal nitric oxide synthase	Mouse	1:500	Sigma N2280	Monoclonal	Olucha-Bordonau et al., 2012
Neuronal nitric oxide synthase	Rabbit	1:1000	Millipore AB5380	Polyclonal	Simmons et al., 2011
Parvalbumin	Guinea Pig	1:1000	Synaptic Systems 195004	Polyclonal	Massi et al., 2012
Pre-proenkephalin	Rabbit	1:5000	LifeSpan Biosciences LS-C23084	Polyclonal	Lee et al., 1997[2]
Secretagogin	Goat	1:1000	R&D systems AF4878	Polyclonal	See below[3]
Secretagogin	Rabbit	1:500	Abcam AB111871	Monoclonal	See below[3]
Specificity protein 8	Goat	1:30000	Santa Cruz SC-104661	Polyclonal	Cai et al., 2013

1 – This antibody recognized a single band of protein along the predicted molecular mass of the targeted protein on Western blots of cell lysates (manufacturer's data)
2 – In control experiments, use of this antibody resulted in immunolabelling that was identifical from what was achieved using an affinity-purified antibody raised against PPE in the guinea pig (Lee et al., 1997)
3 – Goat anti-Scgn and rabbit anti-Scgn were raised against different secretagogin peptide antigens but resulted in a significant overlap in immunoreactive neurons (Abdi et al., 2015)

2.1.3 Sampling and cell-counting strategies

Using a series of partly overlapping, complementary immunofluorescence protocols, striatal neurons were tested for their combinatorial expression of all the molecular markers in Table 2.2. A version of design-based stereology, the 'modified optical fractionator' (West, 1999; Abdi et al., 2015) was used to generate unbiased cell counts, determine the relative expression of molecular markers, and map distributions of striatal interneurons. In all procedures performed, the accuracy of these estimates was ensured by taking absolute counts of all neurons expressing a given molecular marker, thereby allowing for a nearly precise definition of their distribution within the striatum.

The analysis of dorsal striatal expression of specific molecular markers was performed using 13 coronal striatal planes (protocols involving Lhx7 were performed using 9 coronal sections) (Figure 2.1). For protocols performed using mouse striatum, 9 coronal planes were used (Figure 2.2). Stereological cell counts in protocols associated with the rat nucleus accumbens were performed using 5 sections across the rostro-caudal axis of the structure. Each section included both the core and the shell of the nucleus accumbens (Figure 2.3). In many stereological studies looking to investigate the total numbers of neurons in a given structure, unbiased sampling is maintained by giving all coronal planes within the structure (i.e. either the dorsal or ventral striatum) the same probability of being sampled (West, 1993; 1999). The random nature of this sampling should also carry across all animals that were used, such that the sections chosen for one animal do not necessarily have to match those chosen for the next animal in the study. Additionally, sections do not have to be equally distributed throughout the structure as they are chosen at random.

Admittedly, this method of random sampling is, strictly speaking, statistically superior if one is interested entirely in calculating the total number of neurons in a given structure (Oorschot, 1994). However, as this study was also interested in investigating the distribution of interneurons

across all of the striatal planes defined in Figures 2.1, 2.2 and 2.3 in a quantitatively and statistically robust manner, chosen sections from all animals were matched with one another such that sections representing the same distance from Bregma (±50 μm) were chosen. This ensured that the results from all animals studied could be averaged to produce more accurate results regarding the number of counted neurons within a given coronal plane. In order to calculate changes in the density of counted neurons along the rostro-caudal axis, the chosen sections for a given protocol were distributed throughout the entirety of the dorsal or ventral striatum. This allows for a sampling that is consistent rather than random, but carries with it the advantage of providing a detailed look into neuronal distribution along specific planes of the rostro-caudal axis. In this context, a random sampling of sections would therefore not be ideal, as it carries the risk of not choosing large regions of a given structure such that the distribution of counted neurons within those regions would remain unknown. Moreover, as certain striatal planes are more often used for tetrode recordings (Gremel & Costa, 2013; Atallah et al., 2014) in behavioral studies (eg. 0.3 mm ahead of bregma in the case of the dorsal striatum), it is important to specifically include those planes in this study, in order to make the data produced as relevant as possible in the current state of the field as a whole.

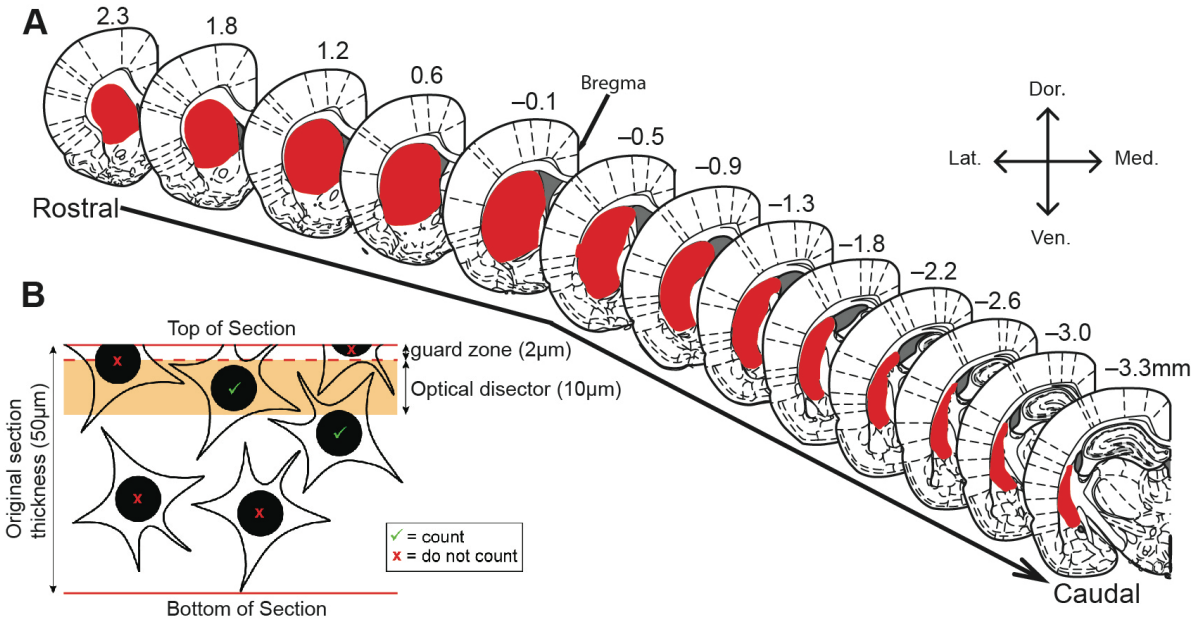


Figure 2.1: Coronal planes associated with the use of the stereological cell counts in the dorsal striatum of the rat. A) Sections of the rat brain taken from Paxinos and Watson, 2007; showing the dorsal striatum (red) at the 13 coronal planes that were used across the rostro-caudal axis of the dorsal striatum. Dorsal (Dor.), ventral (Ven.), lateral (Lat.) and medial (Med.) directions are labeled. The location of the sections with respect to Bregma is noted. **B)** Schematic representation of the optical disector method, showing which neurons would be counted within the 10µm optical disector based on the position of the top of their nuclei.

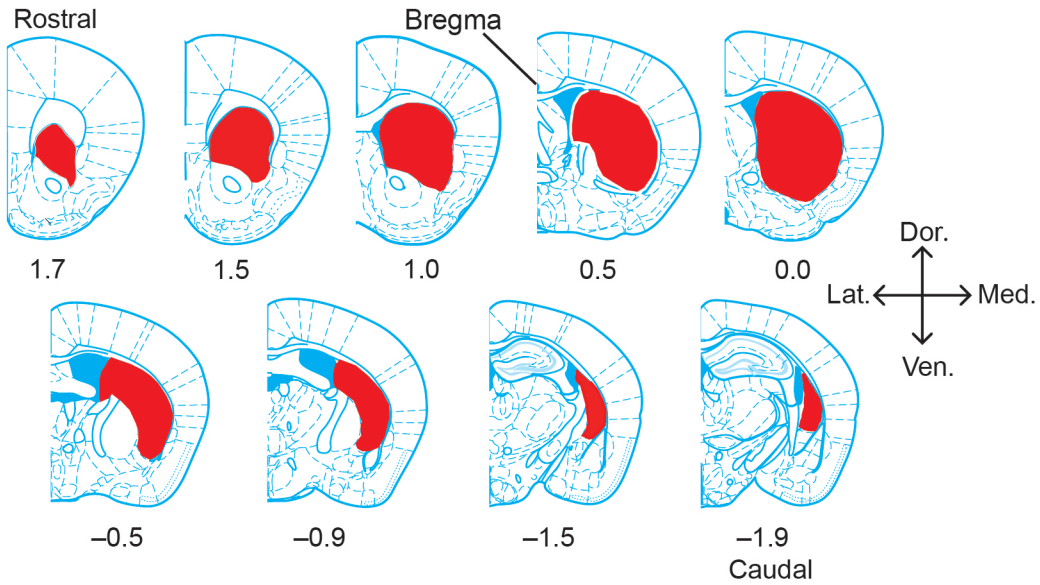


Figure 2.2: Coronal planes associated with the use of the stereological cell counts in the dorsal striatum of the mouse. Sections of the rat brain taken from Franklin & Paxinos, 2008; showing the dorsal striatum (red) at the 9 coronal planes that were used across the rostro-caudal axis of the dorsal striatum. Dorsal (Dor.), ventral (Ven.), lateral (Lat.) and medial (Med.) directions are labeled. The location of the sections with respect to Bregma is noted.

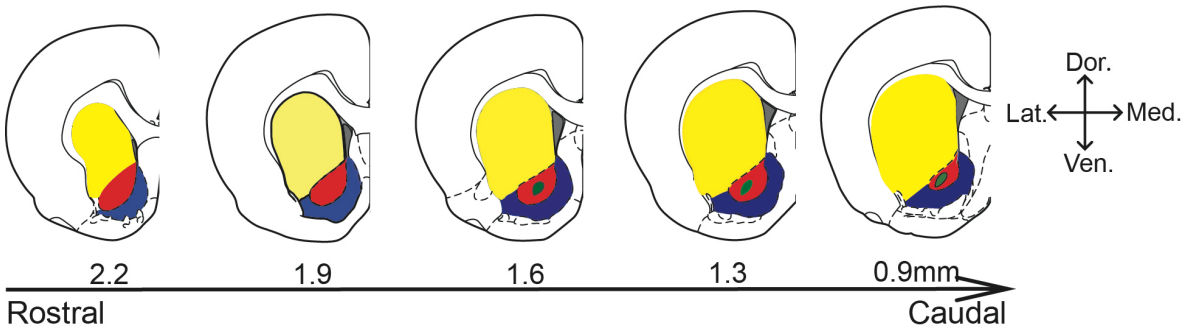


Figure 2.3: Coronal planes associated with the use of the stereological cell counts in the ventral striatum. Sections of the rat brain taken from Paxinos and Watson, 2007; showing the dorsal striatum (yellow), nucleus accumbens shell (red) and core (blue) and anterior commissure (green). Dorsal (Dor.), ventral (Ven.), lateral (Lat.) and medial (Med.) directions are labelled. The location of the sections with respect to Bregma is noted.

Once the chosen striatal coronal planes were identified and incubated in primary and secondary antibodies, a Zeiss Imager M2 epifluorescence microscope (Carl Zeiss, AxioImager.M2) running Axiovision software (Carl Zeiss) and equipped with a 20X (Numerical Aperture = 1.8) objective and StereoInvestigator 9.0 software (MBF Biosciences) were used to delineate the dorsal or ventral striatum. In order to image each fluorescence channel, the following sets of filter cubes were used: AMCA (excitation 299–392 nm, beamsplitter 395 nm, emission 420–470 nm); AlexaFluor-488 (excitation 450–490 nm, beamsplitter 495 nm, emission 500–550 nm); Cy3 (excitation 532–558 nm, beamsplitter 570 nm, emission 570–640 nm); and DyLight 649 (excitation 625–655 nm, beamsplitter 660 nm, emission 665–715 nm). The borders of the dorsal striatum were determined using immunofluorescence for calretinin, calbindin as well as the boundaries defined in standard stereotaxic atlases for rat (Paxinos & Watson, 2007) and mouse (Franklin & Paxinos, 2008). This immunohistochemical combination was done for the 13 specific coronal planes (Figure 2.1) chosen for the rat and the 9 specific coronal planes (Figure 2.2) in the mouse in order to create a "reference" set of delineations. Because calretinin and calbindin could not be used in every experiment, all chosen sections for every protocol were delineated using these reference set of contours in order to ensure that all scanned areas were relatively consistent. Importantly, it should be noted that these references were not strictly

followed for every delineation; since every animal is of course different and slight variations in striatal boundaries were accounted for when contours were drawn.

In order to create similar reference contours for the 5 coronal sections containing the ventral striatum in rats, a novel immunohistochemical combination was required to delineate the boundaries of the nucleus accumbens, as well as the boundary between the shell and the core (see section 1.5). The delineation of these boundaries often represents one of the major difficulties associated with anatomical studies of the ventral striatum. The definition of the medial and lateral borders is particularly poor, with little to no description of its delineation currently existing in the literature (Paxinos & Watson, 2007). Here, a combination of FOXP1, calbindin and calretinin immunofluorescence was used together with the rat brain atlas (Paxinos & Watson, 2007) in order to create a set of reference planes similar to those used for the dorsal striatum (Figure 2.4). FOXP1 was chosen as it is known to label the nuclei of spiny projection neurons within the striatum (Tamura et al., 2004), while CB has been shown to be strongly expressed in the core but not the shell of the nucleus accumbens (Prensa et al., 2003). Immunofluorescent detection of CR for this "reference protocol" was thought to be important given its weak labelling of the nucleus accumbens core (Prensa et al., 2003) and its strong fiber labeleling in the dorsal striatum. As such, CR-expression was used to delineate the boundary between the dorsal and ventral striatum (Figure 2.4). This combination of FOXP1, CB and CR described in this study therefore not only allows for the definition of the medial border of the shell, but also delineates the boundary between the core and the shell, as well as that between the ventral and dorsal striatum as a whole. However, the ventro-lateral border remained ambiguous using this combination of immunohistochemical markers, and so the rat brain atlas (Paxinos & Watson, 2007) was used to guide the delineation.

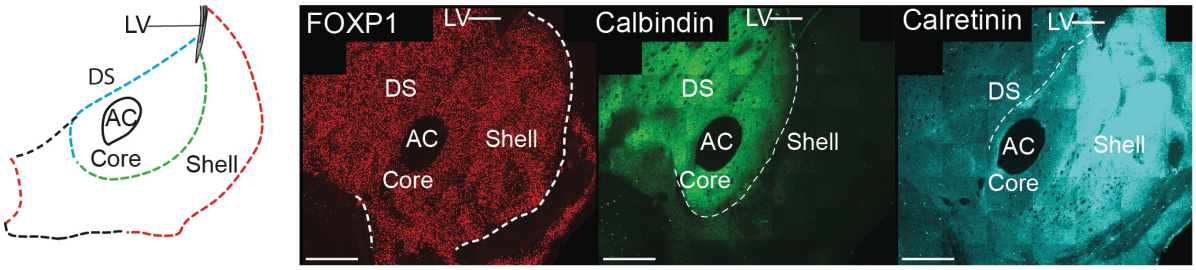


Figure 2.4: Immunohistochemical delineation of the borders in the ventral striatum.
Diagram demonstrating the delineation of multiple borders within the nucleus accumbens within a coronal plane 1.9mm ahead of bregma. FOXP1 reactivity was used to define the medial border of the NAcc (red line), calbindin defined the border between core and shell (green line), and calretinin defined the border between the accumbens core and the dorsal striatum (blue line). The rat brain atlas (Paxinos & Watson, 2007) was used to define the black lines.

Once boundaries were delineated for a given section that had undergone a given immunofluorescence protocol, the selected area was subsequently captured by imaging a series of completely tessellated, z-stacked images (with an optical step size of 1µm) at depths 2 to 12µm from the upper surface of each section at the level of the striatum. This was done using the 20X 1.8 NA objective lens of a Zeiss Imager M2 epifluorescence microscope (Carl Zeiss, AxioImager.M2) running Axiovision software (Carl Zeiss) and StereoInvestigator 9.0 software (MBF Biosciences). The thickness of the section was measured at each counting site and then averaged to obtain a correction factor for tissue shrinkage. The average section thickness was found to be 44.8 ± 0.98µm in rats meaning that the calculated shrinkage factor was ~ 11.4%. In mice, the average section thickness was found to be 46.3 ± 1.2µm, resulting in a calculated shrinkage factor of ~7.4 %. To minimize the confounds arising from surface irregularities, neuropil within a 2µm 'guard zone' at the upper surface was not imaged (Figure 2.1B). By sampling sections in this manner, a 10µm thick "optical disector" was generated which had abutting, unbiased 2D counting frames (320 x 420 µm) consisting of two perpendicular exclusion lines and two inclusion lines. This was used to generate all stereological cell counts and molecular expression profiles presented in this study (West, 1999, 2012; Glaser et al., 2007), and allowed for the generation of robust and unbiased stereological cell counts.

A labeled neuron was counted if the top of its nucleus came into focus within the disector. If the nucleus was already in focus at the top of the 10 μm-thick optical disector, the neuron was excluded (West, 1999). As strongly fluorescent cytoplasmic/nuclear markers can obscure nuclear boundaries, delineation of these nuclei was achieved when necessary by incubating the tissue for 10 minutes in a solution (1:100000) of the DNA dye 4',6-diamidino-2-phenylindole (DAPI). For a given molecular marker, X, positive immunoreactivity (confirmed expression) was denoted as X+ while undetectable immunoreactivity (no expression) was denoted as X−. In all fluorescence analysis, a neuron was classified as not expressing the tested marker only when positive immunoreactivity could be observed in other cells on the same optical section as the tested neuron. Each immunofluorescence protocol described in this study was repeated in a minimum of three adult rats/mice. The data obtained from each count was subsequently exported from StereoInvestigator (MBF Biosciences) into Excel (Microsoft) or Matlab (Mathworks), where they were pooled for further analysis.

2.2 ANALYSES OF DATA OBTAINED FROM STEREOLOGICAL CELL COUNTS

2.2.1 Calculations of section area, volume and estimates of total cell number

Once the number of neurons expressing a marker or markers had been counted and recorded for a given coronal plane, the volume of the striatum in which these neurons had been counted was first calculated. The cross-sectional area of a given delineated region was calculated using StereoInvestigator 9.0 software (MBF Biosciences). The software uses a method that is derivative of the point counting method often cited in older stereological studies (Oorschot, 1996). The value for the cross-sectional area obtained from StereoInvestigator was checked manually in a few cases through the point counting method described below. Since each set of counts was performed within the confines of an optical disector of a depth of 10 μm, the cross sectional area could be multiplied by this depth in order to obtain the volume of striatum in which the counts were performed for a given section. Because each count represents the total number of immunoreactive neurons (i.e. it is not an estimate) within this volume, dividing this number by the calculated volume yields the absolute density of immunoreactive neurons in that specific volume. By assuming that the density of immunoreactive neurons is constant within the 50 μm thick tissue section (corrected for tissue shrinkage in mice and rats), then the calculated value for absolute density applies to the entire section. This absolute density value was calculated for every plane studied for all counted neurons and the values were plotted to demonstrate changes in density along the rostro-caudal axis of the dorsal or ventral striatum. This plot is used to describe the distribution of neurons along the rostro-caudal axis (see below for how distribution along the medio-lateral and dorso-ventral axes was calculated).

In order to calculate an estimate of the total number of neurons in the striatum, the following equation (Oorschot, 1996) was used:

$$\mathbf{N = Nv * V(ref)}$$

where N is the estimate for the total number of neurons in the structure, Nv is the numerical or volume density and V(ref) is the volume of that structure.

It should be noted that numerical density is an inappropriate value to present as a reference value, since it is determined by both the number of neurons in a structure as well as its volume (West, 1999). Indeed, the numerical density is calculated simply as the sum of all counted neurons divided by the volume in which they were counted (i.e. just in the optical disector and not the whole section thickness). Thus, studies looking to compare changes in neuronal number (as a consequence of either physiological or pathological change) to the values obtained by studies in "control animals" (such as this one) must be provided the total number of neurons, and they should always be sure to calculate total numbers as well. This is due to the fact that disease states or other models may change striatal volume, which would impact numerical density despite having no effect on the total cell number. Thus, a calculation of numerical density and total volume of the structure must be performed.

The volume of the dorsal and ventral striatum in rats and the dorsal striatum of mice was calculated using the Cavalieri direct volume estimate (Gundersen & Jensen, 1987) which involves multiplying the sum of the cross sectional area of every nth serial section multiplied by the fixed distance between each of the sampled sections. In studies of this nature, approximately 10-15 sections that span the entirety of the structure along one plane are sufficient for an accurate estimate of volume (Gundersen & Jensen, 1987; West, 1993). For the volume of the nucleus accumbens, 10 equally spaced sections of 50-µm thickness were used while the volume of the dorsal striatum in both rats and mice was calculated using 13 equally spaced 50-µm sections. The striatum in each chosen section is delineated using select immunohistochemical markers (see

above) and the point counting method option of the StereoInvestigator 9.0 software (MBF Biosciences) was then applied in order to obtain an estimate of each of the section's cross-sectional area (which could then be used to calculate the volume of the optical dissector). This involved overlaying a grid of equally-spaced points over each delineation of the structure, and then counting the number of points that lie within the contour of the structure. The spacing of the points is often set such that approximately 100-150 points lie within the entire of set of contours for a given structure. This ensures that the coefficient of error (CE - also referred to as the Gundersen coefficient in this context) is below 0.1 in order to increase the precision of the estimate. In all trials, the spacing between points within the grid was set such that the CE was ~0.03 which meant that approximately 150 points fell within the entire set of contours. Once complete, the volume of the structure V(ref) was calculated according to the following (Oorschot, 1996; West, 1999):

$$\mathbf{V(ref) = \sum P * a(p) * t}$$

where P is the number of points counted within a delineated contour, a(p) is the area represented by each point and t is the fixed distance between each section. When calculated in this manner across the striatum of 9 rats, the mean volume of the dorsal striatum was determined to be 23.2 ± 2.1 mm^3. This value is similar to previous estimations for the volume of the dorsal striatum in the rat (Oorschot, 1999; Rymar et al., 2004). A similar calculation was performed for the ventral striatum, which yielded an estimate of 1.8 ± 0.1 mm^3 (n = 6) for the volume of the nucleus accumbens core and a value of 2.9 ± 0.1 mm^3 (n = 6) for the volume of the nucleus accumbens shell. Once the value of V(ref) for each structure in each animal is determined, multiplying that volume by the absolute neuronal density yields an estimate for the total number of neurons for that animal. The mean value for all animals was then plotted in the form of bar graphs for many of the neuronal populations that were investigated as part of this study. Because most neuronal counts were performed across 3 animals (a sample that is typical of stereological studies), in depth statistics were deemed inappropriate, and so the value calculated from each animal is plotted along with the mean.

2.2.2 Topographical and statistical analysis of interneuron distribution

In order to gain a quantitative understanding of any spatial biases in cell distributions, data obtained using StereoInvestigator regarding the position of individual interneurons and the volume of striatum imaged in a given coronal section were imported into MATLAB software (Mathworks, version: R2014b) for analyses with custom written scripts. For those counts performed in the dorsal striatum, horizontal and vertical lines were first "drawn" from the position of each interneuron within a given coronal plane. Each interneuron was then assigned a value of between -1 and 1 according to its relative distance from the lateral and medial borders of striatum at that same coronal plane. For example, an interneuron located on the lateral border of dorsal striatum would be assigned a value of -1, whereas an interneuron on the medial border have value of 1, and an interneuron located near the centre of the striatum would be assigned a value close to 0. Each interneuron was also assigned a value of between -1 and 1 according to its distance from dorsal and ventral borders. Notably, these two distance values (one in the medio-lateral axis and the other in dorso-ventral axis) were calculated according to the first points along the striatal contours that were contacted by the horizontal and vertical lines drawn from each intern's position. In this manner, the definition of "medial" and "lateral" striatum was shifted depending on the position of the interneuron in the dorso-ventral plane. Likewise, the definition of "dorsal" and "ventral" striatum was also shifted depending on an interneuron's position in the medio-lateral plane. This method of normalisation therefore accommodates the irregular, ever changing shape of the dorsal striatum when viewed over multiple coronal planes.

In the nucleus accumbens however, the definition of medial and lateral nucleus accumbens core and shell are defined anatomically based on the reciprocal inputs and outputs of that structure (Ikimoto et al., 2007). This anatomically defined medio-lateral division is shown in Figure 2.5 as the vertical dashed line for the shell (blue) and core (red) of the nucleus accumbens (Ikimoto et al., 2007). In keeping with these divisions, the core and shell of the nucleus accumbens were divided by a either a vertical line (separating medial and lateral) or a horizontal

line (separating dorsal and ventral) drawn at the midpoint between the 2 extreme values of the structure's contour (in a given coronal section) in both the dorso-ventral plane or the medio-lateral plane (Figure 2.5). Each interneuron was then given a value between -1 and 1 based on its position relative to the lines drawn at the extreme values of the structure's contour (i.e. the medial/lateral most points and the dorsal/ventral most points).

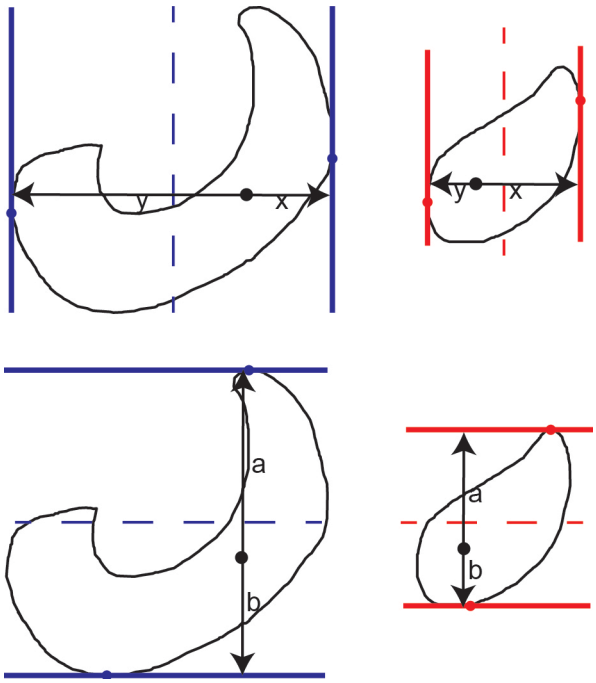


Figure 2.5: Calculating medio-lateral and dorso-ventral bias in shell (blue) and core (red) of rat nucleus accumbens.
For a given interneuron (black dot), distribution values were calculated as a ratio, from most lateral (-1.0) to most medial (1.0). Medio-lateral biases in the core and shell were calculated by x/y to determine the presence of any medial bias, -y/x to determine the presence of any lateral bias. Dorso-ventral bias in the core and shell were calculated by a/b to determine the dorsal bias, and -b/a to determine the ventral bias. This example is given from a section 1.3mm ahead of Bregma.

As each counted interneuron in a section is given a value for each axis analyzed, and at least 3 animals were used for each protocol, the sample size was deemed large enough for the use of the Wilcoxon signed-rank test in order to determine if the mean relative value of a neural population in a given coronal plane differed significantly from 0, a value indicating an unbiased distribution along a given axis. The minimum significance level for these statistical tests was taken to be $p \leq 0.05$, and is denoted in plots by the presence of an asterisk (*). In order to compare the mean positional values of two different interneuron populations along the medio-lateral or dorso-ventral axis within a given coronal plane, the Mann-Whitney U test was performed. The minimum significance level for these statistical tests was taken to be $p \leq 0.05$, and is denoted by

the presence of a box (□). As multiple statistical tests were performed, a multiple test correction known as the false discovery rate (FDR) was used to assess the significance of a given P-value in order to avoid false positives (**Noble, 2009**). Interneuron density within a given coronal plane was calculated by dividing the number of counted cells by the volume of the optical disector in which the cells were counted. With respect to its analysis however, the use of statistics was found to be inappropriate due to the use of a sample size of 3, a value that is often seen in studies of this nature. As such, the results of all 3 animals are plotted, with the mean density value at each plane being shown as a line plot.

2.2.3 Measurements of mean somatic diameters

Immunofluorescent detection of markers that labeled the entirety of the soma of certain classes of interneuron (eg. CR) was used in order to measure the somatic diameters of individual neurons in the dorsal and ventral striatum. A neuron was only measured if the contours of its entire soma were contained within the 10 µm optical dissector along all 3 dimensions. As previously described (Rymar et al., 2004), this was done in order to ensure that the longest axis of a chosen neuron's soma was imaged. The somatic diameter of a labeled neuron was defined as the length of its longest axis, and was measured using StereoInvestigator 9.0 software (MBF Biosciences). For a given class of interneuron, the mean of all somatic diameters measured in this manner was calculated. Statistical comparisons of multiple mean somatic diameters (of multiple classes of interneuron) were performed using one-way ANOVA test followed by post hoc Tukey's HSD (honestly significant difference) test (where appropriate). Significant differences were reported at $P \leq 0.05$.

2.3 JUXTACELLULAR RECORDING AND LABELLING

2.3.1 In vivo electrophysiological recording and juxtacellular labeling of single neurons

Juxtacellular recording and labeling of neurons was performed in 26 anesthetized male Sprague Dawley rats (280-350g) in accordance with the Animals (Scientific Procedures) Act 1986 (UK). The induction of anesthesia was achieved using 4% v/v isoflurane in O_2, and maintained with urethane (1.3g/kg, i.p; ethyl carbamate; Sigma), and supplemental doses of ketamine (30 mg/kg, i.p.; Willows Francis) and xylazine (3 mg/kg i.p.; Bayer). Local anesthetic was used to infiltrate the wound margins (0.5% w/v bupivacaine; Astra). A stereotaxic frame (Kopf) was used to fix the animal in place, and a homeothermic heating device (Harvard Apparatus) was used to maintain the animal's temperature at 37 ± 0.5°C. In addition, the animal's welfare was confirmed via the constant monitoring of its electrocorticogram (ECoG) and its respiration. Recording of the ECoG was performed directly above the frontal (somatic sensory-motor) cortex (4.0 mm rostral and 2.0 mm lateral of Bregma) (Paxinos and Watson, 2007), with the reference screw being placed above the ipsilateral cerebellum (Sharott et al. 2012; Abdi et al., 2015). The signal then underwent bandpass filtration (0.3-1500 Hz, –3dB limits) and amplification (2000x; DPA-2FS filter/amplifier; NPI Electronic Instruments) was applied to the raw ECoG prior to its acquisition. Using a computer-controlled stepper motor (IVM-1000; Scientifica), standard-wall borosilicate glass electrodes (10-30 MΩ in situ with a tip diameter of approximately 1.5 μm) filled with a 0.5M solution of NaCl and neurobiotin (1.5% w/v; Vector Laboratories) were lowered into the dorsal striatum (under stereotaxic guidance). The depth of the electrode was constantly monitored and recorded by the computer at a resolution of 0.1 μm. Action potentials of individual striatal neurons (i.e. single-unit activity) were subsequently recorded after being amplified (10x) (Axoprobe-1A amplifier; Molecular Devices), AC-coupled, bandpass filtered at 300-5000 Hz (DPA-2FS filter/amplifier) and then amplified one more time by a factor of one hundred. Both the ECoG and single-unit activity were recorded at a sampling rate

of 16.6 kHz using a Power1401 Analog-Digital converter and a PC running Spike2 acquisition and analysis software (Version 7.2; Cambridge Electronic Design).

Using the ECoG, the anaesthetized animal's brain state was defined and categorized as slow-wave activity (SWA) or cortical activation (Magill et al., 2001; Sharott et al., 2012). In most experiments, single-unit activity of striatal neurons was recorded in either one or both of these states. Cortical SWA is characterized by the appearance of large-amplitude slow oscillations (~1 Hz), which appear as alternating surface-positive "active components", and surface negative "inactive components" (Mallet et al., 2008) in the ECoG. Both spindle (7-12 Hz) and gamma (27-45 Hz) oscillations also appear in this brain state, which is analogous to what is observed during drowsiness and non-rapid eye movement sleep (Steriade, 2000). In contrast, cortical slow and spindle oscillations are not present in the activated brain state, which is most similar to the brain activity recorded during the alert, behaving state. In addition to recording single-unit activity during spontaneous brain states, recordings were also performed during activated states elicited via the pinching of the hind paw for 15 seconds (Magill et al., 2006). Such pinches were also given during states of spontaneous cortical activation during certain experiments. In all experiments performed, substantial changes to the electrocardiogram or respiration rate did not occur, nor did the animal exhibit a hind paw withdrawal reflex in response to the pinch. Such findings indicate that anesthesia was maintained at an adequate level throughout the experiment. Finally, although neuronal activity recorded under anesthesia is only qualitatively similar to that present in the unanaesthetized brain; the model presented above serves its purpose in demonstrating the effect that different brain states have on the functional connectivity within and between the cortex and the basal ganglia (Magill et al., 2004; Sharott et al., 2012).

Once a neuron was recorded, it was juxtacellularly labeled with neurobiotin (Magill et al., 2001; Sadek et al., 2007; Mallet et al., 2012). Such labeling was achieved by sending continuous positive pulse currents (2-10 nA, 200 ms, 50% duty cycle) through the electrode until the recorded single-unit activity was "entrained" by the injection of current. In most cases, this

entrained state was maintained for an average of 3 minutes in order to ensure adequate labeling. Approximately two to six hours after labeling, animals were given a lethal dose of ketamine (150 mg/kg) followed by a transcardial perfusion using 100ml of PBS, followed by 300 ml of 0.1% w/v glutaraldehyde and 4% w/v paraformaldehyde (PFA) in 0.1 M phosphate buffer, pH 7.4 (PB), and then by 200 ml of 4% w/v PFA in PB. Once retrieved, brains were left for a period of 24 hours in a fixative solution of 4% w/v PFA in PB.

2.3.2 Tissue processing for identification of recorded and labeled neurons

Using a vibrating microtome (VT1000S; Leica Microsystems), 50µm-thick coronal sections were serially collected and subsequently washed in PBS for 10 minutes. Sections were then incubated for a minimum of 4 hours in a solution of Triton PBS (PBS containing 0.3% v/v Triton X-100 [Sigma]) and Cy3-conjugated streptavidin (1:1000; Life Technologies). Sections were analyzed for Cy3 immunoreactivity, and those containing neurobiotin-labelled cells were isolated and subjected to further molecular characterization by indirect immunofluorescence. Neurons appearing to possess dendritic spines were defined as spiny projection neurons (SPNs). In certain cases, they were also tested for their expression of CTip-2, a nuclear marker that has been shown to be exclusively expressed in the SPNs of rats and mice but not in interneurons (Arlotta et al., 2008). Neurons that did not express CTip-2 or possessed aspiny dendrites were tested for their expression of classical markers of striatal interneurons, namely parvalbumin, choline acetyltransferase, nitric oxide synthase, or calretinin. When appropriate, certain labelled neurons were tested for their expression of secretagogin (Mulder et al., 2009). The initial molecular marker test was guided by the labeled cell's somatodendritic structure and position within the striatum, and once a positive expression for one of these markers was established, no other classical marker was tested since these molecules are rarely co-expressed (Kawaguchi et al., 1995).

In order to test for the expression of these markers, the indirect immunofluorescence protocol described by Mallet et al., 2012 was used. Sections containing neurobiotin labeled neuronal somata were incubated in a solution of Triton-PBS and 10% v/v normal donkey serum (NDS; Jackson ImmunoResearch Laboratories) for 1-2 hours. These sections were subsequently incubated overnight at room temperature in a solution containing Triton-PBS and 1% v/v NDS and one or more of the following primary antibodies listed in table 1. Sections were then washed in PBS (3 times 10 minutes) and incubated for a minimum of 4 hours at room temperature in a solution of Triton-PBS and one of the fluorophore-conjugated secondary antibodies (all of which were raised in donkey) described previously in section 2.1.

After being washed one final time in PBS, sections were mounted on glass slides in Vectashield (Vector Laboratories) and single-plane confocal images were acquired using the 20x/40x objective lens of a laser scanning confocal microscope (Zeiss LSM 710). Appropriate sets of laser beams and emission windows were used for Alexa Fluor 488 and DyLight 488 (excitation 488 nm, emission 492–544 nm), Cy3 (excitation 543 nm, emission 552–639 nm), and Cy5 and DyLight649 (excitation 633 nm, emission 639–757 nm). For each section, absence of bleed through or cross talk across channels was ensured by taking sequential and separate images. Importantly, neurons were declared "negative" for a given marker if other neurons along the same focal plane were shown to express the same marker. In cases where neurobiotin labeling of a recorded neuron was deemed highly successful, images were taken at multiple planes in order to form a z-stack to highlight its somatodendritic structure.

2.3.3 Data selection and analysis regarding the firing rate and regularity of identified striatal interneurons

Data from Spike 2 was visually inspected, and epochs of robust cortical SWA or cortical activation were selected based on previous descriptions of these ECoG states (Magill et al., 2006; Mallet et al., 2008; Sharott et al., 2012). Recordings were included for further analysis only if they were artifact free and had a minimum duration of 100 seconds regardless of the brain state.

On average, the majority of epochs analyzed were between 60 and 487s (221 ±16.69 [mean durations ±SEMS]). Spike sorting procedures such as template matching, principal component analysis and clustering (Mallet et al., 2008a) were applied using Spike 2 software in order to isolate single unit activity. Isolation of a single unit was verified by the presence of a distinct refractory period in the interspike interval (ISI) histogram. Further analysis was later conducted after having converted single unit activity into a binary digital event (Spike 2) which was subsequently imported and analyzed using MATLAB software (MathWorks).

The firing frequency (spikes/s) of each recorded neuron was calculated as the number of spikes in a given epoch of data. Statistical comparisons of firing activity between 2 populations were performed using the Mann-Whitney U or Wilcoxon signed rank tests for definition of significant pairwise differences, where appropriate. Compairasons of the firing patterns of 3 or more populations were performed using Kruskal-Wallis ANOVA on ranks. The minimum significance level for these statistical tests was taken to be $p \leq 0.05$ and is indicated by the presence of an asterisk (*) in the appropriate plots. Box plots illustrating the results of these tests display medians; the interquartile ranges (box edges) and extremes of range (whiskers containing 99% of the distribution).

2.3.4 Firing of identified striatal interneurons in relation to cortical oscillatory activity

To investigate how the activity of individual striatal neurons varied in time with respect to ongoing cortical network activity, we analyzed the instantaneous phase relationships between striatal spike times and cortical oscillations of different frequencies during cortical SWA and activation. Electrocorticogram signals containing robust SWA or activation were first filtered, using a neutral-phase bandpass filter (1-3 order Butterworth filter,) in 117 overlapping frequencies with exponentially increasing centre frequencies of 1-80Hz and increasing widths of the plus/minus 1.5x the centre frequency. The instantaneous phase and power of the ECoG in these frequency bands were separately calculated from the analytic signal obtained via the Hilbert transform (Lachaux et al., 1999). In this formalism, peaks in the ECoG oscillations correspond to a phase of 0° and troughs to a phase of 180°. Circular phase plots and circular statistical

measures were calculated using the instantaneous phase values for each spike in relation to each frequency band. Descriptive and inferential circular statistics were then calculated using the CircStat toolbox (Berens, 2009) for MATLAB. We included only those neurons that fired $\geqslant$40 spikes during the entire analyzed epoch. Phase histograms were constructed using 20 phase bins and used to construct pseudocolor plots of probability of firing as a function of phase for each frequency band. These neurons were then tested for significantly phase-locked firing in each frequency band (defined as having $p < 0.05$ in Rayleigh's Uniformity Test). The null hypothesis for Rayleigh's test was that the spike data were distributed in a uniform manner. The power of the ECoG in the SWA band was compared in data epochs used for analyses of phase-locked striatal neuron firing to test whether they were significantly different between groups. For oscillations of frequencies below 5Hz, Rayleigh tests were only carried out after any phase non-uniformities of the slow oscillations were corrected with the empirical cumulative distribution function (Siapas et al. 2005; Nakamura et al, 2014).

2.4 IDENTIFICATION AND QUANTIFICATION OF AXONAL BOUTONS OF JUXTACELLULARLY-LABELED INTERNEURONS

2.4.1 Immunofluorescence labeling and confocal imaging of neurobiotin-filled axonal boutons

In order to determine whether identified PV+/Scgn+ and PV+/Scgn– interneurons innervated different targets in striatum, the following procedures were established. After in vivo recordings and strong juxtacellular labeling of select interneurons, all sections containing intense Cy3 signal for neurobiotin were isolated. The section(s) containing the cell body were separated from those containing neurobiotin-filled dendrites or axons. These cell body containing sections were then subject to tests for PV and Scgn immunohistochemistry in order to determine whether the labeled cell expressed one, both or neither of these proteins. If a cell was determined to be PV+/Scgn+ or PV+/Scgn–, all sections containing the neurobiotin filled axons of the corresponding cell were incubated with the following primary antibodies (see Table 2.2): goat α-DARPP-32, rabbit α-Preproenkaphalin (PPE) and mouse α-gephyrin using the same 2-step incubation method described above for stereological cell counting (see section 2.1.2 for more details). The presence of a DARPP-32 signal was used to mark the somata of spiny projection neurons and the expression of PPE was used to determine whether a DARPP-32 expressing SPN was of the direct pathway (PPE–) or indirect pathway (PPE+). Gephyrin, a post-synaptic protein involved in the anchoring of inhibitory receptors to the neuron's cytoskeleton (Charrier et al., 2006) was used as a marker of putative synapses. Although gephyrin could not be included in all counts, the detection of its expression at the point of contact between a neurobiotin-filled axon bouton and the edge of the DARPP-32 signal was used as indirect evidence of the existence of synapses between axonal boutons and SPN somata.

After one final wash in PBS, each section was mounted on a glass slide in Vectashield (Vector Laboratories) and multiple single-plane confocal images (referred as stacks) were acquired using a 1µm optical dissector and a 63x objective lens of a laser scanning microscope (Zeiss LSM 710). Once again, appropriate sets of laser beams and emission windows were used

for Alexa Fluor 488 and DyLight 488 (excitation 488 nm, emission 492–544 nm), Cy3 (excitation 543 nm, emission 552–639 nm), and Cy5 and DyLight649 (excitation 633 nm, emission 639–757 nm). For each section, bleed through was negated by the taking of sequential and separate images of each fluorescence channel.

2.4.2 Analysis and counting of appositions made by the axons of identified interneurons

Captured images of axon containing sections were analyzed using Zeiss imaging software (Carl Zeiss Microscopy, GmbH). Due to the availability of only 3 fluorescence channels on the confocal microscope, most sections containing neurobiotin-filled axons were incubated with antibodies against DARPP-32 and PPE, and not gephyrin. In such sections, putative synapses made between interneurons and other striatal cells could not be identified, and appositions were instead defined when an axonal bouton (a swelling of the axon) was in close proximity (~0.1 μm) to the cell body of a DARPP-32+ SPN. Appositions were established after verification that there were no detectable pixels between the cell body signal and the neurobiotin signal of the axonal bouton. These appositions could be viewed in 3 planes using the software to ensure that the swelling of the axon defined as a bouton was consistent in 3 dimensions and was not the result of overexposure of the neurobiotin signal. For each section, the number of boutons on the neurobiotin-filled axon of an identified striatal interneuron was counted. These counts included those boutons that apposed the cell bodies of SPNs as well as those that did not. In cases where a bouton contacted an SPN cell body, the expression of PPE (or lack thereof) was used to determine whether that spiny projection neuron was a direct (PPE–) or indirect (PPE+) pathway neuron. This was also counted and recorded.

In total, the neurobiotin filled axons of 4 PV+/Scgn– and 4 PV+/Scgn+ interneurons were assessed in this manner, which allowed for the counting of over 1000 boutons. For each neuron, boutons were classified as either apposed to SPN cell bodies or not apposed. Those boutons that were apposed were further classified as apposed to PPE+ or PPE– cell bodies. The counts for

each neuron were averaged with those of other neurons belonging to the same group (i.e. PV+Scgn– or PV+/Scgn+). These values were then plotted in the form of bar graphs along with the SEMs. Statistical comparisons comparing whether one group significantly differed from another were performed using the Fisher exact test. The minimum significance level for these statistical tests was taken to be $p \leq 0.05$.

2.5 STEREOLOGICAL CELL COUNTS IN THE CAUDATE AND PUTAMEN OF THE RHESUS MONKEY

2.5.1 Tissue preparation and indirect immunofluorescence

All Rhesus monkey (*Macaca mulatta*) tissue used in this study was obtained from Dr. Yoland Smith's group in Emory University, Atlanta, GA, USA. All procedures performed were approved by the Institutional Animal Care and Use Committee at Emory University and conform to the U.S. National Institutes of Health Guide for the Care and Use of Laboratory Animals (Garber et al., 2010). The tissue from 2 female Rhesus monkeys (3–9 years old; 5–8 kg) arrived sectioned and stored in PBS, and only 60µm-thick coronal sections containing the caudate and the putamen were delivered. Unfortunately these sections did not contain the tail of the caudate nucleus, and so it was not possible to include it in this study. A detailed description of the experimental approaches used by the Smith group can be found in Gonzales et al., 2013. Briefly, female Rhesus monkeys from the Yerkes National Primate Research Center colony were anesthetized using an overdose of pentobarbital (100 mg/kg, i.v.). Transcardial perfusion was performed with a cold oxygenated Ringer's solution, followed by a fixative containing 0.1% glutaraldehyde and 4% paraformaldehyde in phosphate buffer (PB; 0.1 M, pH 7.4). Once perfusion was complete, brains were removed and cut into 10 mm-thick blocks along the coronal plane. Each block was refrigerated and stored in phosphate-buffered saline (PBS; 0.01 M, pH 7.4). Blocks were subsequently cut into 60µm thick coronal sections collected in an antifreeze solution (1.4% NaH2PO4-H20, 2.6% Na2HPO4-7H2O, 30% ethylene glycol, 30% glycerol dissolved in distilled water) and stored in a –20^{o}C freezer.

For each of the 2 immunofluorescence protocols performed using monkey tissue, seven evenly-distributed coronal sections which extended from the head of the caudate nucleus to the beginning of the tail of the caudate nucleus were selected from each Rhesus monkey for the purposes of indirect immunofluorescence and stereological cell counting. The seven sections from each monkey were matched such that the overall position of each section relative to Bregma (Paxinos et al., 2000) from one monkey was similar to the sections chosen for the second monkey.

These sections were washed with PBS and pre-incubated for 2 hours in a solution consisting of 10% v/v NDS (normal donkey serum) and 0.3% v/v Triton X-100 in PBS (Triton-PBS). Due to limitations associated with indirect immunofluorescence in monkey tissue, selected sections were incubated over 3 nights at room temperature in a solution of Triton-PBS which contained the following primary antibodies: gtαScgn and gpαPV or gtαScgn and rbαCR. Table 2.2 contains the details, source and the dilutions used for these antibodies as it did not differ from those used for rat and mouse tissue. The tissue was then washed in PBS 5 times (15 minutes per wash) before being incubated overnight at room temperature in a solution of Triton-PBS and one of the fluorophore-conjugated secondary antibodies (all of which were raised in donkey) described previously in section 2.1.

After further washing in PBS, sections were mounted on glass slides (VWR Super Premium Microscope slides) using fluorescence mounting medium (Vectashield; Vector Laboratories), followed by the addition of a coverslip. The caudate and putamen of each section were imaged using a Zeiss Imager M2 epifluorescence microscope equipped with a 20X objective and StereoInvestigator 9.0 software (MBF Biosciences). The delineation of each structure was defined only using the monkey brain atlas (Paxinos et al., 2000) and was done on a section by section basis (no reference was created). Once delineated, the acquisition and subsequent counting of labeled neurons was carried out in precisely the same manner as was done in rodent tissue (see above). It should be noted however that tissues from only 2 monkeys were used to generate this stereological data.

2.5.2 Immunoperoxidase labeling of secretagogin-expressing neurons for light microscopy

Monkey brain sections containing the caudate/putamen were treated with sodium borohydride at room temperature for 20 minutes, after which they were incubated in a solution containing 1% normal horse serum (NHS), 0.3% v/v Triton-X-100 and 1% w/v bovine serum albumin (BSA) in PBS for 1 hour. Sections were subsequently incubated at room temperature in a

solution containing goat anti-secretagogin (Table 2.2), 1% v/v NHS, 0.3% v/v Triton-X-100, and 1% w/v BSA. This was followed by a second room temperature incubation in a solution containing biotinylated horse anti-goat IgGs and 1% normal horse, 0.3% Triton-X-100, and 1% BSA for 90 minutes. Sections were then rinsed in a solution containing PBS, after which they were exposed to an avidin-biotin-peroxidase complex diluted in PBS (ABC; 1:100 [Vector] for 90 minutes followed by rinses in PBS and Tris buffer (50 mM; pH 7.6). The final staining was performed by incubating the sections in a solution containing 0.025% w/v 3,30 -diaminobenzidine tetrahydrochloride (DAB; Sigma, St. Louis, MO), 10 mM imidazole, and 0.005% hydrogen peroxide in Tris buffer for 10 minutes at room temperature. After further rinsing with PBS, each section was placed onto gelatin-coated slides, and coverslipped with Permount. Imaging of sections was performed using a ScanScope light microscope (Aperio Technologies, Vista, CA).

2.5.3 Analysis of stereological cell counts

For each combination of immunofluorescence markers studied, the number of labeled neurons was counted in the caudate or the putamen (they were treated as separate structures) and recorded for a given coronal plane using the same principles described for the rodent. The calculation of V(ref) (i.e. an estimate of the volume of the caudate nucleus and the putamen) could not be accurately performed due to the lack of Rhesus tissue containing the tail of the caudate nucleus (approximately 10 mm of caudate was not acquired). As a result, this study could not accurately report estimates for the total numbers of neurons in the entirety of the caudate nucleus or the putamen. As such, the absolute density for each counted neuron is presented rather than the total number. This was done so that the results obtained from counts of different neuronal populations performed in this study could be compared with one another. The aim is not that these results be compared to those obtained from other studies, as these values represent neuronal densities that are affected by both neuronal number and the volume of the caudate/putamen. However, where neuronal densities have been reported in Rhesus Macaque tissue, the results from this study will be compared in order present the data within the current context of the field.

The distribution of all counted neurons in the caudate nucleus and the putamen was analyzed and presented along the rostro-caudal, dorso-ventral and medio-lateral planes in the same manner as for the dorsal striatum of rodents (see section 2.2.2). Statistical analysis regarding the distributional bias of counted neurons was also performed similarly to what was done for the results obtained in rodent dorsal striatum (see section 2.2.2).

CHAPTER 3.

SECRETAGOGIN EXPRESSION IN THE DORSAL STRIATUM OF RODENTS AND RHESUS MACAQUES

3.1 INTRODUCTION

In the adult brain, calcium-binding proteins (CBPs) are expressed by mature and newly generated neurons. For example, in the neocortex and hippocampus, the selective and combinatorial expression of CBPs has been used to delineate interneuron types that had been previously defined by morphological features (Viney et al, 2013). These and other findings support the notion that differences in the molecular expression profiles of neurons, and particularly those involving CBPs, are well correlated in structural and functional differences at the cellular level. This is perhaps not surprising because different CBPs impart distinct functionality, e.g. they can act as calcium sensors and/or buffers, and can therefore modulate intracellular Ca^{2+} levels throughout the cell, as well as in microscopic cytoplasmic pockets known as microdomains (Willoughby et al., 2010; Ambudkar et al., 2010). Thus, CBPs are in a position to play an important role in governing the electrical activity of cells in the nervous system, while also influencing cellular homeostasis, motility and synaptogenesis. The profound importance of CBP expression is further demonstrated by the epileptic phenotype found in PV knockout –/– mice (Schwaller et al., 2004; Moreno et al., 2011). Although all CBPs fundamentally perform the same function (i.e. bind calcium), it should be noted that each CBP plays a highly specialized (non-redundant) role in cellular activity, as evidenced by the fact that deletion of one CBP leads to functional deficits and does not always result in the up regulation of another CBP (Fossner et al., 2013). This implies that, in cells expressing multiple CPBs (Park et al., 2002), each CBP performs a distinct and complementary set of functions according to their intracellular calcium levels (Fossner et al., 2013; Chernov et al., 2015). It also suggests that cells expressing different CPBs may belong to different neuronal populations. Indeed, the differential expression of CBPs has been widely used to identify a variety of neural population across the central nervous system (Klausberger & Somogyi, 2008; Jonas & Lisman, 2014).

Recently, the novel EF hand CBP secretagogin (Scgn; see section 1.6.1) has been shown to label novel subpopulations of newly-born neurons in the olfactory bulb and the dentate gyrus

(Mulder et al., 2010). Moreover, the expression of Scgn during neurogenesis and neural migration in the developing mouse brain has been used to distinguish subsets of developing neurons that give rise to the granule cells of the dentate gyrus (Wyss et al., 1983; Mulder et al., 2010). In neurons of the adult rodent forebrain, Scgn has been shown to interact with members of the SNARE family of proteins (eg. SNAP-23 and SNAP-25) that regulate the docking and fusion of vesicles with the membrane (Yang et al., 2005; Bauer et al., 2011). This suggests that Scgn expression imparts specific functional properties to the select neuronal populations expressing this CBP. Further emphasising the functional importance of Scgn, this CBP is also found in the primate (human) brain, and to an even greater extent than the rodent brain (Gartner et al., 2007; Attems et al., 2008). Indeed, pyramidal cells of the primate hippocampus are Scgn+, while Scgn expression in the mouse hippocampus is largely limited to the granule cells of the dentate gyrus (Attems et al., 2008; Mulder et al., 2009). Thus, Scgn expression and even structure is retained in both rodents and primates, and its increased expression in primates (along with increases in the expression of CBP, particularly the expression of CR in the forebrain (see Barinka & Druga 2010; Deng et al., 2010)) suggests that Scgn plays an important role in the development and function of larger and larger groups of diverse neuronal populations throughout evolution. Moreover, the extensive distribution of Scgn within a variety of neuronal networks in multiple species implies that its importance as a CBP may mirror that of PV, CR and CB. In the dorsal striatum of rats, Scgn mRNA and protein have been observed in some (non-cholinergic) neurons (Mulder et al., 2009), but the nature, distribution and further cell-type specificity of this expression have yet to be quantified. Moreover, Scgn expression in the striatum of primates has yet to be qualified or quantified.

3.2 AIMS

The presence of the CBP secretagogin within the adult rodent forebrain (including the dorsal striatum), together with its defined role as a functional sensor of intracellular Ca^{2+}, support the idea that the selective expression of Scgn in the dorsal striatum may be an important correlate of functional diversity within the striatum's constituent neurons. With that in mind, the research detailed in this chapter was designed to rigorously define and quantify Scgn expression within the dorsal striatum of rat, mouse and the rhesus macaque monkey. Here, immunofluorescence microscopy and stereological cell counting were used to pursue the following specific aims:

- To quantify Scgn expression in cells of the dorsal striatum of rats and mice.
- To quantify the co-expression of Scgn with other classical markers of striatal interneurons in the dorsal striatum of rodents.
- To quantify Scgn expression in the caudate nucleus and putamen of Rhesus Macaques.

3.3 METHODS

Experimental procedures were carried out on adult male Sprague-Dawley rats (Charles River, Margate, UK) that were 3 months old (Table 2.1), weighing between 280-350g. Some procedures were performed on adult, 6-week old, C57B1/6J male mice (Table 2.1; Charles River, UK). All rodents used were maintained on a 12/12 h light/dark cycle, and had free access to food and water. All experiments were conducted in accordance with the Animals (Scientific Procedures) Act 1986 (UK). Experimental procedures involving primate tissue were performed using tissue from 2 female rhesus monkeys (Table 2.1; 3-9 years old; 5-8 kg). All procedures were approved by the Institutional Animal Care and Use Committee at Emory University and conform to the U.S. National Institutes of Health Guide for the Care and Use of Laboratory Animals.

A detailed description of the techniques and protocols used in this chapter can be found in the appropriate sections of Chapter 2.

- Perfusion and fixation (Section 2.1.1)
- Indirect immunofluorescence (Section 2.1.2)
- Stereological cell counting (Section 2.1.3)
- Calculations of section area, volume and estimates of total cell number (Section 2.2.1)
- Topographical and statistical analysis of interneuron distribution (Section 2.2.2)
- Measurements of mean somatic diameters (Section 2.2.3)
- Tissue preparation and indirect immunofluorescence of monkey tissue (Section 2.5.1)
- Immunoperoxidase labeling of Scgn-expressing neurons for light microscopy (Section 2.5.2)
- Stereological cell counts in the caudate and putamen of the Rhesus monkey (Section 2.5.3)

3.4 RESULTS

3.4.1 The calcium-binding protein secretagogin is an interneuron-specific molecular marker in rat dorsal striatum

It has already been established that Scgn is expressed in some striatal neurons in adult rats (but not in ChAT+ interneurons; (Mulder et al., 2009)). However the prevalence, cellular specificity and topographical distribution of Scgn expression are unknown. Immunofluorescence and stereological cell counting in 13 coronal sections (Figure 2.1 A) was used to map and subsequently quantify the distribution of all Scgn+ neurons in the dorsal striatum of the rat. Immunofluorescent detection of Scgn+ neurons typically labeled the entirety of the soma and the nucleus but not the nucleolus (Figure 3.1 C, Ei), with little labeling of proximal dendrities (Figure 3.1 A, B). To determine the broad identity of Scgn+ cells in the dorsal striatum of the rat, co-expression of Scgn with the neuronal specific marker NeuN (Mullen et al., 1992; Sarnat et al., 1998) revealed that Scgn is exclusively expressed by neurons (Figure 3.1 A) and not by other cell types in the dorsal striatum. Immunofluorescent detection of Scgn and the SPN-specific marker CTIP2 (Arlotta et al., 2008) next demonstrated that striatal Scgn+ neurons do not express CTIP2 and are therefore interneurons (Figure 3.1 B). When tests for the co-expression of Scgn with the 4 classical interneuron markers (i.e. PV, CR, ChAT and NOS) were performed in the dorsal striatum of rats, it was observed that the co-expression of Scgn with either NOS or ChAT was negligible (Figure 3.1C-D, G). Importantly however, Scgn was expressed by some, but not all, PV+ interneurons (see Chapter 4; Figure 3.1 Ei-Eii) and CR+ interneurons (see Chapter 5; Figure 3.1 Fi-Fii). Of all Scgn+ interneurons, nearly half co-expressed PV, while roughly one quarter co-expressed CR (Figure 3.1 G). Because not all PV+ or CR+ striatal interneurons co-expressed Scgn, the selective expression of Scgn represents a novel level of molecular diversity within both of these populations. Importantly, ~25% of Scgn+ interneurons did not express any of the 4 classical markers for striatal interneurons (see below; Figure 3.1 G). It is thus likely that Scgn expression (alone) identifies a group of striatal interneurons that has yet to be described within the dorsal striatum of the rat.

3.4.2 Secretagogin is expressed by a relatively large interneuron population in the dorsal striatum of rats with a novel spatial distribution

The results above suggest that Scgn+ interneurons are relatively abundant in the dorsal striatum of rats. Using stereological quantification, this study estimates that the total number of Scgn+ neurons in the rat dorsal striatum is 27041 ± 507 (n = 3 rats; mean Gundersen's coefficient of error = 0.03), with a mean density of nearly 1166 ± 22 cells/mm^3 (n = 3 rats, mean Gundersen's coefficient of error = 0.03). This value represents approximately 0.9% of all striatal neurons (Oorschot, 1996), and is greater than those reported for the total number of PV-expressing (Luk & Sadikot 2001), NOS-expressing (West, 1996), CR-expressing (Rymar et al., 2004) or ChAT-expressing (Oorschot 1999) interneurons in rat dorsal striatum.

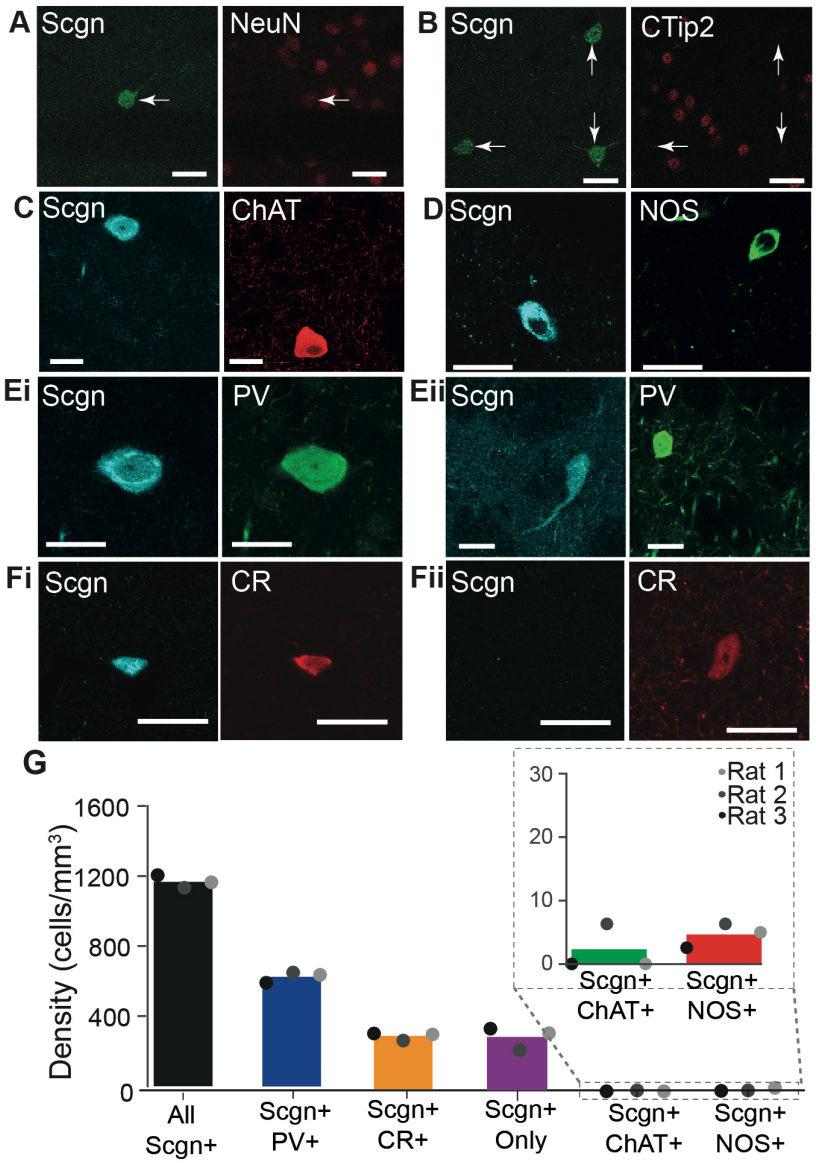


Figure 3.1: The identity of cells expressing Scgn in the dorsal striatum of the rat.
Immunofluorescence images showing the co-expression of Scgn with other markers for striatal projection neurons and interneurons in the dorsal striatum of the rat. **A**) Scgn-expressing cells (arrows) co-express NeuN and are therefore neurons. **B)** Scgn-expressing cells (arrows) do not co-express CTip2, and are therefore interneurons. **C, D**) Scgn+ neurons do not express ChAT (**C**), or NOS (**D**). **E,F**) Some, but not all Scgn+ neurons express PV (**Ei, Eii**) or CR (**Fi, Fii**). Scale bars in A-F represent 20μm.
G) Mean density of Scgn-expressing populations in the dorsal striatum of the rat. Results from each individual rat (n = 3) are plotted as points around the mean. Inset represents the relatively low density of Scgn+/Chat+ interneurons and Scgn+/NOS+ interneurons.

To give further context to this estimate, stereological counts of CR+ interneurons using the same 3 rats and the same 13 sections produced an estimated total number of 13535 ± 392 CR+ interneurons. This value is very similar to that in a previous report (Rymar et al., 2004). This study by Rymar and colleagues is of particular importance as counts were performed across 13 sections that spanned the entirety of the rostro-caudal axis of the striatum, a feature that has not been included in other stereological studies of the rat dorsal striatum (e.g. Luk & Sadikot, 2001). The total cell counts above support the notion that Scgn expression identifies a relatively large population of interneurons within the dorsal striatum of the rat, but they do not offer detailed insights into the spatial distribution of Scgn+ interneurons across this structure. To determine whether (and how) the distribution of Scgn+ interneurons varied across the dorsal striatum, these cells were plotted across the 13 coronal planes in which the stereological cell counts were performed (Figure 3.2 A). When the locations of Scgn+ interneurons were mapped across the rostro-caudal axis of striatum in this manner, they appeared to be particularly abundant in the most rostral and caudal aspects of striatum (e.g. from 2.3 to 1.2 mm and from -2 to -3.5 mm, respectively, in relation to Bregma) and, thus, relatively sparse in the central planes (Figure 3.2 A). In support of this, the density of Scgn+ interneurons was indeed greatest in caudal striatal planes, but was also relatively high in rostral planes (Figure 3.2 B). The high density of Scgn+ interneurons in caudal striatum is of particular interest, since it represents a focal density that is far greater than any other value that has been reported for interneurons in the dorsal striatum (Oorschot, 1996; Oorschot, 2013). In most rostral and caudal planes of dorsal striatum where Scgn+ interneurons were effectively ‘concentrated’, their topographical distribution was such that their locations were significantly biased towards the medial striatum (Figure 3.2 C). In central

planes, Scgn expression was increasingly biased towards the medial border of the dorsal striatum, particularly in those coronal planes immediately behind Bregma (Figure 3.2 C). Along the dorso-ventral axis, Scgn+ interneurons were significantly biased toward ventral locations in some coronal planes, and particularly in those caudal planes 0.9 to 2.2 mm behind Bregma (Figure 3.2 D). The distribution of Scgn expression in all planes of the dorsal striatum is therefore highly variable.

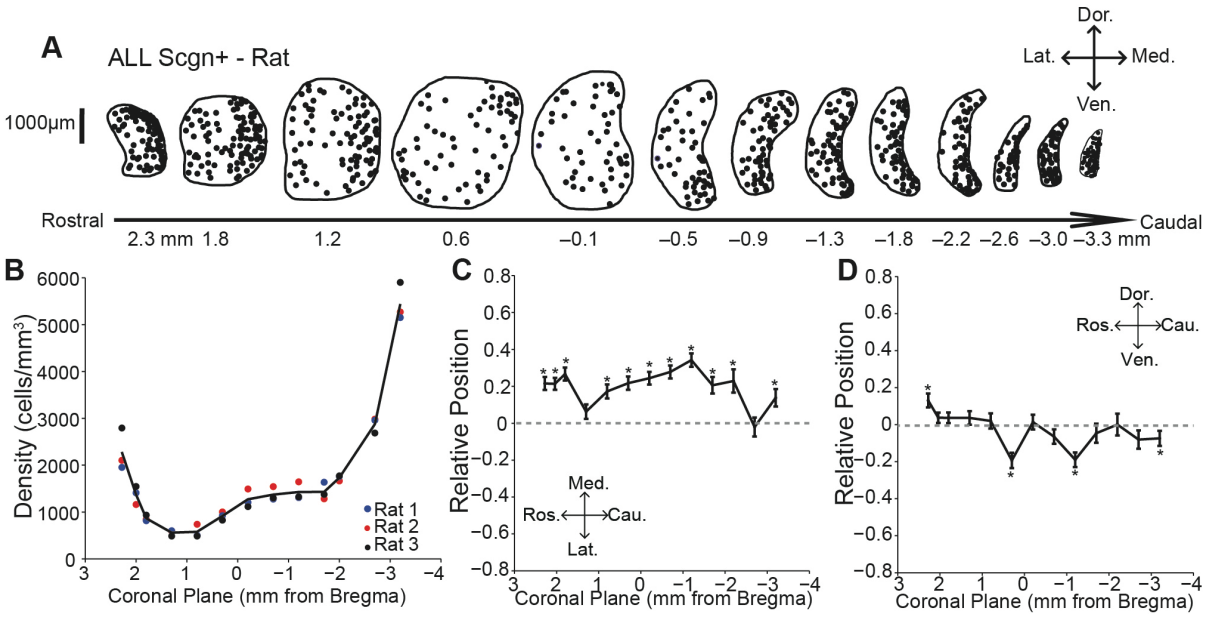


Figure 3.2: The distribution of Scgn-expressing neurons in the dorsal striatum of the rat.
A) Map of Scgn-expressing interneurons across 13 coronal planes encompassing the rostro-caudal axis of the dorsal striatum in one representative rat. **B**) Density of all Scgn-expressing interneurons neurons along the rostro-caudal striatal axis of rats. Note the increased density of Scgn+ interneurons, in the rostral and caudal striatum **C**) Medio-lateral distribution of Scgn+ interneurons along 13 coronal planes. **D**) Dorso-ventral distribution of Scgn+ interneurons along 13 coronal planes. The presence of the asterisk (*) indicates a distribution that is significantly biased in one direction along the specified axis. Data are means of the position of all neurons counted ± SEMs.

3.4.3 A discrete, topographically distinct, striatal interneuron population can be identified by its expression of secretagogin in the dorsal striatum of the rat.

In the dorsal striatum of rats, some Scgn-expressing interneurons did not always co-express one of the 4 classical markers for striatal interneurons (Figure 3.1; 3.2). These interneurons, identified exclusively by their expression of Scgn, were termed "Scgn-only" interneurons and made up nearly one-quarter of all Scgn-expressing interneurons in the rat. In order to further characterize this population, the mean somatic diameter of these neurons was calculated, along with stereological estimates of their mean density, their total number as well as their topographical distribution within the rat dorsal striatum. When the maximal diameter of the immunoreactive signal within the soma is measured, Scgn-only interneurons were of medium size, with an average somatic diameter of 17.2 ± 1.2µm (n = 54). Stereological estimates of this population revealed that its mean density across the striatum was 324.7 ± 22.2 cells/mm^3, which represented a total number of 7532 ± 514 cells across the entire striatum. In the context of all other striatal populations studied, as well as previous reports, these results suggest that Scgn-only interneurons are nearly as numerous as cholinergic interneurons (Oorschot, 1997; Oorschot, 2013). Given these numbers, the possibility that Scgn-only interneurons could represent minor populations of striatal interneuron that have been previously described in the rat (such as those expressing VIP and CCK), was excluded.

When plotted across the dorsal striatum of the rat, Scgn-only interneurons were found to be evenly distributed throughout the rostro-caudal axis, as their density was not relatively greater in one particular set of coronal planes (Figure 3.3 A, B). This therefore meant that these Scgn-only interneurons do not contribute to the high density of Scgn expression in the rostral and caudal regions of the dorsal striatum described previously. When their distribution along the medio-lateral and dorso-ventral axes was assessed, these neurons had a strong medial bias that is particularly evident in central coronal planes (Figure 3.3 C). Along the dorso-ventral axis, Scgn$^+$ only neurons were ventrally biased in their distribution, particularly in coronal planes positioned around Bregma (Figure 3.3 D). Taken together, this biased distribution shows that these

interneurons are particularly clustered within a region of the central striatum referred to in this report as the ventro-medial aspect of the dorsal striatum. This bias is of particular interest, as results from behavioral studies recording in this region have suggested that it may act as a transitional zone between the nucleus accumbens and the dorsal striatum (Roesch et al., 2009). In summary, Scgn+ only interneurons represent a relatively significant striatal population of medium sized neurons that is particularly clustered in the ventro-medial aspect of the rat dorsal striatum.

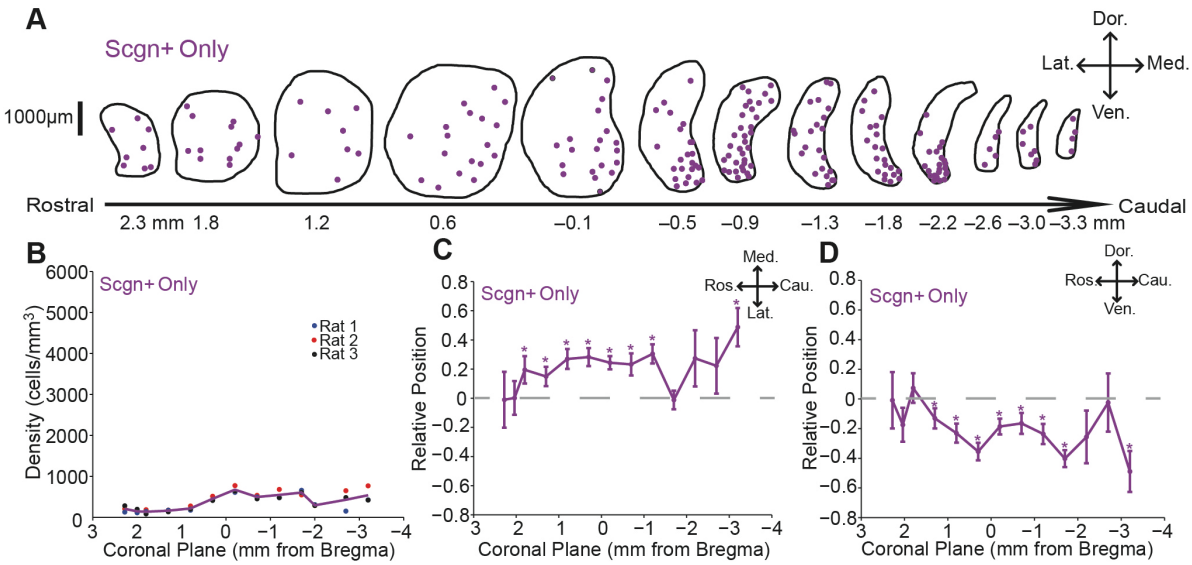


Figure 3.3: Density and distribution of "Scgn+-only" neurons in the dorsal striatum of the rat. **A**) Representative sample of "Scgn+-only" interneurons across 13 coronal planes encompassing the rostro-caudal axis of the dorsal striatum of the rat. **B)** Density of "Scgn+-only" interneurons in each coronal section **C-D**) The Medio-lateral (**C**) and Dorso-ventral (**D**) distribution of "Scgn+-only" interneurons in the dorsal striatum. The presence of the asterisk (*) indicates a distribution that is significantly biased in one direction along the specified axis. Data are means of the position of all neurons counted ± SEMs.

3.4.4 The number and distribution, but not the broad identity, of secretagogin-expressing interneurons varies dramatically according to rodent species

To determine whether and to what extent Scgn-expressing interneurons are present in the mouse striatum, the stereological analyses described above were performed on 9 coronal sections of mouse dorsal striatum whose shape and relative position were similar to those defined for the rat dorsal striatum (Figure 2.1; 2.2). The two antibodies used to detect Scgn in the mouse were the same as those used in the rat (Table 2.2). Importantly, the goat polyclonal antibody produced by R& D Systems is raised against Scgn residues 164-276 while the Rabbit polyclonal antibody produced by Abcam is raised against residues 57-238 of the Secretagogin protein (Pruitt et al., 2013). These two antibodies are therefore directed against different Scgn epitopes, both of which are conserved in mice, rat, human and non-human primates (Pruitt et al., 2013; Gartner et al., 2007). In accordance with data from the rat, Scgn was only expressed in neurons (Figure 3.4 B). Moreover, Scgn was once again not co-expressed with CTIP2, and was very rarely co-expressed with NOS or ChAT in mice (Figure 3.4 C, D, E). Although some PV+ interneurons (Figure 3.4 Fi, Fii) and some CR+ interneurons (Figure 3.4 Gi, Gii) neurons co-expressed Scgn in mouse, the proportional overlap of these markers was different in mouse compared to the rat. Indeed, approximately one-tenth of Scgn+ interneurons co-express PV, 45% co-express CR+ and approximately 45% do not co-express any of the classical striatal interneuron markers (Figure 3.4 H). In all coronal planes tested with both Scgn antibodies, mapping of all Scgn+ interneurons revealed that their overall density is much lower in the mouse compared to the rat, although the increase in density that occurs rostrally and caudally in rat was still apparent in mouse, albeit to a much smaller degree (Figure 3.4 I). Because the volumes of the rat and mouse striatum differ from one another, density was used as a normalized value in order to compare Scgn expression levels between the two species (Figure 3.1; 3.4). In the mouse, the mean density of Scgn-expressing interneurons was 192 ± 51 cells/mm^3 (n = 3 mice; mean Gundersen's coefficient of error = 0.03) (Figure 3.4 H), a value that was nearly one sixth of the result that was calculated for the rat (Figure 3.1 G). Taken together, these results in rats and mice indicate an important species difference in the striatal expression of secretagogin. Due to the scarcity of Scgn+ neurons in

mouse, all of the analysis regarding Scgn expression and distribution that will be performed for the remainder of this report will be in the rat (or the Rhesus Macaque).

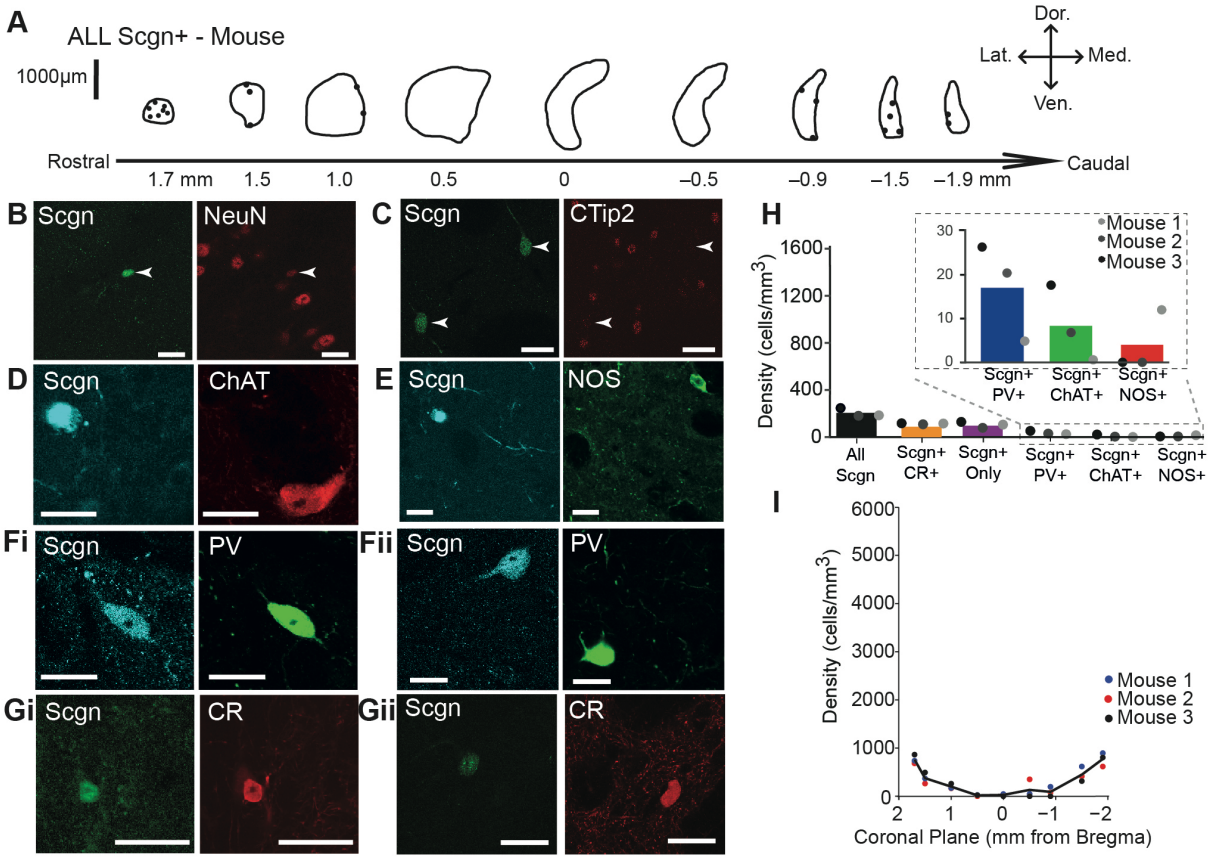


Figure 3.4: The distribution, density and identity of Scgn expression in the dorsal striatum of the mouse. A) Map of all Scgn-expressing interneurons across 9 coronal planes encompassing the rostro-caudal axis of the dorsal striatum in one representative mouse (**B-G**). Immunofluorescence images showing the expression of Scgn in relation to other markers for striatal projection neurons and interneurons in the dorsal striatum of the mouse. **B**) Scgn-expressing cells co-express NeuN and are therefore neurons. **C)** Scgn-expressing cells do not co-express CTip2, and are therefore interneurons. **D, E**) Scgn+ neurons do not typically express ChAT (**D**), or NOS (**E**). **F, G**) Some, but not all Scgn+ neurons express PV (**Fi, Fii**) or CR (**Gi, Gii**). Scale bars in B-G represent 20µm. **H**) Mean densities of different Scgn+ populations in the dorsal striatum of the mouse. Note that the density is much lower than that observed in the rat. Results from each individual mouse (n = 3) are plotted as points around the mean. **I**) Density of all Scgn-expressing interneurons neurons along the rostro-caudal striatal axis of mice. Note the relatively higher densities of Scgn+ neurons in the more rostral and caudal planes of the striatum. Inset represents the relatively small density of Scgn+/PV+ interneurons, Scgn+/Chat+ interneurons and Scgn+/NOS+ interneurons in the mouse.

3.4.5 Secretagogin is expressed in the caudate nucleus and putamen of the rhesus macaque

The disparate results with respect to the expression of Scgn in the dorsal striatum of mouse and rat raise the issues of whether and to what extent Scgn is expressed in the primate striatum. To address these, immunofluorescence and stereological cell counting were used to quantify the distribution of Scgn-expressing cells in the pre-commissural, commissural and post-commissural caudate/putamen of the Rhesus Macaque (Figure 3.5 A). Guided by the results in rats and mice, and using 2-channel immunofluorescence and the same antibodies used in tests of rodent tissue, the broad identity of Scgn+ cells was investigated with a focus on testing whether such cells also co-expressed PV or CR. In both the caudate nucleus and the putamen, immunofluorescent detection of Scgn and PV revealed that some, but not all Scgn+ interneurons co-expressed PV and vice versa (Figure 3.5 B). Of all Scgn+ interneurons, 82.4% co-expressed PV in the caudate while 89.1% co-expressed PV in the putamen. In a separate experiment, co-expression of Scgn with CR was also detected (Figure 3.5 C), with 28.2% of Scgn+ interneurons expressing CR in the caudate nucleus and 17.5% of Scgn+ interneurons expressing CR in the putamen. Unlike the scenario in rodents, PV and CR are co-expressed by a subset of striatal interneurons in monkey (Deng et al., 2010). However, because the tests of PV and CR were necessarily performed as separate incubations, it is unclear whether those neurons expressing Scgn and CR also expressed PV (and vice versa). Due to technical limitations associated with the availability of monkey tissue and the unreliability of select antibodies when used in monkey tissue, the co-expression (or lack thereof) of Scgn with ChAT and/or NOS could not be investigated. Despite these caveats, these results not only suggest that Scgn is expressed by select populations of neurons in Rhesus Macaque striatum, but also (in common with observations in rodents) that Scgn+ neurons can be subdivided into those that do not express PV or CR and those that do co-express PV or CR.

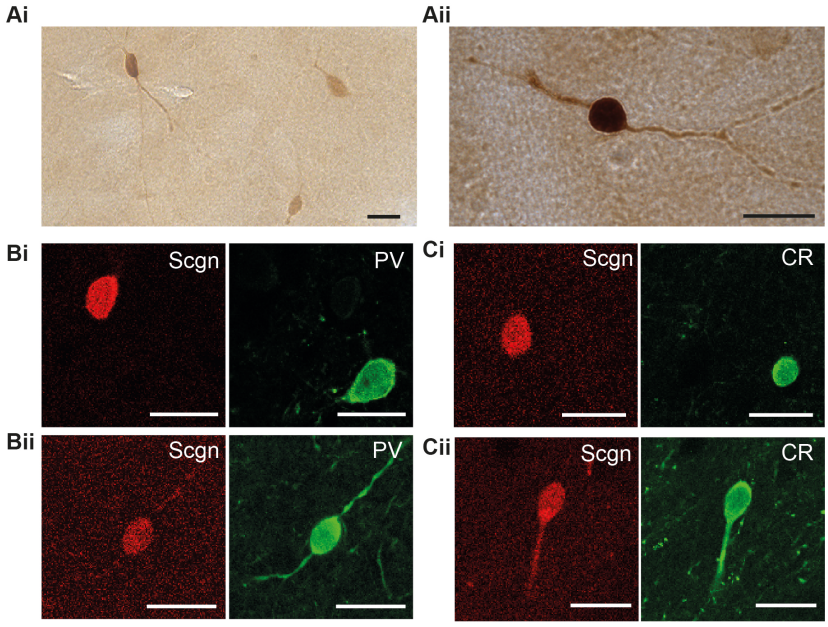


Figure 3.5. The expression of secretagogin in the caudate nucleus and putamen of the rhesus macaque. A) Light microscopic images of DAB-stained sections demonstrating the presence of multiple Scgn-expressing cells in the caudate of the monkey (**Ai**) and an image of a single Scgn-expressing cell in the putamen of the monkey (**Aii**). **B**) Immunofluorscence images showing that some Scgn+ cells do not express parvalbumin (**Bi**) while others co-express parvalbumin (**Bii**). **C**) Immunofluorscent images showing that some Scgn+ cells (in the putamen) do not express calretinin (**Ci**) while others co-express calretinin (**Cii**). Scale bars in A-C represent 20µm.

Stereological counts of Scgn-expression along a portion of the rostro-caudal axis of the monkey striatum revealed that Scgn expression was relatively abundant in both the caudate nucleus and the putamen, which were treated as separate structures for the sake of topographical analysis (Figure 3.6 A). Due to technical limitations associated with the availability of the caudal parts of the caudate/putamen, this study could not accurately provide an estimate for the total number of Scgn+ neurons in the caudate nucleus and the putamen of the monkey. As this was not the primary goal of this study, the neuronal density of 483± 165 cells/mm3 (n=2, mean Gundersen's coefficient of error = 0.04) was calculated for the caudate nucleus and 336.6 ± 122 cells/mm3 (n=2, mean Gundersen's coefficient of error = 0.04) was calculated for the putamen. In both the caudate nucleus and the putamen, the mean density of Scgn-expressing cells was greater

than that of PV-expressing neurons (see chapter 4 for more details) but less than that of CR-expressing neurons (see chapter 5 for more details), indicating that Scgn expression likely identifies a relatively substantial group of cells in the Rhesus Macaque striatum.

The calculation of Scgn neuronal density at each assessed coronal plane revealed that Scgn expression in the monkey qualitatively mirrored results in rats and mice, such that Scgn-expressing interneurons were found at relatively higher densities in the rostral-most and caudal-most planes (Figure 3.6 Bi, Bii). These planes encompassed the pre- (associative) and post (sensorimotor)-commissural caudate/putamen, respectively (Parent, 1990; Fudge et al., 2002; Haber & Knutson, 2010). This distributional bias towards the rostral and caudal planes was particularly evident in the caudate nucleus (Figure 3.6 A, Bi). Within each coronal plane that was stereologically assessed, counts encompassed 100% of the medio-lateral and dorso-ventral axes, allowing for the mapping and quantification of Scgn expression along both of these axes. In the caudate nucleus, Scgn+ cells were biased in their distribution towards the lateral and dorsal borders of the structure across multiple coronal planes (Figure 3.6 Ci, Di). The bias towards the dorsal border among Scgn+ interneurons was also present in the putamen throughout a great proportion of its structure (Figure 3.6 Dii). Such biases in distribution along the dorso-ventral plane (which were not as strong in the rodent striatum) likely reflect the anatomical and functional tripartite subdivision of the dorso-ventral axis of the primate CPu first described by Karachi et al., (2002).

A lateral bias was also noted in the putamen in various planes (Figure 3.6 Di). The coronal planes in which the lateral and dorsal distributional biases of Scgn+ interneurons in the putamen was most apparent are of particular interest, as they were matched for both types of biases. For example, Scgn expression in the coronal plane 2.2mm ahead of bregma demonstrated a significant bias towards both the dorsal and the lateral border, but this bias along both the medio-lateral and dorso-ventral axes disappears around bregma, only to return once again 2.7mm

behind Bregma (Figure 3.6 A, Di, Dii). Clearly, Scgn expression throughout the caudate and putamen of Rhesus Macaques is distributed in a biased fashion across multiple axes, reflecting some of the biases (but not the dorso-ventral bias) that were noted in rodents, particularly across the rostro-caudal striatal axis, in which Scgn was once again found at higher densities rostral and caudally in both the caudate and the putamen. Importantly, Scgn-expression also retains its relatively high level among interneuron populations in both the caudate and the putamen (more details in chapter 4 and 5), mirroring what was found in the rat, but not what was found in the mouse.

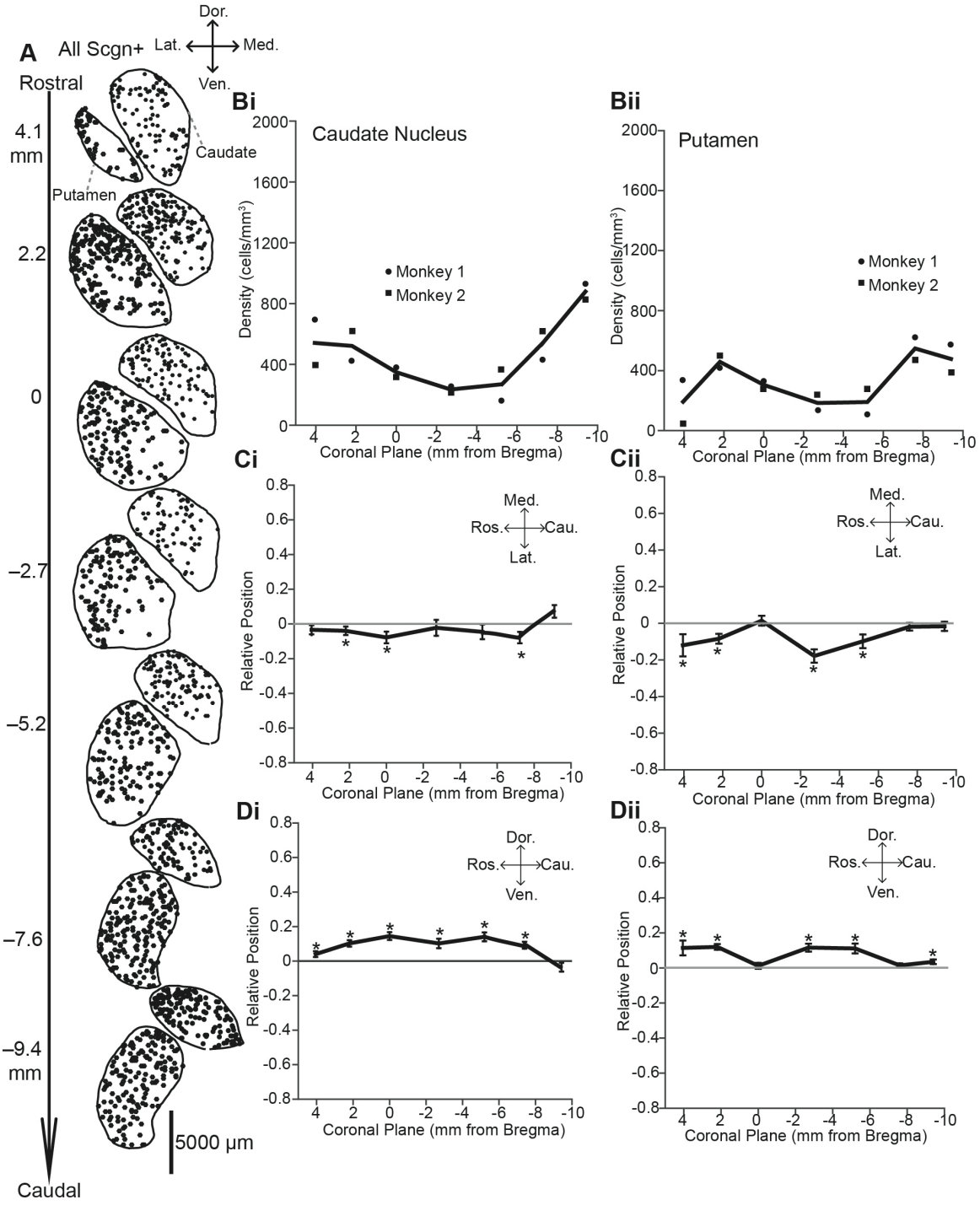


Figure 3.6: The distribution, density and topography of Scgn expression in the caudate and putamen of the rhesus macaque. A) Typical distribution of Scgn expression across 7 coronal planes containing the caudate (grey dots) and putamen (black dots), with each dot representing a single neuron. **B**) Density of Scgn-expressing neurons along the rostro-caudal axis of the caudate (**Bi**) and putamen (**Bii**). As in the rat, Scgn expression in both the caudate nucleus and the putamen was relatively greater at the rostral and caudal planes that were studied. Medio-lateral (**C**) and dorso-ventral (**D**) distribution of $Scgn^{+}$ neurons along 7 coronal planes encompassing the caudate (**Ci, Di**) and putamen (**Cii, Dii**). The presence of the * indicates a distribution that is significantly biased in one direction along the specified axis. Data are means of the position of all neurons counted ± SEMs.

3.5 DISCUSSION

Here, the characterization of secretagogin expression within the dorsal striatum has not only identified a novel population of secretagogin-expressing interneurons, but has also revealed an extensive degree of molecular heterogeneity within 2 classical interneuron populations of the rat, mouse and Rhesus Macaque striatum. Because some, but not all CR+ interneurons and PV+ interneurons in the rat, mouse and the Rhesus Macaque expressed Scgn, the selective expression of this novel CBP highlights potential functional heterogeneity within those populations. Indeed, because Scgn is known to have a specialized intracellular role as a calcium sensor that interacts with the protein machinery involved in vesicle trafficking (Rogstam et al., 2007), the relatively high levels of Scgn expression within the striatum of rats and Rhesus Macaques is in and of itself important, as it may impart specialized functions unto those neurons in which it is selectively expressed. Despite the evidence to suggest that the expression of Scgn alone allows neuronal populations to perform specific functions within their respective microcircuits (Mulder et al., 2009; Alpar et al., 2012), it is not the most important finding presented here. Indeed, the relatively high densities and novel distributions of these Scgn+ interneurons implies that they play a specialized role in, topographically-restricted striatal processes. Such a biased distribution across the rostro-caudal axis of the dorsal striatum is of particular interest when considering that the 4 classical populations of striatal interneuron are often described with little to no bias in their rostro-caudal distribution (Oorschot, 2013; Petryszyn et al., 2014; Ma et al., 2014). Secretaogin therefore represents a robust molecular marker of a spatial distributional bias among the interneuron classes of the dorsal striatum in rodents and the Rhesus Macaque caudate/putamen. This work therefore gives new and important insights into the cellular diversity present within striatal microcircuits, while providing a framework by which this diversity is also reflected in the distributional biases of the various interneuron populations of the dorsal striatum.

3.5.1 Scgn is expressed by a relatively large population of interneurons in the rat dorsal striatum

Over the past decade, more and more heterogeneity has been described among the interneurons that support the microcircuitry of the striatum. Although interneurons as a whole represent a small proportion of the striatum's cellular constituents (Tepper et al., 2010; Kreitzer, 2012), they are able to powerfully influence the activity of projection neurons (Klaus et al., 2011; Szydlowski et al., 2013). Previous studies have described great heterogeneity among striatal interneurons, with "novel" populations expressing CCK, VIP, TH, 5HT-3R and NPY being the most recent (De Deyn et al., 1992; Ibanez-Sandoval et al., 2011; Silberberg & Bolam, 2015). This great heterogeneity in interneurons within a single brain structure has precedent, for example, the CA1 subfield of the hippocampus is known to contain 21 different populations of interneuron within its microcircuit (Klausberger & Somogyi, 2008). With respect to the rat dorsal striatum, stereological studies have been performed by others in order to investigate the total number of each of the 4 major interneuron classes (Luk & Sadikot, 2001; Larsson et al., 2001; Rymar et al., 2004; West, 1996; Oorschot, 1999). Although these studies were all performed using different stereological methods (i.e. probe size and depth were inconsistent, as well as the number of animals used per count), and many studies suffered from under sampling of the dorsal striatum, particularly the caudal most 2.0mm of the structure (Luk & Sadikot, 2001). This caudal most 2.0mm of dorsal striatum that is often not sampled in many rat studies is of particular importance given that it has recently been shown to possess a specialized cellular architecture and, more specifically, an unusual ratio of direct pathway and indirect pathway SPNs (Gangarossa et al., 2013). Despite the limitations of past stereological studies, they provide references for the total numbers of the 4 classical defined populations of striatal interneuron in the rat (Table 1.1). Using a rigorous cell counting strategy and the Cavalieri technique for complex volume estimations, this thesis study is the first to provide a detailed estimate for the number of Scgn+interneurons in the dorsal striatum of the rat and the mouse. In the rat, the number of Scgn+ interneurons was estimated to be approximately 27,000. Based on estimates for the total number of striatal neurons (Oorschot 1996), Scgn+ interneurons likely make up ~0.9% of all striatal neurons. Given the

values cited in Table 1.1 regarding previous estimates for the total numbers of the classical types of striatal interneurons, the estimated here indicates that the expression of Scgn identifies the largest population of rat striatal interneuron (Oorschot, 2013). Clearly then, Scgn expression identifies a relatively large population of striatal interneurons that is found throughout the dorsal striatum of the rat.

3.5.2 The identity, but not the relative level, of Scgn expression in the dorsal striatum is consistent across multiple species

One key feature of Scgn detection in this study was the use of 2 different antibodies raised against epitopes that are conserved in mouse, rat and primate (human and non-human) secretagogin. Indeed, the goat polyclonal antibody produced by R& D Systems is raised against Scgn residues 164-276 while the Rabbit polyclonal antibody produced by Abcam is raised against residues 57-238 of the Secretagogin protein (Pruitt et al., 2013). These two antibodies are therefore directed against different Scgn epitopes, both of which are conserved in mice, rat, human and non-human primates. This ultimately ensures that the immunofluorescent technique used in this study could accurately detect the presence of Scgn in mice, rats and primates. Using both of these antibodies, immunoreactivity for this CBP was mapped in the dorsal striatum of mice, rats and the caudate/putamen of the rhesus macaque. In all 3 species studied, Scgn-expressing cells were identified as interneurons that co-expressed PV or CR, or did not express either of these two CBPs. Secretagogin expression in the Rhesus Macaque caudate/putamen was observed to encompass a proportion of the PV+ interneuron and CR+ interneuron populations, but analyses of other classical markers was not possible due to technical limitations. Data from both of the two separate incubations performed in Rhesus Macaque tissue suggests that PV and CR-immunoreactive neurons do not account for all of the Scgn expression in either the caudate or the putamen, but a definitive answer as to the broad identity of Scgn+ interneurons in the Rhesus Macaque remains unclear.

While Scgn expression identifies a relatively large population of striatal interneurons in the rat (~0.9% of all neurons), it identified a relatively small group of interneurons in the dorsal striatum of the mouse. This disparity raises an important issue regarding the interpretation of these counts in mice. The first issue was whether this value was relatively low or high compared to other interneuron populations of the mouse striatum. The generation of transgenic mice that express GFP under the control of specified regulatory sequences (eg. promoters for D1 or D2 receptors, PV, ChAT etc) has made the mouse the species in which morphological and functional studies of rodent striatum are now most commonly investigated. Indeed, the two most recently discovered classes of "novel" interneuron arose from studies of the dorsal striatum of transgenic mice expressing GFP under the control of the promoters of tyrosine hydroxylase (Ibanez-Sandoval et al. 2010; Unal et al., 2011; Unal et al., 2015) or 5HT3aR (Munoz-Manchado et al., 2014). This shift in the field is perhaps unfortunate given that the current knowledge of neuronal organization in the dorsal striatum of mice is more limited compared to that of rats and Rhesus Macaques. Indeed, one of the few stereological studies investigating the "classical" striatal interneurons in the mouse striatum was that of Graveland and Difiglia(1986), in which the number of indented nuclei (interpreted to be a key feature of interneurons) was counted and compared to the number of non-indented nuclei (projection neurons). This single study has provided the 5% value that is so often cited for the number of interneurons in the mouse striatum. Since then, only the work of Parent and colleagues, who investigated the distribution of CR+ interneurons in the mouse striatum, have performed stereological cell counts of the "classical" interneuron populations of the dorsal striatum of the mouse. Importantly, they estimated the overall density of CR+ interneurons to be 301 cells/mm^3 (Petryszyn et al., 2014). They did not give the total number of neurons counted, but as they used the same strain of mice that was used here (i.e. C57Bl6/j), the density value they provide can be compared to the density for Scgn+ interneurons in the mouse obtained here, that is, ~190 cells/mm^3. Using this recent value for comparison, it is clear that Scgn expression identifies a relatively small group of striatal neurons in the mouse (Figure 3.4). This alone does not necessarily mean that those cell types expressing

Scgn in the rat do not exist in the mouse striatum; it could simply mean that those cell types do not express Scgn in the mouse. Such large scale differences in functionality are not surprising given that some have suggested that the evolutionary distance between mice and rats is potentially as large as that between humans and old-world monkeys (Rats!, 2010). Such a finding implies that the choice between the use of rats or mice to model the anatomy and physiology of the Rhesus Macaque is non-trivial, as many differences likely exist between the nervous systems of these two species (Rats!, 2010).

Importantly, the level and pattern of Scgn expression in the monkey caudate and putamen described in this study appear to more closely approximate those observed in the rat than the mouse. These findings are in line with recent findings that Scgn expression is increased in other regions of the primate central nervous system (Attems et al., 2008; Mulder et al., 2009). Due to technical limitations associated with the availability of the caudal parts of the caudate/putamen, this study could not accurately provide an estimate for the total number of Scgn+ neurons in the dorsal striatum of the monkey. As this was not the primary goal of this study, the neuronal density of ~480 cells/mm^3 was calculated for the caudate nucleus and ~340 cells/mm^3 for the putamen. Unfortunately, many stereological studies investigating the "classical" types of interneurons in the primate do not provide estimates of absolute cell number, but provide neuronal densities in 2 dimensions (Wu and Parent, 2000) or provide percentages (Deng et al., 2010). In contrast, the results presented here are absolute densities in 3 dimensions. For this reason, they are not truly comparable to any previously reported result.

3.5.3 Functional considerations associated with the distributional biases of Scgn-expressing neurons across multiple axes of dorsal striatum

Because Scgn is a cytosolic calcium sensor that interacts with a multitude of intracellular proteins, the expression of Scgn by select groups of striatal interneurons implies that they are able to perform specialized cellular function. Indeed, the findings that Scgn shares similar Ca^{2+} binding proteins to synaptotagmin, in addition to its interaction with components of vesicular

trafficking place Scgn at the heart of intracellular Ca^{2+} signaling. From this position, Scgn expression may influence a variety of cellular functions in a specialized manner, thereby allowing Scgn+ cells to contribute to unique features of the striatal microcircuit.

Despite the functional importance of Scgn expression, the novel distribution of Scgn+ interneurons throughout the striatum is also relevant. In addition to quantifying the density and number of Scgn+ neurons in the dorsal striatum, this study also reports that a relatively high density of Scgn+ cells in the most rostral caudal aspects of the dorsal striatum of the rat and the Rhesus Macaque (Figures 3.2). Importantly, this the distributional bias quantified here continues the ever increasing trend of topographical heterogeneity amongst the cellular constituents of the striatum. Indeed, a recent study has reported a lack of direct pathway SPNs in the caudal striatum (Gangarossa et al., 2012), while several studies have now quantified distributional biases amongst CR+ interneurons (Rymar et al., 2004; Ma et al., 2014) and PV+ interneurons (Ma et al., 2014) in the dorsal striatum of the rat. The study by Ma and colleagues is of particular interest, as they report differences between the dendritic size and length of PV-expressing interneurons in the lateral and medial aspects of the striatum. Importantly, such studies have never reported any distributional biases along the rostro-caudal axis of the dorsal striatum, which contrasts with the strong topographical biases reported here for Scgn+ interneurons. These examples ultimately help to further the notion that the striatum is not one homogenous structure; the inputs may originate from different cortical regions (Albin, Young and Penney, 1989; DeLong, 1990), but the striatum is itself intrinsically organized to process these inputs in a specialized manner.

Ultimately, it should be noted that the total number of neurons does not provide any major hints towards the contribution of different neurons towards striatal processing. However, these numbers are important in the context of pathological or physiological changes to the dorsal striatum (Luk & Sadikot, 2001; Ernst et al., 2014), and so the reporting of these numbers in control models continues to be important. For this reason, the number of Scgn+ interneurons was

reported in this study. In addition to the reporting of these numbers, this study has also shown that Scgn is expressed by subpopulations of CR+ interneurons and PV+ interneurons, while also quantifying significant topographical biases in the expression of Scgn within the striatum of rodents and Rhesus Macaques. This is particularly important in the dorsal striatum, as it receives heterogeneous and topographically organized inputs from a variety of cortical areas (McGeorge 1989; Vertes and Hoover, 2011; Mailly et al., 2013). As this is not the central theme of work in this chapter, specific functions associated with regions of the dorsal striatum containing high densities of Scgn+ neurons will be explored in subsequent chapters. In addition to exploring these topographical biases, these chapters will detail the functional and anatomical properties of PV+/Scgn+ interneurons (Chapter 4) and CR+/Scgn+ interneurons (Chapter 5), as well as their Scgn– counterparts. If it exists, the presence of topographical bias within these specific, molecularly distinct subpopulations will likely provide hints toward their potential roles within the regional processing of the striatal microcircuit. For example, the rostral striatum is known to receive prominent inputs from the cingulate and prefrontal cortices, while receiving little to no input from motor cortices (Mailly et al., 2013). As such, relatively high density of Scgn+ neurons in rostral striatum suggests that Scgn+ interneurons are well portioned to processing information carried by prefrontal cortical inputs. Thus, by defining the distributions of molecularly-defined interneuron populations, stereological studies of the dorsal striatum can provide important new information about the cellular constituents of striatal microcircuits that carry out very different behavioral functions.

3.5.4 Scgn expression identifies a group of interneurons that are topographically biased towards the ventro-medial aspect of the dorsal striatum

Although the expression of Scgn by some PV+ and CR+ interneurons allows for the characterization of molecular heterogeneity within those populations, Scgn was also expressed by a group of neurons that did not express any other classical marker for striatal interneuron. These "Scgn+ only" interneurons were biased in their distribution in coronal planes centred on Bregma

towards the ventro-medial aspects of the dorsal striatum (Figure 3.3). This is particularly interesting, given that ventral biases in distribution have not been previously described for any type of striatal interneuron in the dorsal striatum (Tepper et al., 2010).

Unlike the dorsomedial (DMS) and dorsolateral (DLS) striatum, an understanding of the component structures that comprise the ventral aspect of the dorsal striatum is potentially important given that its cortical input differs from that of the rest of the dorsal striatum (McGeorge & Faull, 1989; Hoover & Vertes, 2011). Indeed, the cortical input to the ventromedial aspects of the dorsal striatum is most similar to that of the nucleus accumbens, particularly the medial aspects of the shell (see Section 1.5). Within the literature, the ventromedial region of the dorsal striatum is often treated as a continuation of the dorsomedial striatum (Burton et al., 2015), but this notion is somewhat inappropriate given that the cortical inputs to these two regions is very different. Indeed, the ventromedial aspects of the dorsal striatum receive a relatively dense and expansive input from the medial orbitofrontal cortex in the rat (Hoover & Vertes, 2011). The medial orbitofrontal cortex, which also sends a smaller, less dense projection to the dorsomedial striatum, is implicated in the dynamic nature of behaviour in response to changing external factors influencing the outcome of said behaviour (Schoenbaum et al., 2006; Schoenbaum & Roesch, 2008; Sul et al., 2010). Moreover, lesions of this cortical area or its cortico-striatal projection produce marked deficits in reversal learning (Burke et al., 2009), suggesting that the ventromedial region of the dorsal striatum (the target of those projections) is heavily involved in the processing of behavioural modification associated with changes in reward valuation. Importantly, the ventromedial striatum is the only region of the dorsal striatum receiving input from the entorhinal cortex (Mcgeorge & Faull, 1989). This unique input pattern may suggest that the ventromedial striatum plays a role in learned behaviours associated with spatial navigation that is functionally associated with the entorhinal cortex (Fyhn et al., 2004; Jacobs et al., 2010). The highly specialised nature of the cortical input to the ventromedial part of the dorsal striatum

is of interest given that it shares some important similarities to the cortical input received by the nucleus accumbens.

Given that the ventromedial aspects of the dorsal striatum receive distinct cortical inputs and are associated with different behaviours (Schoenbaum et al., 2006; Schoenbaum & Roesch, 2008) compared to the rest of the dorsal striatum, it is perhaps not surprising that its cellular composition is unique. Indeed, the relatively high density of "Scgn+ only" interneurons in this particular region of the dorsal striatum provides strong evidence to suggest that the regional cyto-architecture of the dorsal striatum is specialized in order to receive the unique information carried by its particular set of inputs. This theme will be highlighted throughout the rest of this report, as some of the work in Chapter 4 will seek to investigate the topographical biases (if any) of PV+/Scgn+ and PV+/Scgn– while the work presented in Chapter 5 will investigate whether or not these biases exist for the distribution of CR+/Scgn+ and CR+/Scgn– interneurons in the dorsal striatum of the rat.

CHAPTER 4.

DIVERSE ELECTROPHYSIOLOGICAL PROPERTIES AND SPATIAL DISTRIBUTIONS OF PARVALBUMIN- EXPRESSING STRIATAL INTERNEURONS OF RATS AND RHESUS MACAQUES ARE IDENTIFIED BY SELECTIVE EXPRESSION OF SECRETAGOGIN

4.1 INTRODUCTION

In the cerebral cortex, GABAergic interneurons identified by their expression of PV (Kosaka et al, 1987) have been shown to comprise multiple cell types. The divisions between these subsets of PV+ interneurons are apparent upon investigation of their distinct morphological properties, and connectivity within the cortical circuit, as well as their neurochemical and physiological features (Ascoli et al, 2008; Klausberger and Somogyi, 2008). In contrast, striatal interneurons identified by their expression of PV in the rat are still widely believed to belong to one homogenous population that is particularly enriched in the dorsolateral striatum (Gerfen, 1985; Kita et al., 1990; Kreitzer, 2009; Tepper et al., 2010). In the primate, PV+ interneurons have been shown to be found at higher densities in the caudate nucleus compared to the putamen (Wu & Parent, 2000). Although the distributional bias of PV+ interneurons in the rat has yet to be demonstrated in a quantifiable and stereological fashion, it has nevertheless been used to suggest that striatal PV-expressing interneurons may play a specialized role in the processing of cortical sensorimotor inputs (Kubota et al., 1993; Kubota & Kawaguchi 1993; Ma et al., 2014). This notion calls on the topographical nature of cortical inputs to the striatum; i.e. the rather poorly defined "dorsolateral" region of striatum is known to receive prominent inputs from somatosensory and motor cortices in the mouse (Pan et al., 2010) and the rat (Deng et al., 2015). In the primate, stimulation of sensorimotor cortices has been shown to promote the expression of c-fos (a nuclear marker for increased activity) in nearly all PV+ interneurons of the putamen (Parthasarathy & Graybiel, 1997; Ramanthan et al., 2002), while stimulation of the same cortices in the rat produces rapid and robust responses in PV+ interneurons in the dorsal striatum (Mallet et al., 2005, Sharott et al., 2012). These findings have been cited in the past to support the idea that these interneurons are involved in sensorimotor processing in the striatum. This, in combination with the finding that a single cortical axon can make multiple contacts with PV-expressing interneurons (Kita et al., 1990; Kita, 1993) ultimately implies that striatal PV+ interneurons are a key substrate for the processing of direct input from the somatosensory cortices.

Unlike their cortical counterparts, striatal PV+ interneurons have yet to be subdivided on the basis of their afferent and efferent connectivity within the striatum, their broad molecular identities or their electrophysiological features (Tepper et al., 2010; Kreitzer, 2012). However, an in-depth analysis of anecdotal evidence provided by a variety of studies investigating the properties of PV+ interneurons in the striatum reveals a surprising degree of heterogeneity. Indeed, some of the first descriptions of the somatodendritic structure of PV+ interneurons identified some of these cells as having large axonal and dendritic fields whereas other cells were described as having relatively small arborizations (Kawaguchi, 1993). Additionally, in vitro studies of rat dorsal striatum have described a dichotomy within this population with regards to their membrane responses to positive current injections (Bracci et al., 2003). In vivo, PV+ striatal interneurons are consistently fast-spiking neurons, but display highly variable firing rates and patterns (Sharott et al., 2012). For example, during cortical slow-wave activity (SWA), some PV+ interneurons fire a single spike every 30-60 seconds, while others fire high-frequency bursts of spikes activity during the active component of the cortical slow oscillation (Sharott et al., 2012). Taken together, these structural and functional differences (described in the rat) between groups of striatal PV+ interneurons suggest that this classical cell type might in fact encompass 2 or more heterogeneous populations. Although the dorsal striatum of mice is not covered here, recent studies in eGFP-5HT3a mice have also revealed a molecular dichotomy within the PV+ interneuron population, as nearly half of them expressed 5HT3a-R (Munoz-Manchado et al., 2014).

The notion that PV-expressing interneurons in the striatum may not represent a single homogenous population is particularly important given the recent findings regarding the connectivity of these interneurons within the striatal microcircuit in both healthy and disease states. In the dorsal striatum, action potential generation in PV+ (fast spiking) interneurons produces relatively large amplitude IPSPs in SPNs of both the direct and indirect pathways (Koos & Tepper, 1999; Planert et al., 2010). Moreover, evidence from both anatomical reconstructions (Koos & Tepper, 1999) of PV+ interneurons and neighboring spiny projection

neurons suggest that the probability of a synaptic connection between an FSI and an SPN is relatively high, ranging between 25% and 75% (Koos & Tepper, 1999; Gittis et al., 2010; Planert et al., 2010). Importantly, this feed-forward inhibition mediated by FSIs is selective for SPNs, as optogenetic stimulation of PV+ interneurons does not produce detectable IPSPs in cholinergic interneurons, and only occasionally produces small IPSPs in LTS interneurons (Szydlowski et al., 2013). In the healthy brain, striatal FSIs have been shown to be more likely to innervate D1-expressing or direct pathway projection neurons compared to D2-SPNs (Gittis et al., 2010; Gittis et al., 2011). However, the dynamic properties of the FSI to D1-SPN and FSI to D2-SPN connections, including response amplitude and paired-pulse depression, are similar (Planert et al., 2010). The levels of innervation of both direct and indirect pathway SPNs by FSIs is also highly relevant in the context of Parkinson's disease, where dopamine depletion increases the proportion of connections from FSIs unto D2-SPNs without influencing the connectivity of FSIs unto D1-expressing spiny neurons (Gittis et al., 2011). This is thought to be an adaptive response to the increased activity of D2-SPNs after dopamine depletion (Fino et al., 2007; Mallet et al., 2006; Nicola et al., 2000). In contrast, chronic cocaine administration, resulting in increased levels of striatal dopamine (Heiman et al., 2008), produces an increased inhibition of D1-expressing projection neurons via an increase in the innervation of D1-SPNS by PV-expressing interneurons (Flores-Hernandez et al., 2002). Again, this is most likely an adaptive response, but ultimately illustrates the idea that some facets of the feed-forward inhibition provided by FSIs are "pathway specific", and are regulated dynamically to meet the demands of the striatal microcircuit.

4.2 AIMS

The existence of anecdotal evidence to suggest the existence of heterogeneity among the striatal PV-expressing interneuron population, together with the finding that feed-forward inhibition in the striatum is pathway specific supports the notion that quantifiable molecular, electrophysiological and structural differences may exist within the striatum's PV+ cell populations. In chapter 3, secretagogin was shown to be expressed in a significant proportion of PV+ interneurons in the dorsal striatum of rats (see Section 3.4.1) and Rhesus Macaques (see Section 3.4.4) but not in mice (see Section 3.4.3). This suggests that PV+ interneurons in these species can be subdivided on the basis of their molecular expression profiles. In light of these findings, a combination of stereological cell counting, in vivo juxtacellular recordings and immunofluorescence/confocal microscopy were used to address the following aims in rats and Rhesus Macaques:

- To quantify the co-expression of Scgn within the PV+ striatal interneuron population in the rat and Rhesus Macaques.
- To determine whether PV+ interneurons are uniformly distributed throughout the striatum of both rats and Rhesus Macaques.
- To determine whether the selective expression of Scgn by striatal PV+ neurons is reflected by distinct firing properties in vivo.
- To determine whether the molecular heterogeneity within PV+ interneurons is correlated with differences in their efferent connectivity within the striatum.

4.3 METHODS

Experimental procedures were carried out on adult male Sprague-Dawley rats (Charles River, Margate, UK) that were 3 months old, weighing between 280-350g. All rodents used were maintained on a 12/12 h light/dark cycle, and had free access to food and water. All experiments were conducted in accordance with the Animals (Scientific Procedures) Act 1986 (UK). Experimental procedures involving primate tissue were performed using tissue from 2 female rhesus monkeys (3-9 years old; 5-8 kg). All procedures were approved by the Institutional Animal Care and Use Committee at Emory University and conform to the U.S. National Institutes of Health Guide for the Care and Use of Laboratory Animals.

A detailed description of the techniques and protocols used in this chapter can be found in the appropriate sections of Chapter 2.

- Perfusion and fixation (Section 2.1.1)
- Indirect immunofluorescence (Section 2.1.2)
- Stereological cell counting (Section 2.1.3)
- Calculations of section area, volume and estimates of total cell number (Section 2.2.1)
- Topographical and statistical analysis of interneuron distribution (Section 2.2.2)
- Juxtacellular recording and labeling (Section 2.3.1 – 2.3.2)
- Data selection and analysis of electrophysiological data (Section 2.3.3 – 2.3.4)
- Identification and quantification of axonal boutons (Section 2.4.1 – 2.4.2)
- Tissue preparation and indirect immunofluorescence of monkey tissue (Section 2.5.1)
- Stereological cell counts in the caudate and putamen of the rhesus monkey (Section 2.5.3)

4.4 RESULTS

4.4.1 Rat striatal PV+ interneurons can be subdivided into two populations with different topographic distributions and densities based on the expression of Scgn

In the rat dorsal striatum, the hypothesis that the PV-expressing interneurons which co-expressed Scgn (PV+/Scgn+) would have different anatomical features to those with PV alone (PV+/Scgn–) was first tested. The PV+/Scgn+ (Single arrow head; Figure 4.1 A) and PV+/Scgn– (Double arrow head; Figure 4.1 A) neurons appeared similar with respect to their somato-dendritic structure, as they were both medium sized neurons with somatic diameters of 16.8 ± 1.7 μm (n = 56) and 15.8 ± 1.7 μm (n = 62) respectively. Across the entirety of the striatum, stereological counts of all PV+ interneurons revealed that they had a mean density of 2031.7 ± 18.1 cells/mm^3, which represented an estimated total of 47134 ± 419 PV+ interneurons. Given past estimates of the total number of striatal neurons (Oorsthot, 1996), the number of PV+ interneurons estimated in this study represents 1.7% of all striatal neurons, which was greater than the estimated number of Scgn+ interneurons (see section 3.4.2), and is nearly 3 times greater than previous estimates of the total number of PV+ interneurons in the dorsal striatum of the rat (Luk & Sadikot, 2001). Immunofluorescent detection and stereological cell counting of PV and Scgn revealed that nearly half of all Scgn+ neurons also expressed PV (Figure 4.1 B). Approximately one-quarter of all striatal PV+ neurons also expressed Scgn (Figure 4.1 B) meaning that PV+/Scgn+ interneurons represent a relatively large striatal population whose density is approximately 593.8 ± 3.4 cells/mm^3 (Figure 4.1 D), which equates to 13775 ± 79 total cells within the striatum. As PV+/Scgn– interneurons made up nearly three-quarters of all PV+ neurons (Figure 4.1 B), they had a mean density of 1437.9 ± 20.8 cells/mm^3 (Figure 4.1 B), which equates to 33359 ± 482 total cells.

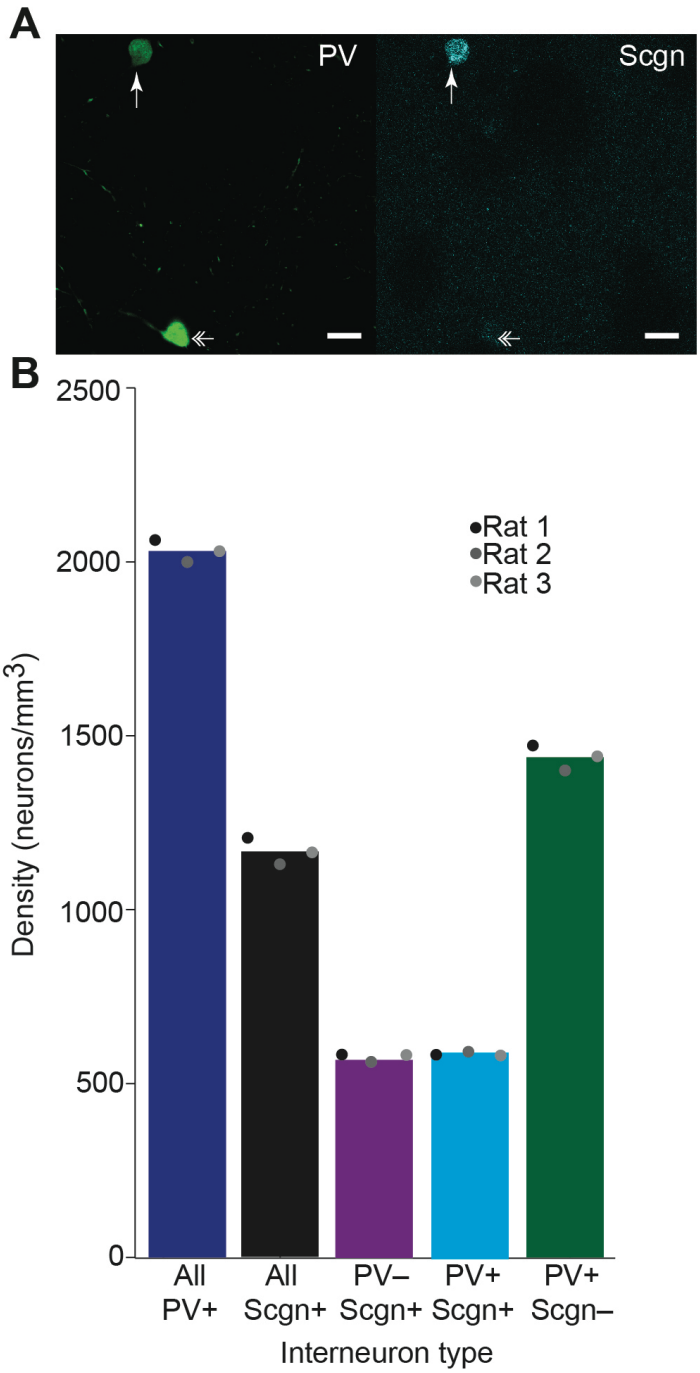


Figure 4.1: A large subpopulation of PV-expressing striatal interneurons co-express Scgn in rats, but not mice. **A)** Confocal micrographs of the rat dorsal striatum showing that PV-expressing interneurons that co-expressed (single arrowhead) and did not co-express (double arrowheads) Scgn. **B)** Density of interneurons with combinations of PV and Scgn expression. Interneurons co-expressing PV accounted for around half of all interneurons expressing Scgn. Interneurons expressing Scgn accounted for around a quarter of all interneurons expressing PV.

Analysis of PV+/Scgn– interneuron distribution in the striatum revealed that the density of these interneurons remains relatively constant along the striatum's rostro-caudal axis, with a small decline in density in most caudal aspects (Figure 4.2 Ai, B). In contrast, the density of PV+/Scgn+ interneurons was relatively low in rostral and central aspects, but dramatically increased in caudal striatum, i.e. in coronal planes from -2.6 mm to -3.3 mm in relation to Bregma (Figure 4.2 Aii, B). This therefore accounts for the relatively high density of Scgn+ neurons in caudal planes (see Figure 3.2A). Further topographical analysis demonstrated that PV+/Scgn− neurons are evenly distributed across the medio-lateral axis throughout the striatum (Figure 4.2 C), whereas PV+/Scgn+ interneurons are biased in distribution towards the lateral border in rostral striatum (i.e. anterior of Bregma), and towards the medial border in caudal striatum (Figure 4.2 C). In contrast, the PV+/Scgn+ interneurons were distributed evenly along the entire dorso-ventral axis throughout striatum, whereas PV+/Scgn− neurons had a dorsal bias in the coronal planes around Bregma (Figure 4.2 D). In summary, the selective expression of Scgn distinguishes two populations of PV+ interneurons that have significantly different spatial distributions in the rat dorsal striatum

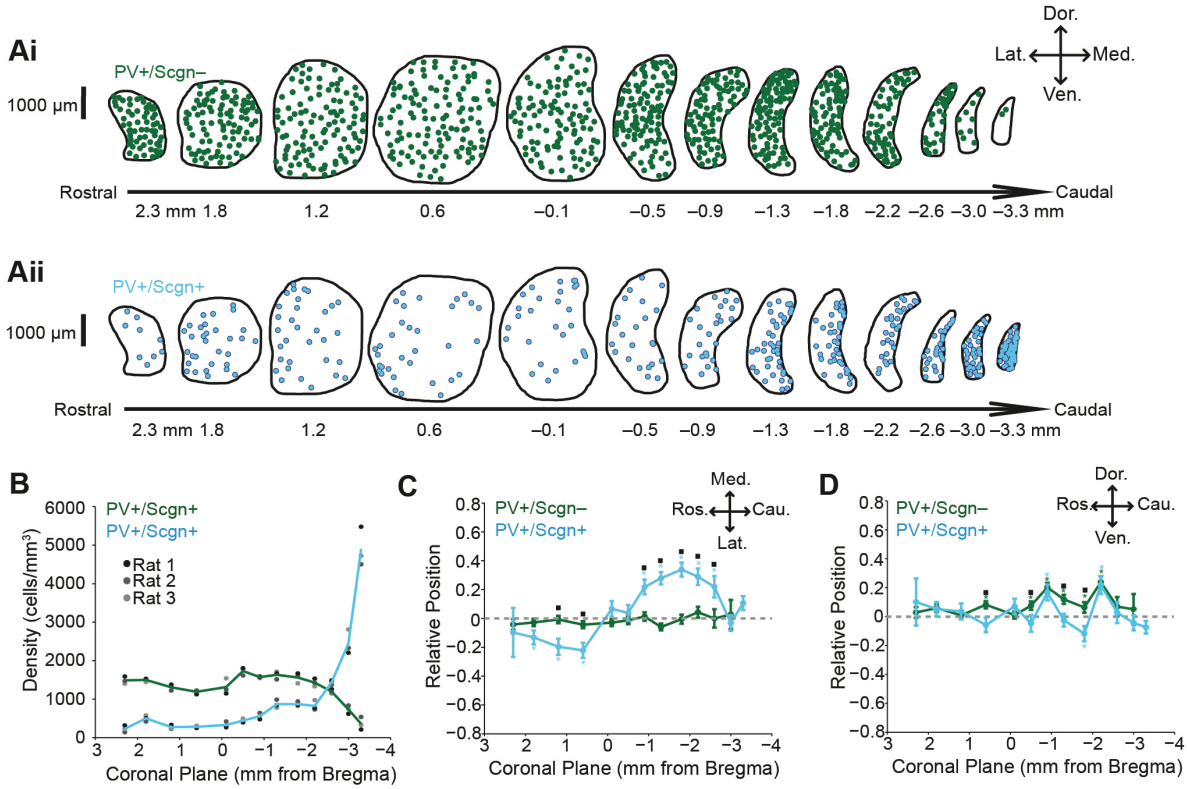


Figure 4.2: PV+/Scgn+ and PV+/Scgn– interneurons have different topographical bias the dorsal striatum of rat. A) Typical distribution of PV+/Scgn+ (**Ai**) and PV+/Scgn– (**Aii**) neurons across 13 coronal planes encompassing the rostro-caudal axis of the dorsal striatum in rat, with each dot representing a single neuron. **B**) Density of PV+/Scgn+ and PV+/Scgn– neurons along the rostro-caudal striatal axis of rats. Note the increase in density of PV+/Scgn+ neurons, and the small decrease in PV+/Scgn– cell density from rostral to caudal striatum **C**) Medio-lateral (**Ci**) and dorso-ventral (**Cii**) distribution of PV+/Scgn+ (blue line) and PV+/Scgn– (green line) neurons along 13 coronal planes. The presence of the asterisk (*) indicates a distribution that is significantly biased in one direction along the specified axis. Squares (□) indicate a significant difference in the distribution of the two populations along the specified axis within a given coronal plane. Data are means of the position of all neurons counted ± SEMs.

4.4.2 A population of unevenly distributed, PV+ interneurons in the caudate and putamen of the monkey can be distinguished by the co-expression of Scgn

Given the prevalence of Scgn expression within a subpopulation of PV+ interneurons in the dorsal striatum of the rat, the existence of this population in the Rhesus Macaque caudate/putamen was also investigated. As in the rat, both PV+/Scgn+ and PV+/Scgn- neurons the Rhesus Macaque caudate nucleus and putamen were medium-sized neurons with similar somatodendritic features (Figure 4.3 A). Unlike the scenario in the rat however, PV+/Scgn+ interneurons outnumbered PV+/Scgn$^-$ neurons (Figure 4.3 C). Indeed, PV+/Scgn+ neurons accounted for nearly 75% of all PV-expressing neurons in both the caudate nucleus and the putamen (Figure 4.3 Ci, Cii). Importantly, although the mean density of all PV+ interneurons in the monkey striatum was lower compared to the rat (Figures 4.1 D and 4.3 C), the mean density of PV+/Scgn+ interneurons was greater in the Rhesus Macaque (Figure 4.3 C), further indicating a potentially important role for this population in modulating the output of the caudate/putamen in Rhesus Macaques. The PV+/Scgn– neuron population in the monkey caudate/putamen was correspondingly less abundant compared to the PV+/Scgn– population in the dorsal striatum of rats (Figure 4.3 C). Along the rostro-caudal axis of the caudate nucleus, and the putamen, the density of PV+/Scgn+ interneurons was relatively low in rostral planes, but was far greater in caudal planes (Figure 4.3 B, Di). Thus, the increased density of Scgn+ neurons that was previously noted in caudal planes of the caudate/putamen (see Figure 3.5 B) is largely accounted for by the PV+/Scgn+ population, an observation that mirrors that made in the rat (see Figure 4.2 B). The distribution of PV+/Scgn– neurons in the Rhesus Macaque caudate nucleus also mirrored what was found in the dorsal striatum of rats, as their density also decreased along the rostro-caudal axis (Figure 4.3 B, Di). Along the medio-lateral axis of the caudate nucleus, both PV+/Scgn+ and PV+/Scgn– interneurons were relatively unbiased in their distribution (Fig. 4.3 Ei). In contrast, PV+/Scgn– interneurons in the putamen were heavily biased towards the lateral region of the striatum in all but the most rostral planes, while PV+/Scgn+ interneurons remained unbiased along the medio-lateral axis (Figure 4.3 Eii). These findings contrast with those of the

dorsal striatum in rats, in which the PV+/Scgn+ population that displayed a strong bias within the medio-lateral striatal axis (Figure 4.2 C). Along the dorso-ventral axis, the results in Rhesus Macaques contrast those in the rat once again, in so far that both the PV+/Scgn+ and PV+/Scgn– populations tended to have a dorsal bias (in both the caudate nucleus and the putamen; Figure Eii and Fii). Taken together, these results show that the expression of Scgn identifies a major subpopulation of PV+ interneurons in the caudate/putamen of the monkey. The existence of this molecular dichotomy in the PV+ interneurons of the Rhesus Macaque further highlights the importance of heterogeneity among striatal interneuron populations, and also that the distinct molecular profiles of these cells is accompanied by differently biased distributions within the striatum.

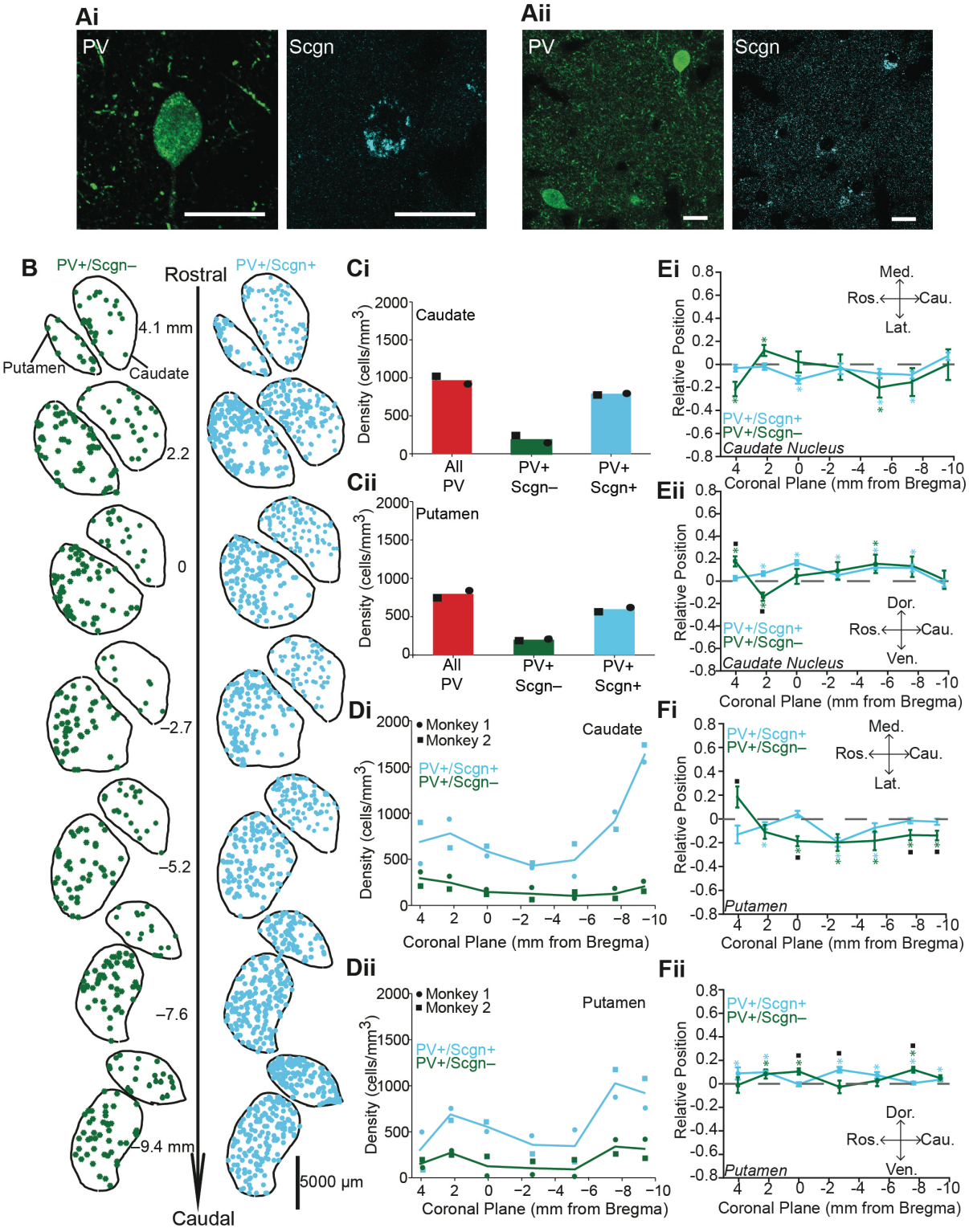

Ai
PV
Scgn
Aii
PV
Scgn
B
PV+/Scgn–
PV+/Scgn+
Rostral
4.1 mm
Putamen
Caudate
2.2
0
–2.7
–5.2
–7.6
–9.4 mm
5000 µm
Caudal
Ci
Caudate
Density (cells/mm3)
All PV
PV+ Scgn–
PV+ Scgn+
Cii
Putamen
Di
Monkey 1
Monkey 2
PV+/Scgn+
PV+/Scgn–
Caudate
Coronal Plane (mm from Bregma)
Dii
Putamen
Ei
Relative Position
Med.
Ros.
Cau.
Lat.
Caudate Nucleus
Eii
Dor.
Ven.
Fi
Putamen
Fii

Figure 4.3: PV+/Scgn+ and PV+/Scgn– interneurons have different topographical bias the caudate and putamen of the rhesus monkey. A, B) Confocal micrographs of the macaque striatum showing that PV-expressing interneurons that co-expressed (**A**) and did not co-express (**Aii**) Scgn. **B**) Typical distribution of PV+/Scgn– (left) and PV+/Scgn+ (right) neurons across 7 coronal planes of macaque caudate and putamen, with each dot representing a single neuron. **C)** Mean density of all PV-expressing interneurons across the entirety of the caudate nucleus (**Ci**) and the putamen (**Cii**), including those populations that express (blue bar) and do not express (green bar) Scgn. In the macaque caudate-putamen, PV+/Scgn+ represent nearly 70% of all PV-expressing neurons. **C**) Density of PV+/Scgn+ (blue) and PV+/Scgn– (green) neurons along the rostro-caudal axis of both the caudate (**Bi**) and the putamen (**Ci**). Note that the PV+/Scgn+ population in the monkey increases in density towards the caudal planes of the caudate and the putamen. **D**) Density of PV+/Scgn+ (blue line) and PV+/Scgn– (green line) along the rostro-caudal axis of the caudate nucleus (**Di**) and the putamen (**Dii**). Dots and squares indicate the values for individual animals. **E-F)** Analysis of medio-lateral (**Ei, Fi**) and dorso-ventral (**Eii, Eii**) distribution of PV+/Scgn+ (blue line) and PV+/Scgn– (green line) neurons along 7 coronal planes encompassing the caudate (**E**) and putamen (**F**). The presence of the asterisk (*) indicates a distribution that is significantly biased in one direction along the specified axis. Squares (□) indicate a significant difference in the distribution of the two populations along the specified axis within a given coronal plane. Data are means of the position of all neurons counted ± SEMs.

4.4.3 Spontaneous in vivo activity of identified PV+/Scgn– and PV+/Scgn+ interneurons during cortical SWA and activation states.

In the cerebral cortex and hippocampus, the expression profile of CPBs often acts as a correlate of specific or specialised intrinsic and network-level physiological properties (Somogyi and Klausberger, 2005). This highlights the possibility that PV+/Scgn- and PV+/Scgn+ interneurons in the dorsal striatum also have distinct physiological properties. To address this, individual PV+/Scgn– and PV+/Scgn+ interneurons (n = 13 and 9, respectively) were extracellularly recorded and juxtacellularly labeled with neurobiotin in both rostral (Figure 4.4 A, C) and caudal (Figure 4.4 B, D) planes of the striatum of urethane-anaesthetised rats. These identified interneurons were recorded during two distinct brain states (SWA and cortical activation – Figure 4.4 Aiii, Aiv, respectively) that have been previously used to give context to recordings of striatal PV+ interneurons in vivo (Mallet et al., 2005; Sharott et al, 2012). Both PV+/Scgn– and PV+/Scgn+ neurons had medium-sized somata (15-25 μm in diameter) and (in those cells that were well labelled) 2-4 aspiny dendrites that extensively ramified close (~300 μm) to the cell body (Figure 4.4 Ai, Bi, Ci, Di). As previously described (Sharott et al, 2012), PV+ interneurons had highly variable firing during cortical SWA, with rates varying from <1 to 10 spike/s (Figure 4.4 Aiii-Diii, Aiv-Div). Some PV+ interneurons, particularly those identified as PV+/Scgn–, displayed high-frequency bursts of spikes during the active component (peaks) of the

cortical slow oscillations, while others fired irregularly with just one for few spikes during some active components (Figure Aiv - Div). In agreement with past studies (Sharott et al., 2012) the firing of PV+ interneurons during cortical activation was less heterogeneous compared to their firing during cortical SWA.

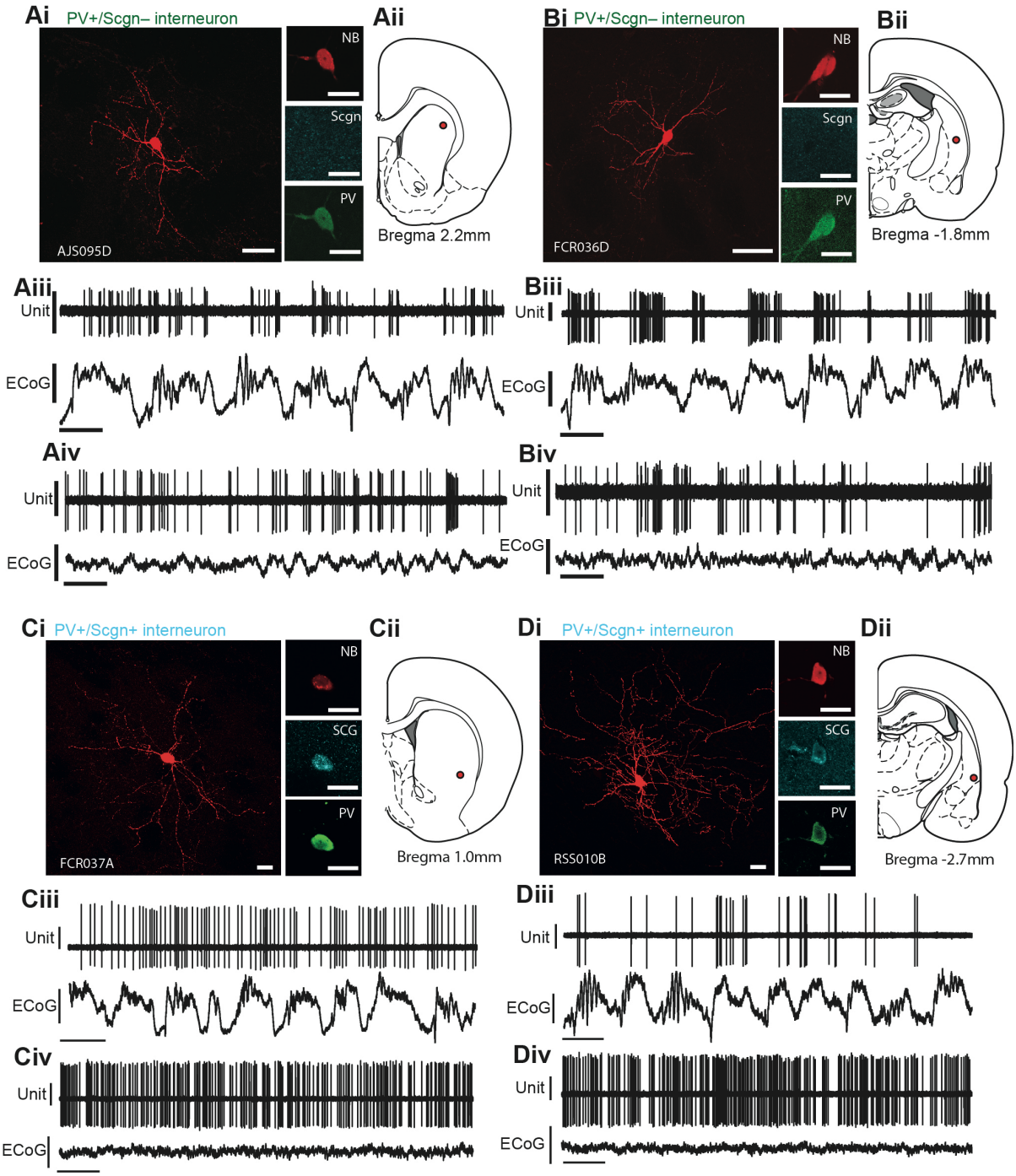


Figure 4.4: Juxtacellular recording of identified PV+/Scgn– and PV+/Scgn+ striatal interneurons. A-D) Juxtacellularly-labeled PV+/Scgn– (**A, B**) and PV+/Scgn+ (**C, D**) interneurons, identified by their co-localization of fluorescent labeling for neurobiotin (NB), PV and Scgn recorded in the dorsal striatum of anaesthetized rats. To ensure a complete characterization of the electrophysiological properties of PV+ interneurons, some PV+/Scgn– and PV+/Scgn+ interneurons were recorded in the rostral striatum (**Aii, Cii**), while others were recorded in the caudal striatum (**Bii, Dii**). **Aiii, Biii**) Spontaneous action potential discharges (unit activity) of individual PV+/Scgn– interneurons during robust cortical slow-wave activity, as recorded in the frontal electrocorticogram (ECoG). **Ciii, Diii**) Spontaneous action potential discharges (unit activity) of individual PV+/Scgn+ interneurons during robust cortical slow-wave activity, as recorded in the frontal electrocorticogram (ECoG). **Aiv, Biv**) Firing of the same PV+/Scgn– interneurons during spontaneous cortical activation. **Civ, Div**) Firing of the same PV+/Scgn+ interneurons during spontaneous cortical activation. Scale bars for recordings represent 0.5mV for the unit activity and 1mV for the ECoG.

It was readily apparent in the extracellular recordings that PV+ interneurons fired spikes that were relatively short in duration (~1 ms; Figure 4.5 A). As has been previously established (Sharott et al., 2012), the length of the waveforms recorded from each identified neuron was divided into 2 segments: the D1 segment which was the length of time needed for the waveform to reach its peak amplitude, and the D2 segment which was the length of time taken for the waveform to return to return to its baseline value (Figure 4.5 A). On average, the durations of spikes of PV+/Scgn+ interneurons (0.81 ± 0.12 ms, n = 7) were shorter than those of PV+/Scgn– interneurons (1.1 ± 1.7 ms, n = 9; Mann-Whitney U test, $p<0.05$; Figure 4.5 A). This was due to the significantly shorter length of the D1 segment of the action potential of PV+/Scgn+ interneurons (0.32 ± 0.06 ms, n = 9) compared to that of PV+/Scgn– interneurons (0.45 ± 0.08 ms, n = 8; Mann-Whitney U test, $p<0.05$; Figure 4.5 A). During juxtacellular recordings, it is well known that the waveforms of recorded neurons can vary depending on the amplitude of said waveforms (Mallet et al., 2005; Magill et al., 2006; Abdi et al., 2015). In this study, the mean waveform amplitude of all analyzed PV+/Scgn+ was 1.2 ± 0.3 mV, (n = 7) while the mean waveform amplitude of all PV+/Scgn– interneurons used in this study was 1.3 ± 0.4 mV (n = 9) (Data not shown). As these were not significantly different from one another, it is unlikely that the shorter waveform lengths of PV+/Scgn+ interneurons reported were caused by differences in the amplitudes of those same waveforms.

Given previous reports that striatal PV+ interneurons have heterogeneous firing patterns in vivo (Sharott et al., 2012), the firing rates of identified PV+/Scgn+ and PV+/Scgn– interneurons were compared in order to determine whether these molecular differences were reflected in distinct firing rates (Figure 4.5 B). During SWA, the firing rate of both PV+Scgn+ and PV+Scgn– interneurons did not differ significantly, while the firing rate of PV+Scgn+ interneurons was significantly greater than that of PV+Scgn– interneurons during spontaneous cortical activation ($p = 0.03$; Mann-Whitney test; Figure 4.5 B). For all analyses that were performed, the power of the following EEG oscillations was compared between recordings of PV+/Scgn+ interneurons and PV+/Scgn– interneurons: the power of the slow oscillations (0.4 – 1.6 Hz) during cortical SWA, the power of the spindle oscillations (7 – 12 Hz) during cortical SWA and the power of gamma oscillations (30 – 80 Hz) during both cortical SWA (sometimes referred to as the "active component" of SWA) and activation. When comparing the power of these various EEG oscillations during recordings of either PV+/Scgn+ interneurons or PV+/Scgn– interneurons, no significant differences were detected, meaning that any significant differences between the firing activity of PV+/Scgn+ and PV+/Scgn– interneurons reported here are not the result of significant differences in the power of the EEG during any recording period used for analysis. In summary, the expression of Scgn within the PV-expressing striatal interneuron population is correlated with differences in firing rate during cortical activation; further suggesting that co-expression of Scgn identifies a novel population of PV+ interneurons.

In comparison to other striatal interneurons, PV+ interneurons show unusually high levels of heterogeneity in their firing rates and patterns in vivo (Sharott et al, 2012), a physiological feature that implies the existence of potential subpopulations. In order to test whether the co-expression of Scgn could explain some of this heterogeneity, correlations between the ISI histograms of pairs of neurons with different PV/Scgn expression were computed (Figure 4.5 C, D). It was hypothesized that PV+/Scgn+ interneurons would have firing patterns more similar to each other than to PV+/Scgn– interneurons during both cortical SWA and cortical activation. As a

point of reference, these analyses also included data from ChAT+ interneurons (Sharott et al., 2012; Doig et al., 2014) recorded under the same conditions (Figure 4.5 C, D), which have a relatively narrow range of ISIs despite having different modes of firing (Sharott et al, 2012). Thus, correlations between the ISI histograms of ChAT+ interneurons often have Spearman correlation coefficients (r-values) close to 1 (Figure 4.5 C, D). During both SWA and cortical activation, the r-values for pairs of PV+/Scgn+ neurons were on average significantly higher than those of PV+/Scgn– neuron pairs, but were not different to those of ChAT+ interneuron pairs (Figure 4.5 C, D). These results show that the firing of the population of PV+/Scgn+ neurons is more homogeneous than the firing of the population of PV+/Scgn– neurons, and further suggest that the highly variable firing rates and patterns of PV+ interneurons previously observed in vivo (Sharott et al, 2012) could arise from the sampling of both PV+/Scgn+ and PV+/Scgn– cell populations, and perhaps biased sampling in favor of the latter.

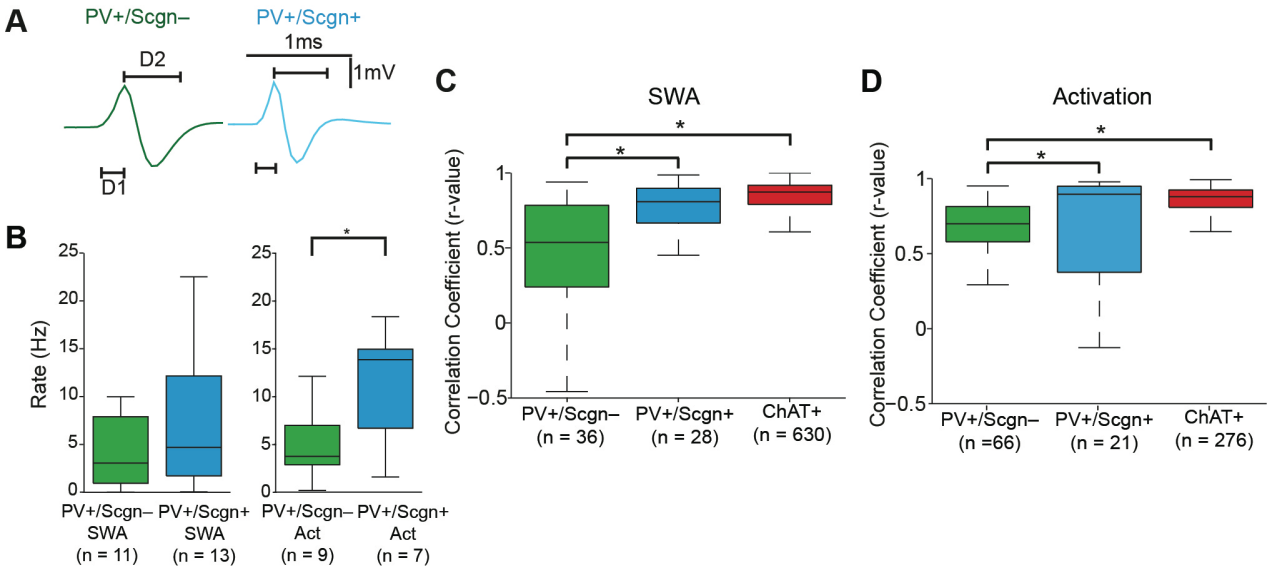


Figure 4.5: Electrophysiological properties of identified PV+/Scgn– and PV+/Scgn+ interneurons recorded in the dorsal striatum of anaesthetized rats. A) The mean action potential waveforms of PV+/Scgn–and PV+/Scgn+ interneurons. Both groups had short waveforms (around 1ms), but those of PV+/Scgn+ interneurons were significantly shorter. **B)** The mean firing rate was not significantly different in SWA, but PV+/Scgn+ interneurons has a significantly higher firing rate during activation. **C-D)** The similarity of firing patterns between individual PV+/Scgn–, PV+/Scgn+ and cholinergic (Chat+) neurons was assessed by calculating the correlation coefficient (Spearman) between interspike interval (ISI) histograms. In both SWA (**C**) and activation (**D**), the correlation coefficients between pairs of PV+/Scgn+ ISI histograms was significantly higher than PV+/Scgn– pairs, but not significantly different to ChAT+ pairs.

4.4.4 PV+/Scgn– and PV+/Scgn+ interneurons show phase locking preferences to different cortical network oscillations

Given that identified striatal PV+ interneurons show a strong tendency to phase lock their firing to cortical oscillations (Sharott et al, 2012), the phase locking of the spikes of PV+/Scgn+ and PV+/Scgn– interneurons to ECoG oscillations across frequencies from 0.4-100 Hz in both SWA and global activation was assessed. As suggested by the raw data (Figure 4.4 Aiv - Div), both types of PV+ interneuron tended to fire in time with the active component of cortical slow oscillations (0.4-1.6 Hz) during SWA, but the resultant phase locking of the PV+/Scgn- cell population was stronger than that of the PV+/Sgcn+ population (Figure 4.6 A, B). In line with these results, the firing of PV+/Scgn– interneurons was more strongly phase locked to cortical spindle oscillations (7-12 Hz), which was also reflected in a greater proportion of significantly locked PV+/Scgn– interneurons during cortical SWA (Figure 4.6 C). In contrast, the firing of PV+/Scgn+ interneurons during cortical SWA was more tightly locked to gamma oscillations (30-80 Hz) as compared to the PV+/Scgn– interneurons (Figure 4.6 A-C). During cortical activation, the phase-locked firing of the PV+/Scgn+ and PV+/Scgn– cell populations was generally more similar across all frequencies (Figure 4.6 D, E). However, around three times more PV+/Scgn+ interneurons were locked at gamma frequencies (30- 60 Hz) as compared to PV+/Scgn– interneurons during cortical activation (Figure 4.6 F). Taken together, these results show that the temporal organization of the firing of PV+/Scgn– and PV+/Scgn+ interneurons with respect to ongoing cortical oscillations is distinct and brain state-dependent.

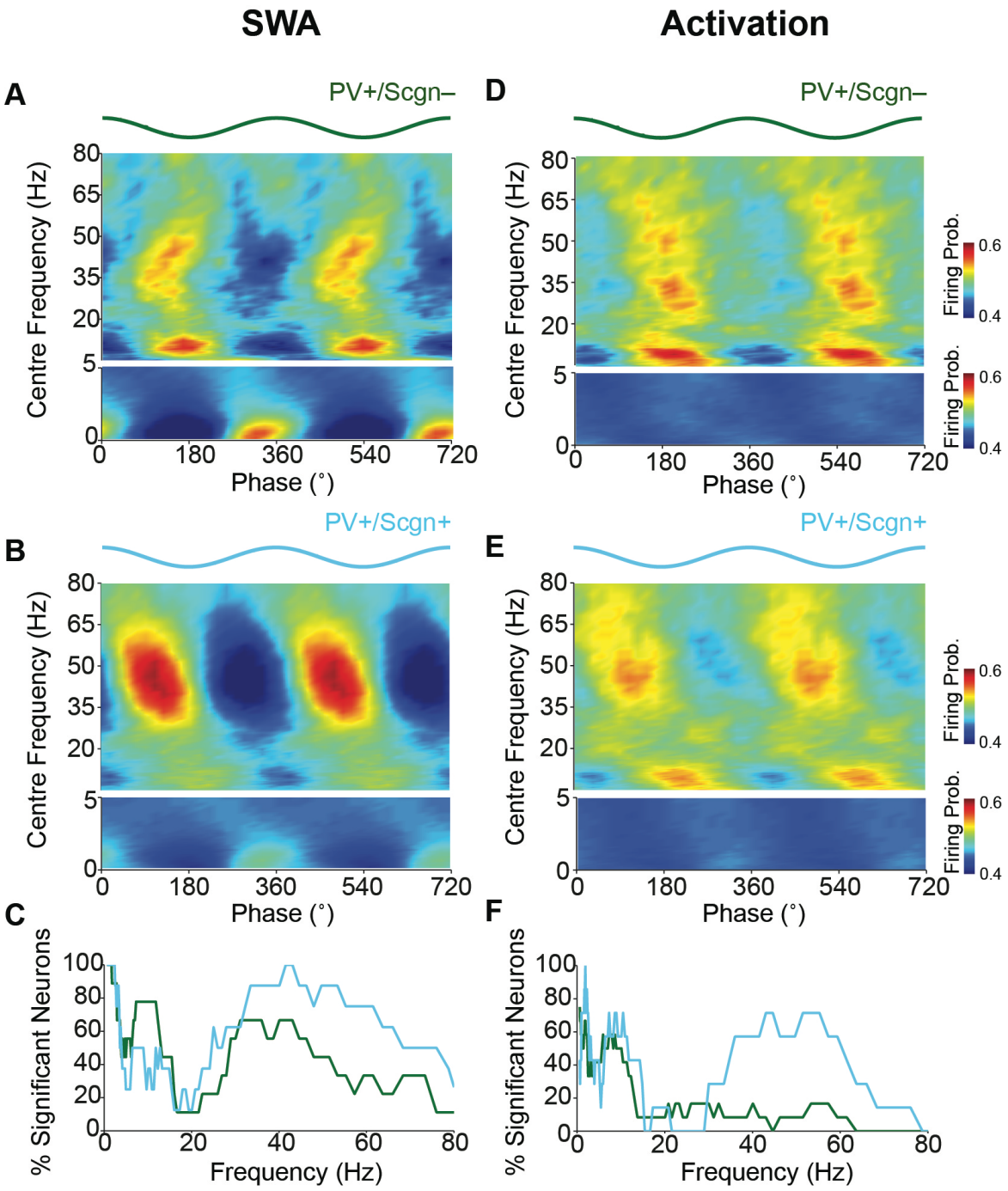


Figure 4.6: PV+/Scgn– and PV+/Scgn+ striatal interneurons have different profiles of phase locking to cortical oscillations. A-B) Mean phase histograms of striatal PV+/Scgn– (**A**) and PV+/Scgn+ (**B**) interneurons for cortical oscillations of 0.4-80Hz during SWA. Note the stronger locking of PV+/Scgn– interneurons to slow (0.4-1.6) and spindle (7-12Hz) frequencies, and the strong locking of PV+/Scgn+ neurons to gamma (30-80Hz) **C)** Histogram showing the percentage of significantly PV+/Scgn– (green) and PV+/Scgn+ (blue) across the above frequency range as measured by the Raliegh test ($p<0.05$) during SWA. **D-E)** Mean phase histograms of striatal PV+/Scgn– (**D**) and PV+/Scgn+ (**E**) interneurons for cortical oscillations of 0.4-80Hz during global activation. Note the difference in frequency and angle in the gamma frequency range. **F)** As in C, for global activation.

4.4.5 A higher proportion of PV+/Scgn– axonal boutons contact SPN cell bodies

The results from the stereological cell counts and electrophysiological recordings of identified neurons that are detailed above converge to suggest that PV+/Scgn+ and PV+/Scgn– are distinct cell types. However, the full definition of a given cell type requires understanding of not only its neurochemical/molecular properties and the temporal organization of its activity, but also of the cellular targets that it innervates. With the latter in mind, a subset of the recorded and well-labelled PV+/Scgn+ and PV+/Scgn– interneurons (n = 4 and 4, respectively) was exploited to gain insight into whether these cell populations target the same types of spiny projection neuron to the same extents. In order to determine whether the neurobiotin filled axonal boutons of labelled PV+Scgn+ and PV+Scgn– differed with respect to their targeting of spiny projection neurons, immunostains against the SPN cell body marker DARPP-32 (Aubry et al., 2008) were performed. Confocal microscopy was thus used to detect and quantify any close appositions between the DARPP-32+ somata of SPNs and the neurobiotin-filled axonal swellings/boutons of the identified interneurons (Figure 4.7 A, B). This sampling strategy takes advantage of the characteristic 'basket-like' innervation of SPN cell bodies by the axons of PV+ interneurons in the dorsal striatum (Kawaguchi et al., 1995; Bolam et al., 2000). The axonal boutons of both PV+/Scgn– and PV+/Scgn+ neurons were commonly apposed to SPN somata (Figure 4.7 A, B). However, PV+/Scgn– interneurons were more likely to target the somata of SPNs; 49.7± 5.8% of the axonal boutons of PV+/Scgn– neurons (n = 249 of 490 boutons counted from 4 interneurons) were apposed to SPN somata, whereas only 28.1± 4.9% of the boutons of PV+/Scgn+ neurons (n = 180 of 709 boutons counted from 3 interneurons) were similarly apposed to SPNs (Figure 4.7 C). Although PV+/Scgn– interneurons differed from PV+/Scgn+ interneurons with respect to the frequency of axonal appositions with SPN somata, it was found that when a single SPN somata was contacted by either a PV+/Scgn+ interneuron or a PV+/Scgn– interneuron, PV+/Scgn+ interneurons made significantly more appositions on each contacted SPN compared to PV+/Scgn– interneurons (Figure 4.7 D). For both groups of interneurons, those boutons classified as not being apposed to SPN somata were defined as not being in contact with any detectable

DARPP-32 signal. In rare cases where the DARPP-32 signal would label proximal dendrites, any boutons apposed to these dendrites were simply treated as not being apposed to a SPN cell body. These results therefore demonstrate that although both PV+/Scgn– and PV+/Scgn+ interneurons innervate SPN somata, the former cell type have a stronger preference to do so.

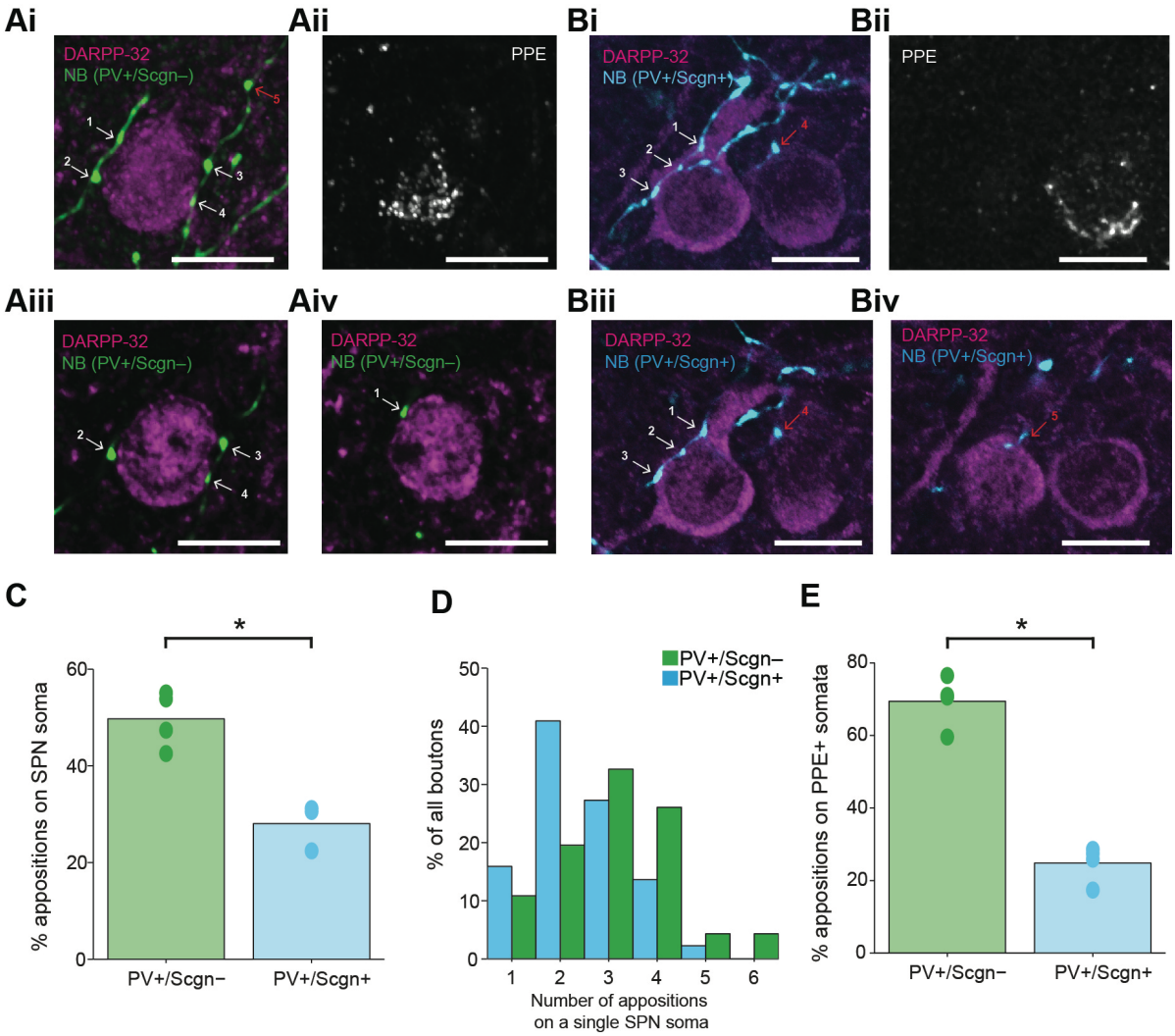


Figure 4.7: PV+/Scgn– and PV+/Scgn+ striatal interneurons have different axonal targets.
Ai) Confocal fluorescent micrograph stack of a neurobiotin-labelled axon (NB) from a PV+/Scgn– interneuron targeting a spiny projection neuron (SPN) revealed with DARRP-32. The axon forms 4 appositions with the SPN soma, marked with white arrows. **Aii)** The SPN expresses PPE, indicating it is in the indirect pathway (iSPN). **Aiii-iv)** Single plane confocal micrographs showing that each of the 4 boutons are opposed to the soma. **Bi)** Confocal fluorescent micrograph stack of a neurobiotin-labelled axon (NB) from a PV+/Scgn+ interneuron traversing two SPNs. The axon forms 3 appositions with the left SPN soma, marked with white arrows, and appears to form a single apposition with the right SPN, marked with a blue arrow. **Bii)** The right SPN expresses PPE, while the left SPN does not, indicating it is in the direct pathway (dSPN). **Biii-iv)** Single plane confocal micrographs showing the boutons 1-3 are opposed to the soma of the dSPN, while boutons 4 and 5 are not opposed to the (PPE–) dSPN. **C)** The boutons of PV+/Scgn– axons formed significantly more somatic appositions with SPNs (as compared to all boutons not contacting an SPN soma) than those of PV+/Scgn+ interneurons. **D)** Histogram of the frequency of different numbers of appositions formed with an individual SPN soma for both types of interneuron. PV+/Scgn+ interneurons made significantly more appositions on each contacted SPN. **E)** PV+/Scgn– interneurons formed a significantly larger percentage of appositions with PPE+ iSPNs (all other boutons were opposed to PPE- dSPNs).

4.4.6 The axons of PV+/Scgn– and PV+/Scgn+ interneurons are preferentially apposed to different types of spiny projection neurons

The results above suggest that PV+/Scgn– and PV+/Scgn+ interneurons target the somata of SPNs to different extents. Given that SPNs are dichotomously organized within the striatum (Gerfen et al., 1990; Yung et al., 1995), an investigation into the identity of the SPNs innervated by these interneurons was conducted. A different set of sections containing the neurobiotin-labeled axons of PV+/Scgn– and PV+/Scgn+ interneurons were immunolabeled for the SPN marker DARPP-32 (Aubry et al., 2008) as well as for preproenkephalin (PPE), a selective marker of SPNs of the so-called "indirect pathway" (Zhou et al., 2003; Figure 4.7 A,B). As gephyrin labeling could not be reliably included in these incubations, all boutons apposed to DARPP-32+ somata were counted. The axonal boutons of PV+/Scgn– interneurons were preferentially apposed to PPE+ SPNs (n = 80 of 119 boutons counted from 4 interneurons), while the axonal boutons of PV+/Scgn+ neurons preferentially contacted the cell bodies of PPE-null or "direct pathway" SPNs (n = 178 of 238 boutons counted from 4 interneurons; Figure 4.7 E). Importantly, both the PV+/Scgn+ and PV+/Scgn– interneurons used in this analysis were located in both rostral (Figure 4.4 A, C) and caudal (Figure 4.4 B, D) planes of the dorsal striatum, meaning that the lack of indirect pathway SPNs (i.e. SPNs that do not express PPE) that has been reported in the caudal striatal pole (Gangarossa et al., 2013 – note that this finding was in the mouse) is unlikely to have affected these results. Combined with the findings from experiments in Section 4.2.6, these data suggest that the connections of PV+/Scgn+ and PV+/Scgn– interneurons within the striatal microcircuit are different, thereby adding further weight to the notion that these two interneuron populations are distinct cell types.

4.5 DISCUSSION

Here, the characterization and quantification of secretagogin and parvalbumin expression by neurons of the dorsal striatum has revealed an extensive degree of molecular heterogeneity within the classical PV+ interneuron population of the rat and Rhesus Macaque striatum. Thus, PV+ interneurons can be subdivided into populations of PV+/Scgn+ and PV+/Scgn– interneurons. This molecular heterogeneity was correlated with specific topographical, anatomical and physiological properties that further distinguish the two populations. This in turn suggests that PV+/Scgn+ and PV+/Scgn– interneurons constitute two potentially novel types of striatal interneuron in rats and Rhesus Macaques. Importantly, this dichotomy does not necessarily imply that each population is homogeneous. Indeed, given the degree of heterogeneity in the electrophysiological properties of PV+/Scgn– interneurons in vivo (Figure 4.4; 4.5), it is likely that further subdivisions may exist among PV+ striatal interneuron populations. This is in accordance with the multitude of PV+ interneuron subtypes that have been identified in other CNS structures, particularly the cortex and the hippocampus (Klausberger and Somogyi, 2008). The finding that the co-expression of secretagogin and parvalbumin is also present, albeit to a relatively tiny degree, in the mouse striatum (see section 3.4.1), is of value because it further supports the existence of a clear disparity between mice and rats with respect to striatal interneuron populations (Oorschot 2013; Petryszyn et al., 2014). Given this crucial species difference, the existence of substantial levels of Scgn and PV co-expression in neurons in both the caudate and putamen of Rhesus Macaques demonstrated in this study is critical, as it supports the hypothesis that, in this particular case, the rat and primate are more “closely related”. This hypothesis is supported not only by the relative numbers of PV+/Scgn+ interneurons in the Rhesus Macaque striatum, but also by the finding that their distributions within the caudate nucleus and the putamen correlated well with what was observed in the rat (Figures 4.2 and 4.3).

4.5.1 Topographical distributions of subtypes of PV+ interneurons and their relationship to the distribution of cortical inputs to the dorsal striatum

Interneurons expressing Scgn are distributed at high densities in the rostral and caudal striatum of both rats and Rhesus Macaques (see sections 3.4.2 and 3.4.4). The preferential distribution of Scgn+ interneurons in the caudal striatum, where their population density reaches a value greater than the mean density of any other reported striatal interneuron population (Oorschot, 1996; Oorschot, 2013), is the result of Scgn co-expression by many PV+ interneurons. Although this study provides estimates for the total numbers of PV+/Scgn+ and PV+/Scgn– interneurons as a reference point for future studies, it is the biased topographical distribution described for these 2 groups that provides hints towards their potential function within the striatal microcircuit. Anatomically, it is already well established that the somata of individual PV+ interneurons are contacted by multiple boutons from corticostriatal neurons (Kita et al., 1990; Kita, 1993). These synapses made with PV+ interneurons therefore provide corticostriatal projections another avenue with which to strongly influence the activity of the striatal microcircuit (Parthasarathy & Graybiel, 1997).

The finding that cortical and thalamic input into the striatum is organized in a partly overlapping, topographical manner was used to suggest that different striatal regions receive, and therefore process, input from different cortical areas (McGeorge and Faull, 1989). Indeed, this has formed the basis for a variety of theories regarding the functional organization of the striatum, most notably the Albin-Delong model (Albin, Young and Penney 1989; DeLong 1990). These parallel pathways of corticostriatal inputs into the striatum are reflected in the different responses of striatal neurons to sensory stimulation in a manner that is dependent on their position along the medio-lateral axis of the striatum (Reig & Silberberg, 2014). In the rat, PV+/Scgn+ interneurons were found to be biased in their distribution towards the medial aspects of the striatum that lie behind Bregma (Figure 4.2), and towards the lateral aspects of the striatum that lie ahead of Bregma (Figure 4.2). In the caudal most planes of the striatum, these interneurons were found

throughout the structure, whereas the presence of PV+/Scgn– interneurons was almost negligeable (Figure 4.2). These striatal areas receive converging input from the orbital prefrontal cortex (Hoover & Vertes, 2011, Mailly et al, 2013), cingulate (Mailly et al, 2013), visual (Khibnik et al., 2014) and auditory cortices (Znamenskiy et al, 2013; Xiong et al, 2015) and receive relatively little input from motor cortex (McGeorge and Faull, 1989; Deng et al., 2015). Given that PV+ interneurons receive direct cortical input (Kita et al., 1990; Kita, 1993), their preferential distribution within areas known to receive a great deal of limbic and sensory cortical input most likely indicates that they are involved in the processing of these inputs. Indeed, a recent study by Graybiel and colleagues (Friedman et al., 2015) found that "high-frequency neurons" (which are likely to be PV+ "fast-spiking interneurons") in the striosomal compartments of the striatum (known to receive input from prelimbic cortices) produced burst like activity when rats were made to perform a cost-benefit analysis (Friedman et al., 2015). This activity produced strong inhibition of neighboring projection neurons, and was reproduced through optogenetic activation of the corticostriatal fibers originating from the prelimbic cortex. These results therefore illustrate the principle that PV+ interneurons, through their biased positioning within the striatum, can receive input from select cortical areas in order to exert a powerful influence over the output from discrete striatal microcircuits, and hence behavior.

4.5.2 The topographical distribution of PV+ subsets is related to heterogenous activity in different striatal regions during behavioral tasks

Such disparity in distribution of fast-spiking interneurons (which are presumed to be PV+ interneurons – Kawaguchi, 1993; although whether all striatal FSIs are PV+ has yet to be demonstrated) along the medio-lateral striatal axis has become particularly important, as a variety of studies have demonstrated that the dorso-medial (DM) and dorso-lateral (DL) striatum located in the coronal planes around Bregma (Gremel & Costa, 2013) each contribute to the striatal processes involved in learning of novel actions as well as their subsequent consolidation in a highly specialized manner (Gremel & Costa, 2013). Indeed, it is now accepted that activity in the

DMS and DLS plays a significant role in goal directed and habit driven behavior, respectively (Balleine & Doherty, 2010). The results described in these studies do not simply apply to the activity of SPNs, as FSIs of the dorsomedial striatum (i.e. those expressing PV but not Scgn) and not those of the dorsolateral striatum (i.e. those PV+ neurons expressing Scgn) have specifically been implicated in the action-specific responses associated with reward prediction error signaling in the striatum (Stalnaker et al., 2012). Importantly, this conclusion is based on the assumption that striatal FSIs are PV+ interneurons (Kawaguchi, 1993). Moreover, although PV+/Scgn– interneurons are not biased towards the medial striatum in the coronal planes located around Bregma, the lack of PV+/Scgn+ interneurons in the medial striatum of those planes implies that PV+ interneurons (and hence FSIs) in the dorsomedial striatum are likely to be PV+/Scgn– (Figure 4.2 A). In the dorsolateral striatum of coronal planes around Bregma, the high density of PV+/Scgn+ interneurons is taken to mean that FSI activity measured in these regions reflects the firing of PV+/Scgn+ interneurons. However, given that PV+/Scgn– interneurons are also present in this region (Figure 4.2 A) and that they outnumber PV+/Scgn+ interneurons by a factor of 3:1 throughout the entirety of the striatum (Figure 4.1 B), it is likely that FSI activity in the DLS is a combination of both PV+/Scgn+ and PV+/Scgn– interneuron activity.

The separate functional contributions of the DLS and DMS to the learning process are well demonstrated when each of these regions are lesioned. Indeed, lesions of the dorsolateral striatum have been shown to impair action generalization while those affecting the dorsomedial striatum impair action discrimination while biasing the animal's behavior towards action generalization (Hilario et al., 2012). As with most studies performing tetrode recordings during behavioral tasks, lesions of the DLS and DMS are often performed in striatal planes located around Bregma (Hilario et al., 2012). The data presented in this study shows that PV+ interneurons in the DMS striatum near Bregma are mostly PV+/Scgn– interneurons with most PV+/Scgn+ interneurons being located in the DLS near Bregma. Thus, the behavioral differences that arise during separate lesions of these 2 regions may be related to the dichotomy of PV+

interneurons presented here, as no other cell population within the striatum has been demonstrated to have any paritulcarly preference in its distribution towards either the DLS or the DMS (Kreitzer, 2009; Tepper et al., 2010; Oorschot, 2013). Finally, divisions of PV+ interneuron activity in the DLS and DMS (around Bregma) have also been reported in addiction, where rodents sensitized to cocaine showed a significant decrease of PV-expressing neurons in the PV+/Scgn+ poor DMS (but not the DLS), following a 2-week withdrawal period (Todtenkopf et al., 2004).

4.5.3 The expression of Scgn identifies subsets of heterogeneously distributed PV-expressing interneurons in the Rhesus Macaque caudate/putamen

In accordance with previous studies in monkeys, PV+ interneurons were more numerous in the caudate nucleus compared to the putamen (Wu & Parent, 2000). As in the rat, the increased density of Scgn-expression in the caudal striatum of Rhesus Macaque (caudate and putamen; see Figure 3.6) is accounted for by its presence in many PV+ interneurons (Figure 4.3). In the monkey, these caudal striatal regions have been implicated in sensorimotor tasks, as they receive strong inputs from primary and supplementary motor and sensory cortices (Parent & Hazrati, 1995; Postuma & Dagher, 2006; Di Martino et al., 2008). This is partially in line with what is known regarding cortical input into the rodent striatum, where caudal regions are known to receive sensory (primarily auditory) inputs (Glynn & Ahmad, 2002), although motor cortices primarily target the dorso-lateral (in central coronal planes around Bregma) striatum (Glynn & Ahmad, 2002; Deng et al., 2010).

In the caudate nucleus, both the PV+Scgn– and the PV+Scgn+ populations once again demonstrated significant biases in their distribution along the medio-lateral and dorso-ventral axes. The dorsal bias displayed by PV+/Scgn+ neurons in monkeys contrasts with results in rats. The existence of this dorsal bias in the caudate nucleus is of particular note because the dorsal, central and ventral regions of the caudate nucleus of non-human and human primates receive

different sensorimotor, associative and limbic cortical inputs, respectively (Karashi et al., 2002; Haber & Knutson, 2010). In the PV+Scgn+ rich dorsal caudate, the activity of various striatal units has been correlated to the location and size of a given reward, and it is believed that this region (much like the DLS in rodents) is thought to encode action-value (Lau & Glimcher, 2008; Stalnaker et al., 2010). These results contrast nicely with those of the ventral caudate, where neural activity is better correlated with reward value (Apicella et al., 1991, Hollerman et al., 1998; Haber & Knutson, 2010). In the putamen, PV+Scgn- interneurons demonstrated a particularly strong lateral bias, a region that has been shown to receive a strong input from the dorso-lateral pre-frontal cortex (DLPFC; Haber et al., 2006). Functionally, the DLPFC is active in the cognitive processing of goal-directed behavior (Amiez & Petrides 2007; Blumenfeld et al., 2011), implying that PV+Scgn– interneurons may help with the processing of the DLPFC inputs responsible for encoding these behaviors in the lateral putamen.

4.5.4 Molecular heterogeneity within the parvalbumin-expressing striatal population correlates with in vivo differences in firing

In the anaesthetized rat, PV+/Scgn+ interneurons fired more rapidly than PV+/Scgn– interneurons during cortical activation, a state most similar to the "awake and behaving" animal. The finding that Scgn expression is correlated with discernable differences in the firing of PV+ interneurons in vivo is perhaps not surprising given the large degree of heterogeneity described for the firing rates of PV+ interneurons in vivo (Sharott et al., 2012). However, when the PV+ interneuron population is subdivided according to the expression of Scgn, this heterogeneity in firing can be explained to some degree. Indeed, by assessing the degree of correlation between ISI histograms (a measure of firing rate and pattern), the firing of PV+/Scgn+ interneurons are significantly more correlated with one another when compared to PV+/Scgn– interneurons. This would appear to indicate that the co-expression of the CBPs parvalbumin and secretagogin identifies a group of interneurons whose electrophysiological properties are strongly correlated with one another. Importantly, these correlations of ISIs revealed that PV+/Scgn- interneurons

have highly variable firing patterns, potentially implying that further heterogeneity may exist within this population.

The finding that PV+Scgn+ interneurons can be distinguished from PV+Scgn– on the basis of their firing rate during cortical activation is particularly important given the current popularity of tetrode recordings in behaving rats (Friedman et al., 2015). Such studies are currently being used to show differences in the firing patterns of topographically distinct striatal FSIs such as those in the DMS and the DLS (Gremel & Costa 2013). Thus, by demonstrating that topographically distinct populations of striatal FSIs can also be distinguished by their firing rate (a property that is easily discernable from the data obtained from probe recordings), these results act as a point of reference for those studies performing blind recordings of FSIs throughout the striatum. Moreover, by providing a CBP as the molecular basis for the distinction between these two populations, it is likely that the heterogeneity of PV+ interneurons in vitro (Bracci et al., 2003; Plotkin et al., 2005) can be partially explained by the existence of these two subsets. As a calcium sensor and buffer known to interact with exocytotic mechanisms within the cell (Rogstam et al., 2007), Scgn is most likely involved in nanodomain coupling with presynaptic Ca2+ channels, a position that allows its activity to influence the cell's synaptic properties (Bucurenciu et al., 2008; Christie et al., 2011). Indeed, the addition of intracelluluar calcium chelators to hippocampal granule cells has been shown to influence mIPSC frequency (Goswani et al., 2012), suggesting that the expression of CBPs have a direct effect on synaptic properties detectable during in vitro recordings. Thus, the molecular and in vivo physiological diversity described in this study is most likely reflected in the heterogeneity that has been previously described for striatal PV+ interneurons (Klaus et al., 2011; Sharott et al., 2012).

In addition to these reported differences in the firing patterns of PV+/Scgn+ interneurons and PV+/Scgn– interneurons, this study also found differences in the strength of phase locking of these classes of striatal PV+ interneuron to different frequencies of cortical activities in the rat. This is particularly interesting given the already established relationship between the activity of dorsal striatal PV+ interneurons in relation to cortical oscillatory activity (Sharott et al., 2012). It should be considered that the differences reported here could be a side effect of having different cortical inputs or intrinsic properties of the neuron resulting in a different output in relation to the oscillation of the motor cortex (as the EEG was recorded directly above the motor cortex). However, as some of the PV+Scgn– neurons that were recorded for this study were located in the caudal striatum and some of the PV+Scgn+ were located in the central or rostral striatum, it is unlikely that these physiological differences can be explained by topographical biases in distribution.

4.5.5 Different types of PV+ interneurons target striatal projection neurons in a pathway-selective manner

Thanks to the widespread availability of D1-EGFP and D2-EGFP mice, the dichotomy of striatal spiny projection neurons first described in the early 1980s (Somogyi & Smith 1979; Preston et al., 1980) has recently been expanded upon in order to reveal a great deal of differences between the two populations (Surmeier et al., 2007; Ericsson et al., 2013). With respect to their distribution, indirect pathway spiny projection neurons (iSPNs) were shown to be relatively sparse in the caudal striatum (Gangarossa et al., 2012), while direct pathway projection neurons (dSPNs) are distributed throughout the structure. PV+Scgn+ interneurons, which are biased in their distribution towards the caudal striatum, were shown in this study to preferentially make appositions with dSPNs over iSPNs. Given the relatively reduced number of iSPNs in the caudal striatum, one could argue that this explains the preference of PV+Scgn+ interneurons. In light of this possibility, the 4 labelled and identified PV+Scgn+ interneurons used in this study were distributed throughout the striatum (Figure 4.4 Ai - Di) in order to ensure that the obtained result

was not a product of the inherent distributional bias present within the various populations of the striatum. Moreover, those PV+/Scgn– interneurons that were located in the caudal striatum (this included 2 of the 4 PV+/Scgn– interneurons used for this analysis) maintained their preference for iSPNs despite their relatively low numbers. Moreover, the locations of PV+/Scgn– interneurons were matched with the locations of the PV+/Scgn+ that were used for this analysis, as this ensured that the comparison between the appositions they made with striatal SPNs was controlled for any potential differences in the distribution of SPNs within the dorsal striatum of rats. Such controls strengthen the finding that Scgn expression within the PV+ population allows for identification of 2 subsets of PV+ interneurons with different and selective preferences for targeting either dSPNs or iSPNs that are unrelated to their overall distribution within the striatum.

Through the use of retrograde tracers and viral vectors, D1-Cre and D2-Cre mice have been used to explore and compare the cortical and thalamic efferents targeting direct (dSPN) and indirect spiny projection neurons (iSPN). These studies have revealed that certain cortical areas preferentially target one spiny projection pathway over another (Wall et al., 2013; Guo et al., 2015). For example, dSPNs receive a higher proportion of their inputs from prefrontal, limbic and somatosensory cortices, while iSPNs receive a greater proportion of their input from motor cortices. Given this target specificity of corticostriatal inputs to dSPNs and iSPNs, it was thought that this might also apply to (some types of) striatal interneurons. Indeed, the topographical data regarding the distribution of PV+Scgn+ and PV+Scgn– interneurons reported in this study, in combination with the finding that PV+ striatal interneurons receive direct cortical input (Kita et al., 1990; Kita, 1993) that is organized in a topographically heterogeneous fashion suggests that PV+Scgn+ interneurons receive prominent inputs from limbic and somatosensory (auditory and visual) cortices whereas PV+Scgn– interneurons are unlikely to receive these same inputs. Together, these findings support the idea of distinct anatomical pathways exist within the striatum such that cortical areas preferentially projecting to one type of SPN also target a PV+ expressing subtype that predominantly contacts the soma of that same type of SPN. As PV-expressing FSIs

are able to exert a powerful inhibition of target SPNs (Koos & Tepper, 1999; Szydlowski et al., 2013), the PV+Scgn+ interneurons that are anatomically and physiologically described in this study may represent an additional, powerful substrate by which limbic and somatosensory cortical areas target spiny projection neurons comprising the striatal origins of the "direct pathway" (particularly in the caudal planes of the rat dorsal striatum). Additionally, in disease states involving disrupted dopamine transmission (Nicola et al., 2000; Mallet et al., 2006; Fino et al., 2007), the increased inhibition of one type of SPN through an increase in the connectivity of FSIs provides a good case for pathway-specific connectivity within the striatum (Gittis et al., 2011). Given that striatal FSIs are capable of selectively increasing their connectivity to one group of SPN, it would perhaps not be surprising that those FSIs belong to their own molecularly and physiologically distinct population.

In conclusion, the novel findings presented above outline an unprecedented amount of molecular heterogeneity among striatal interneurons of rodents and Rs. Despite the functional implications associated with the selective expression of CBPs, it is the finding that the novel populations reported here exist in specific striatal regions that ultimately implies a great deal of functional heterogeneity within the neural populations of the striatum as a whole. The importance of the correlation between molecular and topographical heterogeneity described in the PV+ interneuron population is further strengthened by its existence in both rodents and Rhesus Macaques. The finding that the different molecular profiles of these unevenly distributed interneuron populations is reflected in their firing rates and patterns as well as their connectivity within the striatum ultimately cement the idea that not all striatal microcircuits are equipped to process similar types of information. In chapter 3, Scgn was also shown to be expressed by some, but not all CR+ interneuron in the dorsal striatum rodents and the Rhesus Macaques. Given that the selective expression of Scgn within the PV+ interneuron population was correlated with anatomical, physiological and topographical differences, it follows that selective Scgn expression in CR+ interneurons may also be correlated with functional or structural differences within this poorly understood population. These potential differences are investigated in Chapter 5, with the

intention of further demonstrating the diversity that exists within the regionally specialized circuitry of the dorsal striatum.

CHAPTER 5.

MORPHOLOGICAL AND TOPOGRAPHICAL HETEROGENEITY OF CALRETININ-EXPRESSING INTERNEURONS IN THE STRIATUM OF RATS AND RHESUS MACAQUES

5.1 INTRODUCTION

Although interneurons identified by their expression of the CBP calretinin (CR) are the most abundant class of interneuron in the primate striatum (Cicchetti et al., 2000; Wu and Parent, 2000), they are perhaps the least well understood of the four "classical" types of interneuron (Tepper et al., 2010; Bolam & Silberberg, 2015). In the neocortex, GABAergic interneurons identified using CR (Gulyas et al, 1992) have been shown to comprise multiple cell types with distinct morphological, neurochemical and physiological features (Ascoli et al, 2008; Klausberger and Somogyi, 2008), while striatal CR+ interneurons are often treated as a single homogenous population (Rymar et al., 2004; Petryszyn et al., 2014). In the rat, striatal CR+ neurons were first identified as medium-sized (7-20 μm) aspiny, GABAergic interneurons (Bennet and Bolam, 1993) that are distributed in a decreasing gradient along the rostro-caudal axis (Kubota et al., 1993; Rymar et al., 2004; Petryszyn et al., 2014). Indeed, in the caudal most striatum, the number of CR+ interneurons is markedly reduced (Rymar et al., 2004). Although it has not been quantified, some studies have noted that the number of CR+ interneurons is relatively elevated in the dorso-medial striatum, an observation that is primarily evident in the rostral planes in which the density of these interneurons is elevated (Figueredo-Cardenas et al., 1996; Rymar et al., 2004). Heterogeneity within the CR+ interneuron population has been shown at the level of the morphological properties of CR+ interneurons in the mouse (Tepper et al., 2010). In the rat striatum, there have been reports demonstrating the presence of a small number of CR+ interneurons with large somata (>20 μm) as well as small-sized (<7 μm) CR+ cells. Medium-sized CR+ interneurons (7.1 – 20 μm), are reported to be the largest group in terms of numbers, as they make up nearly ~90% of all CR+ interneurons (Rymar et al., 2004). However, as there are no additional molecular criteria by which to distinguish different subsets of CR+ interneurons, these findings are currently believed to be the result of a normal distribution of cell sizes, such that CR+ interneurons in the rat striatum all belong to one population that varies in size along a single continuum that is centered on the diameter of medium-sized neurons (Petryszyn et al., 2014; Ma et al., 2014). There have been anecdotal descriptions of three "types" of CR+ striatal interneurons

in the mouse striatum, as based on morphological features; those with large somata and infrequently branching dendrites ("Type 1"), those with medium-sized, bipolar somata ("Type 2") and those with small somata and tortuous, spiny dendrites ("Type 3") (Tepper et al., 2010). In this description, a quantification of somatic diameter was not provided in order to define the terms "small", "medium" or "large" (Tepper et al., 2010). Importantly, the electrophysiological properties of striatal CR+ interneurons have not been described in any preparation. Taken together, these observations suggest that CR+ interneurons may comprise multiple, yet poorly defined, cell types. However, due to the relatively small amount of structural or electrophysiological information regarding these interneurons, current studies are limited the use of immunohistochemistry to investigate this potential heterogeneity.

In the primate striatum, CR+ interneurons have been described as being comprised of three different groups based on their morphological properties (Parent et al., 1995). The largest group consists of medium-sized (10-20 μm) neurons, which are similar to the medium-sized CR+ interneurons of the rat striatum. The smallest group is made up of neurons that co-express ChAT and CR, which are preferentially distributed in the putamen (Parent et al., 1995). Their somata are large, ranging from 25 to 40 μm in diameter (Cicchetti et al., 1998). The third group of CR+ interneuron has recently been described in the human caudate nucleus and putamen; their cell bodies have the smallest mean diameter and range from 10-12 μm (Bernacer et al., 2012). Further molecular and morphological characterization of these small CR+ interneurons has yet to be demonstrated (Bernacer et al., 2012). Stereological work in human postmortem tissue has suggested that, on the whole, CR+ interneurons are preferentially distributed in the head of the caudate nucleus and the part of the putamen known as the pre-commissural putamen (Parent, 1990; Bernacer et al., 2012). Although cortical input to the primate striatum is much more diffuse than it is in the rat, this region has been described as the "associative territory" of the primate striatum (Parent 1990; Fudge et al., 2002; Haber & Knutson, 2010). Moreover, the density of CR+ interneurons is relatively high in the striatal region associated with the point of overlap between the associative and the sensorimotor territories (Karachi et al., 2002; Haber, 2003; Haber

et al., 2006; Bernacer et al., 2012; Tziortzi et al., 2014). The morphological and topographical heterogeneity of CR+ interneurons that has been described in the primate and human caudate/putamen most likely underpins further molecular and functional heterogeneity.

In neocortex and hippocampus, combinations of molecular markers have been crucial for defining neuronal diversity. In particular, CBPs, in combination with each other or together with other categories of molecular marker, such as transcription factors and neuropeptides, have been used to delineate interneuron types that had been previously defined by morphological features alone (e.g. Viney et al, 2013). In this thesis, Scgn was shown to be expressed by some, but not all, CR+ interneurons of the rodent and Rhesus Macaque striatum (see Sections 3.4.2 and 3.4.4). Given the morphological diversity of CR+ interneurons in the striatum that has been described in the mouse (Tepper et al., 2010; Petryszyn et al., 2014) and the rat (Rymar et al., 2004), it is possible that the morphological diversity of rat CR+ interneurons correlates with the selective expression of Scgn. Conversely, the expression of transcription factors in the adult neocortex has also been used to distinguish structurally and functionally distinct groups of neurons (Jakob et al., 2015; Prochiantz & Di Nardo 2015), as their selective expression can provide important insights into the developmental origins of a given class of neuron (Marin, 2002; Kepecs & Fischell 2014). For example, in the neostriatum of newly-born rats, some CR+ interneurons are generated from precursors located near the subventricular zone (SVZ; Dayer et al., 2005; Inta et al., 2008; Inta et al., 2015). The SVZ represents an important site of continued neurogenesis throughout adulthood, and is the origin of newly-born neurons that migrate to the olfactory bulb, the hippocampus and the dorsal striatum in both rodents and humans (Inta et al., 2015). Importantly, a subclass of those neurons destined for the olfactory bulb cannot migrate without the expression of the transcription factor known as specificity factor 8 (SP8; Dayer et al., 2005; Inta et al., 2015), which suggests that newly generated striatal CR+ interneurons may also selectively express this protein in the adult rat. The LIM homeodomain protein Lhx7 is required for the development and specification of neurons derived from the medial ganglionic eminence (MGE) into cortical GABAergic interneurons and the cholinergic neurons of the ventral forebrain (Grigoriou et al., 1998; Marin et

al., 2000; Alifragis et al., 2004; Du et al., 2008; Zhao et al., 2008). The use of $Lhx7^{+/nlacZ}$; $Gad67^{GFP}$ adult double transgenic reporter mice has shown that 43% of striatal Lhx7+ cells are GABAergic, while the rest are cholinergic (Fragkouli et al., 2009). Thus, Lhx7 also labels unidentified GABAergic, MGE-derived striatal interneurons, some of which might also express CR.

5.2 AIMS

Anecdotal evidence of a spatial and morphological heterogeneity of the striatal CR-expressing interneuron population supports the notion that quantifiable molecular, morphological, topographical and physiological differences may exist within this population. In light of this hypothesis, a combination of immunofluorescence microscopy, stereological cell counting, and in vivo recording/labelling of identified cells were used to address the following aims:

- To quantify the co-expression of Scgn, SP8 and Lhx7 within the CR+ interneuron populations in the rat striatum.
- To quantify the co-expression of Scgn within the CR+ interneuron populations in the Rhesus Macaque caudate/putamen.
- To determine whether molecular differences amongst CR+ interneurons are reflected in their structural properties.
- To determine whether molecularly-distinct groups of CR+ interneuron are uniformly distributed throughout the striatum of both rats and Rhesus Macaques.
- To gain insight into the in vivo electrophysiological properties of identified CR+ interneurons in the dorsal striatum of anaesthetized rats.

5.3 METHODS

Experimental procedures were carried out on adult male Sprague-Dawley rats (Charles River, Margate, UK) that were 3 months old, weighing between 280-350g. All rodents used were maintained on a 12/12 h light/dark cycle, and had free access to food and water. All experiments were conducted in accordance with the Animals (Scientific Procedures) Act 1986 (UK). Experimental procedures involving primate tissue were performed using tissue from 2 female Rhesus monkeys (3-9 years old; 5-8 kg). All procedures were approved by the Institutional Animal Care and Use Committee at Emory University and conform to the U.S. National Institutes of Health Guide for the Care and Use of Laboratory Animals.

A detailed description of the techniques and protocols used in this chapter can be found in the appropriate sections of Chapter 2.

- Perfusion and fixation (Section 2.1.1)
- Indirect immunofluorescence (Section 2.1.2)
- Stereological cell counting (Section 2.1.3)
- Calculations of section area, volume and estimates of total cell number (Section 2.2.1)
- Topographical and statistical analysis of interneuron distribution (Section 2.2.2)
- Measurements of mean somatic diameters (Section 2.2.3)
- Juxtacellular recording and labeling (Section 2.3.1 – 2.3.2)
- Data selection and analysis of electrophysiological data (Section 2.3.3)
- Tissue preparation and indirect immunofluorescence of monkey tissue (Section 2.5.1)
- Stereological cell counts in the caudate and putamen of the rhesus monkey (Section 2.5.3)

5.4 RESULTS

5.4.1 Topographically-discrete populations of CR+ interneurons can be identified by the selective expression of Scgn in the rat dorsal striatum

The quantification of Scgn+ cells in the dorsal striatum of rats performed in Chapter 3 (see section 3.4.1) showed that some, but not all, CR+ interneurons co-express Scgn. Secretagogin and CR expression in this subpopulation was relatively intense, as immunoreactivity could often be detected in proximal dendrites rather than just in the soma (Figure 5.1 A). Stereological cell counting of CR+/Scgn+ neurons across 3 animals revealed that they represent approximately 40% of all CR+ interneurons (Figure 5.1 B) and 25% of all Scgn-expressing interneurons (see section 3.4.2) in the rat dorsal striatum. Analysis of CR+/Scgn+ neuron density in the coronal plane revealed that these cells are relatively prevalent in the rostral striatum, with an almost negligible number of these neurons being present in the central and caudal striatum (Figure 5.1 C). Thus, they account for the relatively high density of Scgn+ cells in rostral striatal planes that was previously described (see section 3.X). Previous descriptions of all CR+ interneurons in the rat (Rymar et al., 2004) and in the mouse (Petryszyn et al., 2014) have noted (either qualitatively or quantitatively) a strong positional bias towards the rostral and medial borders of the dorsal striatum. In this study, the use of Scgn as a molecular marker to subdivide the CR+ interneuron population of the striatum revealed that the overall bias of the population towards the rostral striatal pole is largely attributable to the prevalence of CR+/Scgn+ interneurons in these striatal regions (Figure 5.1 Ci, Di). This CR+/Scgn+ interneuron population is therefore unique in that, unlike any other molecularly-defined striatal interneuron population, they are highly concentrated in the rostral ("pre-commissural") striatum, and are undetectable in striatal planes caudal to the emergence of the anterior commissure that occurs 0.5 mm ahead of bregma (Figure 5.1 Ci, Di).When averaged across 3 rats, detailed stereological analysis of the positioning of CR+/Scgn+ interneurons also revealed a strong medial (Figure 5.1 Ei) and dorsal bias (Figure 5.1 Eii). In contrast, those CR+ interneurons that did not co-express Scgn were only slightly biased towards the rostral striatum (Figure 5.1 Cii), but were otherwise homogenously

distributed throughout the medio-lateral (Figure 5.1 Ei) and dorso-ventral axes of the rat striatum (Figure 5.1 Eii). In summary, the selective expression of Scgn can be used to parse two topographically-distinct populations of CR+ interneurons in the dorsal striatum of the rat.

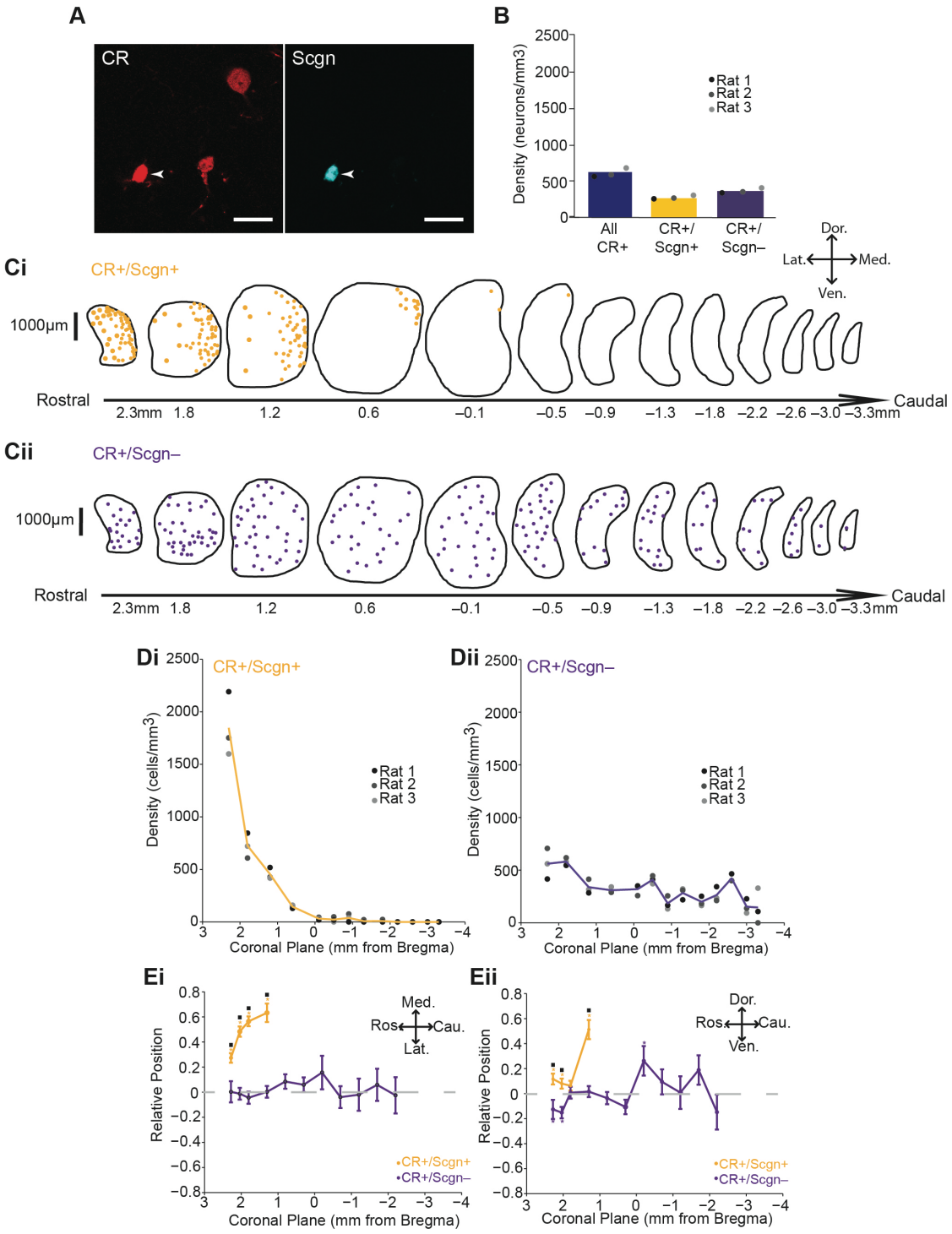


Figure 5.1: CR+/Scgn+ and CR+/Scgn– interneurons have different topographical bias the dorsal striatum of rat. A) Single plane confocal micrographs of the rat dorsal striatum showing that those CR+ interneurons that co-express Scgn (arrow head) have stronger immunofluorescent signals compared to CR+/Scgn– interneurons. Scale bars represent 20 µm. **B**) The mean density of all CR+, CR+/Scgn+ and CR+/Scgn– interneurons within the entirety of the striatum. Note that CR+/Scgn+ interneurons make up two-fifths of all CR+ interneurons in the dorsal striatum of the rat. **C**) Typical distribution of CR+/Scgn+ (**Ci**) and CR+/Scgn– (**Cii**) neurons across 13 coronal planes encompassing the rostro-caudal axis of the dorsal striatum in rat, with each dot representing a single neuron. **D**) Density of CR+/Scgn+ (**Di**) and CR+/Scgn– (**Dii**) neurons along the rostro-caudal striatal axis of rats. Note the decrease in density of CR+/Scgn+ neurons, from rostral to caudal striatum. **E**) Medio-lateral (**Ei**) and dorso-ventral (**Eii**) distribution of CR+/Scgn+ (Orange line) and CR+/Scgn– (Purple line) neurons along 13 coronal planes. In coronal planes where less than 10 neurons were counted per animal, no relative topographical value is given. Asterisks (*) indicate a distribution that is significantly biased in one direction along the specified axis. Squares (□) indicate a significant difference in the distribution of the two populations along the specified axis within a given coronal plane. Data are means of the position of all neurons counted ± SEMs.

5.4.2 The selective expression of Scgn is correlated with differences in the somatic diameters of CR+ interneurons

In accordance with previous reports in the rat dorsal striatum (Rymar et al., 2004), the somatic diameters of all CR+ interneurons (measured as the distance along the longest axis of a CR-expressing interneuron; Rymar et al., 2004) assessed in this study varied from 7.0 to 19.2 µm (Figure 5.2 A). Plotting of these diameters in a frequency histogram revealed a bimodal distribution of soma sizes (Figure 5.2 A). Given previous reports that those CR-expressing interneurons located in the rostral striatum tend to have relatively small somatic diameters (Ma et al., 2014), combined with the preferential distribution of CR+/Scgn+ interneurons in the rostral striatum (Figure 5.1), the somatic diameters of CR+/Scgn+ interneurons were measured and compared against the diameters of all striatal CR+ interneurons in the rat (Figure 5.2 B). Such a comparison revealed that the somata of CR+/Scgn+ interneurons were amongst the smallest of the somata measured for all CR+ interneurons (Figure 5.2). Indeed, CR+/Scgn+ neurons accounted for the vast majority of CR+ interneurons with somata in the range of 7-11 µm, but accounted for none of the CR+ neurons with larger somata (Figure 5.2 B)). Accordingly, the somatic diameter of CR+/Scgn+ interneurons had a mean value of 8.9 ± 1.0 µm (n = 50), which was significantly smaller (Mann-Whitney U test, $P<0.05$) than the mean diameter of CR+/Scgn- interneurons (Figure 5.2 C).

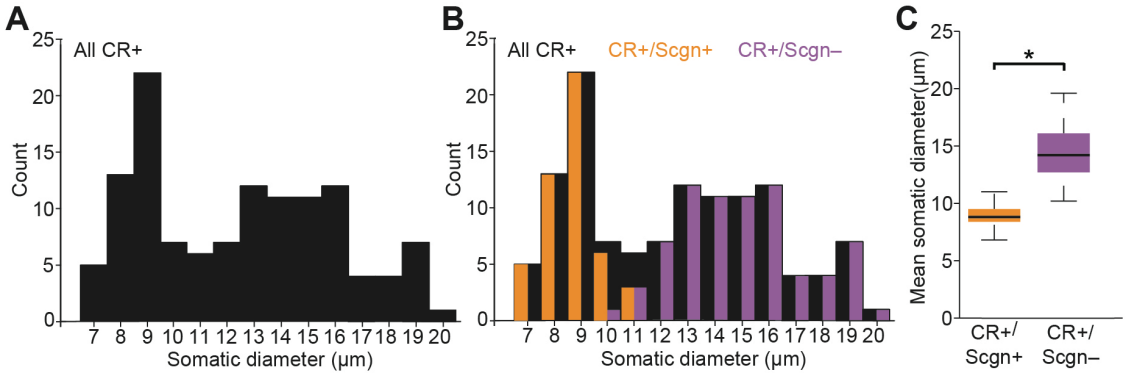


Figure 5.2: CR+/Scgn+ interneurons possess the smallest somatic diameters of all CR+ interneurons, and can be distinguished from CR+/Scgn– interneurons on the basis of their mean somatic diameters. A) Frequency histogram showing the distribution of somatic diameters for all CR+ interneurons in the dorsal striatum of the rat. **B**) Frequency histogram showing the distribution of somatic diameters of all CR+ interneurons (black bars), CR+/Scgn+ interneurons (orange bars) and CR+/Scgn– interneurons (purple bars). Note that CR+/Scgn+ interneurons represent the smallest CR+ interneurons with respect to their somatic diameter. **C**) Mean somatic diameters of CR+/Scgn+ interneurons and CR+/Scgn– interneurons. On average, CR+/Scgn+ interneurons have smaller sized somata compared to CR+/Scgn– interneurons. The presence of the asterisk indicates a significant difference in mean somatic diameter (Mann-Whitney U test, $P < 0.05$)

5.4.3 CR+/Scgn+ interneurons express the transcription factor SP8

Given previous reports that some CR+ interneurons in both rodents and primates are newly generated throughout adulthood from precursors located in the subventricular zone (Inta et al., 2015; Inta et al., 2008), the expression of the transcription factor specificity protein-8 (SP8), a molecular marker of newly generated neurons in the adult olfactory bulb (Jiang et al., 2013) and the inner ear (Chung et al., 2014) was investigated in the dorsal striatum of the rat. Interestingly, nearly all SP8+ neurons were found to express CR and Scgn (Figure 5.3 A, B, C), and most (99.7% ± 0.7%, n = 3 rats) CR+/Scgn+ interneurons expressed SP8 (Figure 5.3 C). These results suggest that those small-sized, rostro-medially biased CR+/Scgn+/SP8+ interneurons likely represent a large proportion of those CR+ interneurons that are generated throughout adulthood (Inta et al., 2015).

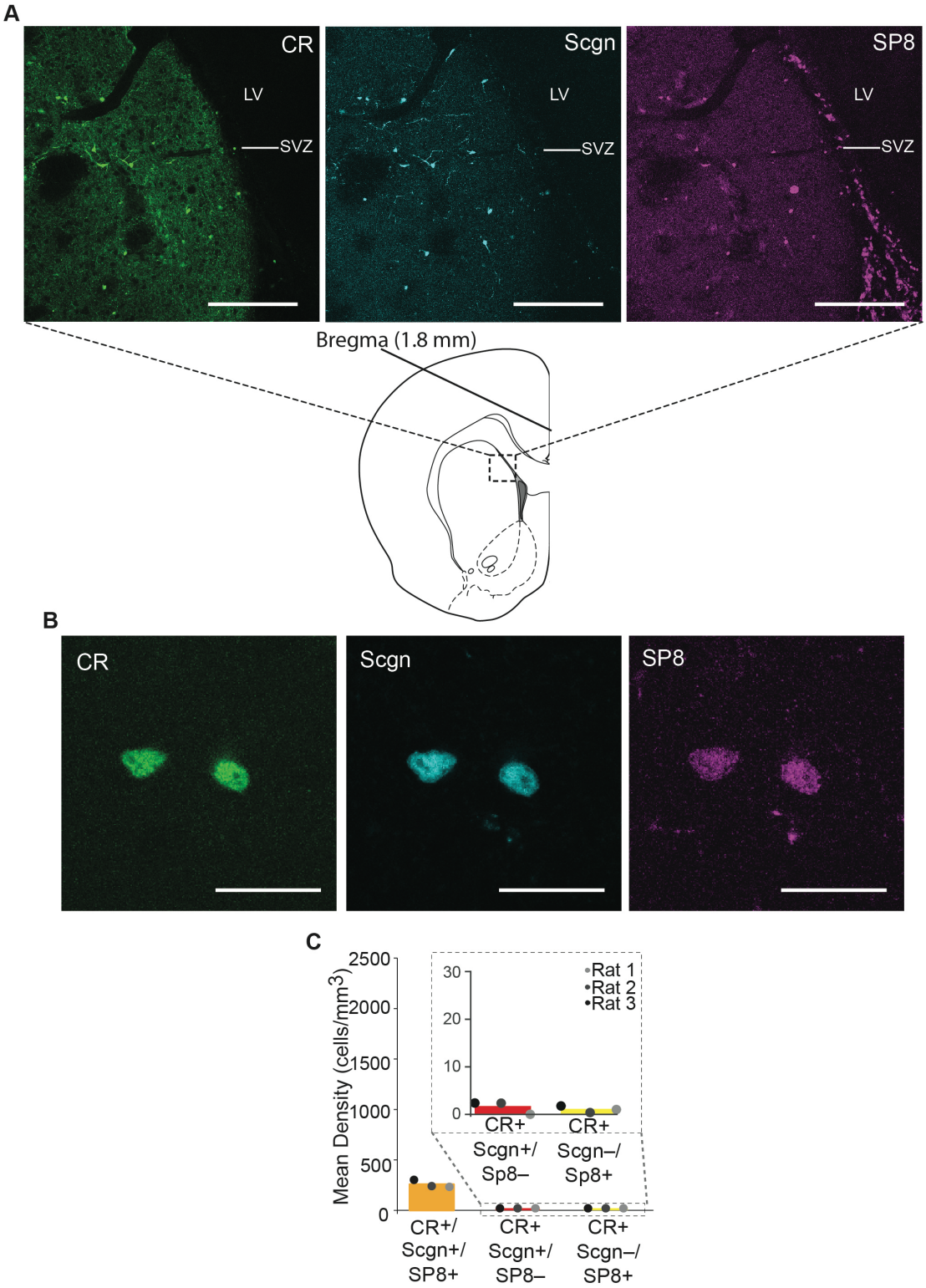


Figure 5.3: CR+/Scgn+ interneurons can also be identified by their expression of SP8, a marker for newly-generated neurons derived from the subventricular zone (SVZ). A) Single plane confocal micrographs of the rat dorsal striatum and the subventricular zone showing the presence of CR+/Scgn+/SP8+ interneurons within the dorso-medial striatum of a coronal plane located 1.8 mm ahead of Bregma. Note the expression of Sp8 in CR+/Scgn+ neurons as well as in the subventricular zone (SVZ), located below the lateral ventricle (LV). Scale bars represent 200µm **B)** Single plane confocal micrographs of CR+/Scgn+/SP8 neurons. Scale bars represent 20µm. **C**) Mean densities of CR+/Scgn+/SP8+ interneurons, CR+/Scgn+/SP8– interneurons and CR+/Scgn-/SP8+ interneurons demonstrating that the co-expression of CR, Scgn and SP8 occurred frequently in the dorsal striatum of the rat..

5.4.4 A discrete population of CR+/Scgn– interneuron expresses the transcription factor Lhx7

After demonstrating that Scgn is a reliable molecular marker of the small-sized CR+ interneurons that have been previously described in the rat (Rymar et al., 2004; Ma et al., 2014), those CR+ interneurons not expressing Scgn were further characterized. In the mouse striatum, there are conflicting reports regarding the existence of a somatodendritic distinction within the "larger" CR+ striatal neural population, with some reports suggesting that it can be further divided based on somatic size and the dendritic features of neurons (Tepper et al., 2010), while others claim that these differences are most likely reflective of a continuum i.e. a single population (Petryszyn et al., 2014). Currently, the degree to which these observations reflect the existence of distinct subpopulations is unclear. In the striatum, one particular transcription factor required for the maintenance of cholinergic interneuron identity is the LIM homeobox protein 7 (Lhx7), also known as Lhx8 or L3 (Zhao et al., 2003; Fragkouli et al., 2009). This transcription factor has also been shown to be expressed in some GABAergic interneurons in the mouse dorsal striatum (Fragkouli et al., 2009). Given that ChAT and CR are co-expressed by some interneurons in the primate striatum (Wu & Parent, 2000), the expression of Lhx7 in the dorsal striatum of adult rats was assessed. When immunoreactivity for Lhx7, CR and Scgn was assessed, it was evident that Lhx7 is expressed by some, but not all, of the CR+/Scgn– neurons in rat dorsal striatum (Figure 5.4 A). Importantly, CR+/Scgn+ interneurons did not express Lhx7 (Figure 5.4 A).

In order to investigate whether CR+/Scgn–/Lhx7+ and CR+/Scgn–/Lhx7– interneurons represented 2 distinct populations, the somatic diameters of these two molecularly-distinct sets of CR+ interneurons were measured and compared to the somatic diameters of all CR+ interneurons in a manner similar to what was performed for CR+/Scgn+ interneurons (see Section 5.4.2). Importantly, the somatic sizes of CR+/Scgn–/Lhx7+ and CR+/Scgn–/Lhx7– interneurons tended to fall within different ranges (11-15 µm and 13-19 µm, respectively), although with some overlap (Figure 5.4 B). The mean somatic diameter of CR+/Scgn–/Lhx7+ interneurons (16.0 ±

2.0 µm, n = 52; Figure 5.4 C) interneurons was on average larger than that of CR+ Scgn–/Lhx7– interneurons (12.9 ± 1.3um, n = 51; Figure 5.4 C). On the other hand, the somatic diameters of CR+/Scgn+/Lhx7– neurons were on average smaller than those of CR+ interneurons that did not express Scgn (Figure 5.4 C). Taken together, these data suggest that the CR+/Scgn– interneurons in rat dorsal striatum can be subdivided into two main populations according to their selective expression of Lhx7 and the sizes of their somata.

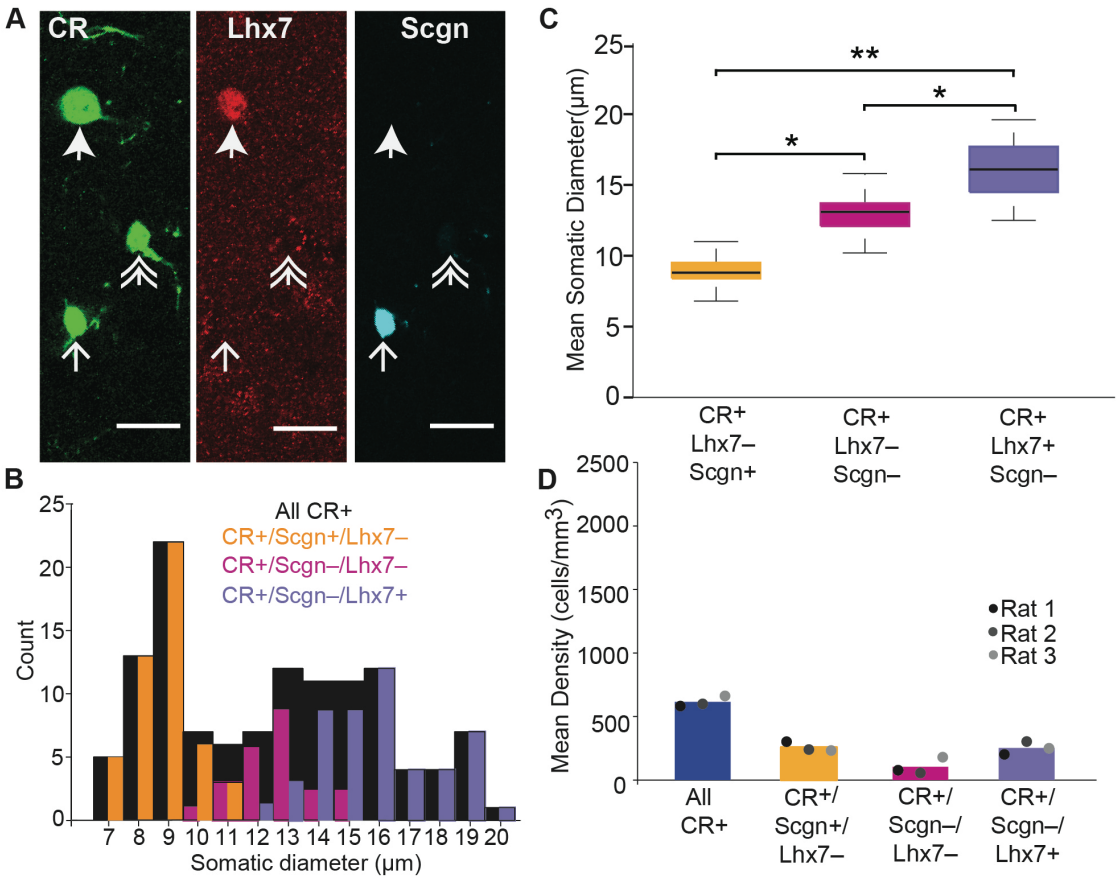


Figure 5.4: The selective expression of Lhx7 distinguishes some CR+/Scgn– interneurons and is correlated with differences in mean somatic diameter. A) Single plane confocal micrographs of the rat dorsal striatum showing that three types of CR+ interneuron can be distinguished on the basis of their molecular expression profiles; CR+/Scgn+/Lhx7– (single slim arrow), CR+/Scgn–/Lhx7– (double arrowhead) and CR+/Scgn–/Lhx7+ (single thick arrowhead). **B**) Frequency histogram showing the distribution of somatic diameters of all CR+ interneurons (black bars), CR+/Scgn+/Lhx7– interneurons (orange bars), CR+/Scgn–/Lhx7– interneurons (magenta bars) and CR+/Scgn–/Lhx7+ interneurons (mauve bars). Note that somatic diameter alone is unlikely to distinguish CR+/Scgn–/Lhx7– interneurons from CR+/Scgn–/Lhx7+ interneurons. **C**) Mean somatic diameter of immunochemically identified subpopulations of CR-expressing interneuron. The presence of a single asterisk indicates a level of significant difference at $P < 0.05$ while the presence of two asterisks indicates a significant difference at $P < 0.01$ as measured by a one way ANOVA test followed by post hoc Tukey's honestly significant difference test. **D**) Density of interneurons with combinations of CR, Scgn and Lhx7 expression. Interneurons co-expressing CR and Scgn accounted for around 40% of all interneurons expressing CR, while CR+/Scgn–/Lhx7+ interneurons represented another 40 % of striatal CR-expression.

Stereological counts of CR+/Scgn–/Lhx7+ interneurons demonstrated that they represent nearly two-fifths of all striatal CR+ interneurons, while CR+/Scgn–/Lhx7– interneurons represented one-fifth of the total CR+ interneuron population (Figure 5.4 D). In accordance with previous results (Rymar et al., 2004), the total number of CR+ neurons in the rat dorsal striatum was estimated to be 13535 ± 392 cells. When the number of each molecularly-distinct subpopulation of CR+ interneuron is estimated in the same manner, the data presented shows that the rat dorsal striatum contains 5550 ± 861 CR+/Scgn–/Lhx7+ interneurons, 2571± 201 CR+/Scgn–/Lhx7– interneurons and 5143 ± 184 CR+/Scgn+/Lhx7– interneurons.

In contrast to the highly-biased distribution of CR+/Scgn+/Lhx7– interneurons within the dorsal striatum of rats (Figure 5.1 Ci), the CR+/Scgn–/Lhx7+ interneurons and CR+/Scgn−/Lhx7–interneurons were only slightly more prevalent in rostral planes, as compared to caudal planes (Figure 5.5 Ai, Aii). These populations may therefore still contribute to the previously described increase in the prevalence of CR+ interneurons in the more rostral aspects of dorsal striatum (Bennett and Bolam, 1993; Kubota et al., 1993; Rymar et al., 2004; Petryszyn et al., 2014). In all coronal planes assessed, CR+/Scgn–/Lhx7+ interneurons and CR+/Scgn−/Lhx7– interneurons were not consistently biased in their distribution in either the medio-lateral or dorso-ventral axis (Figure 5.5 Bi, Bii, Ci, Cii). In summary, the selective expression of the calcium-binding proteins CR and Scgn, as well as of the transcription factors SP8 and Lhx7, can be used

as molecular correlates of three populations of CR-expressing interneurons distinguished by their biased distributions within the striatum as well as the sizes of their somata.

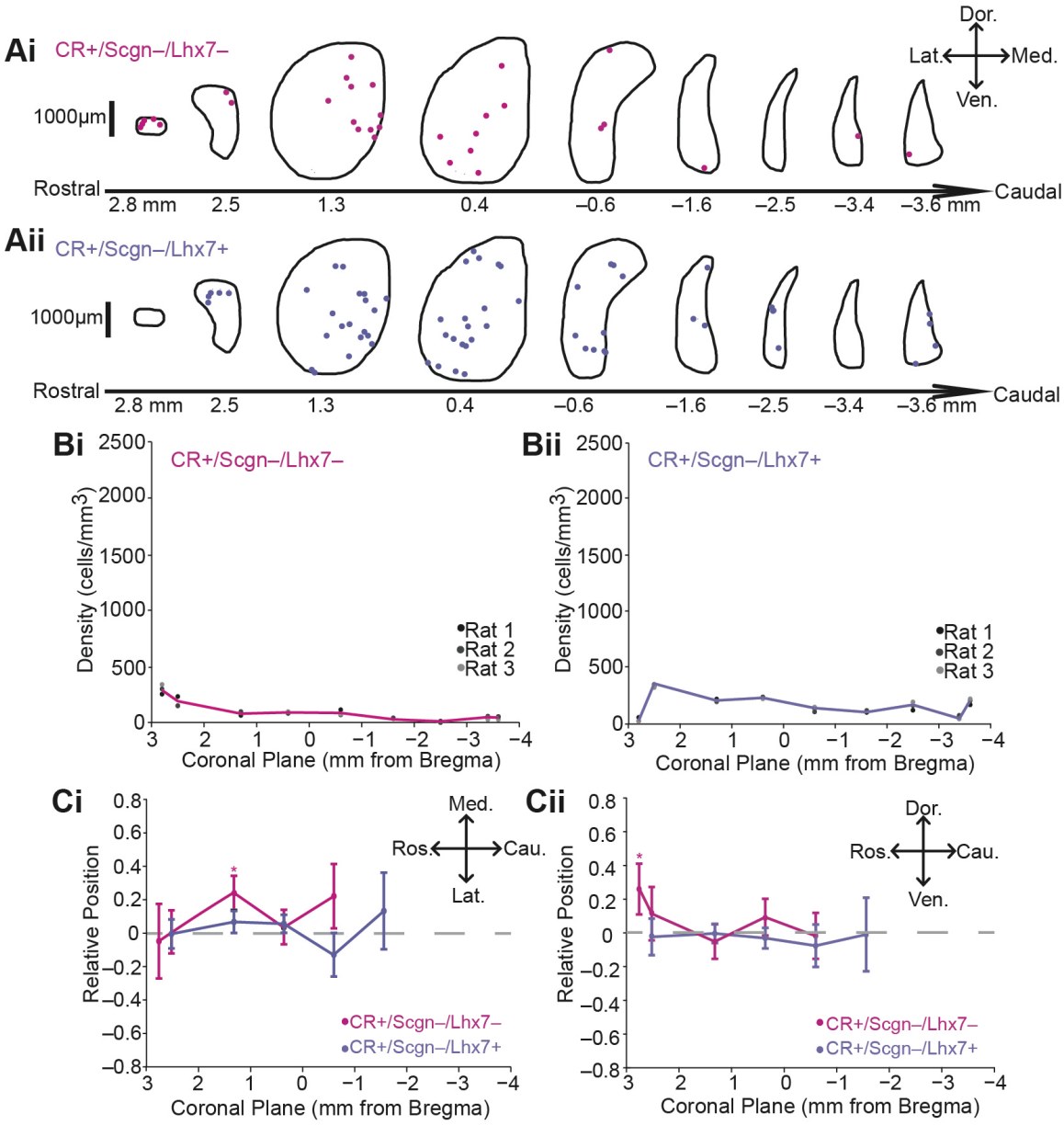


Figure 5.5: CR+/Scgn–/Lhx7– and CR+/Scgn–/Lhx7+ interneurons have similar topographical distribution in the dorsal striatum of rat. A) Typical distribution of CR+/Scgn–/Lhx7– (**Ai**) and CR+/Scgn–/Lhx7+ (**Aii**) neurons across 9 coronal planes encompassing the rostro-caudal axis of the dorsal striatum in rat, with each dot representing a single neuron. **B**) Density of CR+/Scgn–/Lhx7– (Bi) and CR+/Scgn–/Lhx7+ (Bii) neurons along the rostro-caudal striatal axis of rats. Note the decrease in density of of both types of interneuron, from rostral to caudal striatum **C**) Medio-lateral (**Ci**) and dorso-ventral (**Cii**) distribution of CR+/Scgn–/Lhx7– (Magenta line) and CR+/Scgn–/Lhx7+ (Mauve line) neurons along 7 coronal planes. In coronal planes where less than 10 neurons were counted per animal, no relative topographical value is given. The presence of asterisks (*) indicate a distribution that is significantly biased in one direction along the specified axis. Data are means of the position of all neurons counted ± SEMs.

5.4.5 Differences in molecular expression, topographical distribution and somatic size within the dorsal striatal CR+ interneuron population are correlated with previously described differences in the somatodendritic structure of CR+ interneurons

The finding that 3 populations of CR+ interneurons could be distinguished on the basis of their molecular expression profiles and their somatic size suggests that CR+ interneurons are likely comprised of multiple types of interneuron. In previous studies, the somatodendritic structure of 3 loosely defined "types" of CR+ interneuron has been described in the dorsal striatum of the mouse (Tepper et al., 2010): "Type 1" CR+ interneurons were described as having large somata and infrequently branching dendrites; "Type 2" CR+ interneurons were described as being of medium size and possessing bipolar somata, while "Type 3" CR+ interneurons had small somata and tortuous, spiny dendrites (Tepper et al., 2010). Given that the three molecularly and topographically distinct populations of CR+ interneuron described in this study differed in their somatic sizes, whether or not these differences were correlated with the three previously described somatodendritic structures of CR+ interneurons was investigated. Although immunohistochemistry for CR does not consistently or completely label the dendrites of CR+ interneurons, some neurons are often well labeled (Tepper et al., 2010; Petryszyn et al., 2014). Indeed, the fluorescent revelation of CR immunoreactivity was originally used to characterize three "types" of CR+ interneuron in the mouse (Tepper et al., 2010). As such, its use in this study to describe the somatodendritic structures of CR+ interneurons was deemed appropriate. When this is performed, it was found that CR+ interneurons matching the description of Type 1 CR+ interneurons could be found in the rat dorsal striatum, and that they were CR+/Scgn–/Lhx7+ interneurons (Figure 5.6 A). Type 2 CR+ interneurons could also be identified on the basis of their somatodendritic structure, and these were CR+/Scgn–/Lhx7– interneurons (Figure 5.6 B). Finally, the somatodendentric structure of CR+/Scgn+/Lhx7– interneurons was similar to what had been described for Type 3 CR+ interneurons (Figure 5.6 C). These findings therefore suggest that CR+ interneurons in the rat dorsal striatum likely represent at least 3 distinct types of neuron that can be identified on the basis of their molecular expression profiles, their somatodendritic structures as well as their topographical distribution within the striatum.

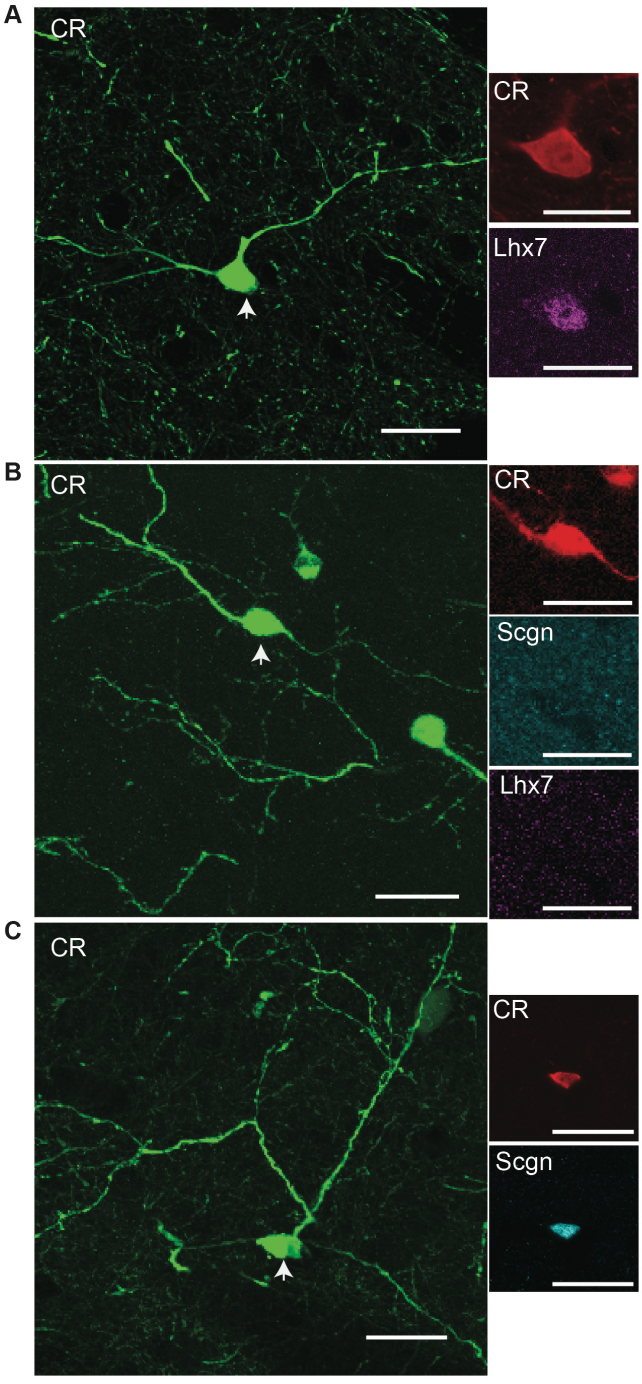

A
CR
CR
Lhx7
B
CR
CR
Scgn
Lhx7
C
CR
CR
Scgn

Figure 5.6: The selective expression of Scgn or Lhx7 identify morphologically distinct "types" of CR-expressing interneurons. A-C) Single plane confocal micrographs of the rat dorsal striatum showing the different morphological characteristics of CR-expressing interneurons. Some CR+ interneurons had large somas with a relatively thick primary dendrites ("Type 1" – **A**) and were CR+/Scgn–/Lhx7+, whereas others were medium sized with 2 major primary dendrites leaving the cell body at opposite poles ("Type 2" – **B**) and were CR+/Scgn–/Lhx7–. Other CR+ interneurons had small somata with tortuous dendrites that appeared to have spines ("Type 3" – **C**) and were CR+/Scgn+/Lhx7–. Scale bars represent 20 μm.

5.4.6 Spontaneous in vivo activity of identified CR-expressing interneurons during cortical SWA and activation states

Despite many studies in both mice and rats, the activity of identified CR+ interneurons in the dorsal striatum has yet to be recorded. To address this, four CR+ interneurons in the dorsal striatum of anaesthetized rats were juxtacellularly recorded, labeled and identified (Figure 5.7 A, B). All identified CR+ neurons were recorded during both cortical slow-wave activity (SWA) and cortical activation (Figure 5.7 A, B). After confirming that these recorded neurons expressed calretinin, their somata were tested for expression of both Scgn and Lhx7; all 4 recorded neurons were CR+/Scgn–/Lhx7–. The action potential waveforms, mean firing rates and interspike intervals (during both cortical SWA and activation) are shown in Figure 5.7 C-F. During cortical SWA, the firing patterns of CR+ neurons were highly variable, with some neurons firing more regularly than others (Figure 5.7 Aii, Bii). For example, some neurons fired bursts of spikes around the peaks of most slow oscillations (Figure 5.7 Aii) while others would fire a single spike in a sporadic fashion (Figure 5.7 Bii). Importantly, these CR+ neurons often displayed tonic activity, particularly during spontaneous cortical activation (Figure 5.7 Aii, Bii), implying that these neurons may represent the third "tonically-firing" interneuron population within the dorsal striatum (Sharott et al., 2012). The action potential waveforms of CR+/Scgn–/Lhx7– interneurons were heterogeneous (Figure 5.7 C), with some neurons displaying fast (<1ms) spikes while others had longer waveforms (>1.5 ms). The firing rates of CR+ interneurons were also highly variable during both cortical SWA and cortical activation (Figure 5.7 D). Importantly, spontaneous changes in cortical activity from SWA to an activated state resulted was accompanied by large increases in the firing rates of 2 neurons, while the other 2 neurons exhibited relatively small decreases in firing rate during similar state transitions (Figure 5.7 D). During SWA, the ISI

histograms of some interneurons was bimodal (Figure 5.7 E; red and purple lines), with a first peak at 100ms and a second peak at ~1 s, which likely reflects their tendency to fire in time with the cortical slow oscillation (Figure 5.7 Aii). During cortical activation, CR+ interneurons fired more regularly (Figure 5.7 F), as ISI histograms for each neuron had a single peak centered on a similar value for their interspike interval (Figure 5.7 F). In summary, this study gives the first insights into the in vivo electrophysiological properties of CR+ interneurons, and have shown that these interneurons are heterogeneous, tonically-active neurons.

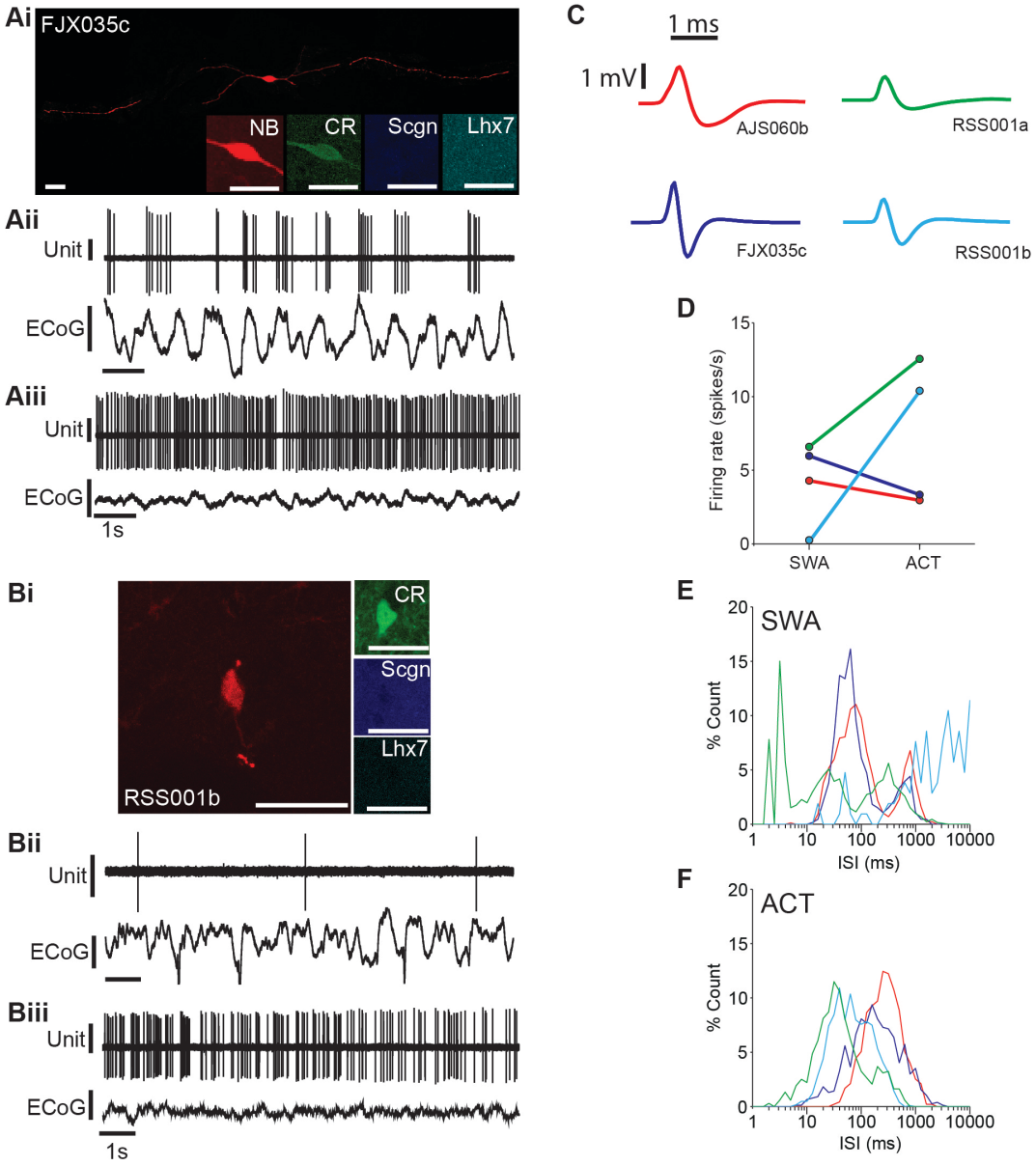


Figure 5.7 Electrophysiological properties of identified CR-expressing striatal interneurons in the rat. A, B) Firing of Juxtacellularly-labeled CR+/Scgn–/Lhx7– interneurons (Ai, Bi), identified by their co-localization of molecular markers and fluorescent labeling for neurobiotin (NB), recorded in the dorsal striatum of rats. **Aii-Bii,** Spontaneous action potential discharges (unit activity) of the same individual CR+ interneurons during robust cortical slow-wave activity, as recorded in the frontal electrocorticogram (ECoG). **Aiii-Biii,** Firing of the same interneurons during spontaneous cortical activation. Scale bars for recordings represent 0.5mV for the unit activity and 1mV for the ECoG. **C)** The mean action potential waveforms of the four CR+/Scgn–/Lhx7– interneurons. **D)** The mean firing rates of CR+/Scgn–/Lhx7– interneurons during both cortical slow-wave activity (SWA) and cortical activation (ACT). **E-F)** ISI histogram of each recorded CR+ interneuon during cortical SWA (**E**) and cortical activation (**F**).

5.4.7 A discrete population of CR+ interneurons expresses Scgn in the Rhesus Macaque caudate/putamen

Given the similarities between CR+ interneurons in the rat and in the primate, for example, regarding overall distribution (with both populations having a prevalence for the rostral pole/head of the caudate nucleus) and somatodendritic structure (with three types existing based on their somatic size and degree of dendritic arborization), whether or not the molecular diversity in CR+ interneurons described above for the rat were also present in the Rhesus Macaque was tested. Unfortunately, the antibodies raised against SP8 and Lhx7 that were used in the rat did not produce reliable and consistent results when used on the Rhesus Macaque tissue, and so its use for stereological estimates of Lhx7+ and SP8+ interneurons was not pursued. However, immunofluorescent detection of CR and Scgn in 7 sections containing the caudate and the putamen of the Rhesus Macaque revealed that some, but not all CR-immunoreactive neurons express Scgn (Figure 5.8 A, B). In agreement with past studies (Deng et al., 2010), the density of all CR+ interneurons was higher in the caudate nucleus (Figure 5.8 Ci, Di) than in the putamen (Figure 5.8 Cii, Dii). The mean densities of CR+ interneurons in Rhesus Macaque striatum (Figure 5.8 Di, Dii) were far greater than the mean density value for CR+ interneurons estimated for the rodent (Figure 5.4 B). These results therefore strengthen the notion that the density of CR+ interneurons is far greater in the primate than in the rodent (Wu & Parent, 2000). Importantly, CR+/Scgn+ interneurons make up the minority (nearly one-tenth) of all CR+ interneurons in Rhesus Macaque (Figure 5.8 Di, Dii), which differs from the situation described for PV+ interneurons in this species (see section 4.4.2). Direct comparison of these results with previous

studies is not possible given that past counts in primates have either provided percentages or densities in cells/mm^2, while the figures in this study were acquired using the optical dissector method.

Topographical analysis of CR+/Scgn+ interneuron distributions in the caudate nucleus and the putamen revealed that the positioning of this cell population is partly conserved between the rat and the Rhesus Macaque (Figure 5.8 A). Indeed, CR+/Scgn+ interneurons were almost entirely restricted to the head of the caudate nucleus and the pre-commissural putamen (Figure 5.8 A, Ci, Cii), which is reminiscent of the strong rostral bias in the positioning of these interneurons in the rat striatum (Figure 5.1 Ci, Di). However, unlike the case in rats, the distribution of CR+/Scgn+ neurons was not consistently biased in the medio-lateral or dorso-ventral axes (Figures 5.8 E,F). Importantly, CR+/Scgn– neurons were distributed throughout the rostro-caudal extent of both the caudate nucleus and the putamen (Figure 5.8 A, Ci Cii), which is again reminiscent of wide distribution of this cell population in rat striatum (Figure 5.1 Cii, Dii). Taken together, these data suggest that CR+/Scgn+ neurons make up about half of all CR-immunoreactive neurons in the head of the caudate nucleus and the pre-commissural putamen. The selective expression of Scgn therefore identifies a topographically-biased subpopulation of CR+ interneurons in the monkey striatum. The existence of this dichotomy in the Rhesus Macaque further highlights the importance of defining heterogeneity among striatal interneuron populations not only on the basis of their molecular profiles, but also on their distributions within the striatum.

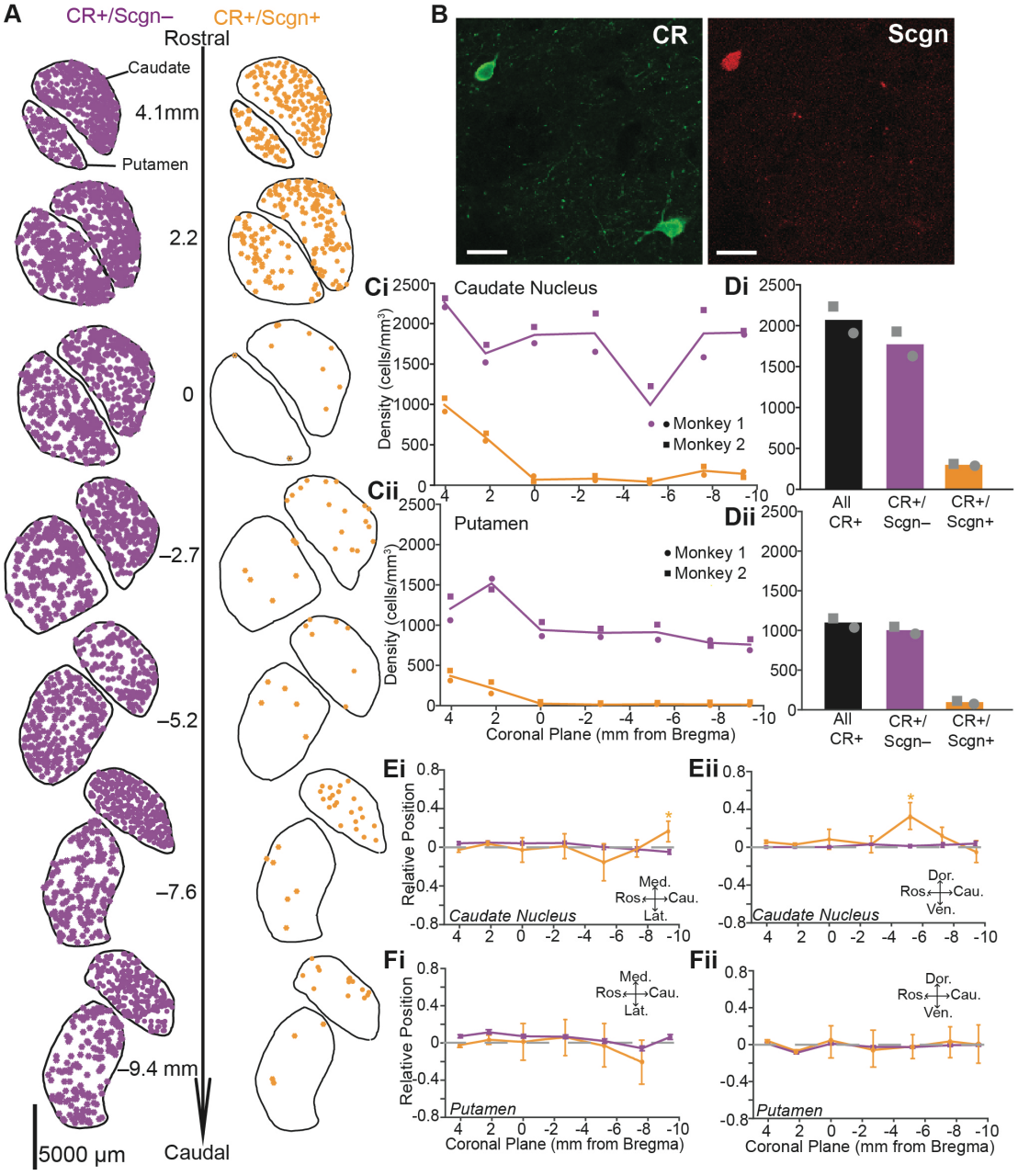

A
CR+/Scgn–
CR+/Scgn+
Rostral
Caudate
4.1mm
Putamen
2.2
0
–2.7
–5.2
–7.6
–9.4 mm
5000 µm
Caudal
B
CR
Scgn
Ci
Caudate Nucleus
Density (cells/mm3)
Monkey 1
Monkey 2
Cii
Putamen
Coronal Plane (mm from Bregma)
Di
Dii
All CR+
CR+/ Scgn–
CR+/ Scgn+
Ei
Eii
Fi
Fii
Relative Position
Med.
Lat.
Dor.
Ven.
Ros.
Cau.
Caudate Nucleus
Putamen

Figure 5.8: CR+/Scgn+ and CR+/Scgn– interneurons have different topographical bias the caudate and putamen of the macaque. A) Typical distribution of CR+/Scgn– (left) and CR+/Scgn+ (right) neurons across 7 coronal planes of the monkey caudate and putamen, with each dot representing a single neuron. **B)** Confocal micrographs of the monkey striatum showing that some CR-expressing interneurons co-expressed Scgn while some did not. **C)** Density of CR+/Scgn+ (orange line) and CR+/Scgn– neurons (purple line) along the rostro-caudal axis of the caudate (**Ci**) and putamen (**Cii**). Note that the CR+/Scgn+ population in the monkey increases in density towards the rostral planes of the caudate and the putamen. **D)** Mean density of CR expression across the entirety of the caudate nucleus (**Di**) and the putamen (**Dii**), including those populations that express (orange bar) and do not express (purple bar) Scgn. In the monkey caudate-putamen, CR+Scgn+ represent nearly 10% of all CR-expressing neurons. **E-F)** Distribution of CR+/Scgn+ (orange line) and CR+/Scgn– neurons (purple line) along the medio-lateral (**Ei, Fi**) and dorso-ventral (**Eii, Fii**) axes of the caudate nucleus (**E**) and putamen (**F**). The presence of asterisks (*) indicate a distribution that is significantly biased in one direction along the specified axis. Data are means of the position of all neurons counted ± SEMs.

5.5 DISCUSSION

The results presented in this study provide the most comprehensive correlations to date between the morphological properties, molecular expression profiles and topographical distributions of CR+ interneurons in the striatum of the rat. Indeed, the co-expression of the calcium-binding protein Scgn (and the transcription factor SP8), or the LIM homebox transcription factor Lhx7 by distinct populations of CR+ interneurons in rat presented here has provided molecular correlates for the morphological diversity previously described in the striatal CR+ interneuron population (Rymar et al., 2004; Tepper et al., 2010; Ma et al., 2014). The correlation between molecular expression patterns and some aspects of spatial distribution for the CR+/Scgn+ population was conserved in the Rhesus Macaque. Through analysis of distribution, somatic size and molecular expression profiles, this study has identified 3 distinct classes of CR+ interneurons in the striatum of the rat. The existence of these 3 "types" of CR-immunoreactive neuron has been alluded to in the past, based on morphological diversity alone (Tepper et al., 2010), but some studies have attributed this diversity to being the product of a single continuum (Rymar et al., 2004; Petryszyn et al., 2014). This disparity has occurred due to the lack of specific and discrete molecular definitions for each subtype of CR+ interneuron, meaning that a clear discrimination between Type 1 and Type 2 CR+ interneurons was not previously possible, even in the rat (Ma et al., 2014).

The molecular expression profiles presented here that identify Type 1 (CR+/Scgn–/Lhx7+), Type 2 (CR+/Scgn–/Lhx7–) and Type 3 (CR+/Scgn+/Lhx7–) CR-expressing interneuron populations are of importance, as they provide an objective method by which to classify morphological disparities among the striatal population of CR+ cells that have been described in the past (Parent and Hazrati, 1995; Rymar et al., 2004; Tepper et al., 2010). This is particularly important given the subjective nature of terms such as "small", "medium" and "large" that have been used to define the heterogeneity in the somatic size and surface area/volume of CR+ interneurons (Rymar et al., 2004; Tepper et al., 2010; Bernacer et al., 2012; Ma et al., 2014).

The existence of a morphologically-distinct class of CR+ interneuron identified by its co-expression of Scgn reported here is in agreement with Scgn expression in the avian brain, where its selective expression was found in classes of neuron with their own unique structural features (Gati et al., 2014). Ultimately, the identification of these 3 types of CR+ interneuron is important given their differences in distribution and molecular expression with respect to CBPs and functional transcriptional factors, as it suggests that each Type of CR+ interneuron is positioned to fulfill specialized functions during the processing of information in the dorsal striatum.

5.5.1 Secretagogin expressing, small sized CR-expressing interneurons are preferentially distributed in the rat and Rhesus Macaque striatum near the subventricular zone, where they might be generated throughout adulthood

In contrast to the PV+/Scgn+ interneuron population in rat striatum described earlier (see Section 4.4.2), the CR+/Scgn+ interneuron population is distributed such that these cells are greatly enriched in the rostro-medial striatum, with very few of them being found centrally or caudally. With respect to its cortical input, this striatal region receives projections primarily from associative cortices rather than limbic or sensorimotor areas in the rat (Vertes & Hoover, 2011, Mailly et al, 2013) and the primate (Parent et al., 1995; Bernacer et al., 2012). Although it is currently unknown whether any CR+ interneurons receive direct cortical or thalamic input, their topographical bias towards the rostro-medial striatum suggests that these Type 3 CR+/Scgn+/Lhx7– interneurons may be involved in the integration of complex information (related to associative tasks) within the striatum, while playing a relatively minor role in the processing of sensorimotor information. Moreover, the bias of these neurons towards the dorsal striatal border places a large number of them close to the lateral ventricles and, thus the subventricular zone (SVZ) (Inta et al., 2008; Inta et al., 2015). These brain regions are important sites of continued neurogenesis throughout adulthood, and are responsible for the generation of newly-born neurons that migrate from the SVZ to the olfactory bulb, the hippocampus and the dorsal striatum. Importantly, a subclass of those neurons destined for the olfactory bulb cannot migrate without the expression of SP8, a transcription factor whose expression also selectively

identifies the Type 3 CR+/Scgn+/Lhx7– interneurons described here. This finding, in combination with reports in which cell-proliferation markers in adult rats were used to demonstrate that newly-born neurons in the subventricular zone migrate to the dorsal striatum of the rat and mature into CR+ interneurons (Dayer et al., 2005; Luzzati et al., 2006; Inta et al., 2015), suggest that some, and perhaps most or all, of these CR+/Scgn+/Lhx7– interneurons are born throughout adulthood. Indeed, recent studies of neuronal migration into the striatum of adult mice have shown that small sized (i.e. 8-10 μm), spiny CR-immunoreactive neurons with a bias towards the medial striatum are generated throughout adulthood (Revishchin et al., 2010a; Revishchin et al., 2010b). As this description matches that of the Type 3 CR+ interneurons defined in this study by their expression of Scgn and SP8, and elsewhere by their morphological characteristics (Tepper et al., 2010), it provides further evidence to suggest that the CR+/Scgn+/Lhx7– neurons described here in the rat are also generated throughout adulthood.

The existence of CR+/Scgn+ neurons biased towards the head of the caudate and the pre-commissural putamen in the Rhesus Macaque further strengthens the hypothesis that neurons belonging to this specific CR+ subtype can be newly generated in adulthood, as the use of carbon-14 dating in human tissue suggests that CR+ interneurons migrate from the subventricular zone into this region of the striatum throughout adulthood (Ernst et al., 2014). The presence of CR+/Scgn+ interneurons in the Rhesus Macaque striatum described in this study thus suggests that this cell type is conserved throughout the mammalian phylogeny. Importantly, interneurons that co-expressed both CR and Scgn in the Rhesus Macaque recapitulated the preferential distribution of the Type 3 CR+/Scgn+/Lhx7– interneurons of the rat dorsal striatum towards the rostral pole of striatum. These regions represent the pre-commissural, associative region of the striatum in the primate (Parent 1990; Fudge et al., 2002; Haber & Knutson, 2010; Bernacer et al., 2012). Thus, CR+/Scgn+ interneurons may perform an equivalent role in the primate and the rat. This hypothesis is further advanced by the fact that CR+/Scgn+ neurons in both rats and Rhesus Macaque are rare in the central and caudal striatum. Thus, past observations that CR+ neurons have a rostral bias in their distribution in both rodents (Rymar et al., 2004; Ma et al., 2014) and

primates (Parent et al., 1995; Cicchetti et al., 1998) are explained by the fact that these CR+/Scgn+ neurons are numerous and are found almost exclusively, and at high density, in these striatal regions.

The hypothesis that CR+/Scgn+/Lhx7– interneurons are born throughout adulthood in rats (and perhaps primates) is particularly important given the prevalence of these neurons in disease states. For example, hypoxic or ischemic lesions of the striatum increase the generation and migration of CR+ interneurons from the subventricular zone (Yang et al., 2008). In humans, both Parkinson's disease (Ordonez et al., 2013) and Huntington's disease (Ernst et al., 2014) involve a decrease of the percentage of newly generated CR+ neurons, but this is slowly recovered over time. Thus, CR+ interneurons, and particularly those co-expressing Scgn are an integral part of neurogenesis that occurs within the dorsal striatum.

5.5.2 The relatively small population of medium sized CR+ interneurons does not express Lhx7 or secretagogin in the rat

The earliest qualitative descriptions of CR+ interneurons in the rat dorsal striatum suggested they were "medium-sized" (Jacobowitz & Winsky, 1991), an observation that was later reiterated in monkeys (Fortin & Parent, 1994) and humans (Parent et al., 1995). Past reports have suggested that these medium-sized interneurons are the major source of CR-immunoreactivity in the rat striatum, making up nearly 90% of all CR+ interneurons (Rymar et al., 2004). These results were based on the assumptions that medium-sized neurons encompassed any neuron whose somatic diameter was between 7-20 μm. Here, the use of Scgn and Lhx7 immunoreactivity, as well as an in-depth investigation of somatic size has revealed that medium-sized CR+ interneurons (as defined by their lack of Scgn or Lhx7 expression and their somatic diameter) make up 20% of all CR+ interneurons in the rat, while the small-sized CR+/Scgn+/Lhx7– neurons and the large-sized CR+/Scgn– /Lhx7+ neurons each make up approximately 40% of the CR+ interneuron population. Importantly, these "type 2" medium-sized CR+/Scgn–/Lhx7– interneurons also demonstrated a preference to distribute in the rostral

striatum in rats, albeit to a much smaller degree than the bias found for type 1 CR+ interneurons. In the Rhesus Macaque striatum, this study reports that CR+ interneurons are more numerous than PV+ interneurons, in accordance with previous descriptions of CR-immunoreactivity in the striatum of primates (Wu and Parent, 2000), but they did not demonstrate any particular bias within either the caudate or the putamen. This lack of inherent distributional bias seems to be a running theme in the primate caudate/putamen, as many studies of interneuron distribution in this species failed to detect any preference for one particular region (Petryszyn et al., 2014; Deng et al., 2010). These findings further highlight the polarized nature of CR+/Scgn+ interneuron distribution of the Rhesus Macaque.

With respect to the function of CR+ interneurons within the striatal microcircuit, very little is known due to the absence of data regarding their synaptic connectivity within the striatum or their electrophysiological properties. Here, the first recordings of medium-sized, Type 2 CR+ interneurons (CR+/Scgn–/Lhx7–) are presented, which show that these are fast-spiking interneurons with highly heterogeneous firing rates and patterns during both cortical activation and cortical slow-wave activity. Although these results alone do not fully elucidate the function of these neurons, they may help future electrophysiological studies recognize their presence within the striatum, particularly given the finding that these interneurons are "tonically active" (4-12 spike/s) during cortical activation; such firing would not be expected of spiny projection neurons, NOS+/NPY+ interneurons or most cholinergic interneurons during this brain state (Sharott et al. 2012). Interestingly, reports of decreases in the number of CR+ interneurons (medium-sized CR+ interneurons in particular) have provided some hypotheses regarding the potential function of these interneurons within the striatum. Studies of medium-sized CR+ interneurons in post-mortem tissue have highlighted their importance in the context of Huntington's disease (HD), where the widespread loss of striatal neurons characteristic of this disease does not apply to medium-sized CR+ interneurons (Kowall et al., 1987; Massouh et al., 2008). After lesions of the nigrostriatal pathway in rats designed to mimic Parkinsonism, the number of CR+ neurons is transiently increased (Mura et al., 2000). This response does not occur when lesioned rats are

treated with L-Dopa, suggesting that CR+ interneurons are particularly sensitive to dopamine depletion (Mura et al., 2000). This is in accordance with past hypotheses suggesting that dopamine can influence CR+ interneurons (Kawaguchi et al., 1995), but recent findings in *Drd1a*-tdTomato/*Drd2*-EGFP double transgenic mice have found that CR+ interneurons do not express D1 or D2 dopamine receptors, meaning that the influence of dopamine on these interneurons is mediated by other types of dopamine receptor or might be indirect (Petryszyn et al., 2014).

5.5.3 Lhx7 expression in the large-sized CR+ interneurons of the rat may link them to the large CR+/ChAT+ expressing interneurons of the primate

Large-sized CR+ interneurons were first described in the striatum of squirrel monkeys (Fortin & Parent, 1995) and humans (Parent et al., 1995) as being highly analogous in somatodendritic structure to the large striatal cholinergic interneurons (Parent et al., 1995). These similarities were not surprising given the large degree of ChAT and CR co-expression by large (>20μm) striatal interneurons which are found in both monkeys and humans (Parent et al., 1995; Massouh et al., 2008). In the rodent striatum, however, ChAT and CR are not co-localized. Interestingly though, "large" CR+ interneurons have been described in the rodent striatum of both mice (Petryzsyn et al., 2014) and rats (Rymar et al., 2004), and have been successfully distinguished from other CR-expressing interneurons in this study on the basis of their molecular expression profile as well as their mean somatic diameter. These findings have raised some important questions regarding the reason that large-sized CR+ interneurons exist in the rodent, and yet do not express ChAT as they do in the primate. Some studies have suggested that CR expression in cholinergic interneurons in the primate may offer them a degree of defence against calcium-mediated "excitotoxicity" (Petryzsyn et al., 2014), but this is unlikely given the degree of cholinergic abnormality seen in large ChAT+ neurons in post-mortem brains of Huntington's disease patients (Smith et al., 2006). Thus, the function of ChAT and CR co-expression by some interneurons in the primate, and the reason for the complete absence of ChAT in the large CR+ neurons in the rodent, remain unclear.

Given this disparity between the presence of large-sized CR+ interneurons in the rodent and the Rhesus Macaque, one could consider whether or not the large CR+ interneurons of the rodent are related to the large CR+/ChAT+ interneurons of the primate. Here, the expression of the LIM homeodomain protein Lhx7 in the rat has allowed for the identification of the largest subpopulation of CR+ striatal interneurons, whose size and somatodendritic structure matches previous descriptions of so-called "Type 1" CR+ interneurons in the mouse (Tepper et al., 2010). While other studies have often treated these large-sized CR+ neurons as being part of the continuum that also encompasses medium-sized CR+ neurons (Rymar et al., 2004; Ma et al., 2014), the unique molecular expression profile of the larger neurons described in this report suggests that they are a separate type of CR+ interneuron. The expression of Lhx7 by Type 1 CR+ interneurons is not entirely surprising, as past studies using $Lhx7^{+/nlacZ}$; $Gad67^{GFP}$ double transgenic reporter mice showed that nearly 43% of striatal β-gal+ cells (indicating the expressing of Lhx7) were also found to express green fluorescent protein (indicating they were GABAergic) (Fragkouli et al., 2005; 2009). Thus, it had been established that Lhx7 also labels GABAergic, MGE-derived striatal neurons (interneurons) whose cell bodies are smaller than those of ChAT+ interneurons in striatum. This suggests that CR+/Scgn–/Lhx7+ interneurons are likely derived from the MGE, while CR+/Scgn+/Lhx7– interneurons expressing SP8 are likely to be derived from the SVZ or CGE (Inta et al., 2008). The quantitative finding that Type 1 CR-expressing interneurons are distributed with a slight descending rostro-caudal gradient within the dorsal striatum presented here is an important one, as it agrees with qualitative descriptions of rat striatal CR+ neurons distributions that have been made in the past (Bennett and Bolam, 1993; Wu and Parent, 2000). The expression of Lhx7 by large Type 1 CR+ interneurons in the adult rat is by itself significant, since Lhx7 is also expressed in the cholinergic interneurons of the adult striatum (Fragkouli et al., 2005). Lhx7 expression in these neurons is functionally relevant as it promotes the migration of cholinergic progenitors during development, while also maintaining their cholinergic identity in the striatum throughout adulthood (Fragkouli et al., 2009). Although Lhx7

is perhaps not performing similar functions in Type 1 rat CR+ interneurons (because they do not have a cholinergic identity *per se*) , its presence in this large, morphologically-distinct population potentially provides developmental insights into the relationship between CR and ChAT that has been described in humans and primates (Cicchetti et al., 1998; Massouh et al., 2008). In summary, the relationship between Lhx7 and cholinergic interneurons, combined with the expression of Lhx7 in large type 1 CR+ interneurons in rat, suggest there is as a link between the large CR+/Scgn–/Lhx7+ neurons of the rat and the large CR+/ChAT+ interneurons of the primate.

Ultimately, the present study has provided a novel approach to identify different populations of morphologically-, topographically- and molecularly-distinct CR+ interneurons in the rat striatum. These molecular correlates were partially conserved in the Rhesus Macaque, while revealing a potential link between rats and primates with respect to the large CR+ interneurons.

CHAPTER 6.

CHARACTERIZATION OF MOLECULARLY DEFINED CLASSES OF INTERNEURON IN THE NUCLEUS ACCUMBENS

6.1 INTRODUCTION

As compared to the dorsal striatum, much less is known about the cellular make-up or organization of the nucleus accumbens (NAcc) core and shell. Indeed, the anatomical and electrophysiological properties of interneurons in the nucleus accumbens are relatively poorly defined. With respect to their distribution, past studies have casually noted that PV-expressing interneurons are less dense in the ventral striatum compared to the dorsal striatum (Kita et al., 1990; Kubota and Kawaguichi, 1993). Other studies have also noted that somatostatin- (and thus, presumably also NOS) expressing interneurons are as equally dense in the ventral striatum as they are in the dorsal striatum (Kubota and Kawaguchi, 1993), while the density of ChAT-expressing interneurons is greater in the ventral striatum (Meredith et al., 1989). Other than the quantitative study of ChAT-expressing interneurons (Meredith et al., 1989), one should appreciate that these observations are all qualitative anecdotes. Thus, no study has provided any quantitative information regarding the absolute numbers and the topographic distribution of the 4 major classes of interneurons (PV+, CR+, ChAT+ and NOS+) in the ventral striatum. Given the striking differences between the structure and the cellular architecture of projection neurons in the core and the shell of the nucleus accumbens (Zhou et al., 2003; Humphries & Prescott, 2010; Kupchik et al., 2015), the lack of quantitative information regarding the presence of the 4 major interneurons in the core vs. the shell is quite surprising. Because GABAergic and cholinergic interneurons neurons have been shown to exert a powerful influence on the output of the dorsal striatum (Koos & Tepper, 1999; Tepper et al., 2010; Klaus et al., 2011; Szydlowski et al., 2013), it is important to clearly define the identities and distributions of these interneurons across the entirety of the core and the shell of the ventral striatum.

The intrinsic connectivity of the ventral striatum has also been relatively poorly elucidated, with many studies making assumptions based on results obtained from the cytoarchitecture of the dorsal striatum. For example, it is assumed that PV-expressing interneurons extend their axons across the boundary between the shell and the core (Humphries &

Prescott, 2010) based on the fact that in the dorsal striatum, the axons of PV-expressing interneurons cross the boundary between the patch and the matrix regions (Kawaguchi et al., 1995). The work of Meredith and colleagues demonstrated that the axon of cholinergic interneurons in the core can pass into the medial shell, although the cellular targets for their output were not defined (Meredith et al., 1989). A further reciprocal connection between the core and the shell has been shown to be mediated by the axon collaterals of SPNs in both regions (vanDongen et al., 2005). This connection has been described on a functional level, as paired recordings of SPNs in the core and shell have found that stimulating SPNs in either region can produce an inhibitory current in the SPNs of another region (Taverna et al., 2004). Thus, the ventral striatum's microcircuit represents a relatively undefined system, whose makeup and overall structure is very poorly understood. Given the multitude of studies that have studied the effects of addictive drugs (Boileau et al., 2003; Bossong et al., 2009) on the activity of post-synaptic structures in the nucleus accumbens (Volkow et al., 1990; Oswald et al., 2005), it is again surprising that the cellular components of the core and the shell of the nucleus accumbens are so unclear. There is therefore a clear need for a better understanding of the identity and distribution of the cellular architecture responsible for this activity, as this will allow the results from these studies to be more accurately interpreted.

With respect to its cortical input, the NAcc receives cortical input from the orbitofrontal division of the prefrontal cortex (Berendse et al., 1992), the amygdala (Wright et al., 1996; Wright & Groenewegen, 1996; Kelley et al., 1982) and the hippocampus (Kelley & Domesick, 1982; Friedman et al., 2002). One particularly prominent input into the nucleus accumbens arises from the ventral and dorsal hippocampal formation (Kelley & Domesick, 1982; Groenewegen et al., 1987) as well as from the lateral entorhinal cortex, which projects to the lateral core and shell, and from the medial entorhinal cortex, which projects to the rostro-medial shell and core (Totterdell & Meredith, 1997). Given the variety of cortical inputs received by the nucleus accumbens, and the similarities these share with the ventromedial aspects of the dorsal striatum, it

is likely that both these regions are sites where spatial properties of the environment, learnt behaviours and reward valuation are at least partially processed.

The functions of the nucleus accumbens suggested by the heterogeneity of its cortical inputs are best demonstrated by behavioural studies looking to investigate the activity of its neural populations during specialized tasks. For example, decision-making tasks in which the predicted value of a reward is modified either by changing the interval between completion of a task and reward delivery or by changing the size of the reward are commonly used to study behavioural modification (Roesch et al., 2009). Recordings made in the nucleus accumbens during such tasks reveal that a relatively high percentage of neurons respond to cues associated with high-value rewards delivered after short delays (Roesch et al., 2009). This suggests that activity in the accumbens changes in response to the predicted value previously associated with a given reward. This also reflects the input the nucleus accumbens receives from the orbitofrontal cortex (Berendse et al., 1992), which has been implicated in similar behavioural tasks (Schoenbaum et al., 2007). Importantly, the responses of neurons in the nucleus accumbens were sensitive to position and direction of the presented cue (Roesch et al., 2009). This may again reflect the extensive inputs into the nucleus accumbens from the entorhinal cortex (Mcgeorge & Faull, 1989; Totterdell & Meredith, 1997). Moreover, the reaction time of animals to the presentation of the reward was significantly correlated with the firing of neurons in the nucleus accumbens, suggesting that some NAcc neurons encodes motivated behaviour in response to reward-associated cues (McGinty et al., 2013; Bissonette et al., 2013).

6.2 AIMS

With its heterogeneous cortical inputs as well as the variety of different behaviours associated with the activity of its neural populations, it is clear that the identity of the microcircuit within the accumbens should be explored in detail. This is especially important given the lack of any quantitative data regarding the microcircuitry of the nucleus accumbens. In order to compare the microcircuitry of the nucleus accumbens with that of the dorsal striatum's dorso-lateral and dorso-medial aspects, immunohistochemistry and stereological cell counting were used to achieve the following aims:

- To determine the densities of ChAT+, PV+, CR+ and NOS+ interneuron populations across the core and shell of the nucleus accumbens.
- To quantify the distributions of these four types of interneuron in the nucleus accumbens.
- To define the prevalence, distribution and extended molecular phenotype of Scgn-expressing interneurons in the nucleus accumbens.

6.3 METHODS

Experimental procedures were carried out on adult male Sprague-Dawley rats (Charles River, Margate, UK) that were ~3 months old, weighing between 280-350g. All rodents used were maintained on a 12/12 h light/dark cycle, and had free access to food and water. All experiments were conducted in accordance with the Animals (Scientific Procedures) Act 1986 (UK).

A detailed description of the techniques and protocols used in this chapter can be found in the appropriate sections of Chapter 2.

- Perfusion and fixation (Section 2.1.1)
- Indirect immunofluorescence (Section 2.1.2)
- Stereological cell counting (Section 2.1.3)
- Calculations of section area, volume and estimates of total cell number (Section 2.2.1)
- Topographical and statistical analysis of interneuron distribution (Section 2.2.2)

6.4 RESULTS

6.4.1 Scgn-expressing neurons in the nucleus accumbens do not express any marker of spiny projection neurons or any classical interneuronal marker

Using 2 antibodies raised against different epitopes along the Scgn protein structure (Table 2.2), Scgn was not found to be co-expressed with the SPN specific marker CTip2 (Arlotta et al., 2008; data not shown), suggesting that Scgn+ neurons in the nucleus accumbens are interneurons. Moreover, immunohistochemical detection of Scgn along with the one or more of the markers of the 4 classical striatal interneuron populations revealed that, first, both core and shell contained Scgn-expressing neurons and secondly, that these Scgn+ neurons did not co-express PV, CR, ChAT or NOS (Figures 6.1, 6.2). These results suggest that Scgn expression identifies a novel group of interneurons in the NAcc. It is unclear whether these Scgn+ interneurons belong to the so-called "Scgn-only" population found in the dorsal striatum (see section 3.4.4). However, investigations of their cell body size as determined from immunohistochemistry showed that their mean somatic diameter was similar to that of "Scgn-only" neurons, as it had a mean value of 15.9 ± 0.9um (n = 41). Thus, these medium sized neurons may potentially represent the same population as the Scgn-expressing neurons described earlier in the ventro-medial aspect of the dorsal striatum (see section 3.4.4).

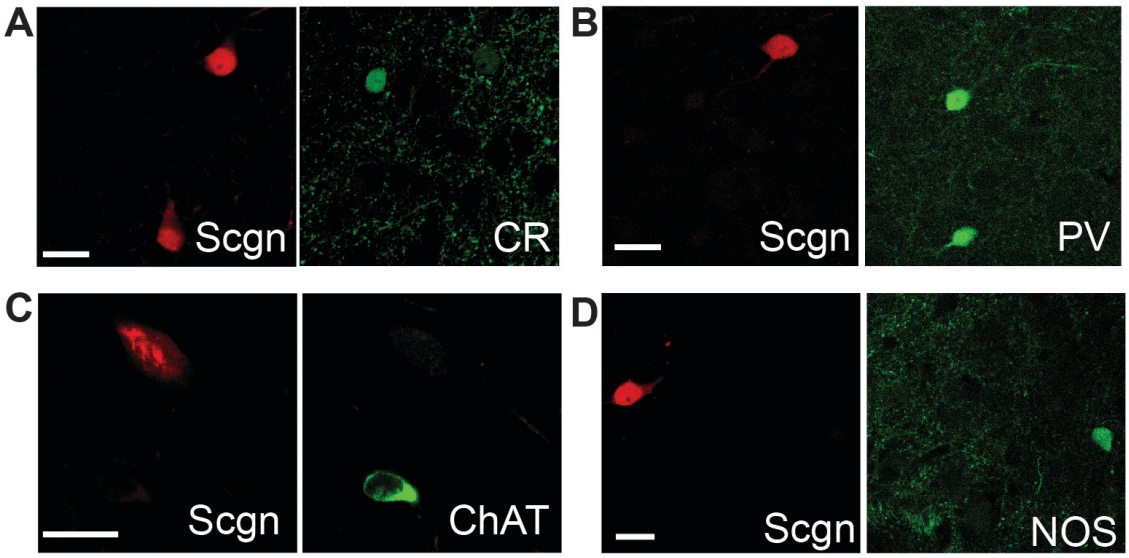


Figure 6.1: Immunofluorescence images of Scgn+, PV+, ChAT+ and NOS+ interneurons in the nucleus accumbens. A) Scgn (red) and CR (green) **B**) Scgn (red) and PV (green) **C**) Scgn (red) and ChAT (green) **D**) Scgn (red) and NOS (green). Scale bars represent 20µm

6.4.2 Scgn+ interneurons have a heterogeneous distribution within the nucleus accumbens

Stereological counting of Scgn-immunoreactive neurons in the core and shell of the nucleus accumbens in rats (Figure 6.2 A) revealed that the proportion of all NAcc Scgn+ neurons located in the shell was substantially larger than that located in the core (Figure 6.2 D). Indeed, averaged across 3 animals, the shell was found to have 2641 ± 386 Scgn+ cells while the core had approximately 866 ± 48 cells. When these numbers are normalised for the larger volume of the shell, the mean density of Scgn+ neurons in the shell was almost double that in core (917 ± 156 and 484 ± 25 cells/mm^3, respectively) (Figure 6.2 Biii). When the locations of Scgn+ neurons was mapped across the nucleus accumbens, those in the core were preferentially distributed towards its rostral and caudal poles (Figure 6.2 Bi). In contrast, Scgn+ interneurons in the shell were preferentially distributed towards only the caudal pole (Figure 6.2 Bii). Because the number of Scgn+ interneurons in the NAcc core was relatively small, quantitative tests of possible bias in

their positioning along the medio-lateral and dorso-ventral axes were limited (Figure 6.2 Ci,Cii) and thus, firm conclusions could not be drawn. However, the locations of Scgn+ neurons in the shell were consistently and significantly biased towards the medial aspects of this structure (Figure 6.2 Ci), but with no clear bias along the dorso-ventral axis (Figure 6.2 Cii).

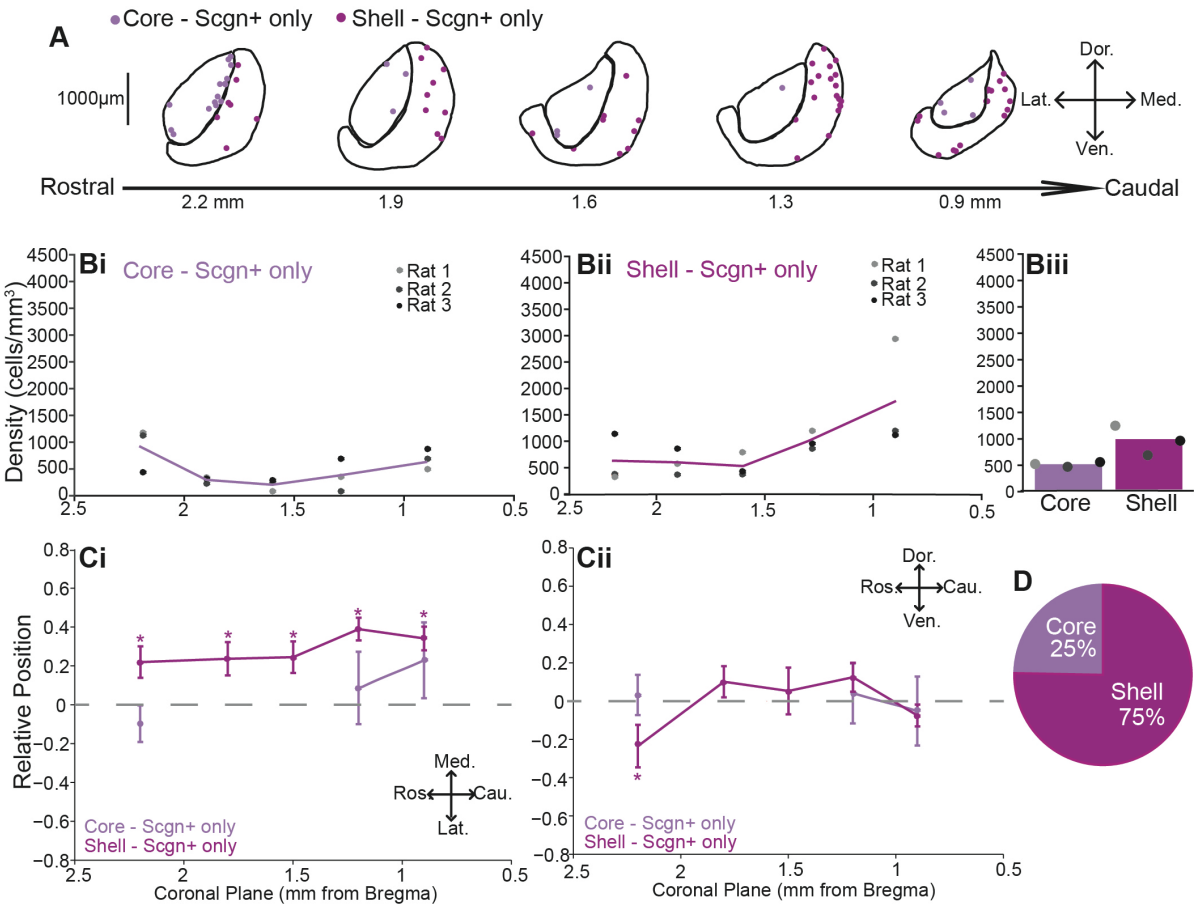


Figure 6.2: Density and distribution of Scgn+ neurons in the core and shell of the NAcc.
A) Representative sample of Scgn+ interneurons in the NAcc of one rat **B**) density of Scgn+ interneurons in each coronal section of the core (**B_i**), the shell (**B_{ii}**) and their mean values (**B_{iii}**) **C**) The medio-lateral (**Ci**) and dorso-ventral (**Cii**) distribution of Scgn+ interneurons in core (light purple line) and shell (dark purple line). In coronal planes where less than 10 neurons were counted per animal, no relative topographical value is given. Asterisks (*) indicate a distribution that is significantly biased in one direction along the specified axis. Data are means of the position of all neurons counted ± SEMs. **D**) Percentage of Scgn+ interneurons in the core and shell.

6.4.3 ChAT+ interneuron density increases in the medial aspects of the nucleus accumbens

Given the scarcity of data regarding the numbers, densities and distributions of the four classical interneuron subtypes in the nucleus accumbens, a quantitative stereological investigation of ChAT+, NOS+, PV+ and CR+ interneurons was carried out in the NAcc core and the shell. Stereological cell counting and mapping of ChAT-immunoreactive neurons in the core and shell in rats (Figure 6.3 A) revealed that a higher proportion of ChAT+ interneurons were located in the shell compared to the NAcc core (Figure 6.3 D). When counts were averaged across 3 animals, the shell was found to have 4589 ± 548 ChAT+ cells while the core had approximately 2038 ± 223 ChAT+ cells. After taking into account the different sizes of the core and shell, the mean density of ChAT+ neurons in the shell was greater than that in the core (1542± 224 and 1139 ± 129cells/mm^3, respectively) (Figure 6.3 Biii). When mapped across the nucleus accumbens, ChAT+ interneurons did not possess a distributional bias along the rostro-caudal axis of either the core or the shell (Figure 6.3 Bi, Bii). In the NAcc shell, ChAT+ neurons were uniformly distributed along the dorso-ventral axis, but displayed a strong medial bias in the central coronal planes that were assessed (Figure 6.3 Ci, Cii). This medial bias has been noted in the past (Meredith et al., 1989), and was consistent across all three animals, and was spatially restricted in the rostro-caudal plane such that it occurred approximately 1.5mm ahead of Bregma, and disappeared entirely in coronal planes 1.0mm ahead of Bregma (Figure 6.3 Ci, Cii). In the NAcc core, ChAT+ interneurons were also biased towards the medial borders in most planes that were assessed, while displaying no significant distributional biases along the dorso-ventral axis (Figure 6.3 Ci, Cii).

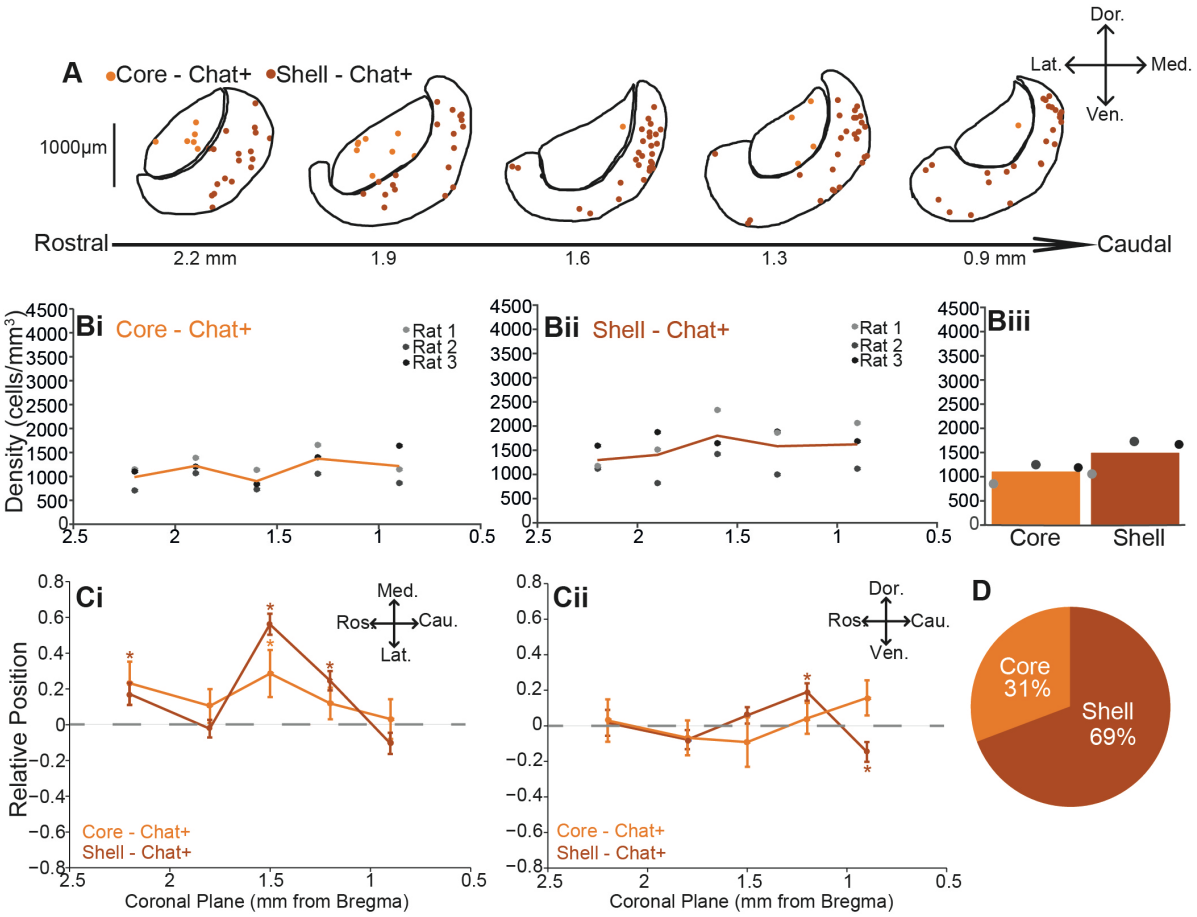


Figure 6.3: Density and distribution of ChAT+ neurons in the core and shell of the nucleus accumbens. **A**) Representative sample of ChAT+ interneurons in the NAcc of one rat **B**) density of ChAT+ interneurons in each coronal section of the core (**B_i**), the shell (**B_{ii}**) and their mean values (**B_{iii}**) **C**) The medio-lateral (**Ci**) and dorso-ventral (**Cii**) distribution of ChAT+ interneurons in core (light purple line) and shell (dark purple line). In coronal planes where less than 10 neurons were counted per animal, no relative topographical value is given. The presence of the asterisk (*) indicates a distribution that is significantly biased in one direction along the specified axis. Data are means of the position of all neurons counted ± SEMs. **D**) Percentage of ChAT+ interneurons in the core and shell.

6.4.4 NOS+ interneurons have a similar distribution to ChAT+ interneurons in both the core and shell of the nucleus accumbens

Stereological cell counting and mapping of NOS-immunoreactive neurons in the core and shell of the nucleus accumbens in rats was performed (Figure 6.4 A). Analysis of this data revealed that a greater proportion of NOS+ interneurons were located in the shell compared to the NAcc core (Figure 6.4 D). Averaged across 3 animals, the shell was found to have 8589 ± 369 NOS+ cells while the core had approximately 3818 ± 531 cells. Normalization of these numbers achieved through the calculation of cell density reveals that the mean density of NOS+ neurons in the shell was 2870 ± 312 cells/mm^3, which was greater than the 2027 ± 190 cells/mm^3 that was measured in the core (Figure 6.4 Biii). These density values are similar to the density values estimated for NOS+ interneurons in the dorsal striatum (West et al., 1996), and therefore are in agreement with previous anecdotal reports of NOS-expression in the ventral striatum (Kubota and Kawaguchi, 1993). When mapped across the nucleus accumbens, the distribution of NOS+ interneurons was similar to that of ChAT-expressing interneurons, in the sense that their distribution was not strongly biased along the rostro-caudal axis of the core (Figure 6.4 Bi) or the shell (Figure 6.4 Bii). Within the core, NOS+ neurons were significantly biased towards its medial border across multiple coronal planes (Figure 6.4 Ci). In the shell, a lateral bias was consistently detected in the caudal most coronal planes i.e. approximately 1.0 mm ahead of Bregma (Figure 6.4 Ci). Along the dorso-ventral axis of both the core and the shell, NOS+ neurons were homogenously distributed (Figure 6.4 Cii).

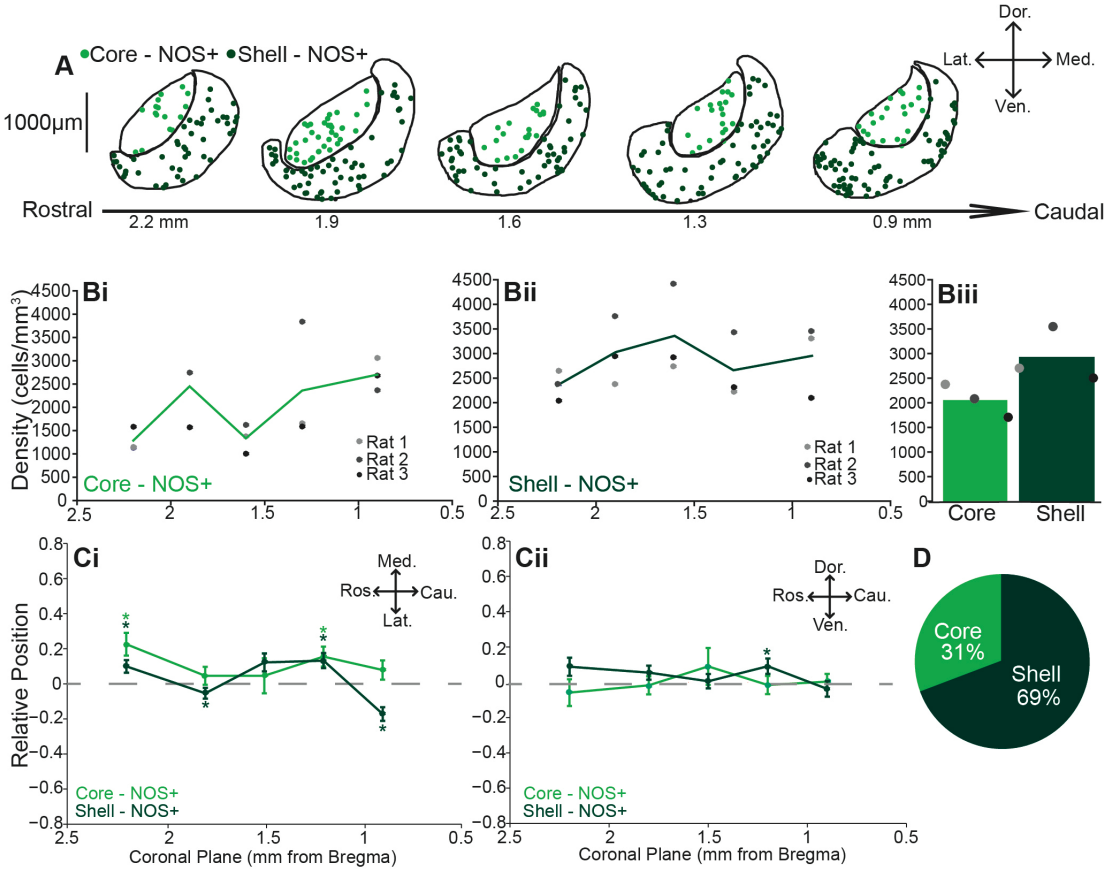


Figure 6.4: Density and distribution of NOS+ neurons in the core and shell of the ventral striatum. **A**) Representative sample of NOS+ interneurons in the NAcc of one rat **B**) density of NOS+ interneurons in each coronal section of the core (**B_i**), the shell (**B_{ii}**) and their mean values (**B_{iii}**) **C**) The medio-lateral (**Ci**) and dorso-ventral (**Cii**) distribution of NOS+ interneurons in core (light purple line) and shell (dark purple line). In coronal planes where less than 10 neurons were counted per animal, no relative topographical value is given. The presence of the asterisk (*) indicates a distribution that is significantly biased in one direction along the specified axis. Data are means of the position of all neurons counted ± SEMs. **D**) Percentage of NOS+ interneurons in the core and shell.

6.4.5 PV+ interneurons are distributed with a decreasing rostro-caudal gradient and a medial bias in the shell but not the core of nucleus accumbens

Stereological cell counting and mapping of PV-immunoreactive neurons in the core and shell of the nucleus accumbens in rats revealed that a higher proportion of PV+ interneurons was found in the shell compared to the NAcc core (Figure 6.4 A, D). Averaged across 3 animals, the shell was found to have 6795± 618 PV+ cells while the core had approximately 3374 ± 180 cells. Normalization of these numbers achieved through the calculation of cell density reveals that the mean density of PV+ neurons in the shell was 2341± 213 cells/mm^3, which was only slightly greater than the 1892± 154cells/mm^3 that was measured in the core (Figure 6.5 Biii). When mapped across the nucleus accumbens, the density of PV+ interneurons in the core generally increases along the rostro-caudal axis (Figure 6.5 Bi). In contrast PV+ interneurons in the shell were more prevalent towards the rostral pole of this structure, where the density of PV+ interneurons was greater than that of any other histochemically defined population that was studied (Figure 6.5 Bii). This quantification of the rostral distributional bias is in agreement with previous anecdotal descriptions of PV+ interneurons in the shell (Wu et al, 2000). There is a significant medial bias in PV+ interneuron distribution throughout the entirety of the shell (Figure 6.5 Ci), while the distribution of PV+ interneurons in the rostral and the caudal poles of the accumbens core was laterally biased (Figure 6.5 Ci). There is a dorsal bias in core PV+ interneurons at the rostral end of the accumbens (Figure 6.5 Cii), and a homogenous distribution throughout the rest of the NAcc core. In the NAcc shell, PV+ interneurons were homogenously distributed along the dorso-ventral axis (Figure 6.5 Cii*)*.

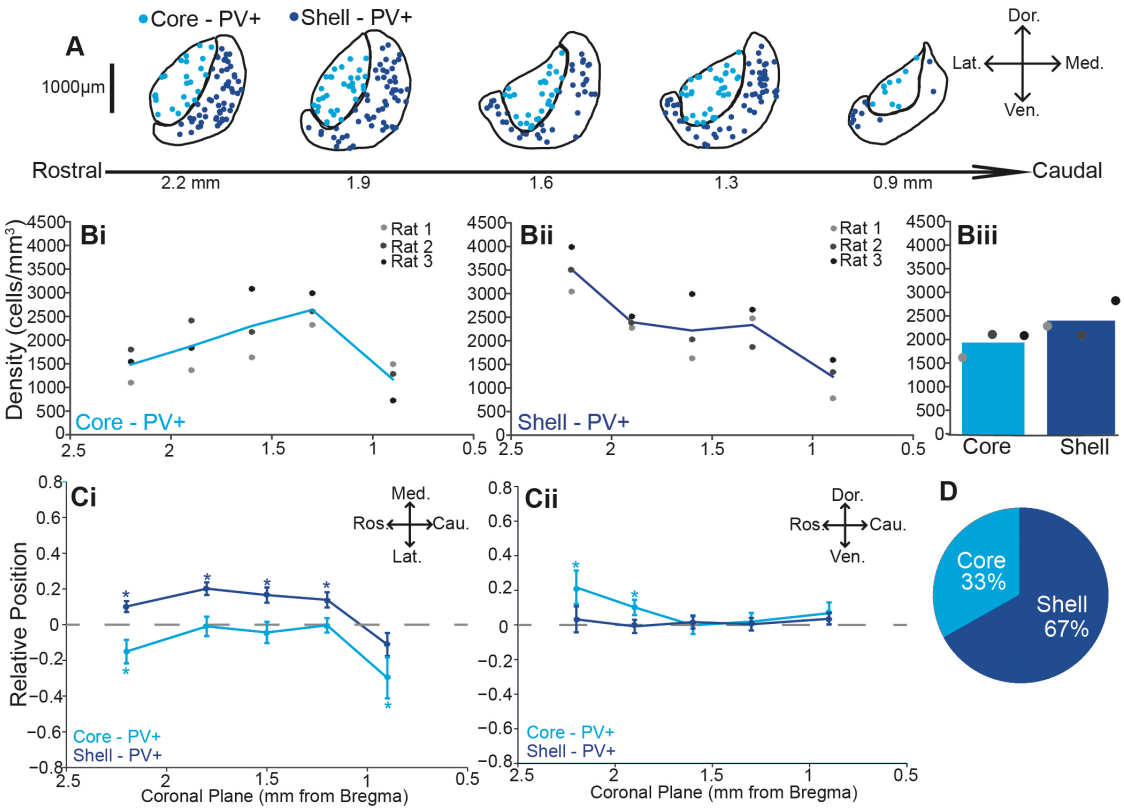


Figure 6.5: Density and distribution of PV+ neurons in the core and shell of the ventral striatum. **A**) Representative sample of PV+ interneurons in the NAcc of one rat **B**) density of PV+ interneurons in each coronal section of the core ($\mathbf{B_i}$), the shell ($\mathbf{B_{ii}}$) and their mean values ($\mathbf{B_{iii}}$) **C**) The medio-lateral (**Ci**) and dorso-ventral (**Cii**) distribution of PV+ interneurons in core (light purple line) and shell (dark purple line). In coronal planes where less than 10 neurons were counted per animal, no relative topographical value is given. The presence of the asterisk (*) indicates a distribution that is significantly biased in one direction along the specified axis. Data are means of the position of all neurons counted ± SEMs. **D**) Percentage of PV+ interneurons in the core and shell.

6.4.6 CR+ interneurons are distributed with an increasing rostro-caudal gradient in the nucleus accumbens

Of all the "classical" interneuron subtypes associated with the striatum in rodents, those identified by their expression of CR within the nucleus accumbens are perhaps the least well characterized. Indeed, even anecdotal observations of interneuron distributions in the NAcc do not include CR+ interneurons (Humphries & Prescott 2010). Stereological assessment and mapping of CR-immunoreactive neurons in the core and shell of the nucleus accumbens in rats (Figure 6.6 A) revealed that the shell possessed a greater proportion of CR+ interneurons than the NAcc core (Figure 6.6 D). Averaged across 3 animals, the shell was found to have 4984 ± 549 CR+ cells while the core had approximately 3308 ± 490 cells. Importantly, when these numbers are adjusted for the larger volume of the shell, the mean density of CR+ neurons in the shell was 1711± 163 cells/mm^3, which was similar to the 1869± 339 cells/mm^3 that was measured in the core (Figure 6.6 Biii). When mapped across the nucleus accumbens, the distribution of CR+ interneurons in both the core and the shell demonstrated an increasing gradient towards the caudal planes of the shell (Figure 6.6 Bi, Bii), where the density of CR+ interneurons was nearly as large as the density of PV+ interneurons in the rostral shell (Figure 6.5 Bii). This increase in the density of CR+ interneurons in the caudal aspects of NAcc has not been described in the past. In the shell, there was a significant medial (Figure Ci) and ventral (Figure Cii) bias in CR+ interneuron distribution which was particularly strong in the shell.

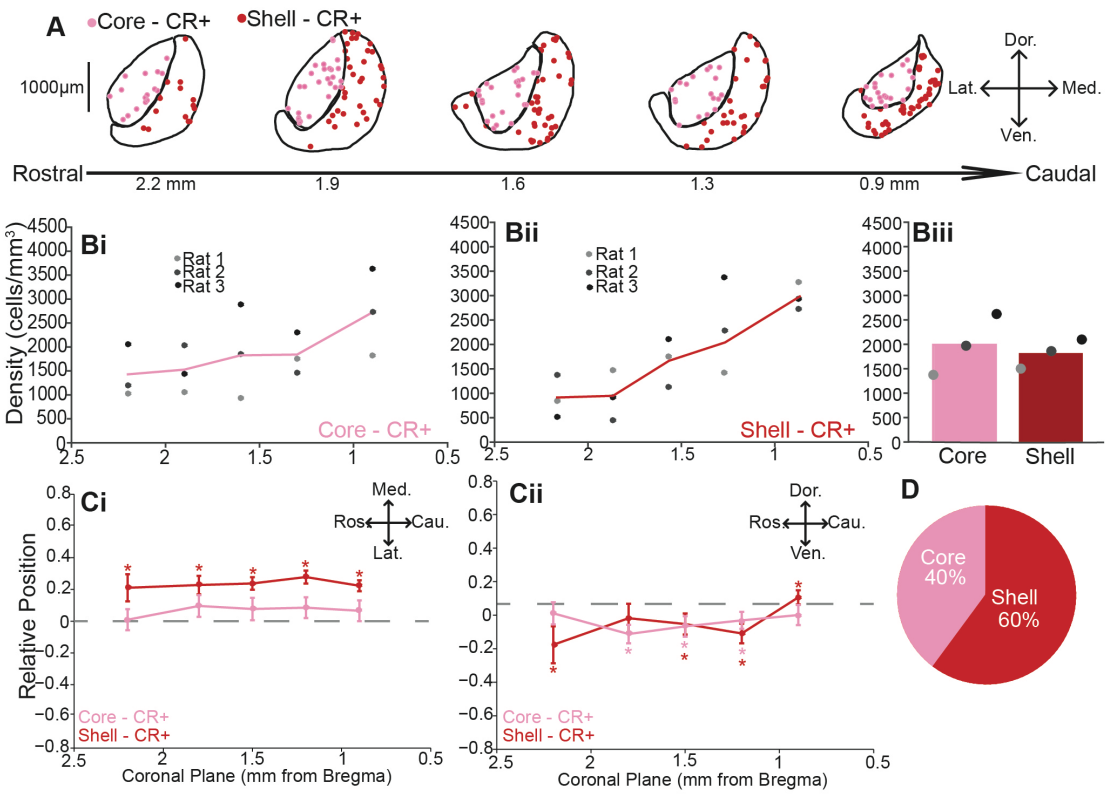


Figure 6.6: Density and distribution of CR+ neurons in the core and shell of the ventral striatum. **A**) Representative sample of CR+ interneurons in the NAcc of one rat **B**) density of CR+ interneurons in each coronal section of the core (**B_i**), the shell (**B_{ii}**) and their mean values (**B_{iii}**) **C**) The medio-lateral (**Ci**) and dorso-ventral (**Cii**) distribution of CR+ interneurons in core (light purple line) and shell (dark purple line). In coronal planes where less than 10 neurons were counted per animal, no relative topographical value is given. The presence of the asterisk (*) indicates a distribution that is significantly biased in one direction along the specified axis. Data are means of the position of all neurons counted ± SEMs. **D**) Percentage of CR+ interneurons in the core and shell.

6.5 DISCUSSION

The present study has provided the first quantitative and stereological definitions of interneuron distributions in the core and shell of the rat nucleus accumbens. It has revealed extensive topographical heterogeneity amongst the "classical" interneuron populations of the nucleus accumbens with respect to their uneven distributions in the core and the shell. A substantial population of interneurons in the NAcc core and shell expressed secretagogin but not any of the other classical markers for striatal interneurons. This differs substantially from what was found in the dorsal striatum, where a subset of PV+ and CR+ interneurons co-expressed Scgn. However, the medium-sized "Scgn-only" interneurons of the NAcc were also found in the dorsal striatum (see section 3.4.3) but, in contrast to the scenario in the NAcc, they represent only one-quarter of all neurons expressing Scgn in the dorsal striatum of the rat (Figures 3.1, 3.2). The distinct distributions of each interneuron population within the NAcc, taken together with the heterogeneous nature of extrinsic glutamatergic and dopaminergic inputs to this structure, suggests that different types of interneuron contribute differently to the processing of specific information within the core and shell of the ventral striatum. The potential functional specializations implied by this heterogeneity are briefly discussed below.

6.5.1 The ventral striatum differs from the dorsal striatum with respect to the relative proportions of the "classical" interneuronal populations

Due to the quantitative nature of the data presented here, this study has revealed a great deal of differences between the relative densities of interneuron populations in the dorsal and ventral striatum. In order to make quantitative comparisons regarding the relative presence of the interneuron populations in the dorsal and ventral striatum, the density of these interneurons was used, as it is a normalized value that takes into consideration the different volumes of these two aspects of the striatum. The results reported in this chapter as well as chapter 4 reveal that PV+ interneurons are denser in the dorsal striatum compared to the ventral striatum, while the data from this chapter and chapter 5 reveals that CR+ interneurons are denser in the ventral striatum.

Additionally, the data from previous estimates of ChAT+ interneuron density in the dorsal striatum (Oorschot, 1999) suggests that their density is greater in the ventral striatum, while NOS+ interneurons were equally as dense in the dorsal striatum (West et al., 1996) as in the ventral striatum. Although these disparities do not necessarily imply the existence of functional differences between the dorsal and the ventral striatum, they provide direct evidence to suggest that the cellular composition of the striatal microcircuit may differ between its dorsal and ventral divisions. Given that the dorsal and ventral striatum are associated with different functional "streams" within the basal ganglia (Smith et al., 1989; Bolam, 2000; Humphries & Prescott, 2010), it is possible that the disparities in the density of different populations of interneuron may suggest that one class of interneuron is more suited to one type of processing over another. This conclusion is particularly strengthened by the finding that the nature of Scgn expression in the ventral striatum differed significantly from the dorsal striatum, as PV+/Scgn+ and CR+/Scgn+ interneurons were not reliably detected in the core or shell of the nucleus accumbens (discussed below). This disparity is also reflected in the three-fold larger density of Scgn+ interneurons in the dorsal striatum compared to the ventral striatum.

6.5.2 The densities of some types of interneuron are greater in the shell than the core

Across all populations studied, stereological estimates of total interneuron number consistently showed that the shell contained a greater number of interneurons than the core. Calculation of cell density to account for the larger size of the shell also showed that, in general, the shell contained a greater density of interneurons when compared to the core. Moreover, the density of interneurons in the shell varied across multiple coronal planes (particularly the density of PV+ and CR+ interneurons) whereas they were more consistent throughout the rostro-caudal axis of the core. In absolute terms, the densities of Scgn+, ChAT+, NOS+ and PV+ interneurons were higher in the shell, whereas the density of CR+ interneurons was slightly higher in the core. These differences are important given that the organization of the projections from the core and the shell are known to differ both with respect to the identity of the neurons themselves (Zhou et al., 2003; Kupchik et al., 2015) as well as the structures they target (Ikimoto, 2007; Bertran-

Gonzalez et al., 2008). Moreover, the core and the shell of the nucleus have been implicated in the encoding of different behavioral functions (Roesch et al., 2009; McGinty et al., 2013; Bissonette et al., 2013). These differences in function are most likely a product of the heterogeneously distributed nature of different cortical inputs into the core and shell. For example, the shell receives an overlapping, input from the basal amygdala and the ventral insular area of the prefrontal cortex, which is heavily restricted to its lateral half (see section 1.5 and Figure 1.3; Humphries & Prescott, 2010). In contrast, the medial shell receives a dense input from the infralimbic cortex which does not target the lateral shell or the core of the nucleus accumbens. The core of the nucleus accumbens receives input from the prelimbic and orbitofrontal cortices, the projections of which do not overlap, but are found in the rostral and caudal poles of the NAcc core, respectively (see Figure 1.3; Berendse et al., 1992).

The presence of spatially restrictive cortical inputs that target the nucleus accumbens, in combination with the results from lesion and behavioral studies, suggest that the Nacc core and shell are involved in the encoding of different behavioral tasks. Indeed, NMDA blockade of the NAcc core degrades the performance of rats in spatial tasks in which the reward has a specific location (Kelley, 1999). This is especially evident in the Morris water maze task, where lesioned animals are unable to locate the platform (Sargolini et al., 2003). In contrast to the core, the shell receives input from the infralimbic cortex while its projections target structures outside of the basal ganglia, including the hypothalamus (Usuda et al., 1998). These anatomical features likely explain why increased dopamine levels in the shell (produced by the local injection of amphetamines) influence the feeding behavior of rats when they are presented with rewards associated with completion of a task (Kelley, 1999; Kelley et al., 2005). Once again, the anatomy of heterogeneous inputs and outputs to different striatal subregions predicts the functional heterogeneity of those same regions. With that in mind, it is likely that the higher proportion of NOS+, Scgn+ and ChAT+ interneurons in the shell may indicate that these subtypes play an important role in the limbic processing that likely occurs in the shell (Kelley et al., 2005). In

contrast, the relatively high number of CR+ interneurons in the core may reflect their possible role in coordinating motor activity.

6.5.3 Secretagogin is expressed heterogeneously within the nucleus accumbens

This study demonstrated that the expression of Scgn in the core and shell identified a group of neurons that did not co-express any other classical interneuron markers. Importantly, Scgn expression was limited to these neurons, as it was not co-expressed with any other marker for striatal interneurons or projection neurons. The lack of PV+/Scgn+ or CR+/Scgn+ interneurons in the ventral striatum is of interest, as it suggests that the cellular organization of the ventral striatum differs significantly from that of the dorsal striatum. This is particularly interesting given the large numbers of anatomical and electrophysiological differences that are correlated with the expression of Scgn in both PV+ (see Chapter 4) and CR+ (see Chapter 5) interneuron populations of the dorsal striatum. Thus, the functional and anatomical division between the dorsal and the ventral striatum that has been established in the past (Bolam et al., 2000) is ultimately reflected in the molecular identity of some of the neurons that make up the cellular architecture of these two structures.

Despite these differences, it should be noted that Scgn+ "only" neurons were also found in the dorsal striatum, where they were preferentially distributed ventro-medially (see section 3.4.4). Scgn+ only interneurons may therefore constitute a novel class of interneuron that is found in both dorsal and ventral striatal domains; but is found at higher densities in the ventral striatum compared to the dorsal striatum. The finding that "Scgn-only" interneurons are present within the cyto-architecture of the ventral aspect of the dorsal striatum (see section 3.4.3) as well as the medial shell of the nucleus accumbens strengthens the hypothesis that this region of the dorsal striatum might be involved in the encoding of neural processes similar to those of the nucleus accumbens (particularly the medial shell). These similarities of intrinsic cyto-architecture are not surprising, given that these two regions receive overlapping and highly specialized input from the

orbitofrontal cortex and the entorhinal cortex (McGeorge & Faull, 1989; Totterdell & Meredith, 1997). In addition to its specific cortical input, the medial shell and the ventro-medial aspect of the dorsal striatum also receives dopaminergic input from a different set of VTA (ventral tegmental area)-dopaminergic neurons (distinguished from other VTA-dopaminergic neurons by their different inputs and output targets; Beier et al., 2015). This strengthens the hypothesis that these regions are responsible for the processing of different streams of information. As the projections targeting the ventral aspect of the dorsal striatum and the medial shell of the nucleus accumbens originates from similar cortical and midbrain areas, the information carried by their projections is likely related, meaning that the processing units within the target structures should also be similar. Thus, the finding that "Scgn+-only" neurons are biased towards the medial shell is likely to be important, as the same entorhinal cortical input that targets the ventral aspect of the dorsal striatum also targets the medial shell of the NAcc (Humphries & Prescott, 2010). This ultimately suggests that Scgn+ only interneurons may play an important role in the processing of reward-associated behaviors that occurs within the medial shell (Kelley 1999; Kelley et al., 2005).

6.5.4 Heterogeneous distribution of ChAT-expressing interneurons matches the uneven nature of dopamine-acetylcholine signaling in the nucleus accumbens

The stereological and quantitative description of ChAT+ interneuron distribution in the nucleus accumbens performed in this study has demonstrated that their density is greater in the shell compared to the core. This is in accordance with previous studies that have investigated ChAT immunoreactivity in the nucleus accumbens (Merredith et al., 1989). Within the shell, ChAT-expressing interneurons were biased towards the medial aspect of this structure; a region known to receive a dopaminergic input that is anatomically and physiologically different from the input that targets the rest of the ventral striatum (Chuma et al., 2014; Beier et al., 2015). Indeed, recent studies investigating the firing patterns of ChAT+ interneurons during the stimulation of dopaminergic fibers originating in the substantia nigra pars compacta (SNc) demonstrated that the typical burst-pause firing sequence of ChAT+ interneurons was present in the nucleus accumbens, but the strongest responses were noticeably restricted to the medial shell (Chuma et al., 2014).

Originally, these findings were interpreted as being the product of regional variation in dopamine-neuron glutamate co-transmission (Kiyatkin, 2002), but the firing of dopamine neurons throughout both the VTA and the SNc during classic conditioning tasks is remarkably similar, implying that the level of dopamine across all regions of striatum is likely to be the same (Kiyatkin, 2002). Importantly, synchronized activity of ChAT+ interneurons is known to influence the release of dopamine from dopaminergic terminals (Threlfell et al., 2012), meaning that the biased distribution of ChAT+ interneurons towards the medial shell presented here is valuable as it provides additional evidence to suggest that dopaminergic transmission within the medial shell is likely to be specialized. Ultimately, the increased density of ChAT+ interneurons in the shell over the core may contribute to differences in dopaminergic activity within the nucleus accumbens, which likely translates into the shell's function in reward prediction and associative learning behaviors.

6.5.5 CR+ and PV+ interneuron populations have contrasting distributional biases along the rostro-caudal axis of the ventral striatum

The stereological work presented here shows that PV+ interneurons are most prevalent in the rostral aspects of the NAcc shell. In contrast, CR+ interneurons were more prevalent in the caudal aspects of both the core and shell. This contrast of PV+ and CR+ interneuron densities expression along the rostro-caudal axis is the opposite of what has been reported in the dorsal striatum (see Section 4.4.1 and 4.5.1), where the rostral pole contains the highest density of CR-expressing interneurons and the caudal pole contains the highest density of PV-expressing interneurons. The findings presented in this report demonstrating that PV and CR-expressing interneurons are preferentially distributed in different regions of both the dorsal and ventral striatal domains may imply that they are unlikely to neither contact one another nor process the same types of information within the striatal microcircuit.

The finding that PV+ and CR+ interneurons are preferentially distributed in opposing ends of the rostro-caudal axis of the ventral striatum is of interest given that the rostral and caudal poles of the nucleus accumbens differ with respect to their chemical organization. Indeed, the caudal core is known to contain regions that stain poorly for calbindin, which could be considered the equivalent of the striosomes/patches of dorsal striatum (see section 1.5). In contrast, the rostral core contains discrete calbindin-rich regions and it has been hypothesized in the past that the patch/matrix relationship of the striatum appears to be inverted in the rostral nucleus accumbens (Berendse et al., 1992b). Despite the finding that the chemical signatures of the striosomes in this region of the nucleus accumbens is inverted, the identity and the origin (i.e. the anatomy) of inputs into the patch and matrix compartments in the rostral and caudal aspects of the NAcc are organized in a manner analogous to that of the dorsal striatum. The reversal of these chemical signatures may ultimately imply that these regions are intrinsically different from one another. As is a recurring theme of stereological work, the chemical and stereological differences between the rostral core and shell reported here are reflected in their cortical input. For example, the rostral nucleus accumbens (particularly the shell) is the only region of the ventral striatum known to receive input from the anterior cingulate cortex (Humphries & Prescott 2010). In contrast, the caudal pole of the nucleus accumbens (particularly the shell) receives exclusive inputs from the hippocampal CA1 as well as the entorhinal cortex (Kelley & Domesick, 1982; Friedman et al., 2002; Humphries & Prescott 2010). This suggests that the rostral pole of the NAcc shell may play a greater role in the processing of reward anticipation and motivational decision making while the caudal pole of the NAcc shell may preferentially encode learned behaviors associated with spatial navigation such as those required in the Morris water maze (Sargolini et al., 2003). Taken together with the results presented here, this ultimately suggests that PV+ interneurons may be preferentially involved in the processing of motivated behaviors towards cue-associated rewards while CR+ interneurons may compute inputs associated with spatial memory. This hypothesis is particularly enticing given that past reports have suggested that the localized distribution of PV

interneurons within the microcircuit provide neurochemical specializations within different anatomical compartments that may influence addiction (Todtenkopf et al., 2004).

CHAPTER 7.

GENERAL DISCUSSION

7.1 SUMMARY

The objective of this study was to investigate the extent of potential heterogeneity within the interneuron populations of the dorsal and ventral striatum. To achieve this, a combination of techniques was used to identify and quantify discrete cell populations. This included immunofluorescence detection of molecular markers, stereological cell counting, objective analyses of cell distributions and somatic diameters, and juxtacellular recording and labelling of single interneurons in vivo as well as the use of confocal microscopy to elucidate how specific sets of spiny projection neurons are targeted by the axons of identified interneurons. By using a combination of these techniques when appropriate, PV+/Scgn+, PV+/Scgn–, CR+/Scgn+/Lhx7–, CR+/Scgn–/Lhx7–, CR+/Scgn–/Lhx7+ and Scgn+only interneurons were distinguished from one another by differences in their molecular expression profiles, and these differences were subsequently correlated with differences in the structural and physiological features of distinct populations of striatal interneuron. Importantly, PV+/Scgn+ and CR+/Scgn+ interneurons were also found in both the caudate and the putamen of the Rhesus Macaque, where they were unevenly distributed along the rostro-caudal axis in a manner similar to what was found in the rat dorsal striatum. Additionally, the application of a robust, quantitative stereological method in the core and shell of the nucleus accumbens revealed that nearly all of the "classical" interneuron populations were unevenly distributed within the ventral striatum. Moreover, Scgn was not expressed by any PV+ or CR+ interneurons in the ventral striatum, but "Scgn-only" interneurons were present in both the core and the shell. Although the observations detailed in this thesis open up new vistas on the substrates for interneuron function and specialisation within the striatum, it is likely that further heterogeneity exists among these interneuron populations, such that the extent of their diversity may one day rival that of their neocortical and hippocampal counterparts (Klausberger & Somogyi, 2008).

7.1.1 A comprehensive look at the numbers and densities of interneurons in the dorsal and ventral striatum

By investigating the heterogeneity of interneurons in the dorsal and ventral striatum of the rat, this study has generated comprehensive sets of stereological data that define the total numbers and mean densities of "classical" and other interneuron populations within these structures. The results obtained from the stereological cell counts performed in this study are summarized in Figure 7.1 and 7.2. These summaries are of particular value in addressing the inconsistent methods and data of published stereological studies of interneurons in the dorsal striatum, and the lack of published quantitative characterizations of interneurons in the ventral striatum.

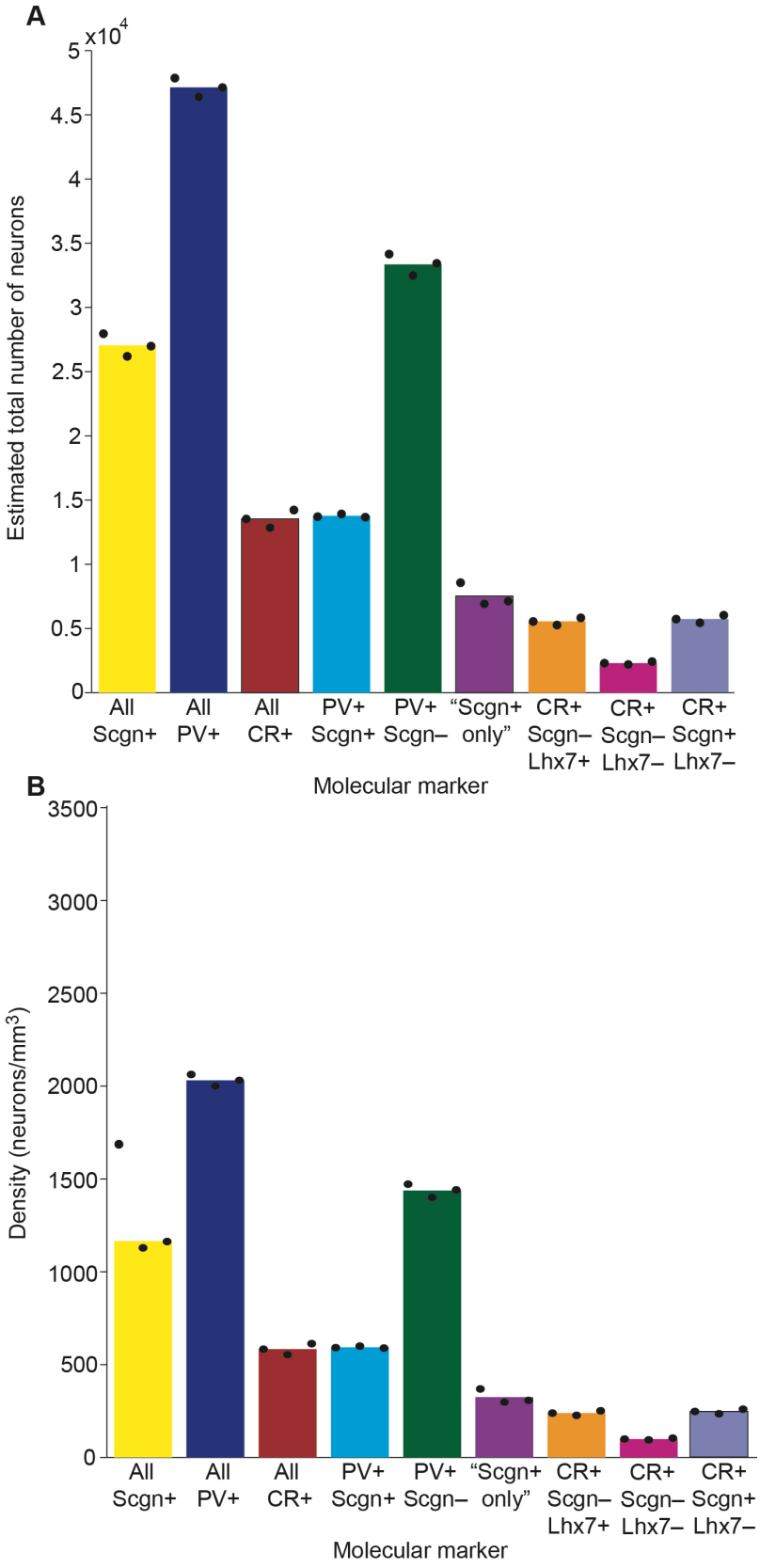


Figure 7.1 Estimated total numbers and mean densities of molecularly-distinct interneuron populations in the dorsal striatum of the rat. A) The estimated total numbers of different types of striatal interneuron. **B**) Mean densities of different types of striatal interneuron. The results from 3 rats are represented as 3 points around the mean.

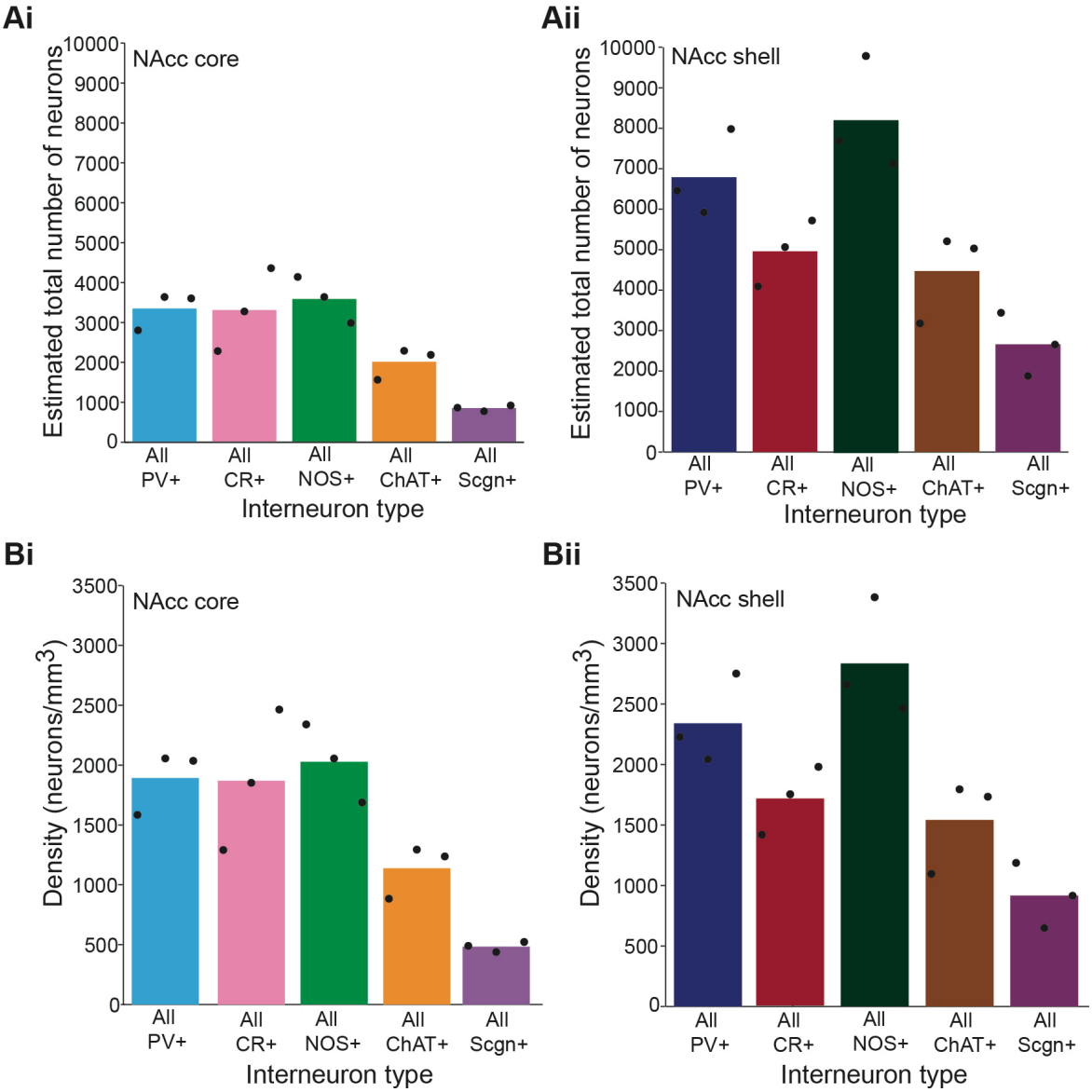


Figure 7.2 Estimated total number and mean density of molecularly distinct interneuron populations in the core and the shell of the rat ventral striatum. A) The estimated total number of neurons stereologically counted in the core (**Ai**) and the shell (**Aii**) of the rat ventral striatum. **B**) Mean density of different classes of striatal interneuron in the core (**Bi**) and shell (**Bii**) ventral striatum. The results from 3 rats are represented as 3 points around the mean.

In figure 7.1, it should be noted that the total number of all PV+ interneurons is high in comparison to previous studies, which have estimated their numbers at ~16, 000 (Luk & Sadikot, 2001). Importantly, this number was calculated from counts performed in a small sample of striatal planes centred around Bregma. As a result, it likely represents an underestimation as they did not include striatal planes from –1.6 mm to –3.2 mm behind Bregma, where the density of

PV+ interneurons is far greater than in in the rest of the striatum (see section 4.4.1). Additionally, the estimates for total cell number provided in this report are likely to be accurate as the number of CR+ neurons which were counted in the same sections and animals as those PV-expressing interneurons is similar to what was found by Rymar and colleagues (Rymar et al., 2004), who estimated their numbers to be approximately 13, 000. This is important given that Rymer et al. (2004) performed cell counts in 13 coronal sections, which were similar to those analyzed in this study, and their determined value for the total volume of the dorsal striatum was similar to what was calculated for this report (see section 2.2.1). Given these considerations, it is likely that PV-expressing interneurons make up 1.6% (0.4% PV+/Scgn+ and 1.2% PV+/Scgn–) of all neurons in the dorsal striatum of the rat, CR-expressing interneurons make up 0.5% (0.2% CR+/Scgn–/Lhx7+, 0.1% CR+/Scgn–/Lhx7– and 0.2% CR+/Scgn+/Lhx7–), and Scgn-expressing interneurons make up 0.9% (0.3% Scgn+-only, 0.4% PV+/Scgn+ and 0.2% CR+/Scgn+/Lhx7–). These percentages were calculated on the assumption that the total number of neurons in the dorsal striatum is 2.79 million (Oorschot, 1996); a value that was estimated on the assumption that the volume of the dorsal striatum is 19.9 +/- 2.7 mm3, which is similar to the volume calculated in this study (see section 2.2.1).

In the ventral striatum, the need for a comprehensive account of interneuron number and distribution in both the core and shell of the nucleus accumbens was evident given the lack of quantitative data regarding the "major" classes of interneuron. These results are summarized in figure 7.2, and represent the first quantitative estimation for the number of interneurons in the core and shell of the ventral striatum. In chapter 6, the density of these interneuron populations was compared to the density of those same populations in the dorsal striatum (as described in this report or in the literature), with the key finding being that most classes of interneuron had greater densities in the ventral striatum except for PV+ interneurons. These numbers, while not as informative as the distributional biases of each interneuron population reported in chapter 6 (see below), are likely to become important references for the large number of studies investigating

the effects of manipulating the dopaminergic projections (either chemically, optogenetically or through behavioural tasks) targeting the nucleus accumbens. This is particularly relevant given that drugs of abuse have been shown to significantly alter the density and number of interneurons in the dorsal striatum (Todtenkopf et al., 2004).

7.1.2 The value of distribution and regional density as compared to total cell number

The earliest characterization of interneurons in the striatum from a stereological point of view was focused on quantifying the total number of neurons identified by the expression of a detectable marker (Graveland and DiFiglia, 1985; Oorschot, 1996). This has resulted in many or most publications on striatal circuitry contending that projection neurons make up nearly 95% of all striatal interneurons while interneurons make up 3-5% (Kreitzer, 2012; Tepper et al., 2010; Silberberg & Bolam, 2015). This gives the impression that the relative number of neurons is of paramount importance for determining the influence of a particular population on the overall activity of the striatal microcircuit, but this does not adequately capture some important features of the functional organisation of different types of interneuron. This is exemplified by the cholinergic, ChAT-expressing interneurons of the striatum, which represent one of the smallest populations, but have been attributed with a variety of functional roles revolving primarily around the feedback control of the dopaminergic system (Threlfell et al., 2012). The total number of neurons is therefore just one of many indicators of the relative importance of that specific population for the overall activity of a given structure, but remains important when considering how it can be influenced in the context of disease. Indeed, studies investigating cocaine addiction have shown that repeated cocaine administration resulting in sensitization increased the number of PV-immunoreactive neurons throughout the ventral and dorsal striatum (Todtenkopf et al., 2004). Here, an increase in the total number of inhibitory interneurons can be interpreted as indicating an increase in the inhibition of striatal projection neurons, but this is not concrete, once again demonstrating the weakness of studies only providing the total number of interneurons. Indeed, the value of these studies is well contrasted by those recent studies that have characterized

the increased synaptic connectivity of PV+ interneurons unto indirect pathway SPNs in rodent models of Parkinson's disease (Gittis et al., 2011).

Given that the total number of neurons is not by itself directly related to that population's influence on the striatal circuit, the value of stereological studies in highlighting the functional composition of a given microcircuit can be obtained by analysing the distributional biases of different populations within a given structure. These regional biases in distribution were emphasized throughout this study for a variety of reasons, the most important of which was that the cortical input into the striatum is also regionally biased. Thus, if distributional biases of certain striatal interneurons were to be correlated with certain cortico-striatal inputs, it would provide important insights into the function of those populations within their respective micro-circuits. Additionally, the existence of distributional biases can also be used to distinguish between different populations of interneurons, as these biases likely reflect specific developmental programs, thereby providing evidence to suggest that those molecularly distinct neurons may belong to different neural populations. Despite the inherent value of understanding distributional biases within the circuitry of a given structure, it ultimately relies on the important assumption that a neuron's influence within its microcircuit occurs in close proximity to its soma. This may not always be the case, as computational models suggest that dendritic processors can exhibit both linear and nonlinear mechanisms, allowing them to perform basic computations of synaptic input, suggesting that the principal site of neural activity does not always coincide with the position of the neuron's soma (London & Hausser, 2005; Lazar & Slutskiy, 2014; Zheng et al., 2014). Thus, the value of quantitative stereology is best extracted when in-depth analyses of distributional biases are carried out, as indicated by the increasing number of recent such studies that focus particularly on regional density, rather than total cell number (Ma et al., 2014; Petryszyn et al., 2014).

7.2 TECHNICAL CONSIDERATIONS

Although great care was taken to control for the technical caveats associated with the immunohistochemical and electrophysiological techniques used in this study, certain aspects could not always be controlled, or simply remain an issue that will likely always be associated with studies of this nature. As such, these are discussed below in an attempt to identify where improvements to this work could have made, but also to demonstrate how future studies of this nature could be designed in order to better avoid such technical limitations.

7.2.1 Secretagogin-expressing neurons in the rat and the mouse: a weakness of chemically based methods of neural identification?

One of the key findings reported in this study was that the density of secretagogin-expressing interneurons in the dorsal striatum of mouse was tiny in comparison to that observed in rat (and Rhesus Macaque). Scgn was also found to be expressed by some, but not all, PV+ and CR+ interneurons in both rats and mice (albeit in different proportions), and some neurons were only identified thanks to their expression of Scgn (the so-called "Scgn-only" neuron). The existence of relatively high numbers of Scgn+ interneurons in the Rhesus Macaque caudate/putamen, in addition to its expression by some, but not all CR+ and PV+ interneurons in the Rhesus Macaque seemed to indicate that it was indeed a powerful marker for heterogeneity amongst certain interneuron populations of the striatum. This conclusion was ultimately strengthened by the finding that certain aspects of the specialized distribution of those Scgn+ populations of the rat (PV+/Scgn+ and CR+/Scgn+) were also observed in the Rhesus Macaque. Given the number of differences that were illuminated in this study regarding how structural and functional properties of certain interneurons correlated with the (co-expression of Scgn in the rat, the low numbers of Scgn-expressing interneurons (thus, of PV+/Scgn+ neurons) in the mouse could be interpreted as indicating that this functional diversity (cell type) is lacking in the mouse. Although this might indeed be the case, this species difference highlights one of the inherent weaknesses of using a single molecular marker to identify a group of neurons. More specifically, molecular markers are not always sufficient to unambiguously define 'cell type' (see section 7.3

below), and in any case, the levels of expression of a marker might not be fixed or otherwise stable in postnatal life. For example, in Huntington's disease, the earliest reports of CR+ interneuron numbers in the human striatum seemed to suggest that the number of large-sized CR+/ChAT+ interneurons was greatly reduced compared to healthy post-mortem brains (Cicchetti & Parent., 1996). However, recent studies using the neurokinin-1 receptor as a marker of these CR+/ChAT+ interneurons have found that it is not the numbers of these interneurons that is disrupted in Huntington's disease but rather, it is their expression of CR and ChAT that is decreased (Massouh et al., 2008). Thus, in theory, the mouse striatum could contain a group of interneurons that do not express Scgn but yet still have other functional properties in common with the Scgn+ cell types that populate the rat and Rhesus Macaque striatum.

Although this is one potential explanation for the significantly reduced levels of Scgn-expression in the mouse striatum, it is unlikely given that Scgn expression was detected in the mouse striatum. As such, most of the Scgn+ cell populations identified in the rat probably exist in the mouse, but they are simply minor populations of interneurons within the mouse striatum. Importantly, there is a precedent to suggest that neuronal expression of Scgn can vary dramatically in the mouse and rat: nearly 7% of neurons in the dorsal root ganglion of mice express secretagogin, whereas rat dorsal root ganglion neurons do not express Scgn (Shi et al., 2012). Whether or not this disparity has functional implications with respect to circuit activity and the processing of information in both species is unclear. It does however raise an important issue regarding the need for multiple methods by which to identify neural populations within the central nervous system given the dynamic nature of protein expression to meet the demands of the microcircuit.

This thesis study was focussed on analyses of marker expression in neurons of the adult striatum. A technical short coming of this approach is that it cannot account for the possibility that the expression of Scgn is widespread at an early developmental stage in mouse but is then downregulated in adulthood. More specifically, and given the established role of Scgn in the development and migration of neural populations in the forebrain of the mouse (Mulder et al.,

2009), there is a possibility that a host of fully-matured mouse striatal neurons once expressed Scgn. This could be a likely explanation for the relatively low levels of Scgn-expression in the mouse striatum, given that the downregulation of markers required for development of striatal interneurons (such as Nkx2-1) is known to occur in the adult (Marin et al., 2000). Importantly, this downregulation is not consistent across an entire group of interneurons (eg. Not all CR+ interneurons express Nkx2-1 in the adult striatum of mice), as some interneurons down regulate the expression of these markers while others (presumably belonging to the same class of interneuron) do not (Marin et al., 2000). Thus, those Scgn-expressing neurons detected in the adult mouse may represent a small group that did not downregulate its expression after completing their development, in turn implying that a larger group of Scgn+ interneurons may exist in the embryonic mouse striatum. The detection of these interneurons is likely to be possible through the use of EGFP-Scgn+ mouse lines, an avenue of research that is further discussed in section 7.4. If Scgn+ interneurons are numerous before birth, it still raises the issue that those neurons that have downregulated Scgn are no longer using its calcium sensor function (see section 1.6). Thus, although this explanation may account for the lack of Scgn-expression in the dorsal striatum of the mouse, it ultimately does not explain why the adult mouse striatum does not generate extensive interneuron diversity through selective expression of Scgn in the same manner as the rat and Rhesus Macaque striatum.

7.2.2 Calibrated immunofluorescence signals: the key to replacing binary based stereological investigations?

In this study, a great deal of heterogeneity was demonstrated within "classical" populations of striatal interneuron in both rodents and Rhesus Macaques. For example, distinct firing patterns, distribution and anatomical connectivity within the striatum could be used to distinguish two distinct sets of PV+ interneurons in the rat. Calretinin-expressing interneurons could also be parsed according to morphological features and distributions within the dorsal striatum. In all cases, this heterogeneity was correlated with (partly defined by) the selective expression of molecular markers (i.e. secretagogin, Lhx7) that were detected using indirect immunofluorescence. In essence, expression of these markers was defined using a discontinuous

or discrete (binary) scoring system i.e. detectable expression (+) or no detectable expression (–). Although this scoring system is time efficient, and is widely used in the field, it does not capture the potential continuum of protein expression levels that could arise from the functional requirements of a given cell or perhaps an entire population of cells. This is particularly relevant for this study, where the expression of CR and PV, as defined with a binary scoring system, was shown to identify multiple cell types (eg. PV+/Scgn+ and PV+/Scgn– interneurons), rather than identifying single, functionally distinct populations of neurons. This is because it is possible that the levels of PV or CR expression within those subpopulations might have been different, and so the use of multiple markers may not have been necessary. Indeed, the levels of CR immunoreactivity detected in small "type 3" CR-expressing interneurons (CR+/Scgn+/SP8+) were noticeably higher than those detected in type 2 (CR+/Scgn–/Lhx7–) and type 1 (CR+/Scgn–/Lhx7+) interneurons. This indicates that CR expression is upregulated in the population of type 3 interneurons. Given that calretinin is a CBP that behaves as both a calcium sensor and a calcium chelator (Winsky and Kuznicki, 1995; Schwaller et al., 1997; Marilley and Schwaller, 2000), this finding could potentially give insights into the functional output of this cell population. The idea that differences in the levels of CBPs expression exist (and are functionally relevant) has been shown in the past (Donato et al., 2013), and its functional relevance is best studied using mouse models in which a particular protein of interest is deleted ('knocked out') or over expressed (D'Orlando et al., 2001; Pecze et al., 2013). For example, single PV+ basket cells in the cerebellum express PV at a concentration of ~ 500μM (Schwaller et al., 2002; Eggermann and Jonas, 2012), whereas PV+ basket cells of the hippocampus express ~10 μM PV (Muller et al., 2005). In PV-null mice, pairs of IPSCs evoked in target neurons by cerebellar basket cells exhibit an abnormal facilitation, such that the ratio of the second and first IPSCs ($IPSC_2/IPSC_1$) increases from ~1.0 to ~1.5 (Caillard et al., 2000; Eggermann and Jonas, 2012). This effect is believed to be caused by the increase in residual Ca^{2+} concentration that occurs at presynaptic varicosities in the absence of PV, but is entirely absent from basket cells in the hippocampus (Eggermann and Jonas, 2012). Thus, when identifying neurons on the basis of protein expression, it might prove insightful to quantify the degree of this expression on a continuous scale (even if it is relative), as

this has been shown to differ among groups of neurons that seemingly perform the same function in their respective structures.

In order to use the level of protein expression as a further determinant of cell identity in the future, calibration of a continuous scale of immunoreactvity is required. This calibration would ultimately require a single standard to be adopted by many laboratories, and although this is difficult, it has been established in other fields. For example, the quantifiable detection of HER-2 overexpression in breast cancer cells (Couturier et al., 2000) is important for the identification of potential carcinomas. In this field, the calibration of immunohistochemistry was successfully standardized across all laboratories performing these measurements (Vincent-Saloon et al., 2002) to produce a relative scale that anyone could use. A similar system should ideally be implemented in studies of neurons in the central nervous system, as this would allow for the detection of potentially functional heterogeneity that exist within pre-existing populations. In the case of CBPs such as PV or CR, which are known to influence the firing pattern of the cells in which they are expressed (Caillard et al., 2000; Bearzatto et al., 2006), the use of a calibrated 'sliding scale' of immunoreactvity could in theory provide readouts that are correlated with previously described electrophysiological heterogeneity within those populations (Chapter 5 and Sharott et al., 2012). Clearly, the calibration of continuum of immunoreactvity signals has the potential for refining the criteria by which neuronal types are defined within the central nervous system.

The use of calibrated readouts of immunoreactvity, or any method that allows for the quantification of relative protein concentrations within a cell is unfortunately not free from flaws. Although the results demonstrated by Jonas and colleagues (Schwaller et al., 2002) suggest that the total concentration of a given protein within a cell can be indicative of its relative importance for the overall function of a neuron, this is unlikely to be the case in a consistent fashion. Indeed, calcium sensors such as CR, PV and Scgn carry out their primary functions within $Ca2^{+}$ microdomains and nanodomains, where their concentration is likely locally regulated to meet the cell's physiological requirements (Reddy et al., 2014). Moreover, it is possible that, during sustained periods of a particular network activity or animal behaviour (Donato et al., 2013), the

neurons of a given microcircuit may increase or decrease their expression of multiple proteins, and so an assumption has to be made regarding the "resting" levels of protein expression within a given neural population. Whether or not the total concentration of CBPs within a neuron is indicative of its importance for the cell's overall function is therefore unclear, and this should always be considered when attempts are made to understand function from different levels of protein expression. Ultimately, although the use of calibration to define the degree of protein expression represents an important step towards further elucidating potential heterogeneity within existing neuronal populations, it should always be noted that expression levels are not always indicative of that protein's relevance to a neuron's functional output.

7.2.3 The variability associated with the axonal labelling of neurons using the juxtacelluluar technique

The juxtacellular recording and labelling technique is a powerful tool that allows for direct correlations between the *in vivo* electrophysiological, molecular and structural properties of single neurons. In this study, the labelling of PV+/Scgn– and PV+/Scgn+ interneurons with neurobiotin was used to investigate and compare their respective axonal connectivity. One potential issue associated with this method concerns the extent to which individual neurons can be 'filled' by the neurobiotion, which will directly influence the degree to which the entire axonal arborisation of a recorded neuron can be visualized. Currently, there is an assumption that the extent of labelling is directly proportional to the amount of time a given neuron was subjected to the current pulses that deliver the tracer, although this is highly unreliable after the first minute of labelling. As a result, observations regarding the axonal arborisation of individual PV+ interneurons from either class were not possible given the variability of their labelling. Moreover, as the axons of PV+/Scgn+ interneurons were on average labelled to a greater extent than those of PV+/Scgn– interneurons, the number of axonal boutons counted for PV+/Scgn+ neurons was greater. This issue was ultimately resolved by normalising bouton counts and the appositions they made with spiny projection neurons. It is however still possible that the differences in the striatal targets of PV+/Scgn+ and PV+/Scgn– neurons reported in this study may reflect the fact that the distal parts of the axons of PV+/Scgn+ interneurons were often labelled while those of PV+Scgn–

interneurons were not. Because it is not yet possible to rule out the possibility that the proximal and distal axons of these neurons innervate different sets of targets, these caveats should be kept in mind when interpreting the data presented here.

7.3 THEORETICAL CONSIDERATIONS

7.3.1 The definition of a "novel cell type": a consideration of neural development and maturation

A recurring theme in this thesis is the definition of cellular heterogeneity within the striatal microcircuit. Given the importance of this microcircuit in the processing of learnt behaviours and habit formation, an in-depth understanding of its component parts (i.e. the cells) is necessary in order to fully appreciate the extent of the functional roles it plays. While a great deal of heterogeneity was found to exist within certain pre-existing or classical striatal interneurons populations, some other interneurons were identified for the first time due to their unique molecular expression profiles. In the case of striatal PV+ interneurons, 2 'subtypes' were identified according to their molecular, electrophysiological, topographical and anatomical differences, while 3 'subtypes' of CR+ interneurons were identified on the basis of their distinct topographical, morphological and molecular characteristics. Finally, populations of "Scgn-only" neurons in the nucleus accumbens and dorsal striatum were identified by their specialised molecular profiles. The identification of these neurons raises an important issue regarding the requirements for the successful characterization of a "novel cell type" or population. If one considers the differences that arise when the connectivity, genetic back ground (i.e. which genes a neuron chooses to express, and the levels of that expression), physiological properties and molecular profiles that exist within the central nervous system are compared, it is conceivable that novel cell types could be endlessly identified on the basis that they differ from their neighbours in just one of these rather general categories. In a system where the classification of cells allows for a fundamental understanding of how neural circuits function, the continued identification of novel cell types on the basis of single physiological or anatomical differences is simply untenable. This inherent complexity can be partially resolved by considering how neurons are generated within the embryonic brain, as well as how they develop through their interactions with other neurons within their respective microcircuit. These concepts are considered briefly below in the context of the cell types that have been described in this study.

One of the landmark discoveries for cortical interneuron development in the central nervous system was the finding that these interneurons are generated in subcortical proliferative zones (Wichterle et al., 2001). This discovery has led to the hypothesis that specific classes of interneurons arise from specific regions of the embryonic brain (eg. The ganglionic eminences) and then migrate to their target structures. This is best exemplified by the PV-expressing "fast spiking" basket cells that exist within the striatum, the hippocampus, the neocortex and the amygdala (Kawaguchi 1993; Kepecs & Fischell, 2014). If one uses a strictly developmental definition of cell type (Kepecs & Fischell, 2014) one could argue that these interneurons likely belong to a different class of interneuron than those that originate from different regions of the embryonic brain. Developmental origin therefore represents an important criteria in the definition of a discrete neural population. For example, neurogliaform cells of the cortex are derived from the caudal ganglionic eminence, while hippocampal neurogliaform cells are derived from the medial ganglionic eminence (Tricoire et al., 2010). In the striatum, the majority of striatal interneurons are believed to be derived from the Nkx2-1 expressing cell lineages within the medial ganglionic eminence (Marin, 2002; Nobrega-Pereira et al., 2008; Villar-Cervino et al., 2015), while calretinin-expressing interneurons are thought to be derived from the caudal ganglionic eminence (Kepecs & Fishell 2014). In this study, the finding that that the small-sized "type 3" CR+/Scgn+/Lhx7– interneurons co-express SP8 suggests that their developmental origin differs from that of other striatal interneurons. Instead, it is likely that they belong to the same family as the newly-generated CR+ neurons that migrate from the subventricular zone to the olfactory bulb (Wei et al., 2013). The importance of calretinin expression for the generation and maintenance of these cell populations is evidenced by their absence in CR-null mice (Wei et al., 2013). Thus, it is likely that the CR+/Scgn+/Lhx7– population identified in this study represents a novel neural population, while it remains unclear whether the two other CR+ populations presented here are truly distinct from one another. Although type 1 and type 2 CR+ interneurons can be distinguished by their selective expression of Lhx7 (a finding that likely exists in the primate given the existence of ChAT+/CR+ interneurons), and somewhat parsed according to the somatodendritic structure, some would argue that this alone is insufficient evidence that they

belong to distinct classes of striatal interneuron, as the inputs and outputs of these 2 CR+ interneuron types have not been elucidated (Klausberger & Somogyi 2008). However, given the limited utility of current CR-Cre mouse lines (which could be bred with GFP reporter mice in order to investigate the structure and developmental origins of CR+ interneurons; see section 7.4), it is unlikely that further investigation into the differences between striatal CR+ interneurons can be elucidated in the near future. Thus, given the tools currently available, the results presented here provide new insights that help define CR-expression in the dorsal striatum of both rodents and Rhesus Macaques.

If many cortical and striatal interneurons develop from the same MGE-derived progenitors (Mayer et al., 2015), then further diversity is generated from both excitatory and inhibitory cues that migrating neurons receive as they mature (Cancedda et al., 2007; Bortone & Polleux, 2009). Recent evidence seems to suggest that these cues, which can be chemical (Mckinsey et al., 2013) or electrophysiological (De Marco Garcia et al., 2011), are region specific, a hypothesis supported by the finding that the concentration of regulatory markers varies across the different axes of a given structure (West & Greenberg, 2011). The importance of this regional specification for interneuron development and differentiation is one of the major reasons that the distribution of identified interneuron subtypes was so heavily emphasized in this study, as it may reflect differences in their development, which ultimately suggests that they may indeed represent novel populations of striatal interneuron. For this reason, the migration of neurons is the second criteria that can be used to distinguish different cell types from one another, as different classes of neuron are likely to respond to those chemical gradients in a specialized manner.

One particularly important signal for the differential development of migrating populations is calcium influx through voltage-gated calcium channels (West & Greenberg 2011). This suggests that calcium binding proteins, such as secretagogin, that are expressed during these critical periods (Mulder et al., 2009; 2010) are key factors in the development of different interneuron classes. Whether or not these cues are responsible for the maturation of previously specified neurons or the differentiation of non-specific progenitors remains unclear, although the

latter is more likely given the finding that that unspecified MGE progenitors are capable of functionally integrating into abnormally functioning striatal circuits such as those produced by dopaminergic lesion (Martinez-Cerdone et al., 2010). In this study, 2 classes of PV+ interneurons were distinguished by the selective expression of Scgn, which was correlated with differences in regional density, electrophysiological properties and anatomical connectivity within the striatum. Importantly, these 2 molecularly distinct groups of interneurons are unlikely to originate from different embryonic progenitors (Marin et al., 2000), and so developmental origins cannot be used to distinguish them as 2 separate classes of interneuron. However, given the extensive role of Scgn in the migration and development of many forebrain populations (Mulder et al., 2009), it is likely that the expression of Scgn by a subset of PV+ interneurons allows them to become more or less receptive to the variety of calcium based cues that they are subjected to during their migration (i.e. the second criteria). This may ultimately explain why PV+/Scgn+ interneurons are so heavily biased in their distribution within the striatum.

Electrophysiologically, although both populations were fast-spiking neurons that likely perform the same function within their respective microcircuits (i.e. the powerful inhibition of target projection neurons), their firing patterns in relation to cortical oscillatory activity differed significantly. Importantly, PV+/Scgn+ and PV+/Scgn– interneurons were distinguished by their preferential targeting of SPNs, indicating that during their maturation in the striatum, their integration into the microcircuit was significantly different. This therefore represents a third criterion by which to distinguish different classes of neurons, and has been used in the past to distinguish between different classes of PV+ neurons in the hippocampus (Klausberger & Somogyi 2008). In conclusion, when future investigators attempt to broadly define novel cell types, one potential avenue is to examine how the distinguishing features of their cell classes are reflected in the development of the microcircuit. In doing so, rather than asking “is this a novel neural population?”, investigators can directly examine whether the nervous system itself recognizes these cells as belonging to a distinct group of neurons.

7.4 FUTURE STUDIES

The work presented in this thesis has provided a great deal of evidence to suggest that a great deal molecular, anatomical and physiological heterogeneity likely exists in the dorsal (and ventral) striatum of the rat (and the Rhesus Macaque). However, given certain limitations associated with the methods used in this study (see section 7.2), further heterogeneity amongst striatal interneurons could be investigated using novel approaches as they are generated in the future. These techniques, as well as their utility in demonstrating further interneuron heterogeneity in the striatum, are discussed below.

7.4.1 The use of genetic mouse models to investigate further heterogeneity within Scgn-expressing striatal interneuron populations

One of the major hurdles associated with the study of Scgn expression in the adult rodent neostriatum is the relatively small density of Scgn+ interneurons (see section 3.4.3). This has ultimately meant that EGFP-mouse lines (which provide researchers with an important tool by which the composition and the function of neuronal microcircuits can be studied) could not be used in this study. In addition to this problem, it should also be noted that a Scgn-Cre mouse line has not yet been generated, but given the popularity of these models, it is likely that one will be produced in the near future. The generation of this model would likely allow for in-depth investigations into the nature of Scgn-expression in the mouse neostriatum. For example, a genetic "fate mapping approach" could be used in which a Scgn-Cre mouse is bred with a floxed GFP reporter mouse in order to ensure that the long term expression of GFP is triggered in any neuron that has ever expressed Scgn (even during development. This ultimately means that if some Scgn+ neurons in the mouse downregulate Scgn expression post-maturation, they would still express GFP, allowing for a unique perspective regarding the expression of Scgn in the neostriatum of the mouse. Moreover, the GFP-guided labelling of Scgn+ interneurons would allow for the in-vitro characterization of the intrinsic physiological properties of some of the relatively minor Scgn+ interneuron populations within the dorsal striatum of the mouse (see section 7.4.2 for details).

Studies of this nature have been performed in EGFP-TH+ mice (Ibanez-Sandoval et al., 2010; Unal et al., 2015) and in EGFP-5HT3a mice (Munoz-Manchado et al., 2014) to identify and subsequently characterize the electrophysiological properties of striatal TH-expressing interneurons and 5HT3a-expressing interneurons in the dorsal striatum. Similarly to what has been done for Scgn-expression in the rat, the identification of 5HT3a-expression (which is only possible thanks to this mouse model) in particular has revealed further heterogeneity among existing populations of striatal interneurons as some 5HT3a+ interneurons expressed PV (Munoz-Manchado et al., 2014). Moreover, the in vitro characterization of the intrinsic firing (and structural) properties of TH+ interneurons made possible thanks to the EGFP –TH+ mouse line has suggested that they may encompass several classes of interneuron (Ibanez-Sandoval et al., 2010). These examples therefore provide an important precedent to suggest that the application of these models for studies can be used as an additional tool by which to demonstrate further heterogeneity within striatal interneuron populations.

7.4.2 The use of genetic rat models to investigate heterogeneity amongst striatal PV-expressing interneurons

Given the prevalence of Scgn-expression in the rat striatum compared to the mouse, it is likely that a great deal of information regarding the activity of Scgn+ interneurons in the striatum could be elucidated from studies performing in-vivo and in-vitro recordings in Scgn-Cre rats. Although this model is unlikely to be developed in the near future (indeed, a Scgn-Cre mouse has yet to be developed), the recent successful development of TH-Cre and ChAT-Cre rat lines (Witten et al., 2011) suggests that a PV-Cre rat line may be developed in the near future. As the results from this study suggest that nearly all PV+ interneurons in the caudal pole of the striatum belong to the PV+/Scgn+ population, it is possible that PV-Cre rat lines (injected with a viral vector expressing “floxed” opsins) could be used to isolate and optogenetically stimulate channel rhodopsin-expressing PV+/Scgn+ cells in the caudal striatum, while simultaneously recording from neighbouring spiny projection neurons. This simultaneous optogenetic stimulation and recording can be performed either in vivo (Brown et al., 2012) or in vitro (Threlfall et al., 2012; Szydlowski et al., 2013). Cre-expressing lines have also been recently used to determine the

"whole-brain input connectome" of a genetically defined cell type (Wall et al., 2013; Guo et al., 2015), meaning that it would be possible to use a PV-Cre line to map the inputs of those PV+/Scgn+ interneurons in the caudal pole of the dorsal striatum. Unfortunately, it is unlikely that one could effectively isolate PV+/Scgn– interneurons in a similar manner, as this study demonstrates that they are not exclusively present in one particular region of the striatum. However, the use of the topographical information presented here to optogenetically manipulate PV+/Scgn+ interneurons may provide additional evidence for target selectivity within a particular class of striatal PV+ interneuron.

7.4.3 Correlating differences in molecular expression profiles with the morphological characteristics of PV+ interneurons

The first descriptions of striatal PV+ neurons characterized two different types based on the overall size and density of their dendritic arborisation (Kawaguchi, 1993).The idea that these differences may correlate with molecular and physiological heterogeneity within the PV-expressing striatal population was one of the underlying principles repeatedly mentioned in this report. Whether or not the morphological disparities first described in 1993 correlate with the molecular dichotomy described in this report (i.e. PV+/Scgn+ or PV+/Scgn– interneurons) remains unclear. However, the anatomical reconstruction (Koos & Tepper, 1999; Tukker et al., 2013; Katona et al., 2014) of juxtacellularly labelled PV+/Scgn+ and PV+/Scgn– neurons would allow for an investigation of the dendritic arborisation of these two classes of interneuron in order to determine whether they correspond to Kawaguchi's original description nearly 2 decades ago. Given the variability associated with the labelling of neurons using neurobiotin, it is unlikely that the axonal arborisation of these interneurons could be fully reconstructed. Ultimately, a study of this nature would likely further highlight the potential for further heterogeneity among striatal PV+ interneurons, although given the small number of neurons often reconstructed in studies of this nature (Kawaguchi 1993; Koos & Tepper, 1999), any differences may ultimately reflect a continuum that cannot be fully explored when 3 or 4 interneurons are studied.

7.4.4 Electron microscopy as a powerful tool for investigating synaptic connectivity within the striatal microcircuit

One of the key findings reported in this study demonstrated that PV+Scgn+ neurons preferentially target SPNS of the direct pathway, whereas PV+/Scgn– neurons preferentially target contact SPNs of the indirect pathway. The presence of this dichotomy within the striatum is of value, as it implies that different subsets of inhibitory fast-spiking interneurons can act as substrates through which the preferential inhibition of one group of SPNs can be rapidly and powerfully achieved. Importantly, this study was unable to show that axonal boutons contacting the cell bodies of SPNs were forming functional synapses. Although pre- and postsynaptic markers of GABAergic synapses, such as VGAT and gephyrin (Gittis et al., 2011), have been used in the past to provide evidence for the presence of these synapses, electron microscopy remains the "gold standard". Thus, the use of electron microscopy to analyse the synapses formed between juxtacellularly labelled PV+/Scgn+ or PV+/Scgn– neurons and different types of SPNs would be a good follow-up study to provide more robust evidence of the targetsof these two subtypes of interneuron.

7.4.5 In vivo recordings of striatal interneurons in the ventral striatum of the rat

In this study, the number and distribution of the "classical types" of interneurons in the core and shell of the ventral striatum was extensively quantified. Given the structural differences between the dorsal striatum and the core and the shell of the ventral striatum, in addition to the disparate distributions of interneurons within the core and the shell described in this report, the electrophysiological characteristics of these same interneurons may also differ from those reported in the dorsal striatum (Sharott et al., 2012). A study of the in vivo physiological characteristics of these interneurons is likely to be relevant given the increasing number of studies performing tetrode recordings in the ventral striatum (Lansink et al., 2007; Lansink et al., 2010). As these studies allow for the simultaneous recording of multiple units but cannot identify those neurons from which they are recording, their increasing popularity highlights the need for studies recording and identifying individual units within the nucleus accumbens. As this can be achieved using the juxtacellular recording and labelling technique described in this report, a follow up

study investigating the firing patterns of individual projection neurons and interneurons in both the core and the shell of the ventral striatum will provide valuable information for future studies looking to perform tetrode recordings in the nucleus accumbens. When paired with the distributional data provided in this report, the results from such a study will provide researchers with a much-needed understanding of both the composition and intrinsic activity dynamics of the circuits that exist within the ventral striatum.

7.4.6 Profiling the genetic, electrophysiological and morphological features of single neurons using the Patch-seq technique

Throughout this dissertation, a great deal of work was done in order to distinguish populations of striatal interneurons based on their molecular, morphological and electrophysiological features. Although this multidisciplinary approach has proven to be successful in the past (Sharott et al., 2012; Viney et al., 2013), it is highly inefficient, and usually identifies groups of neurons based on the expression of one or two molecular markers while ignoring the remainder of that particular group's molecular profile. By utilizing these approaches in a complimentary fashion over many years, the neural components of certain microcircuits (cortical and hippocampal in particular) have been elucidated (Klausberger and Somogyi, 2008). Recently, this entire process has been revolutionized thanks to the "patch-seq" technique, in which a neuron's electrophysiological properties are determined through patch clamping, followed by the aspiration of its cytoplasmic contents through the patch-clamp pipette. These contents can be subsequently prepared for RNA-sequencing (Zeisel et al., 2015; Fuzik et al., 2016), allowing investigators to determine all genes currently expressed by the recorded neuron.

Using this technique, several groups have begun investigating the relationships between the electrophysiological properties and molecular expression profiles of different groups of cortical neurons. This is done by clustering and through dimensionality-reduction analysis using the most variable genes amplified in the sample (Fuzik et al., 2016). In one study, Cadwell and colleagues were able to predict (with an accuracy greater than 85%) the electrophysiological (eg. response to current injection, amplitude of individual spikes) and morphological (eg. axonal and

dendritic arborisation) properties of 2 groups of cortical interneurons thanks to the cluster analysis of their genetic profiles (Cadwell et al., 2016). Clearly, this technique allows for a powerful characterization of single neurons, and will ultimately allow for a precise definition of a particular neuronal population, as it combines molecular, morphological and physiological features of each neuron.

7.5 GENERAL CONCLUSIONS

In conclusion, the studies encompassed by this thesis have shown that the discrete expression of functional molecular markers such as calcium binding proteins and transcription factors can be correlated with differences in the electrophysiological, structural and topographical of striatal units originally believed to belong to a single homogenous population. PV+ interneurons were divided into at least 2 types of interneuron identified by their differential expression of Scgn, their distributional biases within the striatum (indicative of differences in their development and their corticostriatal input), their electrophysiological properties as well as their proportional targeting of the different types of striatal projection neuron. CR+ interneurons were divided into 3 potential types of neurons on the basis of their distinct structural features, their expression of Scgn (and SP8) and Lhx7 as well as their distributional biases within the dorsal striatum. By itself, Scgn identified a group of neurons that did not express any of the classical markers for striatal interneuron. This population was biased towards the ventro-medial aspects of the dorsal striatum, and was also found in the nucleus accumbens, whose constituent populations did not express Scgn to a significant degree.

In the nucleus accumbens, stereological cell counting and topographical analysis revealed large biases in the distribution of nearly all of the major classes of interneurons along one or multiple axes of the core or the shell. What is perhaps most interesting was that in some areas of the core and shell, certain classes of interneuron were almost entirely absent, while possessing relatively high regional densities in others (particularly the medial shell). Unlike the dorsal striatum, where the Scgn-expressing subclasses of interneuron were heavily biased but the classical populations were widely spread throughout the stricture (except perhaps CR-expressing interneurons), the ventral striatum is unique in that its supposed major populations of interneuron were heavily biased towards certain poles of the structure. This may indicate that the nucleus accumbens as a whole possesses an additional number of yet to be identified cell populations, or that the processing of inputs within the ventral striatum is carried out in a regionally specific manner.

Finally, the observation that the overall topographical distribution of the novel interneuron populations identified in this study are well conserved from the rat to the Rhesus Macaque are of potential interest, as they suggest that not only are cell types conserved throughout multiple phylogenies, but the overall composition of those microcircuits receiving similar excitatory inputs is also well conserved. Taken together, the data detailed in the studies performed in this report have provided important insights into the electrophysiological, neurochemical, structural and topographical properties that distinguish a large number of novel interneuron populations within the striatum.

BIBLIOGRAPHY

1. Abdi, A. *et al*. Prototypic and arkypallidal neurons in the dopamine-intact external globus pallidus. *J. Neurosci.* **35**, 6667-6688 (2015).

2. Albin, R. L., Young, A. B. & Penney, J. B. The functional anatomy of basal ganglia disorders. *Trends Neurosci.* **12**, 366-375 (1989).

3. Alexander, G. E., Crutcher, M. D. & DeLong, M. R. Basal ganglia-thalamocortical circuits: parallel substrates for motor, oculomotor, 'prefrontal' and 'limbic' functions. *Prog. Brain Res.* **85**, 119-146 (1990).

4. Alexander, G. E., DeLong, M. R. & Strick, P. L. Parallel organization of functionally segregated circuits linking basal ganglia and cortex. *Annu. Rev. Neurosci.* **VOL. 9**, 357-381 (1986).

5. Alifragis, P., Liapi, A. & Parnavelas, J. G. Lhx6 regulates the migration of cortical interneurons from the ventral telencephalon but does not specify their GABA phenotype. *J. Neurosci.* **24**, 5643-5648 (2004).

6. Alpár, A., Attems, J., Mulder, J., Hökfelt, T. & Harkany, T. The renaissance of Ca 2+-binding proteins in the nervous system: Secretagogin takes center stage. *Cell. Signal.* **24**, 378-387 (2012).

7. Ambudkar, I. S., Ong, H. L. & Singh, B. B. Molecular and functional determinants of Ca2+ signaling microdomains. *Sign. Transduction: Pathways, Mechanisms and Dis.*, 237-253 (2010).

8. Amiez, C. & Petrides, M. Selective involvement of the mid-dorsolateral prefrontal cortex in the coding of the serial order of visual stimuli in working memory. *Proc. Natl. Acad. Sci. U. S. A.* **104**, 13786-13791 (2007).

9. Andressen, C., Blümcke, I. & Celio, M. R. Calcium-binding proteins: selective markers of nerve cells. *Cell Tissue Res.* **271**, 181-208 (1993).

10. Aoki, C. & Pickel, V. M. Neuropeptide Y-containing neurons in the rat striatum: ultrastructure and cellular relations with tyrosine hydroxylase-containing terminals and with astrocytes. *Brain Res.* **459**, 205-225 (1988).

11. Aosaki, T., Kiuchi, K. & Kawaguchi, Y. Dopamine D1-like receptor activation excites rat striatal large aspiny neurons in vitro. *J. Neurosci.* **18**, 5180-5190 (1998).

12. Aosaki, T. *et al*. Responses of tonically active neurons in the primate's striatum undergo systematic changes during behavioral sensorimotor conditioning. *J. Neurosci.* **14**, 3969-3984 (1994).

13. Apicella, P., Scarnati, E. & Schultz, W. Tonically discharging neurons of monkey striatum respond to preparatory and rewarding stimuli. *Exp. Brain Res.* **84**, 672-675 (1991).

14. Arlotta, P., Molyneaux, B. J., Jabaudon, D., Yoshida, Y. & Macklis, J. D. Ctip2 controls the differentiation of medium spiny neurons and the establishment of the cellular architecture of the striatum. *J. Neurosci.* **28**, 622-632 (2008).

15. Aron, A. R. & Poldrack, R. A. Cortical and subcortical contributions to stop signal response inhibition: Role of the subthalamic nucleus. *J. Neurosci.* **26**, 2424-2433 (2006).

16. Aronin, K., Chase, K. & DiFiglia, M. Glutamic acid decarboxylase and enkephalin immunoreactive axon terminals in the rat neostriatum synapse with striatonigral neurons. *Brain Res.* **365**, 151-158 (1986).

17. Ascoli, G. A. *et al*. Petilla terminology: Nomenclature of features of GABAergic interneurons of the cerebral cortex. *Nat. Rev. Neurosci.* **9**, 557-568 (2008).

18. Atallah, H. E., McCool, A. D., Howe, M. W. & Graybiel, A. M. Neurons in the ventral striatum exhibit cell-type-specific representations of outcome during learning. *Neuron* **82**, 1145-1156 (2014).

19. Attems, J. *et al*. Calcium-binding protein secretagogin-expressing neurones in the human hippocampus are largely resistant to neurodegeneration in Alzheimer's disease. *Neuropathol. Appl. Neurobiol.* **34**, 23-32 (2008).

20. Attems, J. *et al*. Immunoreactivity of calcium binding protein secretagogin in the human hippocampus is restricted to pyramidal neurons. *Exp. Gerontol.* **42**, 215-222 (2007).

21. Aubry, L. *et al*. Striatal progenitors derived from human ES cells mature into DARPP32 neurons in vitro and in quinolinic acid-lesioned rats. *Proc. Natl. Acad. Sci. U. S. A.* **105**, 16707-16712 (2008).

22. Balleine, B. W. & O'Doherty, J. P. Human and rodent homologies in action control: Corticostriatal determinants of goal-directed and habitual action. *Neuropsychopharmacology* **35**, 48-69 (2010).

23. Barinka, F. & Druga, R. Calretinin expression in the mammalian neocortex: A review. *Physiol. Res.* **59**, 665-677 (2010).

24. Batens, K. *et al*. Subthalamic nucleus stimulation and spontaneous language production in Parkinson's disease: A double laterality problem. *Brain Lang.* **147**, 76-84 (2015).

25. Bauer, M. C. *et al*. Identification of a high-affinity network of secretagogin-binding proteins involved in vesicle secretion. *Mol. Biosyst.* **7**, 2196-2204 (2011).

26. Bearzatto, B. *et al*. Targeted calretinin expression in granule cells of calretinin-null mice restores normal cerebellar functions. *FASEB J.* **20**, 380-382 (2006).

27. Beier, K. T. *et al*. Circuit Architecture of VTA Dopamine Neurons Revealed by Systematic Input-Output Mapping. *Cell* **162**, 622-634 (2015).

28. Ben-Ari, Y. Cell death and synaptic reorganizations produced by seizures. *Epilepsia* **42**, 5-7 (2001).

29. Bennett, B. D. & Bolam, J. P. Synaptic input and output of parvalbumin-immunoreactive neurons in the neostriatum of the rat. *Neuroscience* **62**, 707-719 (1994).

30. Bennett, B. D. & Bolam, J. P. Two populations of calbindin D28k-immunoreactive neurones in the striatum of the rat. *Brain Res.* **610**, 305-310 (1993).

31. Bennett, B. D. & Bolam, J. P. Characterization of calretinin-immunoreactive structures in the striatum of the rat. *Brain Res.* **609**, 137-148 (1993).

32. Bennett, B. D., Callaway, J. C. & Wilson, C. J. Intrinsic membrane properties underlying spontaneous tonic firing in neostriatal cholinergic interneurons. *J. Neurosci.* **20**, 8493-8503 (2000).

33. Bennett, B. D. & Wilson, C. J. Spontaneous activity of neostriatal cholinergic interneurons in vitro. *J. Neurosci.* **19**, 5586-5596 (1999).

34. Berendse, H. W., Galis-de Graaf, Y. & Groenewegen, H. J. Topographical organization and relationship with ventral striatal compartments of prefrontal corticostriatal projections in the rat. *J. Comp. Neurol.* **316**, 314-347 (1992).

35. Berens, P.. CircStat: A MATLAB Toolbox for Circular Statistics. *Journal of Statistical Software* **31**, 1-21. (2009).

36. Bergson, C. *et al*. Regional, cellular, and subcellular variations in the distribution of D1 and D5 dopamine receptors in primate brain. *J. Neurosci.* **15**, 7821-7836 (1995).

37. Berke, J. D. Uncoordinated firing rate changes of striatal fast-spiking interneurons during behavioral task performance. *J. Neurosci.* **28**, 10075-10080 (2008).

38. Berke, J. D. & Hyman, S. E. Addiction, dopamine, and the molecular mechanisms of memory. *Neuron* **25**, 515-532 (2000).

39. Bernácer, J., Prensa, L. & Giménez-Amaya, J. M. Distribution of GABAergic interneurons and dopaminergic cells in the functional territories of the human striatum. *PLoS ONE* **7** (2012).

40. Bernard, V., Laribi, O., Levey, A. I. & Bloch, B. Subcellular redistribution of m2 muscarinic acetylcholine receptors in striatal interneurons in vivo after acute cholinergic stimulation. *J. Neurosci.* **18**, 10207-10218 (1998).

41. Bernard, V., Normand, E. & Bloch, B. Phenotypical characterization of the rat striatal neurons expressing muscarinic receptor genes. *J. Neurosci.* **12**, 3591-3600 (1992).

42. Bertran-Gonzalez, J. *et al*. Opposing patterns of signaling activation in dopamine D1 and D2 receptor-expressing striatal neurons in response to cocaine and haloperidol. *J. Neurosci.* **28**, 5671-5685 (2008).

43. Bevan, M. D. Selective innervation of neostriatal interneurons by a subclass of neuron in the globus pallidus of the rat. *J. Neurosci.* **18**, 9438-9452 (1998).

44. Bevan, M. D., Hallworth, N. E. & Baufreton, J. GABAergic control of the subthalamic nucleus. *Prog. Brain Res.* **160**, 173-188 (2007).

45. Bissonette, G. B., Powell, E. M. & Roesch, M. R. Neural structures underlying set-shifting: Roles of medial prefrontal cortex and anterior cingulate cortex. *Behav. Brain Res.* **250**, 91-101 (2013).

46. Blackwell, K. T., Czubayko, U. & Plenz, D. Quantitative estimate of synaptic inputs to striatal neurons during up and down states in vitro. *J. Neurosci.* **23**, 9123-9132 (2003).

47. Blomeley, C. & Bracci, E. Substance P depolarizes striatal projection neurons and facilitates their glutamatergic inputs. *J. Physiol.* **586**, 2143-2155 (2008).

48. Blomeley, C. P. & Bracci, E. Opioidergic interactions between striatal projection neurons. *J. Neurosci.* **31**, 13346-13356 (2011).

49. Blomeley, C. P., Kehoe, L. A. & Bracci, E. Substance p mediates excitatory interactions between striatal projection neurons. *J. Neurosci.* **29**, 4953-4963 (2009).

50. Blumenfeld, R. S., Parks, C. M., Yonelinas, A. P. & Ranganath, C. Putting the pieces together: The role of dorsolateral prefrontal cortex in relational memory encoding. *J. Cogn. Neurosci.* **23**, 257-265 (2011).

51. Bockaert, J., Premont, J., Glowinski, J., Thierry, A. M. & Tassin, J. P. Topographical distribution of dopaminergic innervation and of dopaminergic receptors in the rat striatum. II. Distribution and characteristics of dopamine adenylate cyclase - Interaction of d-LSD with dopaminergic receptors. *Brain Res.* **107**, 303-315 (1976).

52. Boileau, I. *et al*. Alcohol promotes dopamine release in the human nucleus accumbens. *Synapse* **49**, 226-231 (2003).

53. Bolam, J. P., Clarke, D. J., Smith, A. D. & Somogyi, P. A type of aspiny neuron in the rat neostriatum accumulates [3H]γ-aminobutyric acid: Combination of Golgi-staining, autoradiography, and electron microscopy. *J. Comp. Neurol.* **213**, 121-134 (1983).

54. Bolam, J. P., Hanley, J. J., Booth, P. A. C. & Bevan, M. D. Synaptic organisation of the basal ganglia. *J. Anat.* **196**, 527-542 (2000).

55. Bolam, J. P. *et al*. Substance P-Containing terminals in synaptic contact with cholinergic neurons in the neostriatum and basal forebrain: a double immunocytochemical study in the rat. *Brain Res.* **397**, 279-289 (1986).

56. Bolam, J. P. & Smith, Y. The GABA and substance P input to dopaminergic neurones in the substantia nigra of the rat. *Brain Res.* **529**, 57-78 (1990).

57. Bolam, J. P., Somogyi, P., Totterdell, S. & Smith, A. D. A second type of striatonigral neuron: a comparison between retrogradely labelled and golgi-stained neurons at the light and electron microscopic levels. *Neuroscience* **6**, 2141-"2151,2153-2157" (1981).

58. Bolam, J. P., Wainer, B. H. & Smith, A. D. Characterization of cholinergic neurons in the rat neostriatum. A combination of choline acetyltransferase immunocytochemistry, Golgi-impregnation and electron microscopy. *Neuroscience* **12**, 711-718 (1984).

59. Bortone, D. & Polleux, F. KCC2 Expression Promotes the Termination of Cortical Interneuron Migration in a Voltage-Sensitive Calcium-Dependent Manner. *Neuron* **62**, 53-71 (2009).

60. Bossong, M. G. *et al*. Δ9-tetrahydrocannabinol induces dopamine release in the human striatum. *Neuropsychopharmacology* **34**, 759-766 (2009).

61. Bracci, E., Centonze, D., Bernardi, G. & Calabresi, P. Voltage-dependent membrane potential oscillations of rat striatal fast-spiking interneurons. *J. Physiol.* **549**, 121-130 (2003).

62. Bracci, E., Centonze, D., Bernardi, G. & Calabresi, P. Dopamine excites fast-spiking interneurons in the striatum. *J. Neurophysiol.* **87**, 2190-2194 (2002).

63. Brown, M. T. C., Henny, P., Bolam, J. P. & Magill, P. J. Activity of neurochemically heterogeneous dopaminergic neurons in the substantia nigra during spontaneous and driven changes in brain state. *J. Neurosci.* **29**, 2915-2925 (2009).

64. Brown, M. T. C. *et al*. Ventral tegmental area GABA projections pause accumbal cholinergic interneurons to enhance associative learning. *Nature* **492**, 452-456 (2012).

65. Bucurenciu, I., Kulik, A., Schwaller, B., Frotscher, M. & Jonas, P. Nanodomain Coupling between Ca2+ Channels and Ca2+ Sensors Promotes Fast and Efficient Transmitter Release at a Cortical GABAergic Synapse. *Neuron* **57**, 536-545 (2008).

66. Burke, M. V., Nocjar, C., Sonneborn, A. J., McCreary, A. C. & Pehek, E. A. Striatal serotonin 2C receptors decrease nigrostriatal dopamine release by increasing GABA-A receptor tone in the substantia nigra. *J. Neurochem.* **131**, 432-443 (2014).

67. Burton, A. C., Nakamura, K. & Roesch, M. R. From ventral-medial to dorsal-lateral striatum: Neural correlates of reward-guided decision-making. *Neurobiol. Learn. Mem.* **117**, 51-59 (2015).

68. Cadwell, C. *et al.* Electrophysiological, transcriptomic and morphologic profiling of single neurons using Patch-seq. *Nat. Biotechology.* **34**, 199-203 (2016).

69. Caillard, O. *et al*. Role of the calcium-binding protein parvalbumin in short-term synaptic plasticity. *Proc. Natl. Acad. Sci. U. S. A.* **97**, 13372-13377 (2000).

70. Calabresi, P., Centonze, D., Gubellini, P., Pisani, A. & Bernardi, G. Acetylcholine-mediated modulation of striatal function. *Trends Neurosci.* **23**, 120-126 (2000).

71. Calabresi, P., Centonze, D., Gubellini, P., Pisani, A. & Bernardi, G. Endogenous ACh enhances striatal NMDA-responses via M1-like muscarinic receptors and PKC activation. *Eur. J. Neurosci.* **10**, 2887-2895 (1998).

72. Calabresi, P. *et al*. Muscarinic IPSPs in rat striatal cholinergic interneurones. *J. Physiol.* **510**, 421-427 (1998).

73. Calabresi, P. *et al*. A critical role of the nitric oxide/cGMP pathway in corticostriatal long-term depression. *J. Neurosci.* **19**, 2489-2499 (1999).

74. Calabresi, P., Picconi, B., Tozzi, A. & Di Filippo, M. Dopamine-mediated regulation of corticostriatal synaptic plasticity. *Trends Neurosci.* **30**, 211-219 (2007).

75. Cancedda, L., Fiumelli, H., Chen, K. & Poo, M. -. Excitatory GABA action is essential for morphological maturation of cortical neurons in vivo. *J. Neurosci.* **27**, 5224-5235 (2007).

76. Carr, D. B. & Sesack, S. R. Projections from the rat prefrontal cortex to the ventral tegmental area: Target specificity in the synaptic associations with mesoaccumbens and mesocortical neurons. *J. Neurosci.* **20**, 3864-3873 (2000).

77. Carter, A. G. & Sabatini, B. L. State-dependent calcium signaling in dendritic spines of striatal medium spiny neurons. *Neuron* **44**, 483-493 (2004).

78. Caruncho, H. J., Liste, I. & Labandeira-García, J. L. GABAA receptor a1-subunit-immunopositive neurons in the rat striatum. *Brain Res.* **722**, 185-189 (1996).

79. Cauli, B. *et al*. Molecular and physiological diversity of cortical nonpyramidal cells. *J. Neurosci.* **17**, 3894-3906 (1997).

80. Celio, M. R. Calbindin D-28k and parvalbumin in the rat nervous system. *Neuroscience* **35**, 375-475 (1990).

81. Centonze, D. *et al*. Activation of dopamine D1-like receptors excites LTS interneurons of the striatum. *Eur. J. Neurosci.* **15**, 2049-2052 (2002).

82. Centonze, D. *et al*. Receptor subtypes involved in the presynaptic and postsynaptic actions of dopamine on striatal interneurons. *J. Neurosci.* **23**, 6245-6254 (2003).

83. Centonze, D., Gubellini, P., Pisani, A., Bernardi, G. & Calabresi, P. Dopamine, acetylcholine, and nitric oxide systems interact to induce corticostriatal synaptic plasticity. *Rev. Neurosci.* **14**, 207-216 (2003).

84. Centonze, D. *et al*. Stimulation of nitric oxide-cGMP pathway excites striatal cholinergic interneurons via protein kinase G activation. *J. Neurosci.* **21**, 1393-1400 (2001).

85. Chang, H. T. & Kita, H. Interneurons in the rat striatum: relationships between parvalbumin neurons and cholinergic neurons. *Brain Res.* **574**, 307-311 (1992).

86. Chang, H. T. & Tian, Q. Vasoactive intestinal polypeptide (VIP) immunoreactive elements in the caudal ventral striatum of the rat: A light and electron microscopic study. *Brain Res. Bull.* **26**, 947-956 (1991).

87. Charrier, C., Ehrensperger, M. -., Dahan, M., Lévi, S. & Triller, A. Cytoskeleton regulation of glycine receptor number at synapses and diffusion in the plasma membrane. *J. Neurosci.* **26**, 8502-8511 (2006).

88. Chernov, A. V. *et al*. The calcium-binding proteins S100a8 and S100a9 initiate the early inflammatory program in injured peripheral nerves. *J. Biol. Chem.* **290**, 11771-11784 (2015).

89. Chesselet, M. -. & Robbins, E. Characterization of striatal neurons expressing high levels of glutamic acid decarboxylase messenger RNA. *Brain Res.* **492**, 237-244 (1989).

90. Choi, S. & Lovinger, D. M. Decreased probability of neurotransmitter release underlies striatal long-term depression and postnatal development of corticostriatal synapses. *Proc. Natl. Acad. Sci. U. S. A.* **94**, 2665-2670 (1997).

91. Christie, J. M., Chiu, D. N. & Jahr, C. E. Ca2+-dependent enhancement of release by subthreshold somatic depolarization. *Nat. Neurosci.* **14**, 62-69 (2011).

92. Chronister, R. B., Farnell, K. E., Marco, L. A. & White Jr., L. E. The rodent neostriatum: A golgi analysis. *Brain Res.* **108**, 37-46 (1976).

93. Chuhma, N., Mingote, S., Moore, H. & Rayport, S. Dopamine neurons control striatal cholinergic neurons via regionally heterogeneous dopamine and glutamate signaling. *Neuron* **81**, 901-912 (2014).

94. Chung, H. A., Medina-Ruiz, S. & Harland, R. M. Sp8 regulates inner ear development. *Proc. Natl. Acad. Sci. U. S. A.* **111**, 6329-6334 (2014).

95. Cicchetti, F., Beach, T. G. & Parent, A. Chemical phenotype of calretinin interneurons in the human striatum. *Synapse* **30**, 284-297 (1998).

96. Cicchetti, F., Prensa, L., Wu, Y. & Parent, A. Chemical anatomy of striatal interneurons in normal individuals and in patients with Huntington's disease. *Brain Res. Rev.* **34**, 80-101 (2000).

97. Contant, C., Umbriaco, D., Garcia, S., Watkins, K. C. & Descarries, L. Ultrastructural characterization of the acetylcholine innervation in adult rat neostriatum. *Neuroscience* **71**, 937-947 (1996).

98. Couturier, J. *et al*. Strong correlation between results of fluorescent In situ hybridization and immunohistochemistry for the assessment of the ERBB2 (HER-2/neu) gene status in breast carcinoma. *Mod. Pathol.* **13**, 1238-1243 (2000).

99. Cowan, R. L., Wilson, C. J., Emson, P. C. & Heizmann, C. W. Parvalbumin-containing GABAergic interneurons in the rat neostriatum. *J. Comp. Neurol.* **302**, 197-205 (1990).

100. Cragg, S. J., Baufreton, J., Xue, Y., Bolam, J. P. & Bevan, M. D. Synaptic release of dopamine in the subthalamic nucleus. *Eur. J. Neurosci.* **20**, 1788-1802 (2004).

101. Czubayko, U. & Plenz, D. Fast synaptic transmission between striatal spiny projection neurons. *Proc. Natl. Acad. Sci. U. S. A.* **99**, 15764-15769 (2002).

102. Dautan, D. *et al*. A major external source of cholinergic innervation of the striatum and nucleus accumbens originates in the Brainstem. *J. Neurosci.* **34**, 4509-4518 (2014).

103. Dayer, A. G., Cleaver, K. M., Abouantoun, T. & Cameron, H. A. New GABAergic interneurons in the adult neocortex and striatum are generated from different precursors. *J. Cell Biol.* **168**, 415-427 (2005).

104. De Deyn, P. P., D'hooge, R., Block, J. D., Llona, I. & De Potter, W. P. Biochemical characterization of particles from rat striatum containing dopamine, cholecystokinin or both. *Arch. Physiol. Biochem.* **100**, 175-179 (1992).

105. De Marco García, N. V., Karayannis, T. & Fishell, G. Neuronal activity is required for the development of specific cortical interneuron subtypes. *Nature* **472**, 351-355 (2011).

106. DeLong, M. R. Primate models of movement disorders of basal ganglia origin. *Trends Neurosci.* **13**, 281-285 (1990).

107. DeLong, M. R. The neurophysiologic basis of abnormal movements in basal ganglia disorders. *Neurobehav. Toxicol. Teratol.* **5**, 611-616 (1983).

108. Delong, M. R. *et al*. Functional organization of the basal ganglia: contributions of single-cell recording studies. *Ciba Found. Symp.* **107**, 64-82 (1984).

109. Deng, Y. *et al*. Differential organization of cortical inputs to striatal projection neurons of the matrix compartment in rats. *Front. Syst. Neurosci.* **9** (2015).

110. Deng, Y. -., Shelby, E. & Reiner, A. J. Immunohistochemical localization of AMPA-type glutamate receptor subunits in the striatum of rhesus monkey. *Brain Res.* **1344**, 104-123 (2010).

111. Deniau, J. M., Mailly, P., Maurice, N. & Charpier, S. The pars reticulata of the substantia nigra: a window to basal ganglia output. *Prog. Brain Res.* **160**, 151-172 (2007).

112. Deniau, J. M., Menetrey, A. & Thierry, A. M. Indirect nucleus accumbens input to the prefrontal cortex via the substantia nigra pars reticulata: A combined anatomical and electrophysiological study in the rat. *Neuroscience* **61**, 533-545 (1994).

113. Di Giovanni, G., Di Matteo, V., Pierucci, M. & Esposito, E. Serotonin-dopamine interaction: electrophysiological evidence. *Prog. Brain Res.* **172**, 45-71 (2008).

114. Di Martino, A. *et al*. Functional connectivity of human striatum: A resting state fMRI study. *Cereb. Cortex* **18**, 2735-2747 (2008).

115. DiFiglia, M. & Aronin, N. Ultrastructural features of immunoreactive somatostatin neurons in the rat caudate nucleus. *J. Neurosci.* **2**, 1267-1274 (1982).

116. DiFiglia, M., Aronin, N. & Martin, J. B. Light and electron microscopic localization of immunoreactive Leu-enkephalin in the monkey basal ganglia. *J. Neurosci.* **2**, 303-320 (1982).

117. Dodson, P. D. *et al*. Distinct developmental origins manifest in the specialized encoding of movement by adult neurons of the external globus pallidus. *Neuron* **86**, 501-513 (2015).

118. Doig, N. M., Magill, P. J., Apicella, P., Bolam, J. P. & Sharott, A. Cortical and thalamic excitation mediate the multiphasic responses of striatal cholinergic interneurons to motivationally salient stimuli. *J. Neurosci.* **34**, 3101-3117 (2014).

119. Doig, N. M., Moss, J. & Bolam, J. P. Cortical and thalamic innervation of direct and indirect pathway medium-sized spiny neurons in mouse striatum. *J. Neurosci.* **30**, 14610-14618 (2010).

120. Donato, F., Rompani, S. B. & Caroni, P. Parvalbumin-expressing basket-cell network plasticity induced by experience regulates adult learning. *Nature* **504**, 272-276 (2013).

121. D'Orlando, C. *et al*. Calretinin and calbindin D-28k delay the onset of cell death after excitotoxic stimulation in transfected P19 cells. *Brain Res.* **909**, 145-158 (2001).

122. Doya, K. & Kimura, M. The basal ganglia and the encoding of value. *Neuroecon.*, 407-416 (2009).

123. Du, T., Xu, Q., Ocbina, P. J. & Anderson, S. A. NKX2.1 specifies cortical interneuron fate by activating Lhx6. *Development (Cambridge)* **135**, 1559-1567 (2008).

124. Duque, A., Gazula, V. -. & Kaczmarek, L. K. Expression of Kv1.3 potassium channels regulates density of cortical interneurons. *Dev. Neurobiol.* **73**, 841-855 (2013).

125. Eggermann, E. & Jonas, P. How the 'slow' Ca 2+ buffer parvalbumin affects transmitter release in nanodomain-coupling regimes. *Nat. Neurosci.* **15**, 20-22 (2012).

126. Ellender, T. J., Huerta-Ocampo, I., Deisseroth, K., Capogna, M. & Paul Bolam, J. Differential modulation of excitatory and inhibitory striatal synaptic transmission by histamine. *J. Neurosci.* **31**, 15340-15351 (2011).

127. Ernst, A. *et al*. Neurogenesis in the striatum of the adult human brain. *Cell* **156**, 1072-1083 (2014).

128. Eskenazi, D., Brodsky, M. & Neumaier, J. F. Deconstructing 5-HT6 receptor effects on striatal circuit function. *Neuroscience* **299**, 97-106 (2015).

129. Faust, T. W., Assous, M., Shah, F., Tepper, J. M. & Koós, T. Novel fast adapting interneurons mediate cholinergic-induced fast GABAA inhibitory postsynaptic currents in striatal spiny neurons. *Eur. J. Neurosci.* **42**, 1764-1774 (2015).

130. Figueredo-Cardenas, G., Medina, L. & Reiner, A. Calretinin is largely localized to a unique population of striatal interneurons in rats. *Brain Res.* **709**, 145-150 (1996).

131. Figueredo-Cardenas, G., Morello, M., Sancesario, G., Bernardi, G. & Reiner, A. Colocalization of somatostatin, neuropeptide Y, neuronal nitric oxide synthase and NADPH-diaphorase in striatal inerneurons in rats. *Brain Res.* **735**, 317-324 (1996).

132. Fino, E., Glowinski, J. & Venance, L. Effects of acute dopamine depletion on the electrophysiological properties of striatal neurons. *Neurosci. Res.* **58**, 305-316 (2007).

133. Fishell, G. & Heintz, N. The neuron identity problem: Form meets function. *Neuron* **80**, 602-612 (2013).

134. Flaherty, A. W. & Graybiel, A. M. Output architecture of the primate putamen. *J. Neurosci.* **13**, 3222-3237 (1993).

135. Flores-Hernández, J. *et al*. Dopamine enhancement of NMDA currents in dissociated medium-sized striatal neurons: Role of D1 receptors and DARPP-32. *J. Neurophysiol.* **88**, 3010-3020 (2002).

136. Fortin, M. & Parent, A. Calretinin labels a specific neuronal subpopulation in primate globus pallidus. *Neuroreport* **5**, 2097-2100 (1994).

137. Fosser, N. S., Ronco, L., Bejarano, A., Paganelli, A. R. & Ríos, H. Calbindin-D28k and calretinin in chicken inner retina during postnatal development and neuroplasticity by dim red light. *Dev. Neurobiol.* **73**, 530-542 (2013).

138. Foxworthy, W. A., Clemo, H. R. & Meredith, M. A. Laminar and connectional organization of a multisensory cortex. *J. Comp. Neurol.* **521**, 1867-1890 (2013).

139. Fragkouli, A. *et al*. Loss of forebrain cholinergic neurons and impairment in spatial learning and memory in LHX7-deficient mice. *Eur. J. Neurosci.* **21**, 2923-2938 (2005).

140. Fragkouli, A., van Wijk, N. V., Lopes, R., Kessaris, N. & Pachnis, V. LIM homeodomain transcription factor-dependent specification of bipotential MGE progenitors into cholinergic and GABAergic striatal interneurons. *Development (Cambridge)* **136**, 3841-3851 (2009).

141. Franklin K, Paxinos G. The Mouse Brain in Stereotaxic Coordinates **3rd ed.** *London: Academic Press*. (2008).

142. Freiman, I., Anton, A., Monyer, H., Urbanski, M. J. & Szabo, B. Analysis of the effects of cannabinoids on identified synaptic connections in the caudate-putamen by paired recordings in transgenic mice. *J. Physiol.* **575**, 789-806 (2006).

143. Freund, T. F. & Buzsáki, G. Interneurons of the Hippocampus. *Hippocampus* **6**, 347-470 (1996).

144. Friedman, A. *et al*. A corticostriatal path targeting striosomes controls decision-making under conflict. *Cell* **161**, 1320-1333 (2015).

145. Friedman, D. P., Aggleton, J. P. & Saunders, R. C. Comparison of hippocampal, amygdala, and perirhinal projections to the nucleus accumbens: Combined anterograde and retrograde tracing study in the macaque brain. *J. Comp. Neurol.* **450**, 345-365 (2002).

146. Fudge, J. L., Kunishio, K., Walsh, P., Richard, C. & Haber, S. N. Amygdaloid projections to ventromedial striatal subterritories in the primate. *Neuroscience* **110**, 257-275 (2002).

147. Fuzik, J. *et al*. Integration of electrophysiological recordings with single-cell RNA-seq data identifies neuronal subtypes. *Nat. Biotechnology.* **4(2)**,175-83 (2016)

148. Fyhn, M., Molden, S., Witter, M. P., Moser, E. I. & Moser, M. -. Spatial representation in the entorhinal cortex. *Science* **305**, 1258-1264 (2004).

149. Gage, G. J., Stoetzner, C. R., Wiltschko, A. B. & Berke, J. D. Selective Activation of Striatal Fast-Spiking Interneurons during Choice Execution. *Neuron* **67**, 466-479 (2010).

150. Galarreta, M. & Hestrin, S. Electrical and chemical synapses among parvalbumin fast-spiking GABAergic interneurons in adult mouse neocortex. *Proc. Natl. Acad. Sci. U. S. A.* **99**, 12438-12443 (2002).

151. Galarreta, M. & Hestrin, S. Spike transmission and synchrony detection in networks of GABAergic interneurons. *Science* **292**, 2295-2299 (2001).

152. Galarreta, M. & Hestrin, S. Electrical synapses between GABA-releasing interneurons. *Nat. Rev. Neurosci.* **2**, 425-433 (2001).

153. Galarreta, M. & Hestrin, S. A network of fast-spiking cells in the neocortex connected by electrical synapses. *Nature* **402**, 72-75 (1999).

154. Galvan, A., Devergnas, A. & Wichmann, T. Alterations in neuronal activity in basal ganglia-thalamocortical circuits in the Parkinsonian State. *Front. Neuroanat.* **9**, 1-21 (2015).

155. Gangarossa, G. *et al*. Spatial distribution of D1R- and D2R-expressing medium-sized spiny neurons differs along the rostro-caudal axis of the mouse dorsal striatum. *Front. Neural Circuits* (2013).

156. Garber JC, Barbee RW, Bielitzki JT, Clayton LA, Donovan JC, Hendriksen CFM, Kohn DF, Lipman NS, Locke PA, Melcher J, Quimby FW, Turner PV, Wood GA, Würbel H. Guide for the care and use of laboratory animals, Washington, DC: *The National Academies Press*. (2010).

157. Gardiner, T. W. & Kitai, S. T. Single-unit activity in the globus pallidus and neostriatum of the rat during performance of a trained head movement. *Exp. Brain Res.* **88**, 517-530 (1992).

158. Gartner, W. *et al*. New functional aspects of the neuroendocrine marker secretagogin based on the characterization of its rat homolog. *Am. J. Physiol. Endocrinol. Metab.* **293**, E347-E354 (2007).

159. Gáti, G., Lendvai, D., Hökfelt, T., Harkany, T. & Alpár, A. Revival of calcium-binding proteins for neuromorphology: Secretagogin typifies distinct cell populations in the avian brain. *Brain Behav. Evol.* **83**, 82-92 (2014).

160. Gerfen, C. R. The neostriatal mosaic: Multiple levels of compartmental organization. *Trends Neurosci.* **15**, 133-139 (1992).

161. Gerfen, C. R. D1 and D2 dopamine receptor regulation of striatonigral and striatopallidal neurons. *Semin. Neurosci.* **4**, 109-118 (1992).

162. Gerfen, C. R. The neostriatal mosaic: multiple levels of compartmental organization. *J. Neural Transm. Suppl.* **36**, 43-59 (1992).

163. Gerfen, C. R., Baimbridge, K. G. & Miller, J. J. The neostriatal mosaic: Compartmental distribution of calcium-binding protein and parvalbumin in the basal ganglia of the rat and monkey. *Proc. Natl. Acad. Sci. U. S. A.* **82**, 8780-8784 (1985).

164. Gerfen, C. R. *et al*. D1 and D2 dopamine receptor-regulated gene expression of striatonigral and striatopallidal neurons. *Science* **250**, 1429-1432 (1990).

165. Gerfen, C. R. & Surmeier, D. J. Modulation of striatal projection systems by dopamine. *Annu. Rev. Neurosci.* **34**, 441-466 (2011).

166. Gertler, T. S., Chan, C. S. & Surmeier, D. J. Dichotomous anatomical properties of adult striatal medium spiny neurons. *J. Neurosci.* **28**, 10814-10824 (2008).

167. Gittis, A. *et al*. Rapid target-specific remodeling of fast-spiking inhibitory circuits after loss of dopamine. *Neuron* **71**, 858-868 (2011).

168. Gittis, A. H., Nelson, A. B., Thwin, M. T., Palop, J. J. & Kreitzer, A. C. Distinct roles of GABAergic interneurons in the regulation of striatal output pathways. *J. Neurosci.* **30**, 2223-2234 (2010).

169. Glynn, G. & Ahmad, S. O. Three-dimensional electrophysiological topography of the rat corticostriatal system. *J. Comp. Physiol. A Neuroethol. Sens. Neural. Behav. Physiol.* **188**, 695-703 (2002).

170. Goldberg, J. H., Farries, M. A. & Fee, M. S. Integration of cortical and pallidal inputs in the basal ganglia-recipient thalamus of singing birds. *J. Neurophysiol.* **108**, 1403-1429 (2012).

171. Gonzales, K. K., Pare, J. -., Wichmann, T. & Smith, Y. GABAergic inputs from direct and indirect striatal projection neurons onto cholinergic interneurons in the primate putamen. *J. Comp. Neurol.* **521**, 2502-2522 (2013).

172. Graveland, G. A. & Difiglia, M. The frequency and distribution of medium-sized neurons with indented nuclei in the primate and rodent neostriatum. *Brain Res.* **327**, 307-311 (1985).

173. Graybiel, A. M., Aosaki, T., Flaherty, A. W. & Kimura, M. The basal ganglia and adaptive motor control. *Science* **265**, 1826-1831 (1994).

174. Graybiel, A. M., Pickel, V. M., Joh, T. H., Reis, D. J. & Ragsdale Jr., C. W. Direct demonstration of a correspondence between the dopamine islands and acetylcholinesterase patches in the developing striatum. *Proc. Natl. Acad. Sci. U. S. A.* **78**, 5871-5875 (1981).

175. Gremel, C. M. & Costa, R. M. Orbitofrontal and striatal circuits dynamically encode the shift between goal-directed and habitual actions. *Nat. Commun.* **4** (2013).

176. Grenhoff, J., Ugedo, L. & Svensson, T. H. Firing patterns of midbrain dopamine neurons: Differences between A9 and A10 cells. *Acta Physiol. Scand.* **134**, 127-132 (1988).

177. Grigoriou, M., Tucker, A. S., Sharpe, P. T. & Pachnis, V. Expression and regulation of Lhx6 and Lhx7, a novel subfamily of LIM homeodomain encoding genes, suggests a role in mammalian head development. *Development (Cambridge)* **125**, 2063-2074 (1998).

178. Grillner, S., Hellgren, J., Ménard, A., Saitoh, K. & Wikström, M. A. Mechanisms for selection of basic motor programs - Roles for the striatum and pallidum. *Trends Neurosci.* **28**, 364-370 (2005).

179. Groenewegen, H. J., Berendse, H. W. & Haber, S. N. Organization of the output of the ventral striatopallidal system in the rat: Ventral pallidal efferents. *Neuroscience* **57**, 113-142 (1993).

180. Groenewegen, H. J., Wright, C. I., Beijer, A. V. J. & Voorn, P. Convergence and segregation of ventral striatal inputs and outputs. *Ann. New York Acad. Sci.* **877**, 49-63 (1999).

181. Gulyás, A. I., Miettinen, R., Jacobowitz, D. M. & Freund, T. F. Calretinin is present in non-pyramidal cells of the rat hippocampus-I. A new type of neuron specifically associated with the mossy fibre system. *Neuroscience* **48**, 1-27 (1992).

182. Gundersen, H. J. & Jensen, E. B. The efficiency of systematic sampling in stereology and its prediction. *J. Microsc.* **147**, Pt 3/ (1987).

183. Guo, Q. *et al*. Whole-brain mapping of inputs to projection neurons and cholinergic interneurons in the dorsal striatum. *PLoS ONE* **10** (2015).

184. Haber, S. N. The primate basal ganglia: Parallel and integrative networks. *J. Chem. Neuroanat.* **26**, 317-330 (2003).

185. Haber, S. N., Fudge, J. L. & McFarland, N. R. Striatonigrostriatal pathways in primates form an ascending spiral from the shell to the dorsolateral striatum. *J. Neurosci.* **20**, 2369-2382 (2000).

186. Haber, S. N., Kim, K. -., Mailly, P. & Calzavara, R. Reward-related cortical inputs define a large striatal region in primates that interface with associative cortical connections, providing a substrate for incentive-based learning. *J. Neurosci.* **26**, 8368-8376 (2006).

187. Haber, S. N. & Knutson, B. The reward circuit: Linking primate anatomy and human imaging. *Neuropsychopharmacology* **35**, 4-26 (2010).

188. Hakan, R. L., Berg, G. I. & Henriksen, S. J. Electrophysiological evidence for reciprocal connectivity between the nucleus accumbens septi and ventral pallidal region. *Brain Res.* **581**, 344-350 (1992).

189. Hanley, J. J. & Bolam, J. P. Synaptology of the nigrostriatal projection in relation to the compartmental organization of the neostriatum in the rat. *Neuroscience* **81**, 353-370 (1997).

190. Hassani, O. -., François, C., Yelnik, J. & Féger, J. Evidence for a dopaminergic innervation of the subthalamic nucleus in the rat. *Brain Res.* **749**, 88-94 (1997).

191. Hauber, W., Lutz, S. & Münkle, M. The effects of globus pallidus lesions on dopamine-dependent motor behaviour in rats. *Neuroscience* **86**, 147-157 (1998).

192. Heimer, L., Zahm, D. S., Churchill, L., Kalivas, P. W. & Wohltmann, C. Specificity in the projection patterns of accumbal core and shell in the rat. *Neuroscience* **41**, 89-125 (1991).

193. Hersch, S. M. *et al*. Electron microscopic analysis of D1 and D2 dopamine receptor proteins in the dorsal striatum and their synaptic relationships with motor corticostriatal afferents. *J. Neurosci.* **15**, 5222-5237 (1995).

194. Hersch, S. M., Gutekunst, C. -., Rees, H. D., Heilman, C. J. & Levey, A. I. Distribution of m1-m4 muscarinic receptor proteins in the rat striatum: Light and electron microscopic immunocytochemistry using subtype-specific antibodies. *J. Neurosci.* **14**, 3351-3363 (1994).

195. Hikosaka, O. GABAergic output of the basal ganglia. *Prog. Brain Res.* **160**, 209-226 (2007).

196. Hilario, M., Holloway, T., Jin, X. & Costa, R. M. Different dorsal striatum circuits mediate action discrimination and action generalization. *Eur. J. Neurosci.* **35**, 1105-1114 (2012).

197. Hollerman, J. R. & Schultz, W. Dopamine neurons report an error in the temporal prediction of reward during learning. *Nat. Neurosci.* **1**, 304-309 (1998).

198. Hollerman, J. R., Tremblay, L. & Schultz, W. Influence of reward expectation on behavior-related neuronal activity in primate striatum. *J. Neurophysiol.* **80**, 947-963 (1998).

199. Hoover, W. B. & Vertes, R. P. Projections of the medial orbital and ventral orbital cortex in the rat. *J. Comp. Neurol.* **519**, 3766-3801 (2011).

200. Huang, Z., Yu, Y., Shimoda, Y., Watanabe, K. & Liu, Y. Loss of neural recognition molecule NB-3 delays the normal projection and terminal branching of developing corticospinal tract axons in the mouse. *J. Comp. Neurol.* **520**, 1227-1245 (2012).

201. Humphries, M. D. & Prescott, T. J. The ventral basal ganglia, a selection mechanism at the crossroads of space, strategy, and reward. *Prog. Neurobiol.* **90**, 385-417 (2010).

202. Hutcherson, L. & Roberts, R. C. The immunocytochemical localization of substance P in the human striatum: A postmortem ultrastructural study. *Synapse* **57**, 191-201 (2005).

203. Ibáñez-Sandoval, O. *et al*. A novel functionally distinct subtype of striatal neuropeptide Y interneuron. *J. Neurosci.* **31**, 16757-16769 (2011).

204. Ibáñez-Sandoval, O. *et al*. Electrophysiological and morphological characteristics and synaptic connectivity of tyrosine hydroxylase-expressing neurons in adult mouse striatum. *J. Neurosci.* **30**, 6999-7016 (2010).

205. Ibáñez-Sandoval, O., Xenias, H. S., Tepper, J. M. & Koós, T. Dopaminergic and cholinergic modulation of striatal tyrosine hydroxylase interneurons. *Neuropharmacology* **95**, 468-476 (2015).

206. Ikemoto, S. Dopamine reward circuitry: Two projection systems from the ventral midbrain to the nucleus accumbens-olfactory tubercle complex. *Brain Res. Rev.* **56**, 27-78 (2007).

207. Inta, D. *et al*. Neurogenesis and widespread forebrain migration of distinct GABAergic neurons from the postnatal subventricular zone. *Proc. Natl. Acad. Sci. U. S. A.* **105**, 20994-20999 (2008).

208. Inta, D., Cameron, H. A. & Gass, P. New neurons in the adult striatum: From rodents to humans. *Trends Neurosci.* **38**, 517-523 (2015).

209. Ito, C., Onodera, K., Sakurai, E., Sato, M. & Watanabe, T. Effects of dopamine antagonists on neuronal histamine release in the striatum of rats subjected to acute and chronic treatments with methamphetamine. *J. Pharmacol. Exp. Ther.* **279**, 271-276 (1996).

210. Ito, R., Dalley, J. W., Robbins, T. W. & Everitt, B. J. Dopamine release in the dorsal striatum during cocaine-seeking behavior under the control of a drug-associated cue. *J. Neurosci.* **22**, 6247-6253 (2002).

211. Izzo, P. N. & Bolam, J. P. Cholinergic synaptic input to different parts of spiny striatonigral neurons in the rat. *J. Comp. Neurol.* **269**, 219-234 (1988).

212. Jacobowitz, D. M. & Winsky, L. Immunocytochemical localization of calretinin in the forebrain of the rat. *J. Comp. Neurol.* **304**, 198-218 (1991).

213. Jacobs, J., Kahana, M. J., Ekstrom, A. D., Mollison, M. V. & Fried, I. A sense of direction in human entorhinal cortex. *Proc. Natl. Acad. Sci. U. S. A.* **107**, 6487-6492 (2010).

214. Jaeger, D., Kita, H. & Wilson, C. J. Surround inhibition among projection neurons is weak or nonexistent in the rat neostriatum. *J. Neurophysiol.* **72**, 2555-2558 (1994).

215. Jakob, T. F., Döring, U. & Illing, R. -. The pattern of Fos expression in the rat auditory brainstem changes with the temporal structure of binaural electrical intracochlear stimulation. *Exp. Neurol.* **266**, 55-67 (2015).

216. Janssen, M. L. F. *et al*. Mild dopaminergic lesions are accompanied by robust changes in subthalamic nucleus activity. *Neurosci. Lett.* **508**, 101-105 (2012).

217. Jiang, X., Zhang, M., You, Y. & Liu, F. The Production of Somatostatin Interneurons in the Olfactory Bulb Is Regulated by the Transcription Factor Sp8. *PLoS ONE* **8** (2013).

218. Jiang, Z. G. & North, R. A. Pre- and postsynaptic inhibition by opioids in rat striatum. *J. Neurosci.* **12**, 356-361 (1992).

219. Jongen-Relo, A. L., Voom, P. & Groenewegen, H. J. Immunohistochemical characterization of the shell and core territories of the nucleus accumbens in the rat. *Eur. J. Neurosci.* **6**, 1255-1264 (1994).

220. Joshua, M., Adler, A., Mitelman, R., Vaadia, E. & Bergman, H. Midbrain dopaminergic neurons and striatal cholinergic interneurons encode the difference between reward and aversive events at different epochs of probabilistic classical conditioning trials. *J. Neurosci.* **28**, 11673-11684 (2008).

221. Karachi, C. *et al*. Three-dimensional cartography of functional territories in the human striatopallidal complex by using calbindin immunoreactivity. *J. Comp. Neurol.* **450**, 122-134 (2002).

222. Kasanetz, F., Riquelme, L. A. & Murer, M. G. Disruption of the two-state membrane potential of striatal neurones during cortical desynchronisation in anaesthetised rats. *J. Physiol.* **543**, 577-589 (2002).

223. Katona, L. *et al*. Sleep and Movement Differentiates Actions of Two Types of Somatostatin-Expressing GABAergic Interneuron in Rat Hippocampus. *Neuron* **82**, 872-886 (2014).

224. Kawagoe, R., Takikawa, Y. & Hikosaka, O. Expectation of reward modulates cognitive signals in the basal ganglia. *Nat. Neurosci.* **1**, 411-416 (1998).

225. Kawaguchi, Y. Physiological, morphological, and histochemical characterization of three classes of interneurons in rat neostriatum. *J. Neurosci.* **13**, 4908-4923 (1993).

226. Kawaguchi, Y., Aosaki, T. & Kubota, Y. Cholinergic and GABAergic interneurons in the striatum. *JPN. J. PSYCHOPHARMACOL.* **17**, 87-90 (1997).

227. Kawaguchi, Y., Wilson, C. J., Augood, S. J. & Emson, P. C. Striatal interneurones: chemical, physiological and morphological characterization. *Trends Neurosci.* **18**, 527-535 (1995).

228. Kawaguchi, Y., Wilson, C. J. & Emson, P. C. Projection subtypes of rat neostriatal matrix cells revealed by intracellular injection of biocytin. *J. Neurosci.* **10**, 3421-3438 (1990).

229. Kawaguchi, Y., Wilson, C. J. & Emson, P. C. Intracellular recording of identified neostriatal patch and matrix spiny cells in a slice preparation preserving cortical inputs. *J. Neurophysiol.* **62**, 1052-1068 (1989).

230. Kelley, A. E. Functional specificity of ventral striatal compartments in appetitive behaviors. *Ann. New York Acad. Sci.* **877**, 71-90 (1999).

231. Kelley, A. E. Neural integrative activities of nucleus accumbens subregions in relation to learning and motivation. *Psychobiology* **27**, 198-213 (1999).

232. Kelley, A. E., Baldo, B. A., Pratt, W. E. & Will, M. J. Corticostriatal-hypothalamic circuitry and food motivation: Integration of energy, action and reward. *Physiol. Behav.* **86**, 773-795 (2005).

233. Kelley, A. E. & Domesick, V. B. The distribution of the projection from the hippocampal formation to the nucleus accumbens in the rat: An anterograde and retrograde-horseradish peroxidase study. *Neuroscience* **7**, 2321-2335 (1982).

234. Kelley, A. E., Domesick, V. B. & Nauta, W. J. H. The amygdalostriatal projection in the rat-an anatomical study by anterograde and retrograde tracing methods. *Neuroscience* **7**, 615-"625,627-630" (1982).

235. Kemp, J. M. & Powell, T. P. The synaptic organization of the caudate nucleus. *Philos Trans R Soc Lond B Biol Sci* **262**, 403-412 (1971).

236. Kepecs, A. & Fishell, G. Interneuron cell types are fit to function. *Nature* **505**, 318-326 (2014).

237. Khibnik, L. A., Tritsch, N. X. & Sabatini, B. L. A direct projection from mouse primary visual cortex to dorsomedial striatum. *PLoS ONE* **9**, e104501 (2014).

238. Kincaid, A. E., Zheng, T. & Wilson, C. J. Connectivity and convergence of single corticostriatal axons. *J. Neurosci.* **18**, 4722-4731 (1998).

239. Kita, H. Parvalbumin-immunopositive neurons in rat globus pallidus: a light and electron microscopic study. *Brain Res.* **657**, 31-41 (1994).

240. Kita, H. GABAergic circuits of the striatum. *Prog. Brain Res.* **99**, 51-72 (1993).

241. Kita, H. & Kita, S. T. The morphology of globus pallidus projection neurons in the rat: an intracellular staining study. *Brain Res.* **636**, 308-319 (1994).

242. Kita, H., Kosaka, T. & Heizmann, C. W. Parvalbumin-immunoreactive neurons in the rat neostriatum: a light and electron microscopic study. *Brain Res.* **536**, 1-15 (1990).

243. Kita, T., Kita, H. & Kitai, S. T. Passive electrical membrane properties of rat neostriatal neurons in an in vitro slice preparation. *Brain Res.* **300**, 129-139 (1984).

244. Klaus, A. *et al*. Striatal fast-spiking interneurons: From firing patterns to postsynaptic impact. *Front. Syst. Neurosci.* (2011).

245. Klausberger, T. & Somogyi, P. Neuronal diversity and temporal dynamics: The unity of hippocampal circuit operations. *Science* **321**, 53-57 (2008).

246. Koós, T. & Tepper, J. M. Dual cholinergic control of fast-spiking interneurons in the neostriatum. *J. Neurosci.* **22**, 529-535 (2002).

247. Koós, T. & Tepper, J. M. Inhibitory control of neostriatal projection neurons by GABAergic interneurons. *Nat. Neurosci.* **2**, 467-472 (1999).

248. Koralek, A. C., Jin, X., Long II, J. D., Costa, R. M. & Carmena, J. M. Corticostriatal plasticity is necessary for learning intentional neuroprosthetic skills. *Nature* **483**, 331-335 (2012).

249. Kosaka, T., Katsumaru, H., Hama, K., Wu, J. -. & Heizmann, C. W. GABAergic neurons containing the Ca2+-binding protein parvalbumin in the rat hippocampus and dentate gyrus. *Brain Res.* **419**, 119-130 (1987).

250. Kowall, N. W., Ferrante, R. J. & Martin, J. B. Patterns of cell loss in Huntington's disease. *Trends Neurosci.* **10**, 24-29 (1987).

251. Kreitzer, A. C. Physiology and pharmacology of striatal neurons. *Annu. Rev. Neurosci.* **32**, 127-147 (2009).

252. Kreitzer, A. C. & Malenka, R. C. Dopamine modulation of state-dependent endocannabinoid release and long-term depression in the striatum. *J. Neurosci.* **25**, 10537-10545 (2005).

253. Kretsinger, R. H. Structure and evolution of calcium-modulated proteins. *CRC Crit. Rev. Biochem.* **8**, 119-174 (1980).

254. Kubota, Y. *et al*. Neuropeptide Y-immunoreactive neurons receive synaptic inputs from dopaminergic axon terminals in the rat neostriatum. *Brain Res.* **458**, 389-393 (1988).

255. Kubota, Y., Inagaki, S., Kito, S. & Wu, J. -. Dopaminergic axons directly make synapses with GABAergic neurons in the rat neostriatum. *Brain Res.* **406**, 147-156 (1987).

256. Kubota, Y., Ito, C., Kuramasu, A., Sato, M. & Watanabe, T. Transient increases of histamine H1 and H2 receptor mRNA levels in the rat striatum after the chronic administration of methamphetamine. *Neurosci. Lett.* **275**, 37-40 (1999).

257. Kubota, Y. & Kawaguchi, Y. Dependence of GABAergic synaptic areas on the interneuron type and target size. *J. Neurosci.* **20**, 375-386 (2000).

258. Kubota, Y. & Kawaguchi, Y. Spatial distributions of chemically identified intrinsic neurons in relation to patch and matrix compartments of rat neostriatum. *J. Comp. Neurol.* **332**, 499-513 (1993).

259. Kubota, Y., Mikawa, S. & Kawaguchi, Y. Neostriatal gabaergic interneurones contain nos, calretinin or parvalbumin. *Neuroreport* **5**, 205-208 (1993).

260. Kupchik, Y. M. *et al*. Coding the direct/indirect pathways by D1 and D2 receptors is not valid for accumbens projections. *Nat. Neurosci.* (2015).

261. Lachaux, J. -., Rodriguez, E., Martinerie, J. & Varela, F. J. Measuring phase synchrony in brain signals. *Hum. Brain Mapp.* **8**, 194-208 (1999).

262. Lansink, C. S. *et al*. A split microdrive for simultaneous multi-electrode recordings from two brain areas in awake small animals. *J. Neurosci. Methods* **162**, 129-138 (2007).

263. Lansink, C. S., Goltstein, P. M., Lankelma, J. V. & Pennartz, C. M. A. Fast-spiking interneurons of the rat ventral striatum: Temporal coordination of activity with principal cells and responsiveness to reward. *Eur. J. Neurosci.* **32**, 494-508 (2010).

264. Lapper, S. R. & Bolam, J. P. Input from the frontal cortex and the parafascicular nucleus to cholinergic interneurons in the dorsal striatum of the rat. *Neuroscience* **51**, 533-545 (1992).

265. Lapper, S. R., Smith, Y., Sadikot, A. F., Parent, A. & Bolam, J. P. Cortical input to parvalbumin-immunoreactive neurones in the putamen of the squirrel monkey. *Brain Res.* **580**, 215-224 (1992).

266. Larsson, E., Lindvall, O. & Kokaia, Z. Stereological assessment of vulnerability of immunocytochemically identified striatal and hippocampal neurons after global cerebral ischemia in rats. *Brain Res.* **913**, 117-132 (2001).

267. Lau, B. & Glimcher, P. W. Value Representations in the Primate Striatum during Matching Behavior. *Neuron* **58**, 451-463 (2008).

268. Lazar, A. A. & Slutskiy, Y. B. Spiking neural circuits with dendritic stimulus processors. *J. Comput. Neurosci.* (2014).

269. Lee, S., Hjerling-Leffler, J., Zagha, E., Fishell, G. & Rudy, B. The largest group of superficial neocortical GABAergic interneurons expresses ionotropic serotonin receptors. *J. Neurosci.* **30**, 16796-16808 (2010).

270. Lee, T., Kaneko, T., Taki, K. & Mizuno, N. Preprodynorphin-, preproenkephalin-, and preprotachykinin-expressing neurons in the rat neostriatum: An analysis by immunocytochemistry and retrograde tracing. *J. Comp. Neurol.* **386**, 229-244 (1997).

271. Lenz, S., Perney, T. M., Qin, Y., Robbins, E. & Chesselet, M. -. GABA-ergic interneurons of the striatum express the shaw-like potassium channel Kv3.1. *Synapse* **18**, 55-66 (1994).

272. London, M. & Häusser, M. Dendritic computation. *Annu. Rev. Neurosci.* **28**, 503-532 (2005).

273. Lopez-Huerta, V. G., Tecuapetla, F., Guzman, J. N., Bargas, J. & Galarraga, E. Presynaptic modulation by somatostatin in the neostriatum. *Neurochem. Res.* **33**, 1452-1458 (2008).

274. Lotharius, J. & Brundin, P. Pathogenesis of Parkinson's disease: dopamine, vesicles and alpha-synuclein. *Nat. Rev. Neurosci.* **3**, 932-942 (2002).

275. Lovinger, D. M., Tyler, E. C. & Merritt, A. Short- and long-term synaptic depression in rat neostriatum. *J. Neurophysiol.* **70**, 1937-1949 (1993).

276. Luk, K. C. & Sadikot, A. F. GABA promotes survival but not proliferation of parvalbumin-immunoreactive interneurons in rodent neostriatum: An in vivo study with stereology. *Neuroscience* **104**, 93-103 (2001).

277. Luzzati, F., De Marchis, S., Fasolo, A. & Peretto, P. Neurogenesis in the caudate nucleus of the adult rabbit. *J. Neurosci.* **26**, 609-621 (2006).

278. Ma, Y. *et al*. Morphological diversity of GABAergic and cholinergic interneurons in the striatal dorsolateral and ventromedial regions of rats. *Cell. Mol. Neurobiol.* **34**, 351-359 (2014).

279. Magill, P. J., Bolam, J. P. & Bevan, M. D. Relationship of activity in the subthalamic nucleus-globus pallidus network to cortical electroencephalogram. *J. Neurosci.* **20**, 820-833 (2000).

280. Magill, P. J. *et al*. Changes in functional connectivity within the rat striatopallidal axis during global brain activation in vivo. *J. Neurosci.* **26**, 6318-6329 (2006).

281. Magill, P. J., Sharott, A., Bevan, M. D., Brown, P. & Bolam, J. P. Synchronous unit activity and local field potentials evoked in the subthalamic nucleus by cortical stimulation. *J. Neurophysiol.* **92**, 700-714 (2004).

282. Magill, P. J., Sharott, A., Bolam, J. P. & Brown, P. Delayed synchronization of activity in cortex and subthalamic nucleus following cortical stimulation in the rat. *J. Physiol.* **574**, 929-946 (2006).

283. Magill, P. J., Sharott, A., Bolam, J. P. & Brown, P. Brain state-dependency of coherent oscillatory activity in the cerebral cortex and basal ganglia of the rat. *J. Neurophysiol.* **92**, 2122-2136 (2004).

284. Mahon, S., Deniau, J. -. & Charpier, S. Relationship between EEG potentials and intracellular activity of striatal and cortico-striatal neurons: An in vivo study under different anesthetics. *Cereb. Cortex* **11**, 360-373 (2001).

285. Mahon, S. *et al*. Distinct patterns of striatal medium spiny neuron activity during the natural sleep-wake cycle. *J. Neurosci.* **26**, 12587-12595 (2006).

286. Mailly, P., Aliane, V., Groenewegen, H. J., Haber, S. N. & Deniau, J. -. The rat prefrontostriatal system analyzed in 3D: Evidence for multiple interacting functional units. *J. Neurosci.* **33**, 5718-5727 (2013).

287. Mallet, N., Ballion, B., Le Moine, C. & Gonon, F. Cortical inputs and GABA interneurons imbalance projection neurons in the striatum of parkinsonian rats. *J. Neurosci.* **26**, 3875-3884 (2006).

288. Mallet, N., Le Moine, C., Charpier, S. & Gonon, F. Feedforward inhibition of projection neurons by fast-spiking GABA interneurons in the rat striatum in vivo. *J. Neurosci.* **25**, 3857-3869 (2005).

289. Mallet, N. *et al*. Dichotomous Organization of the External Globus Pallidus. *Neuron* **74**, 1075-1086 (2012).

290. Mallet, N. *et al*. Parkinsonian beta oscillations in the external globus pallidus and their relationship with subthalamic nucleus activity. *J. Neurosci.* **28**, 14245-14258 (2008).

291. Marilley, D. & Schwaller, B. Association between the calcium-binding protein calretinin and cytoskeletal components in the human colon adenocarcinoma cell line WiDr. *Exp. Cell Res.* **259**, 12-22 (2000).

292. Marín, O. Origin of cortical interneurons: Basic concepts and clinical implications. *Rev. Neurol.* **35**, 743-751 (2002).

293. Marín, O., Anderson, S. A. & Rubenstein, J. L. R. Origin and molecular specification of striatal interneurons. *J. Neurosci.* **20**, 6063-6076 (2000).

294. Martínez-Cerdeño, V. *et al*. Embryonic MGE Precursor Cells Grafted into Adult Rat Striatum Integrate and Ameliorate Motor Symptoms in 6-OHDA-Lesioned Rats. *Cell Stem Cell* **6**, 238-250 (2010).

295. Massi, L. *et al*. Temporal dynamics of parvalbumin-expressing axo-axonic and basket cells in the rat medial prefrontal cortex in vivo. *J. Neurosci.* **32**, 16496-16502 (2012).

296. Massouh, M., Wallman, M. -., Pourcher, E. & Parent, A. The fate of the large striatal interneurons expressing calretinin in Huntington's disease. *Neurosci. Res.* **62**, 216-224 (2008).

297. Matsuda, W. *et al*. Single nigrostriatal dopaminergic neurons form widely spread and highly dense axonal arborizations in the neostriatum. *J. Neurosci.* **29**, 444-453 (2009).

298. Matsumoto, Y., Yoshida, M., Watanabe, S. & Yamamoto, T. Involvement of cholinergic and glutamatergic functions in working memory impairment induced by interleukin-1ß in rats. *Eur. J. Pharmacol.* **430**, 283-288 (2001).

299. Matthews, E. A. & Dietrich, D. Buffer mobility and the regulation of neuronal calcium domains. *Front. Cell. Neurosci.* **9** (2015).

300. Maurice, N., Deniau, J. -., Glowinski, J. & Thierry, A. -. Relationships between the prefrontal cortex and the basal ganglia in the rat: Physiology of the cortico-nigral circuits. *J. Neurosci.* **19**, 4674-4681 (1999).

301. Maurice, N., Deniau, J. M., Menetrey, A., Glowinski, J. & Thierry, A. M. Position of the ventral pallidum in the rat prefrontal cortex-basal ganglia circuit. *Neuroscience* **80**, 523-534 (1997).

302. Maurice, N. *et al*. D2 dopamine receptor-mediated modulation of voltage-dependent Na+ channels reduces autonomous activity in striatal cholinergic interneurons. *J. Neurosci.* **24**, 10289-10301 (2004).

303. Mayer, C. *et al*. Clonally Related Forebrain Interneurons Disperse Broadly across Both Functional Areas and Structural Boundaries. *Neuron* **87**, 989-998 (2015).

304. McGeorge, A. J. & Faull, R. L. M. The organization of the projection from the cerebral cortex to the striatum in the rat. *Neuroscience* **29**, 503-537 (1989).

305. McGinty, J. F., Zelek-Molik, A. & Sun, W. -. Cocaine self-administration causes signaling deficits in corticostriatal circuitry that are reversed by BDNF in early withdrawal. *Brain Res.* (2013).

306. McKinsey, G. L. *et al*. Dlx1&2-Dependent Expression of Zfhx1b (Sip1, Zeb2) Regulates the Fate Switch between Cortical and Striatal Interneurons. *Neuron* **77**, 83-98 (2013).

307. Meredith, G. E., Blank, B. & Groenewegen, H. J. The distribution and compartmental organization of the cholinergic neurons in nucleus accumbens of the rat. *Neuroscience* **31**, 327-345 (1989).

308. Middleton, F. A. & Strick, P. L. Basal ganglia output and cognition: Evidence from anatomical, behavioral, and clinical studies. *Brain Cogn.* **42**, 183-200 (2000).

309. Middleton, F. A. & Strick, P. L. Basal ganglia and cerebellar loops: Motor and cognitive circuits. *Brain Res. Rev.* **31**, 236-250 (2000).

310. Milovanovic, D. & Jahn, R. Organization and dynamics of SNARE proteins in the presynaptic membrane. *Front. Physiol.* **6** (2015).

311. Misgeld, U. Innervation of the substantia nigra. *Cell Tissue Res.* **318**, 107-114 (2004).

312. Mogenson, G. J., Swanson, L. W. & Wu, M. Neural projections from nucleus accumbens to globus pallidus, substantia innominata, and lateral preoptic-lateral hypothalamic area: An anatomical and electrophysiological investigation in the rat. *J. Neurosci.* **3**, 189-202 (1983).

313. Morris, G., Arkadir, D., Nevet, A., Vaadia, E. & Bergman, H. Coincident but distinct messages of midbrain dopamine and striatal tonically active neurons. *Neuron* **43**, 133-143 (2004).

314. Morrow, B. A., Redmond Jr., D. E., Roth, R. H. & Elsworth, J. D. Development of A9/A10 dopamine neurons during the second and third trimesters in the African green monkey. *J. Comp. Neurol.* **488**, 215-223 (2005).

315. Moss, J. & Bolam, J. P. A dopaminergic axon lattice in the striatum and its relationship with cortical and thalamic terminals. *J. Neurosci.* **28**, 11221-11230 (2008).

316. Mulder, J. *et al*. Secretagogin is a Ca2+-binding protein identifying prospective extended amygdala neurons in the developing mammalian telencephalon. *Eur. J. Neurosci.* **31**, 2166-2177 (2010).

317. Mulder, J. *et al*. Secretagogin is a Ca2+-binding protein specifying subpopulations of telencephalic neurons. *Proc. Natl. Acad. Sci. U. S. A.* **106**, 22492-22497 (2009).

318. Mullen, R. J., Buck, C. R. & Smith, A. M. NeuN, a neuronal specific nuclear protein in vertebrates. *Development* **116**, 201-211 (1992).

319. Müller, A. *et al*. Endogenous Ca2+ buffer concentration and Ca2+ microdomains in hippocampal neurons. *J. Neurosci.* **25**, 558-565 (2005).

320. A.B. Munoz-Manchado, C. Foldi, S. Szydlowski, L. Sjulson, M. Farries, C. Wilson, G. Silberberg, J. Hjerling-Leffler. Novel striatal GABAergic interneuron populations labeled in the 5HT3aEGFP mouse. *Cereb. Cortex* (2014).

321. Mura, A., Linder, J. C., Young, S. J. & Groves, P. M. Striatal cells containing aromatic L-amino acid decarboxylase: An immunohistochemical comparison with other classes of striatal neurons. *Neuroscience* **98**, 501-511 (2000).

322. Nakamura, K. C., Sharott, A. & Magill, P. J. Temporal coupling with cortex distinguishes spontaneous neuronal activities in identified basal ganglia-recipient and cerebellar-recipient zones of the motor thalamus. *Cereb. Cortex* **24**, 81-97 (2014).

323. Navailles, S., Carta, M., Guthrie, M. & de Deurwaerdère, P. L-dopa and serotonergic neurons: Functional implication and therapeutic perspectives in parkinson's disease. *Cent. Nerv. Syst. Agents Med. Chem.* **11**, 305-320 (2011).

324. Navailles, S. & De Deurwaerdère, P. Presynaptic control of serotonin on striatal dopamine function. *Psychopharmacology* **213**, 213-242 (2011).

325. Nicola, S. M., James Surmeier, D. & Malenka, R. C. Dopaminergic modulation of neuronal excitability in the striatum and nucleus accumbens. *Annu. Rev. Neurosci.* **23**, 185-215 (2000).

326. Nisenbaum, E. S. & Wilson, C. J. Potassium currents responsible for inward and outward rectification in rat neostriatal spiny projection neurons. *J. Neurosci.* **15**, 4449-4463 (1995).

327. Nisenbaum, E. S., Wilson, C. J., Foehring, R. C. & Surmeier, D. J. Isolation and characterization of a persistent potassium current in neostriatal neurons. *J. Neurophysiol.* **76**, 1180-1194 (1996).

328. Niv, Y. & Schoenbaum, G. Dialogues on prediction errors. *Trends Cogn. Sci.* **12**, 265-272 (2008).

329. Noble, W. S. How does multiple testing correction work? *Nat. Biotechnol.* **27**, 1135-1137 (2009).

330. Nóbrega-Pereira, S. *et al*. Postmitotic Nkx2-1 Controls the Migration of Telencephalic Interneurons by Direct Repression of Guidance Receptors. *Neuron* **59**, 733-745 (2008).

331. Olucha-Bordonau, F. E. *et al*. Distribution and targets of the relaxin-3 innervation of the septal area in the rat. *J. Comp. Neurol.* **520**, 1903-1939 (2012).

332. Ölveczky, B. P., Andalman, A. S. & Fee, M. S. Vocal experimentation in the juvenile songbird requires a basal ganglia circuit. *PloS Biol.* **3**, 0902-0909 (2005).

333. Oorschot, D. E. The percentage of interneurons in the dorsal striatum of the rat, cat, monkey and human: A critique of the evidence. *Basal Ganglia* **3**, 19-24 (2013).

334. Oorschot, D. E. Total number of neurons in the neostriatal, pallidal, subthalamic, and substantia nigral nuclei of the rat basal ganglia: A stereological study using the cavalieri and optical disector methods. *J. Comp. Neurol.* **366**, 580-599 (1996).

335. Oorschot, D. E. Are you using neuronal densities, synaptic densities or neurochemical densities as your definitive data? there is a better way to go. *Prog. Neurobiol.* **44**, 233-247 (1994).

336. Oorschot, D.E. Zhang, R. Wickens, J.R. Absolute number and three-dimensional spatial distribution of rat neostriatal large interneurons: a first and second order stereological study. *Proceedings of the Xth International Congress of Stereology*. p. 87, (1999).

337. Ordoñez, C. *et al*. Sox-2 Positive Neural Progenitors in the Primate Striatum Undergo Dynamic Changes after Dopamine Denervation. *PLoS ONE* **8** (2013).

338. Orduz, D., Bischop, D. P., Schwaller, B., Schiffmann, S. N. & Gall, D. Parvalbumin tunes spike-timing and efferent short-term plasticity in striatal fast spiking interneurons. *J. Physiol.* **591**, 3215-3232 (2013).

339. Oswald, L. M. *et al*. Relationships among ventral striatal dopamine release, cortisol secretion, and subjective responses to amphetamine. *Neuropsychopharmacology* **30**, 821-832 (2005).

340. Overstreet-Wadiche, L. & McBain, C. J. Neurogliaform cells in cortical circuits. *Nat. Rev. Neurosci.* **16**, 458-468 (2015).

341. Pan, W. X., Mao, T. & Dudman, J. T. Inputs to the dorsal striatum of the mouse reflect the parallel circuit architecture of the forebrain. *Front. Neuroanat.* (2010).

342. Pang, Z. P. & Südhof, T. C. Cell biology of Ca2+-triggered exocytosis. *Curr. Opin. Cell Biol.* **22**, 496-505 (2010).

343. Pangas, S. A. *et al*. Oogenesis requires germ cell-specific transcriptional regulators Sohlh1 and Lhx8. *Proc. Natl. Acad. Sci. U. S. A.* **103**, 8090-8095 (2006).

344. Parent, A. Extrinsic connections of the basal ganglia. *Trends Neurosci.* **13**, 254-258 (1990).

345. Parent, A., Cicchetti, F. & Beach, T. G. Calretinin-immunoreactive neurons in the human striatum. *Brain Res.* **674**, 347-351 (1995).

346. Parent, A., Côté, P. -. & Lavoie, B. Chemical anatomy of primate basal ganglia. *Prog. Neurobiol.* **46**, 131-197 (1995).

347. Parent, A. & Hazrati, L. -. Functional anatomy of the basal ganglia. I. The cortico-basal ganglia-thalamo-cortical loop. *Brain Res. Rev.* **20**, 91-127 (1995).

348. Park, H. -. *et al*. The distribution and morphology of calbindin D28K- and calretinin-immunoreactive neurons in the visual cortex of mouse. *Mol. Cells* **14**, 143-149 (2002).

349. Parthasarathy, H. B. & Graybiel, A. M. Cortically driven immediate-early gene expression reflects modular influence of sensorimotor cortex on identified striatal neurons in the squirrel monkey. *J. Neurosci.* **17**, 2477-2491 (1997).

350. Partridge, J. G. *et al*. Excitatory and inhibitory synapses in neuropeptide Y-expressing striatal interneurons. *J. Neurophysiol.* **102**, 3038-3045 (2009).

351. Parush, N., Tishby, N. & Bergman, H. Dopaminergic balance between reward maximization and policy complexity. *Front. Syst. Neurosci.* (2011).

352. Paxinos, G., Huang, X., and Toga, A. The Rhesus Monkey Brain in Stereotaxic Coordinates *San Diego: Academic Press*. (2000).

353. Paxinos G, Watson C. The rat brain in Stereotaxic Coordinates **6th ed.** *London: Academic Press*. (2007).

354. Pecze, L., Blum, W. & Schwaller, B. Mechanism of capsaicin receptor TRPV1-mediated toxicity in pain-sensing neurons focusing on the effects of Na+/Ca2+ fluxes and the Ca2+-binding protein calretinin. *Biochim. Biophys. Acta Mol. Cell Res.* **1833**, 1680-1691 (2013).

355. Petryszyn, S., Beaulieu, J. -., Parent, A. & Parent, M. Distribution and morphological characteristics of striatal interneurons expressing calretinin in mice: A comparison with human and nonhuman primates. *J. Chem. Neuroanat.* **59-60**, 51-61 (2014).

356. Phelps, P. E., Houser, C. R. & Vaughn, J. E. Immunocytochemical localization of choline acetyltransferase within the rat neostriatum: A correlated light and electron microscopic study of cholinergic neurons and synapses. *J. Comp. Neurol.* **238**, 286-307 (1985).

357. Pickel, V. M., Chan, J. & Sesack, S. R. Cellular basis for interactions between catecholaminergic afferents and neurons containing Leu-enkephalin-like immunoreactivity in rat caudate- putamen nuclei. *J. Neurosci. Res.* **31**, 212-230 (1992).

358. Planert, H., Szydlowski, S. N., Hjorth, J. J. J., Grillner, S. & Silberberg, G. Dynamics of synaptic transmission between fast-spiking interneurons and striatal projection neurons of the direct and indirect pathways. *J. Neurosci.* **30**, 3499-3507 (2010).

359. Plenz, D. & Kitai, S. T. Up and down states in striatal medium spiny neurons simultaneously recorded with spontaneous activity in fast-spiking interneurons studied in cortex-striatum-substantia nigra organotypic cultures. *J. Neurosci.* **18**, 266-283 (1998).

360. Plenz, D. & Kital, S. T. A basal ganglia pacemaker formed by the subthalamic nucleus and external globus pallidus. *Nature* **400**, 677-682 (1999).

361. Plotkin, J. L., Wu, N., Chesselet, M. -. & Levine, M. S. Functional and molecular development of striatal fast-spiking GABAergic interneurons and their cortical inputs. *Eur. J. Neurosci.* **22**, 1097-1108 (2005).

362. Pollard, H., Moreau, J., Arrang, J. M. & Schwartz, J. C. A detailed autoradiographic mapping of histamine H3 receptors in rat brain areas. *Neuroscience* **52**, 169-189 (1993).

363. Postuma, R. B. & Dagher, A. Basal ganglia functional connectivity based on a meta-analysis of 126 positron emission tomography and functional magnetic resonance imaging publications. *Cereb. Cortex* **16**, 1508-1521 (2006).

364. Prast, H., Fischer, H. & Philippu, A. Release of acetylcholine in the ventral striatum is influenced by histamine receptors. *Agents Actions* **41**, C85-C86 (1994).

365. Prast, H. *et al*. Modulation of acetylcholine release in the ventral striatum by histamine receptors. *Inflamm. Res.* **46**, S37-S38 (1997).

366. Prensa, L., Giménez-Amaya, J. M. & Parent, A. Morphological features of neurons containing calcium-binding proteins in the human striatum. *J. Comp. Neurol.* **390**, 552-563 (1998).

367. Prensa, L., Richard, S. & Parent, A. Chemical anatomy of the human ventral striatum and adjacent basal forebrain structures. *J. Comp. Neurol.* **460**, 345-367 (2003).

368. Preston, R. J., Bishop, G. A. & Kitai, S. T. Medium spiny neuron projection from the rat striatum: An intracellular horseradish peroxidase study. *Brain Res.* **183**, 253-263 (1980).

369. Prochiantz, A. & Di Nardo, A. A. Homeoprotein signaling in the developing and adult nervous system. *Neuron* **85**, 911-925 (2015).

370. Pruitt KD, Brown GR, Hiatt SM, Thibaud-Nissen F, Astashyn A, Ermolaeva O, Farrell CM, Hart J, Landrum MJ, McGarvey KM, Murphy MR, O'Leary NA, Pujar S, Rajput B, Rangwala SH, Riddick LD, Shkeda A, Sun H, Tamez P, Tully RE, Wallin C, Webb D, Weber J, Wu W, Dicuccio M, Kitts P, Maglott DR, Murphy TD, Ostell JM. RefSeq: an update on mammalian reference sequences. *Nucleic Acids Res.* (2013).

371. Qin, Y., Ouyang, Q., Pablo, J. & Mash, D. C. Cocaine abuse elevates alpha-synuclein and dopamine transporter levels in the human striatum. *Neuroreport* **16**, 1489-1493 (2005).

372. Rats!. Editorial. Nature Methods, Vol. 7, No. 6 (2010, June 20).

373. Ravel, S., Legallet, E. & Apicella, P. Tonically active neurons in the monkey striatum do not preferentially respond to appetitive stimuli. *Exp. Brain Res.* **128**, 531-534 (1999).

374. Reddy, P. P. *et al*. Molecular dynamics of the neuronal EF-hand Ca2+-sensor Caldendrin. *PLoS ONE* **9** (2014).

375. Reig, R. & Silberberg, G. Multisensory Integration in the Mouse Striatum. *Neuron* **83**, 1200-1212 (2014).

376. Revishchin, A. V., Okhotin, V. E., Korochkin, L. I. & Pavlova, G. V. A new population of calretinin-positive cells, presumptively neurons, with polymorphous spines in the mouse forebrain. *Neurosci. Behav. Physiol.* **40**, 541-552 (2010).

377. Revishchin, A. V., Okhotin, V. E. & Pavlova, G. V. New calretinin-positive cells with polymorphous spines in the mouse forebrain during early postnatal ontogeny. *Neurosci. Behav. Physiol.* **40**, 833-840 (2010).

378. Reynolds, J. N. J., Hyland, B. I. & Wickens, J. R. A cellular mechanism of reward-related learning. *Nature* **413**, 67-70 (2001).

379. Rice, M. E. & Cragg, S. J. Dopamine spillover after quantal release: Rethinking dopamine transmission in the nigrostriatal pathway. *Brain Res. Rev.* **58**, 303-313 (2008).

380. Roesch, M. R., Singh, T., Leon Brown, P., Mullins, S. E. & Schoenbaum, G. Ventral striatal neurons encode the value of the chosen action in rats deciding between differently delayed or sized rewards. *J. Neurosci.* **29**, 13365-13376 (2009).

381. Rogstam, A. *et al*. Binding of calcium ions and SNAP-25 to the hexa EF-hand protein secretagogin. *Biochem. J.* **401**, 353-363 (2007).

382. Romanov, R. A. *et al*. A secretagogin locus of the mammalian hypothalamus controls stress hormone release. *EMBO J.* **34**, 36-54 (2015).

383. Rudy, B. & McBain, C. J. Kv3 channels: Voltage-gated K+ channels designed for high-frequency repetitive firing. *Trends Neurosci.* **24**, 517-526 (2001).

384. Rymar, V. V., Sasseville, R., Luk, K. C. & Sadikot, A. F. Neurogenesis and Stereological Morphometry of Calretinin-Immunoreactive GABAergic Interneurons of the Neostriatum. *J. Comp. Neurol.* **469**, 325-339 (2004).

385. Sadek, A. R., Magill, P. J. & Bolam, J. P. A single-cell analysis of intrinsic connectivity in the rat globus pallidus. *J. Neurosci.* **27**, 6352-6362 (2007).

386. Sakagami, H. *et al*. Distinct synaptic localization patterns of brefeldin A-resistant guanine nucleotide exchange factors BRAG2 and BRAG3 in the mouse retina. *J. Comp. Neurol.* **521**, 860-876 (2013).

387. Sargolini, F., Roullet, P., Oliverio, A. & Mele, A. Effects of intra-accumbens focal administrations of glutamate antagonists on object recognition memory in mice. *Behav. Brain Res.* **138**, 153-163 (2003).

388. Sarnat, H. B., Nochlin, D. & Born, D. E. Neuronal nuclear antigen (NeuN): A marker of neuronal maturation in the early human fetal nervous system. *Brain Dev.* **20**, 88-94 (1998).

389. Schlösser, B., Klausa, G., Prime, G. & Bruggencate, G. T. Postnatal development of calretinin- and parvalbumin-positive interneurons in the rat neostriatum: An immunohistochemical study. *J. Comp. Neurol.* **405**, 185-198 (1999).

390. Schmidt, R., Leventhal, D. K., Mallet, N., Chen, F. & Berke, J. D. Canceling actions involves a race between basal ganglia pathways. *Nat. Neurosci.* **16**, 1118-1124 (2013).

391. Schoenbaum, G., Saddoris, M. P. & Stalnaker, T. A. Reconciling the roles of orbitofrontal cortex in reversal learning and the encoding of outcome expectancies. *Ann. New York Acad. Sci.* **1121**, 320-335 (2007).

392. Schultz, W. Dopamine signals for reward value and risk: Basic and recent data. *Behav. Brain Funct.* **6** (2010).

393. Schultz, W. Dopamine neurons and their role in reward mechanisms. *Curr. Opin. Neurobiol.* **7**, 191-197 (1997).

394. Schultz, W. The Phasic Reward Signal of Primate Dopamine Neurons. *Adv. Pharmacol.* **42**, 686-690 (1997).

395. Schultz, W., Dayan, P. & Montague, P. R. A neural substrate of prediction and reward. *Science* **275**, 1593-1599 (1997).

396. Schultz, W., Tremblay, L. & Hollerman, J. R. Reward prediction in primate basal ganglia and frontal cortex. *Neuropharmacology* **37**, 421-429 (1998).

397. Schwaller, B., Durussel, I., Jermann, D., Herrmann, B. & Cox, J. A. Comparison of the Ca2+-binding properties of human recombinant calretinin-22k and calretinin. *J. Biol. Chem.* **272**, 29663-29671 (1997).

398. Schwaller, B., Meyer, M. & Schiffmann, S. 'New' functions for 'old' proteins: The role of the calcium-binding proteins calbindin D-28k, calretinin and parvalbumin, in cerebellar physiology. Studies with knockout mice. *Cerebellum* **1**, 241-258 (2002).

399. Schwaller, B. *et al*. Parvalbumin deficiency affects network properties resulting in increased susceptibility to epileptic seizures. *Mol. Cell. Neurosci.* **25**, 650-663 (2004).

400. Schwartz, R. D., Lehmann, J. & Kellar, K. J. Presynaptic nicotinic cholinergic receptors labeled by [3H]acetylcholine on catecholamine and serotonin axons in brain. *J. Neurochem.* **42**, 1495-1498 (1984).

401. Sesack, S. R., Aoki, C. & Pickel, V. M. Ultrastructural localization of D2 receptor-like immunoreactivity in midbrain dopamine neurons and their striatal targets. *J. Neurosci.* **14**, 88-106 (1994).

402. Sharott, A., Doig, N. M., Mallet, N. & Magill, P. J. Relationships between the firing of identified striatal interneurons and spontaneous and driven cortical activities in vivo. *J. Neurosci.* **32**, 13221-13236 (2012).

403. Shink, E., Bevan, M. D., Bolam, J. P. & Smith, Y. The subthalamic nucleus and the external pallidum: Two tightly interconnected structures that control the output of the basal ganglia in the monkey. *Neuroscience* **73**, 335-357 (1996).

404. Siapas, A. G., Lubenov, E. V. & Wilson, M. A. Prefrontal phase locking to hippocampal theta oscillations. *Neuron* **46**, 141-151 (2005).

405. Silberberg, G. & Bolam, J. P. Local and afferent synaptic pathways in the striatal microcircuitry. *Curr. Opin. Neurobiol.* **33** (2015).

406. Simmons, D. A. & Yahr, P. Nitric oxidergic cells related to ejaculation in gerbil forebrain contain androgen receptor and respond to testosterone. *J. Comp. Neurol.* **519**, 900-915 (2011).

407. Simmons, D. D., Tong, B., Schrader, A. D. & Hornak, A. J. Oncomodulin identifies different hair cell types in the mammalian inner ear. *J. Comp. Neurol.* **518**, 3785-3802 (2010).

408. Smith, K. S. & Graybiel, A. M. Investigating habits: Strategies, technologies and models. *Front. Behav. Neurosci.* **8** (2014).

409. Smith, R. *et al*. Cholinergic neuronal defect without cell loss in Huntington's disease. *Hum. Mol. Genet.* **15**, 3119-3131 (2006).

410. Smith, Y., Bennett, B. D., Bolam, J. P., Parent, A. & Sadikot, A. F. Synaptic relationships between dopaminergic afferents and cortical or thalamic input in the sensorimotor territory of the striatum in monkey. *J. Comp. Neurol.* **344**, 1-19 (1994).

411. Smith, Y., Bevan, M. D., Shink, E. & Bolam, J. P. Microcircuitry of the direct and indirect pathways of the basal ganglia. *Neuroscience* **86**, 353-387 (1998).

412. Smith, Y. & Kieval, J. Z. Anatomy of the dopamine system in the basal ganglia. *Trends Neurosci.* **23**, S28-S33 (2000).

413. Smith, Y. & Parent, A. Neuropeptide Y-immunoreactive neurons in the striatum of cat and monkey: Morphological characteristics, intrinsic organization and co-localization with somatostatin. *Brain Res.* **372**, 241-252 (1986).

414. Smith, Y., Shink, E. & Sidibe, M. Neuronal circuitry and synaptic connectivity of the basal ganglia. *Neurosurg. Clin. North Am.* **9**, 203-222 (1998).

415. Somogyi, P., Bolam, J. P. & Smith, A. D. Monosynaptic cortical input and local axon collaterals of identified striatonigral neurons. A light and electron microscopic study using the Golgi-peroxidase transport-degeneration procedure. *J. Comp. Neurol.* **195**, 567-584 (1981).

416. Somogyi, P. & Klausberger, T. Defined types of cortical interneurone structure space and spike timing in the hippocampus. *J. Physiol.* **562**, 9-26 (2005).

417. Somogyi, P. & Smith, A. D. Projection of neostriatal spiny neurons to the substantia nigra. Application of a combined golgi-staining and horse-radish peroxidase transport procedure at both light and electron microscopic levels. *Brain Res.* **178**, 3-15 (1979).

418. Soomro, G. M., Altman, D., Rajagopal, S. & Oakley-Browne, M. Selective serotonin re-uptake inhibitors (SSRIs) versus placebo for obsessive compulsive disorder (OCD). *Cochrane Database Syst. Rev.* (2008).

419. Stacy, R. C., Demas, J., Burgess, R. W., Sanes, J. R. & Wong, R. O. L. Disruption and recovery of patterned retinal activity in the absence of acetylcholine. *J. Neurosci.* **25**, 9347-9357 (2005).

420. Stalnaker, T. A., Calhoon, G. G., Ogawa, M., Roesch, M. R. & Schoenbaum, G. Reward prediction error signaling in posterior dorsomedial striatum is action specific. *J. Neurosci.* **32**, 10296-10305 (2012).

421. Stalnaker, T. A., Calhoon, G. G., Ogawa, M., Roesch, M. R. & Schoenbaum, G. Neural correlates of stimulus-response and response-outcome associations in dorsolateral versus dorsomedial striatum. *Front. Integr. Neurosci.* (2010).

422. Stateva, S. R., Salas, V., Anguita, E., Benaim, G. & Villalobo, A. Ca2+/calmodulin and apo-calmodulin both bind to and enhance the tyrosine kinase activity of c-Src. *PLoS ONE* **10** (2015).

423. Stephenson-Jones, M., Samuelsson, E., Ericsson, J., Robertson, B. & Grillner, S. Evolutionary conservation of the basal ganglia as a common vertebrate mechanism for action selection. *Curr. Biol.* **21**, 1081-1091 (2011).

424. Steriade, M. Corticothalamic resonance, states of vigilance and mentation. *Neuroscience* **101**, 243-276 (2000).

425. Stern, E. A., Jaeger, D. & Wilson, C. J. Membrane potential synchrony of simultaneously recorded striatal spiny neuronsin vivo. *Nature* **394**, 475-478 (1998).

426. Sul, J. H., Kim, H., Huh, N., Lee, D. & Jung, M. W. Distinct roles of rodent orbitofrontal and medial prefrontal cortex in decision making. *Neuron* **66**, 449-460 (2010).

427. Surmeier, D. J., Ding, J., Day, M., Wang, Z. & Shen, W. D1 and D2 dopamine-receptor modulation of striatal glutamatergic signaling in striatal medium spiny neurons. *Trends Neurosci.* **30**, 228-235 (2007).

428. Surmeier, D. J., Song, W. -. & Yan, Z. Coordinated expression of dopamine receptors in neostriatal medium spiny neurons. *J. Neurosci.* **16**, 6579-6591 (1996).

429. Szydlowski, S. N. *et al*. Target selectivity of feedforward inhibition by striatal fast-spiking interneurons. *J. Neurosci.* **33**, 1678-1683 (2013).

430. Tamura, S., Morikawa, Y., Iwanishi, H., Hisaoka, T. & Senba, E. Foxp1 gene expression in projection neurons of the mouse striatum. *Neuroscience* **124**, 261-267 (2004).

431. Tassin, J. P., Cheramy, A., Blanc, G., Thierry, A. M. & Glowinski, J. Topographical distribution of dopaminergic innervation and of dopaminergic receptors in the rat striatum. I. Microestimation of [3H]dopamine uptake and dopamine content in microdiscs. *Brain Res.* **107**, 291-301 (1976).

432. Taverna, S., Van Dongen, Y. C., Groenewegen, H. J. & Pennartz, C. M. A. Direct Physiological Evidence for Synaptic Connectivity between Medium-Sized Spiny Neurons in Rat Nucleus Accumbens In Situ. *J. Neurophysiol.* **91**, 1111-1121 (2004).

433. Tepper, J. M. & Bolam, J. P. Functional diversity and specificity of neostriatal interneurons. *Curr. Opin. Neurobiol.* **14**, 685-692 (2004).

434. Tepper, J. M., Koós, T. & Wilson, C. J. GABAergic microcircuits in the neostriatum. *Trends Neurosci.* **27**, 662-669 (2004).

435. Tepper, J. M., Tecuapetla, F., Koós, T. & Ibáñez-Sandoval, O. Heterogeneity and diversity of striatal GABAergic interneurons. *Front. Neuroanat.* (2010).

436. Thomas, T. M., Smith, Y., Levey, A. I. & Hersch, S. M. Cortical inputs to m2-immunoreactive striatal interneurons in rat and monkey. *Synapse* **37**, 252-261 (2000).

437. Thorn, C. A., Atallah, H., Howe, M. & Graybiel, A. M. Differential Dynamics of Activity Changes in Dorsolateral and Dorsomedial Striatal Loops during Learning. *Neuron* **66**, 781-795 (2010).

438. Threlfell, S. *et al*. Striatal dopamine release is triggered by synchronized activity in cholinergic interneurons. *Neuron* **75**, 58-64 (2012).

439. Todtenkopf, M. S., Stellar, J. R., Williams, E. A. & Zahm, D. S. Differential distribution of parvalbumin immunoreactive neurons in the striatum of cocaine sensitized rats. *Neuroscience* **127**, 35-42 (2004).

440. Totterdell, S. & Meredith, G. E. Topographical organization of projections from the entorhinal cortex to the striatum of the rat. *Neuroscience* **78**, 715-729 (1997).

441. Tricoire, L. *et al*. Common origins of hippocampal ivy and nitric oxide synthase expressing neurogliaform cells. *J. Neurosci.* **30**, 2165-2176 (2010).

442. Tukker, J. J. *et al*. Distinct dendritic arborization and in vivo firing patterns of parvalbumin-expressing basket cells in the hippocampal area CA3. *J. Neurosci.* **33**, 6809-6825 (2013).

443. Tziortzi, A. C. *et al*. Connectivity-based functional analysis of dopamine release in the striatum using diffusion-weighted MRI and positron emission tomography. *Cereb. Cortex* **24**, 1165-1177 (2014).

444. Ünal, B., Ibáñez-Sandoval, O., Shah, F., Abercrombie, E. D. & Tepper, J. M. Distribution of tyrosine hydroxylase-expressing interneurons with respect to anatomical organization of the neostriatum. *Front. Syst. Neurosci.* (2011).

445. Ünal, B., Shah, F., Kothari, J. & Tepper, J. M. Anatomical and electrophysiological changes in striatal TH interneurons after loss of the nigrostriatal dopaminergic pathway. *Brain Struct. Funct.*, 1-19 (2013).

446. Usuda, I., Tanaka, K. & Chiba, T. Efferent projections of the nucleus accumbens in the rat with special reference to subdivision of the nucleus: Biotinylated dextran amine study. *Brain Res.* **797**, 73-93 (1998).

447. Van Dongen, Y. C. *et al*. Anatomical evidence for direct connections between the shell and core subregions of the rat nucleus accumbens. *Neuroscience* **136**, 1049-1071 (2005).

448. Villar-Cerviño, V. *et al*. Molecular mechanisms controlling the migration of striatal interneurons. *J. Neurosci.* **35**, 8718-8729 (2015).

449. Vincent, S. R. & Johansson, O. Striatal neurons containing both somatostatin- and avian pancreatic polypeptide (APP)-like immunoreactivities and NADPH-diaphorase activity: A light and electron microscopic study. *J. Comp. Neurol.* **217**, 264-270 (1983).

450. Viney, T. J. *et al*. Network state-dependent inhibition of identified hippocampal CA3 axo-axonic cells in vivo. *Nat. Neurosci.* **16**, 1802-1811 (2013).

451. Volkow, N. D. *et al*. Effects of chronic cocaine abuse on postsynaptic dopamine receptors. *Am. J. Psychiatry* **147**, 719-724 (1990).

452. Volkow, N. D. & Li, T. -. Drug addiction: The neurobiology of behaviour gone awry. *Nat. Rev. Neurosci.* **5**, 963-970 (2004).

453. Von Engelhardt, J., Eliava, M., Meyer, A. H., Rozov, A. & Monyer, H. Functional characterization of intrinsic cholinergic interneurons in the cortex. *J. Neurosci.* **27**, 5633-5642 (2007).

454. Vuillet, J., Dimova, R. -., Nieoullon, A. & Goff, L. K. -. Ultrastructural relationships between choline acetyltransferase- and neuropeptide Y-containing neurons in the rat striatum. *Neuroscience* **46**, 351-360 (1992).

455. Vuillet, J., Kerkerian, L., Kachidian, P., Bosler, O. & Nieoullon, A. Ultrastructural correlates of functional relationships between nigral dopaminergic or cortical afferent fibers and neuropeptide Y-containing neurons in the rat striatum. *Neurosci. Lett.* **100**, 99-104 (1989).

456. Wagner, L. *et al*. Cloning and expression of secretagogin, a novel neuroendocrine- and pancreatic islet of Langerhans-specific Ca2+-binding protein. *J. Biol. Chem.* **275**, 24740-24751 (2000).

457. Wall, N., DeLaParra, M., Callaway, E. & Kreitzer, A. Differential innervation of direct- and indirect-pathway striatal projection neurons. *Neuron* **79**, 347-360 (2013).

458. Walsh, J. P. Depression of excitatory synaptic input in rat striatal neurons. *Brain Res.* **608**, 123-128 (1993).

459. Walsh, J. P. & Dunia, R. Synaptic activation of N-methyl-d-aspartate receptors induces short-term potentiation at excitatory synapses in the striatum of the rat. *Neuroscience* **57**, 241-248 (1993).

460. Wang, B., Lufkin, T. & Rubenstein, J. L. R. Dlx6 regulates molecular properties of the striatum and central nucleus of the amygdala. *J. Comp. Neurol.* **519**, 2320-2334 (2011).

461. Wei, H., Lang, M. -. & Jiang, X. Calretinin is expressed in the intermediate cells during olfactory receptor neuron development. *Neurosci. Lett.* **542**, 42-46 (2013).

462. Weiner, I. Neural substrates of latent inhibition: The switching model. *Psychol. Bull.* **108**, 442-461 (1990).

463. West, A. E. & Greenberg, M. E. Neuronal activity-regulated gene transcription in synapse development and cognitive function. *Cold Spring Harbor Perspect. Biol.* **3**, 1-21 (2011).

464. West, M. J. Stereological methods for estimating the total number of neurons and synapses: Issues of precision and bias. *Trends Neurosci.* **22**, 51-61 (1999).

465. West, M. J. New stereological methods for counting neurons. *Neurobiol. Aging* **14**, 275-285 (1993).

466. West, M. J., Østergaard, K., Andreassen, O. A. & Finsen, B. Estimation of the number of somatostatin neurons in the striatum: An in situ hybridization study using the optical fractionator method. *J. Comp. Neurol.* **370**, 11-22 (1996).

467. Wichterle, H., Turnbull, D. H., Nery, S., Fishell, G. & Alvarez-Buylla, A. In utero fate mapping reveals distinct migratory pathways and fates of neurons born in the mammalian basal forebrain. *Development (Cambridge)* **128**, 3759-3771 (2001).

468. Wickens, J. R., Begg, A. J. & Arbuthnott, G. W. Dopamine reverses the depression of rat corticostriatal synapses which normally follows high-frequency stimulation of cortex in vitro. *Neuroscience* **70**, 1-5 (1996).

469. Willoughby, D., Wachten, S., Masada, N. & Cooper, D. M. F. Direct demonstration of discrete Ca2+ microdomains associated with different isoforms of adenylyl cyclase. *J. Cell. Sci.* **123**, 107-117 (2010).

470. Wilson, C. J. GABAergic inhibition in the neostriatum. *Prog. Brain Res.* **160**, 91-110 (2007).

471. Wilson, C. J. The mechanism of intrinsic amplification of hyperpolarizations and spontaneous bursting in striatal cholinergic interneurons. *Neuron* **45**, 575-585 (2005).

472. Wilson, C. J. The generation of natural firing patterns in neostriatal neurons. *Prog. Brain Res.* **99**, 277-297 (1993).

473. Wilson, C. J., Chang, H. T. & Kitai, S. T. Firing patterns and synaptic potentials of identified giant aspiny interneurons in the rat neostriatum. *J. Neurosci.* **10**, 508-519 (1990).

474. Wilson, C. J. & Goldberg, J. A. Origin of the slow afterhyperpolarization and slow rhythmic bursting in striatal cholinergic interneurons. *J. Neurophysiol.* **95**, 196-204 (2006).

475. Wilson, C. J. & Groves, P. M. Spontaneous firing patterns of identified spiny neurons in the rat neostriatum. *Brain Res.* **220**, 67-80 (1981).

476. Wilson, C. J. & Groves, P. M. Fine structure and synaptic connections of the common spiny neuron of the rat neostriatum: A study employing intracellular injection of horseradish peroxidase. *J. Comp. Neurol.* **194**, 599-615 (1980).

477. Wilson, C. J., Groves, P. M., Kitai, S. T. & Linder, J. C. Three-dimensional structure of dendritic spines in the rat neostriatum. *J. Neurosci.* **3**, 383-398 (1983).

478. Wilson, C. J. & Kawaguchi, Y. The origins of two-state spontaneous membrane potential fluctuations of neostriatal spiny neurons. *J. Neurosci.* **16**, 2397-2410 (1996).

479. Wiltschko, A. B., Pettibone, J. R. & Berke, J. D. Opposite effects of stimulant and antipsychotic drugs on striatal fast-spiking interneurons. *Neuropsychopharmacology* **35**, 1261-1270 (2010).

480. Winsky, L. & Kuznicki, J. Distribution of calretinin, calbindin D28k, and parvalbumin in subcellular fractions of rat cerebellum: Effects of calcium. *J. Neurochem.* **65**, 381-388 (1995).

481. Witten, I. *et al*. Recombinase-driver rat lines: Tools, techniques, and optogenetic application to dopamine-mediated reinforcement. *Neuron* **72**, 721-733 (2011).

482. Wright, C. I., Beijer, A. V. J. & Groenewegen, H. J. Basal amygdaloid complex afferents to the rat nucleus accumbens are compartmentally organized. *J. Neurosci.* **16**, 1877-1893 (1996).

483. Wright, C. I. & Groenewegen, H. J. Patterns of overlap and segregation between insular cortical, intermediodorsal thalamic and basal amygdaloid afferents in the nucleus accumbens of the rat. *Neuroscience* **73**, 359-373 (1996).

484. Wu, Y. & Parent, A. Striatal interneurons expressing calretinin, parvalbumin or NADPH-diaphorase: A comparative study in the rat, monkey and human. *Brain Res.* **863**, 182-191 (2000).

485. Wu, Y., Richard, S. & Parent, A. The organization of the striatal output system: A single-cell juxtacellular labeling study in the rat. *Neurosci. Res.* **38**, 49-62 (2000).

486. Wyss, J. M. & Sripanidkulchai, K. The indusium griseum and anterior hippocampal continuation in the rat. *J. Comp. Neurol.* **219**, 251-272 (1983).

487. Xenias, H. S., Ibáñez-Sandoval, O., Koós, T. & Tepper, J. M. Are striatal tyrosine hydroxylase interneurons dopaminergic? *J. Neurosci.* **35**, 6584-6599 (2015).

488. Xiong, Q., Znamenskiy, P. & Zador, A. M. Selective corticostriatal plasticity during acquisition of an auditory discrimination task. *Nature* **521**, 348-351 (2015).

489. Yamada, T., McGeer, P. L., Baimbridge, K. G. & McGeer, E. G. Relative sparing in Parkinson's disease of substantia nigra dopamine neurons containing calbindin-D28K. *Brain Res.* **526**, 303-307 (1990).

490. Yan, R., Luo, X. -., Bi, G. -., Feng, J. & Zhang, C. -. Influence of astrocyte-conditioned medium on the formation of synapses in neural stem cells: The role of neurotrophin proteins. *Nat. Med. J. China* **88**, 2508-2512 (2008).

491. Yan, Z., Flores-Hernandez, J. & Surmeier, D. J. Coordinated expression of muscarinic receptor messenger RNAs in striatal medium spiny neurons. *Neuroscience* **103**, 1017-1024 (2001).

492. Yan, Z. & Surmeier, D. J. Muscarinic (m2/m4) receptors reduce N- and P-type Ca2+ currents in rat neostriatal cholinergic interneurons through a fast, membrane-delimited, G-protein pathway. *J. Neurosci.* **16**, 2592-2604 (1996).

493. Yang, H. *et al*. A simulation study on the Ca2+-independent but voltage-dependent exocytosis and endocytosis in dorsal root ganglion neurons. *Eur. Biophys. J.* **34**, 1007-1016 (2005).

494. Yang, Z., You, Y. & Levison, S. W. Neonatal hypoxic/ischemic brain injury induces production of calretinin-expressing interneurons in the striatum. *J. Comp. Neurol.* **511**, 19-33 (2008).

495. Yin, H. H. *et al*. Dynamic reorganization of striatal circuits during the acquisition and consolidation of a skill. *Nat. Neurosci.* **12**, 333-341 (2009).

496. Yung, K. K. L. Synaptic connections between spiny neurons of the direct and indirect pathways in the neostriatum of the rat: Evidence from dopamine receptor and neuropeptide immunostaining. *Eur. J. Neurosci.* **8**, 861-869 (1996).

497. Yung, K. K. L. & Bolam, J. P. Localization of dopamine D1 and D2 receptors in the rat neostriatum: Synaptic interaction with glutamate- and GABA-containing axonal terminals. *Synapse* **38**, 413-420 (2000).

498. Zeisel, A. *et al.* Brain structure. Cell types in the mouse cortex and hippocampus revealed by single-cell RNA-seq. *Science* **347**, 1138-1142 (2015).

499. Zhao, Y. *et al*. Distinct molecular pathways of development of telencephalic interneuron subtypes revealed through analysis of Lhx6 mutants. *J. Comp. Neurol.* **510**, 79-99 (2008).

500. Zhao, Y. *et al*. The LIM-homeobox gene Lhx8 is required for the development of many cholinergic neurons in the mouse forebrain. *Proc. Natl. Acad. Sci. U. S. A.* **100**, 9005-9010 (2003).

501. Zheng, Y., Schwabe, L. & Plotkin, J. L. Location-dependent dendritic computation in a modeled striatal projection neuron. *Lect. Notes Comput. Sci.* **8681 LNCS**, 741-748 (2014).

502. Zhou, F. -., Wilson, C. J. & Dani, J. A. Cholinergic interneuron characteristics and nicotinic properties in the striatum. *J. Neurobiol.* **53**, 590-605 (2002).

503. Zhou, L., Furuta, T. & Kaneko, T. Chemical organization of projection neurons in the rat accumbens nucleus and olfactory tubercle. *Neuroscience* **120**, 783-798 (2003).

504. Zierhut, B. *et al*. Setagin and secretagogin-R22: Posttranscriptional modification products of the secretagogin gene. *Biochem. Biophys. Res. Commun.* **329**, 1193-1199 (2005).

505. Znamenskiy, P. & Zador, A. M. Corticostriatal neurons in auditory cortex drive decisions during auditory discrimination. *Nature* **497**, 482-485 (2013).